FLOW DYNAMICS IN HIGH DENSITY CIRCULATING FLUIDIZED BEDS

By

Allan Shorusaeli Issangya

B. Sc., University of Dar es Salaam, 1983

M. Sc., University of Leeds, 1985

A THESIS SUBMITTED IN PARTIAL FULFILLMENT OF

THE REQUIREMENTS FOR THE DEGREE OF

DOCTOR OF PHILOSOPHY

in

THE FACULTY OF GRADUATE STUDIES

(Department of Chemical and Bio-Resource Engineering)

We accept this thesis as conforming

to the required standard

THE UNIVERSITY OF BRITISH COLUMBIA

April 1998

In presenting this thesis in partial fulfilment of the requirements for an advanced degree at the University of British Columbia, I agree that the Library shall make it freely available for reference and study. I further agree that permission for extensive copying of this thesis for scholarly purposes may be granted by the head of my department or by his or her representatives. It is understood that copying or publication of this thesis for financial gain shall not be allowed without my written permission.

Department of CHEMICAL AND BIO-RESOURCE ENGINEERING

The University of British Columbia
Vancouver, Canada

Date April 8, 1998

DE-6 (2/88)

ABSTRACT

Almost all previous circulating fluidized bed hydrodynamic data reported in the literature have been for suspension densities and solids circulation rates well below values used in fluid catalytic cracking and other catalytic reactors. A dual-loop circulating fluidized bed unit capable of achieving solids hold-ups as high as 15 to 25% by volume over the entire riser and solids circulation fluxes of 400 kg/m^2s and beyond was designed and constructed. Measurements were obtained in a riser of inside diameter 76.2 mm and height 6.1 m at superficial air velocities between 4 and 8 m/s with FCC particles of mean diameter 70 μm and density 1600 kg/m^3.

Longitudinal solids hold-up profiles, inferred from differential pressures, showed that a dense zone formed when the solids circulation rate exceeded the saturation carrying capacity of the gas. On further increasing the solids circulation rate, the solids volumetric concentration levelled off at 0.2 ± 0.05 while the height of the dense zone continued to expand. Low density (LDCFB) conditions are delineated from high density CFB (HDCFB) conditions by a transition point, defined as the intersection of the two linear portions when solids hold-up is plotted against solids circulation rate. Cross-sectional solids hold-ups in HDCFB conditions are not significantly affected by the superficial gas velocity. Average slip velocities are as high as 40 times the single particle terminal velocity, with slip factors as high as 15. The total pressure drop across the riser increases linearly with solids-to-gas mass flow ratio, then levels off once the dense zone occupies the whole riser. Correlations are suggested for longitudinal mean solids hold-up profiles. At a fixed solids circulation rate and air velocity, increasing solids inventories in the downcomer do not affect suspension densities in the risers.

Reflective-type optical fiber probes were employed to measure radial local voidage profiles. A non-linear relationship between the reflected light intensity and voidage was obtained using a new calibration method. Local time-mean voidages for high density conditions were nearly as low as ε_{mf} at the wall and as high as 0.9 at the axis. Local voidages were correlated as a function of the cross-sectional mean voidage, with the correlation covering a broader range of conditions than previous correlations. Visual observations indicate that solids refluxing, observed near the wall of dilute CFB risers, no longer exists for high density conditions; instead the whole suspension appears relatively homogeneous.

Radial profiles of local solids flux were measured using a suction tube for upflow fluxes and an inclined tube for downflowing solids. Net solids flux profiles are roughly parabolic and indicate the net flow to be, on average, upwards over the entire cross-section. Measurements from a solids momentum probe confirm that solids rise rapidly in the core and slowly near the wall. Local voidages, voidage frequency distributions, intermittency indices and voidage spectral density are also used to characterize the local flow dynamics. The core is a relatively uniform dilute flow interspersed with particle structures whose frequency and density increase with radius. The standard deviation of local voidage fluctuations reaches a peak at some distance from the wall. The location of the peak is quite different from the core-annulus boundary for LDCFB risers. Intermittency vs. local voidage plots are "bell-shaped", with a maximum when the local time-mean voidage is approximately 0.75. The fast fluidization regime is redefined to incorporate the HDCFB findings of this study.

A novel method is also developed to determine the accumulative (Type A) and classical (Type C) choking velocities in a single experiment in the dual-loop system.

TABLE OF CONTENTS

LIST OF TABLES

LIST OF FIGURES

ACKNOWLEDGEMENT

I wish to express my deepest gratitude to my main supervisor Dr. John R. Grace for his continuous guidance and support over the entire course of this work. My appreciation also goes to the co-supervisors Dr. J. -X. Zhu and Dr. K. S. Lim for their helpful discussion and encouragement. The key role played by Dr. Zhu in initiating this research project deserves a special recognition. I thank Dr. D. Bai for assisting with some of the experiments. Thanks are also due to the faculty members of Chemical and Bio-Resource Engineering for their interest and criticisms. I acknowledge also the inspiration I received from my former professors at the Universities of Dar es Salaam and Leeds and from the late Prof. Friedrich Lóffler of the University of Karlsruhe.

I am indebted to the entire staff of the Department's Workshop for their professional work in the construction of the experimental unit and their critical inputs during the design phase. Thanks to Mr. Horace Lam and the staff of Stores who assisted with the procurement of construction materials. Instrumentation of the unit owes a great deal to Mr. Alex Thng of the Electronics Shop. The friendship and discussions of my fellow graduate students in the Fluidization Group will always be cherished.

A scholarship from the German Academic Exchange Service (DAAD) and additional funding from the Natural Sciences and Engineering Research Council of Canada are gratefully acknowledged.

A special mention goes to my mother Maria for her love and her dedication to my education. I thank my wife Ndeninsia for her cooperation and inspiration. Lastly, but not the least, the following people deserve special thanks from me: Abraham, Brenda, Callilla, Elinkunde, Ellyns, Frank, Josehn, Nicolas and Ruth.

CHAPTER 1

INTRODUCTION

A large number of chemical processes require that two or more phases be brought into intimate contact with each other. The reactor performance is determined both by the process itself and by the relative motion between the lighter and the heavier phases. Fluidization, whereby a gas or liquid is passed upwards through a bed of particles supported on a porous distributor, involves relative motion between the fluid and solid particles in such a manner that the solid phase is supported and maintained in a suspended state by the fluid. In high velocity fluidization, where particles are massively entrained and transported out of the reactor, a relatively dense suspension can be maintained in the column by proper control of the air velocity and solids recycle rate.

The fluidized bed appeared on the industrial scene in the early 1920's when Winkler gasification of coal was first carried out (Leva, 1959). For a variety of reasons the technique did not attract much attention and lay dormant until World War II, when increased demand for aviation fuel led to the construction of the first fluidized bed catalytic cracker (Squires, 1986). The success of FCC technology led to the proliferation of the technique throughout the modern chemical process industry as well as other industries. As a result an enormous amount of research work has been carried out in fluidization and allied subjects during the past 50 years. Advantages of fluidized bed reactors over other gas-solid contacting reactors often include such factors as the capability of operating with small catalyst particles and hence high effectiveness factors, favorable bed-to-immersed-surface heat transfer coefficients, ability to withdraw and add particulate solids continuously, and the possibility of operation on very large scales.

Gas fluidized beds exhibit a number of distinct hydrodynamic regimes. Figure 1.1 illustrates schematically a sequence of fluidization regimes encountered in a vertical flow gas-solids system when the gas superficial velocity is raised gradually from zero to over 10 m/s. At low velocity, the gas merely percolates through the void spaces between particles and emerges at the surface. The solids in this case remain stationary, and the system is referred to as a fixed bed. As the gas velocity is gradually increased, the drag force acting on the particles also increases until the drag force balances the gravitational force on the particles. At this point the particles begin to move apart, and the bed expands upwards. The particles are then said to be fluidized, and the superficial gas velocity, U, at which this occurs is called the minimum fluidization velocity, U_{mf}. According to the two-phase theory (Toomey and Johnstone, 1952; Clift and Grace, 1985) once the velocity of the gas exceeds the minimum necessary to just fluidize the solids, any excess flow passes through in the form of gas bubbles (also referred to as voids). Group A powders are an exception in that they show an appreciable bubble-free range of gas velocities between U_{mf} and the velocity at which bubbles start to appear, the minimum bubbling velocity, U_{mb}. While there continue to be contrary views, supported by instability theory based purely on hydrodynamic considerations (e.g. Foscolo and Gibilaro, 1987; Gibilaro et al., 1988), most fluidization researchers describe the bubble-free range as being dominated by interparticle forces, which become more prevalent for small particles. U_{mf} and U_{mb} can be calculated from the equation due to Grace (1982) and the dimensional correlations of Geldart and Abrahamsen (1978):

$$Re_{mf} = \sqrt{27.2^2 + 0.0408 Ar} - 27.2 \qquad (1.1)$$

$$U_{mb} = 33 d_p \left(\frac{\rho}{\mu}\right)^{0.1} \qquad \text{(SI units)} \qquad (1.2)$$

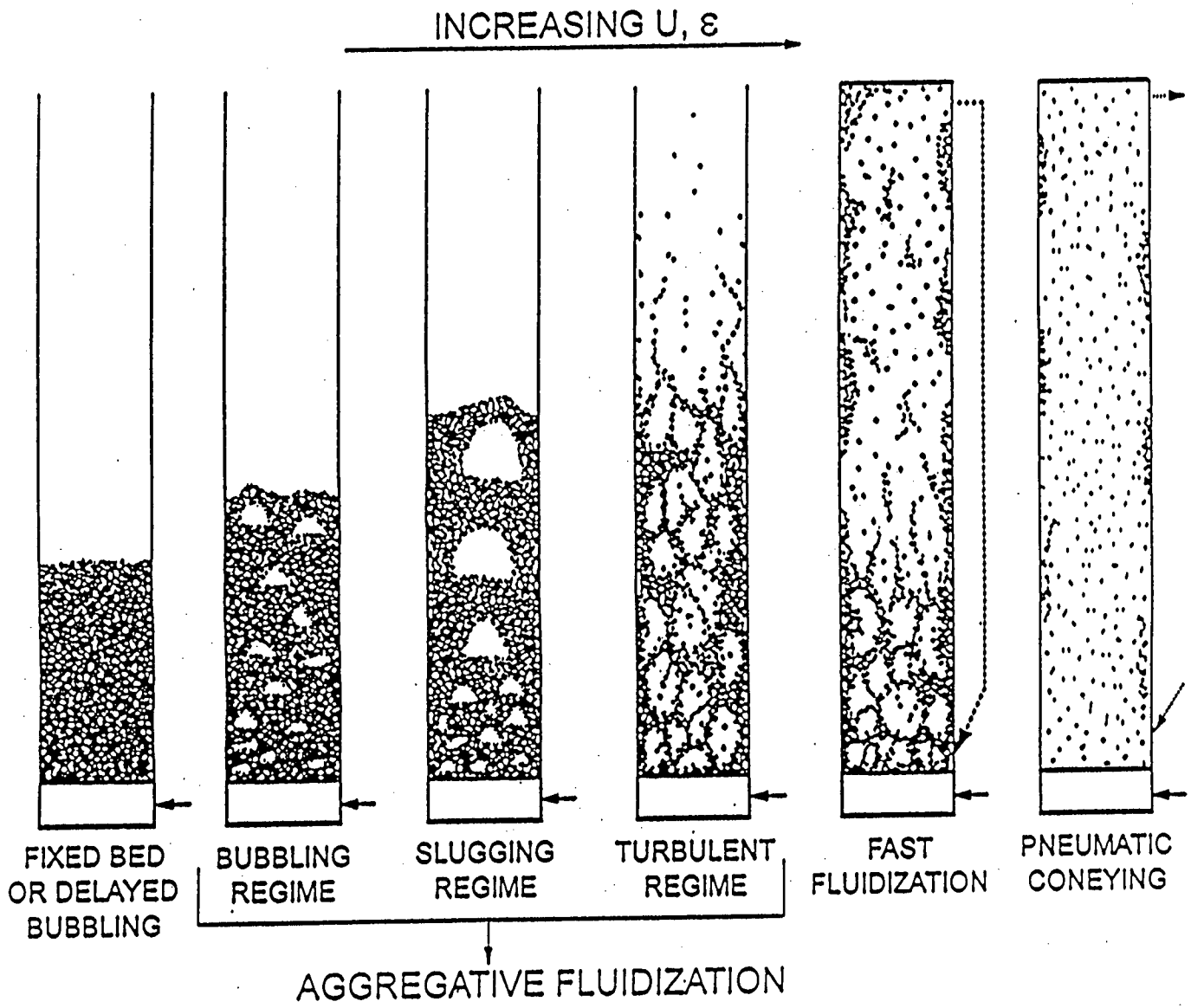

Fig. 1.1 Schematic diagram showing hydrodynamic regimes of fluidization, from Grace et al. (1997)

Beyond U_{mf} or U_{mb} the bed is in a state of bubbling fluidization where bubbles form at the distributor and rise, coalescing and growing larger as they move upwards, inducing mixing of particles in the bed. The gas flowing inside bubbles has limited contact with the bed solids, affecting the extent of reactions which can be achieved. Depending on the bed geometry and the material being fluidized, bubbles may grow large enough to fill most of the column cross-section; they then elongate to become slugs, leading to slugging fluidization. Slugging is generally undesirable since it further reduces the gas-solid contacting and causes vibrations in the fluidized bed. Not all systems are capable of slugging, however. If particles are sufficiently small, the column diameter is sufficiently large or the bed is shallow, void sizes do not approach the column diameter. Under these circumstances, there can be no slug flow. Such systems have often been termed non-choking systems (Yousfi and Gau, 1974; Yang, 1975; Leung, 1980; Bi et al., 1993).

The next regime encountered as the gas velocity is increased is turbulent fluidization. The transition from bubbling to turbulent fluidization is generally characterized by the superficial velocity U_c at which the amplitude of pressure fluctuations measured at the bottom of the column reaches a maximum (Yerushalmi and Cankurt, 1979). There have, however, been wide variations in the manner in which pressure fluctuations have been measured and analyzed (Brereton and Grace; 1992), some workers preferring absolute or dimensional values, while others employ differential values and/or normalize to give dimensionless values. These variations significantly affect measurements of U_c (Bi and Grace, 1995). Measurements based on differential rather than absolute pressure are preferred since the data are more indicative of local conditions. U_c determined from differential pressure measurements is well correlated (Lim et al., 1995) by

$$Re_c = \frac{\rho U_c d_p}{\mu} = 1.24 Ar^{0.45} \qquad (2 < Ar < 1 \times 10^8) \qquad (1.3)$$

By considering bubble-bubble interaction and coalescence, Bi et al. (1995) derived U_c for small particles and non-slugging systems as,

$$U_c = U_{mf} + \frac{1.21 Ar^{0.04} (g\nu_d)^{1/3}}{(Y - 0.3 Ar^{0.04})} \qquad (1.4)$$

Y is typically 1 for group A particles; ν_d, the kinematic viscosity of the emulsion phase, has been correlated (Bi et al., 1996) by

$$\nu_d = 0.000374 Ar^{0.0764} \qquad \text{(SI units)} \qquad (1.5)$$

In fully turbulent fluidized beds bubbles no longer exist. Some studies (e.g. Kehoe and Davidson, 1971) describe the flow as rapid, chaotic, small scale motions, with transient voids darting obliquely up the column. Others (e.g. Yerushalmi and Cankurt, 1979) indicate that a turbulent fluidized bed consists of refluxing strands or packets of particles where neither a dense nor a dilute phase can truly be said to be continuous. Other observations (e.g. Brereton, 1987; Brereton and Grace, 1992) suggest that the bed is composed of periods when there are slug-like structures, interspersed with periods of particle clusters and dilute zones. The decrease in amplitude of pressure fluctuations above U_c has also been explained differently. Some studies (e.g. Chehbouni et al., 1994; Bi et al., 1995) attribute it to bubble break-up increasingly dominating over coalescence as the superficial velocity is raised until bubbles completely disappear, while others (e.g. Rhodes and Geldart, 1986) suggest that it is due to solids being increasingly transferred from the bed to the freeboard. Brereton and Grace (1992) suggest that intermittent bursts of particle agglomerates become dominant over slug-like behaviour as the gas velocity is increased. Despite the different descriptions, it is generally agreed that gas/solid contacting

is better than in bubbling/slugging fluidized beds because there is less tendency for gas to bypass the particles. Entrainment from a turbulent fluidized bed is higher and the bed surface more diffuse than for lower-velocity fluidized beds. The onset of turbulent fluidization appears to occur in most cases when the overall voidage is of order 0.7 to 0.8 and for $(U - U_{mf})$ of 0.4 to 0.6 m/s (Sun and Chen, 1989).

When the superficial gas velocity is raised further, the overall bed voidage increases and the top surface between the "dense bed" and the freeboard becomes less and less distinct. At the same time, the rate of particle entrainment increases and, unless the entrained material is replaced, the column empties very rapidly. Continuous operation is normally sustained by capturing the entrained solids in cyclones or other gas-solid separation devices and returning them to the base of the column (often called a 'riser') through a standpipe and a seal, e.g. a mechanical valve (e.g. slide valve) or non-mechanical valve (e.g. L-valve). Such a system, shown schematically in Fig. 1.2, consisting of the riser and the associated recirculation loop, is referred to as a circulating fluidized bed (CFB).

Two flow regimes may be distinguished in CFB systems. If the solids feed rate is low enough and the gas velocity high enough, all particles are conveyed up the column, leaving no accumulation at the bed bottom. This represents dilute phase pneumatic transport and corresponds to solids volumetric concentrations of typically 1 to 5%. On the other hand, at lower gas velocity or high solids flowrate, some particles start refluxing and accumulate at the bottom in a dense phase; the riser is then said to be in the fast fluidization regime. In this regime overall suspension compositions are typically 2 to 15% by volume solids. The point where solids accumulation commences on lowering the gas velocity corresponds to what has been called (Bi et al., 1993) type A (or accumulative) choking and represents the transition between fast fluidization and pneumatic transport.

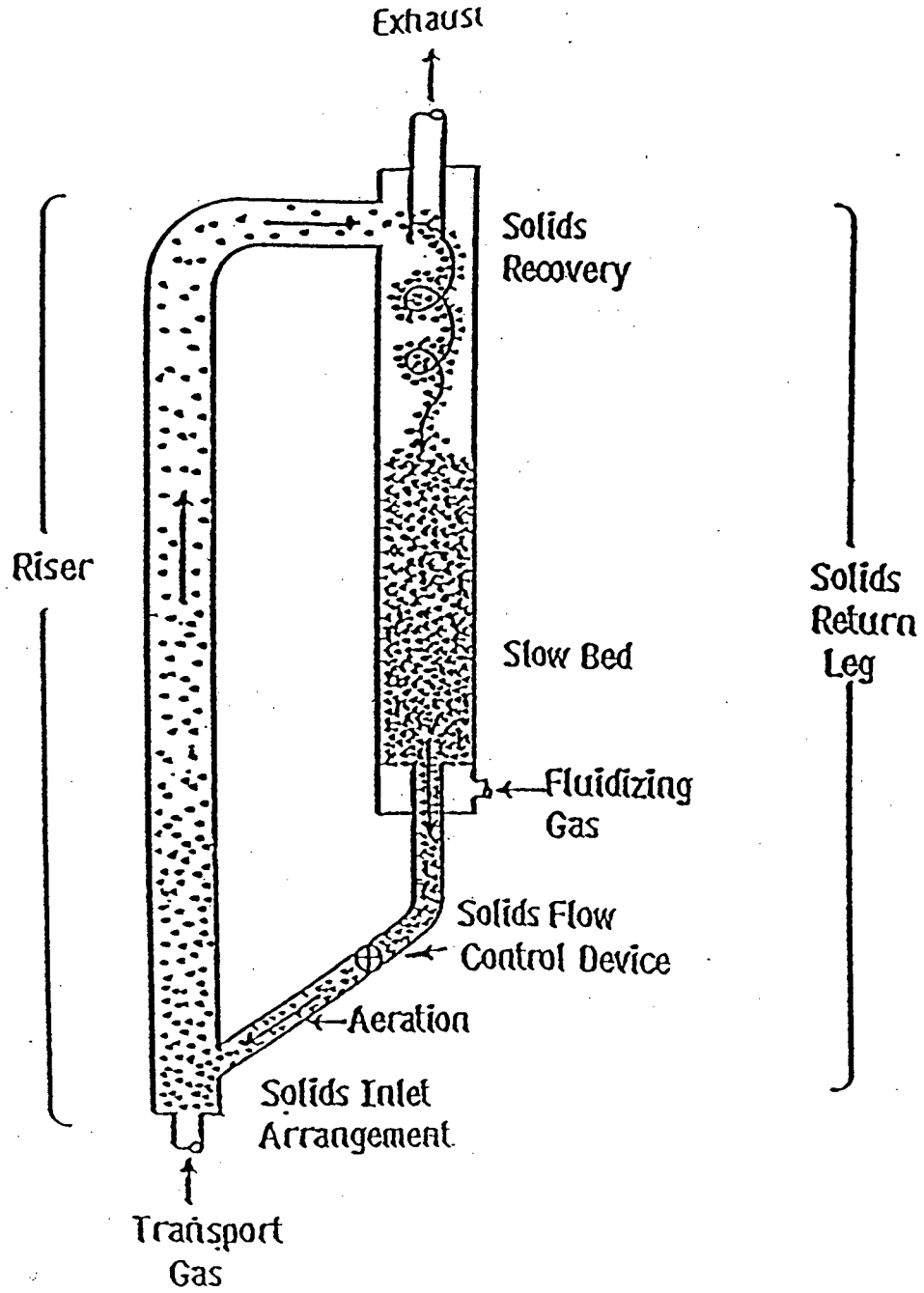

Fig. 1.2 Schematic of a typical setup of a circulating fluidized bed adopted from Yang (1993).

This superficial velocity, designated U_{CA}, is well predicted by an equation due to Bi and Fan (1991):

$$U_{CA} = 7.34(gd_p)^{0.324}(G_s/\rho)^{0.352}Ar^{0.068} \qquad \text{(SI units)} \qquad (1.6)$$

The mean voidage of the bed at the transition is normally around 0.95 (Avidan and Yerushalmi, 1982; Monceaux et al., 1986a), although transition voidages from 0.93 to 0.98 have been observed (Horio, 1988; Li and Kwauk, 1980).

The transition velocity between turbulent and fast fluidization proposed by Yerushalmi and Cankurt (1979) was based on the measured differential pressure gradient (dP/dL) between two points near the bottom of the column. Below the transition velocity, referred to as the transport velocity, U_{tr}, the suspension collapses, leading to a step change in the pressure gradient. Above it the pressure gradient varies smoothly with increasing G_S. Determining the transport velocity by this method has been found to be tedious and difficult (Rhodes and Geldart, 1986; Schnitzlein and Weinstein, 1988; Yoshida and Mineo, 1989). Bi et al. (1995) defined the transition from turbulent to fast fluidization as the superficial velocity U_{se} corresponding to the onset of significant particle entrainment from the column. Values of U_{se} were well correlated by

$$U_{se} = 1.53\sqrt{\frac{gd_p\Delta\rho}{\rho}} \qquad (1.7)$$

In fast fluidization the average solids holdup is usually lower than 0.2. Riser superficial gas velocities typically exceed 5 m/s, compared to less than 1 m/s in conventional bubbling beds. Average slip velocities are high, in some cases > 30 times the terminal velocity of individual particles (Yerushalmi and Avidan, 1985). The high slip velocities are generally considered to result from the hydrodynamic formation of relatively large and dense particle clusters, streamers, strands, swarms or particle sheets (Brereton, 1987; Horio, et al., 1988; Horio and Kuroki, 1994; Bi, 1994). Agglomeration due to other forces, e.g.

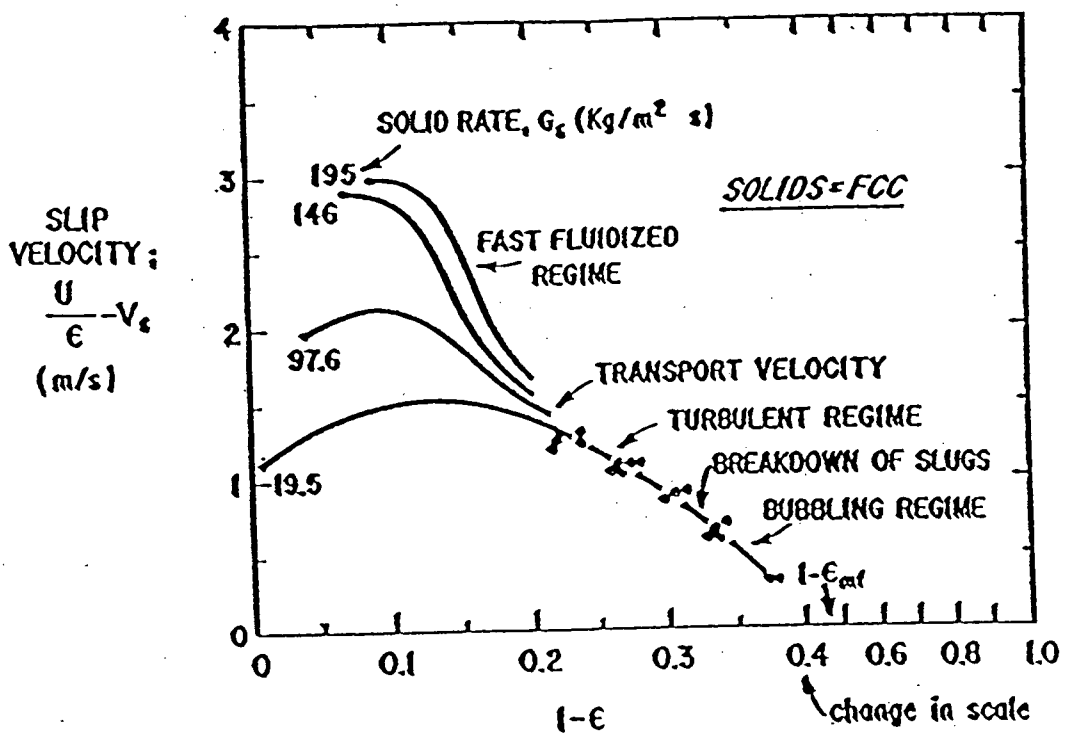

Fig. 1.3 Slip velocity in fluidized beds according to Yerushalmi and Cankurt (1979).

electrostatics, may also be significant, especially for very fine solids systems. As shown in Fig. 1.3, slip velocities are highest in the fast fluidization regime.

A number of factors other than gas velocity and solids circulation rate may affect the flow regime transitions. These include particle size distribution (Abrahamsen and Geldart, 1980; Sun and Grace, 1992), gas properties and the associated effects of pressure and temperature (Sun and Chen, 1989; Knowlton, 1992; Bi and Grace, 1996), column diameter and height, presence of internals in the bed (Sitnai and Whitehead, 1985; Jiang et al., 1991) and interparticle forces, both naturally occurring (Rietema, 1981) and artificially induced, e.g. magnetic forces (Agbim et al., 1971). Typical operating ranges are summarized in a regime map by Grace (1986), later extended by Bi et al. (1995) to include curves for the transition velocities U_c, U_{se} and U_{CA} as shown in Fig. 1.4. As noted above, the flow behavior in a circulating fluidized bed depends on solids circulation rate in addition to the superficial gas velocity. Therefore the solid-to-gas volumetric flowrate ratio, $m = G_s/\rho_p U$, is included as a parameter to provide boundaries between the fast fluidization and pneumatic transport regimes. It is apparent from Fig. 1.4 that in current applications, circulating fluidized bed reactors are primarily of interest for Groups A and B of the Geldart (1973) particle classification. The present study is concerned with circulating beds of group A particles operating in the fast fluidization regime, with emphasis on high density, high solids flux suspensions.

The earliest fluidized bed reactors used for the catalytic cracking of hydrocarbons operated at superficial gas velocities of 1.5 m/s or more, velocities now associated with the fast fluidization regime (Grace, 1990). However, insufficient methods were then used to separate and return entrained solids, leading to high catalyst losses. These reactors also faced difficulties in controlling solids holdup (Turner, 1979). They were therefore soon replaced by bubbling fluidized beds (Jahnig et al., 1980; Squires, 1985). In 1954 a

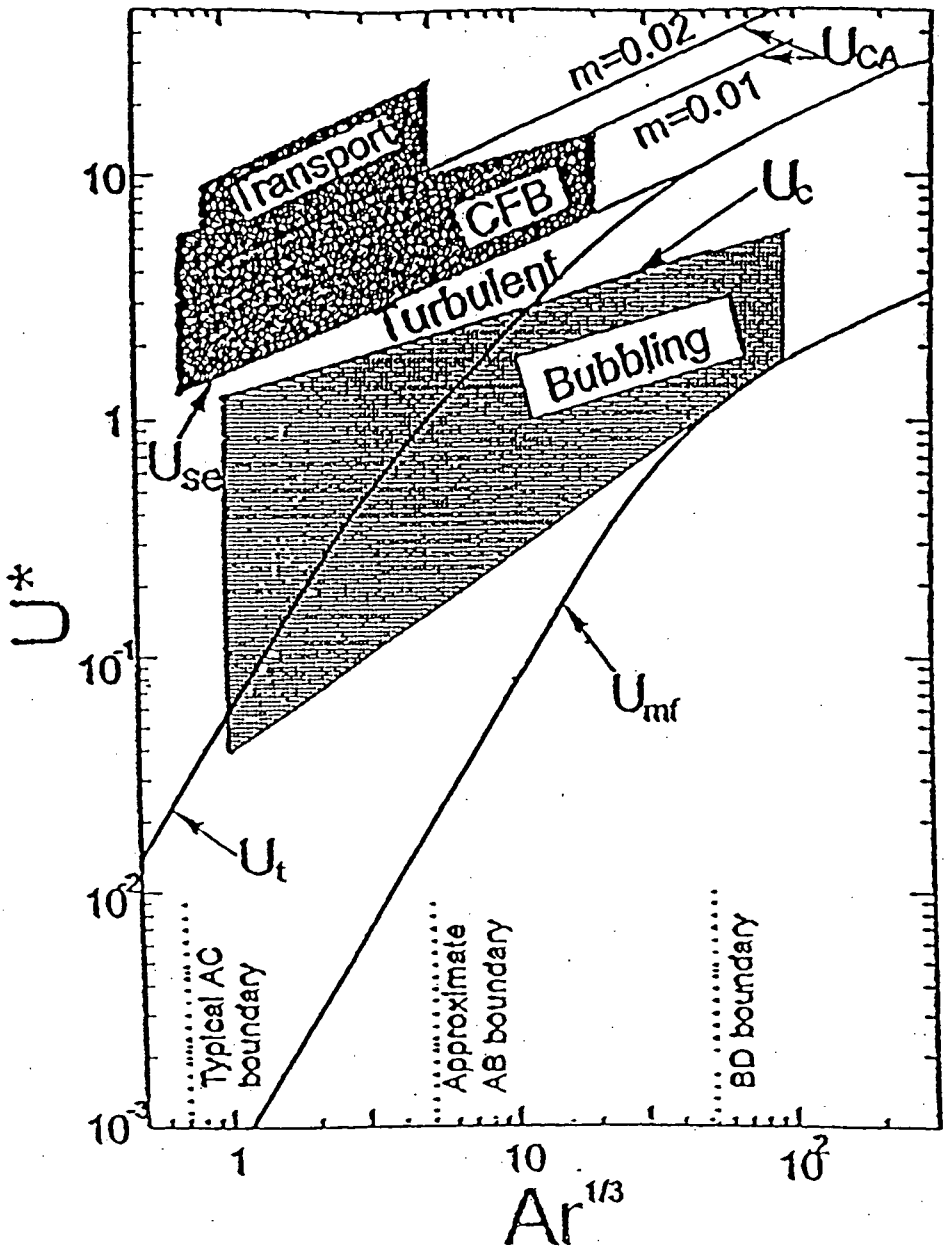

Fig. 1.4 Fluidization regime map adopted from Bi et al. (1996).

commercial circulating fluidized bed Fischer-Tropsch plant was constructed in South Africa. Only in the early 1970s did CFB reactors return to prominence with the development of alumina calcining CFB reactors (Reh, 1971). In the late 1970s these were extended to CFB coal combustion due to environmental advantages over low-velocity fluidized bed combustors. At about the same time, the introduction of ultra-high activity and durable zeolite catalysts and advances in solids flow control systems helped push fluid catalytic cracking technology back to high velocity riser operation (Avidan et al., 1989). By 1991 there were over 220 CFB combustors worldwide (Engstrom and Lee, 1991), while in 1992 there were over 350 fluid catalytic cracking units in the US alone (Reichle, 1992).

Circulating fluidized beds offer several advantages over conventional bubbling/turbulent fluidized bed reactors. These include (Yerushalmi, 1986; Grace, 1990; Berruti et al., 1995) high gas and solids throughput, absence of gas bypassing by bubbles and therefore better gas-solids contacting efficiency, reduced axial gas and solids backmixing, near thermal uniformity throughout the reactor, independent adjustment of solids and gas retention time, possibility of desirable reactions or other operations in the return loop, staged addition of reactants along the riser height, and reduced tendency for particles to agglomerate. A notable advantage for gas-phase catalytic reactions is that the extent of gas backmixing is reduced since most particles are entrained upwards giving near plug flow condition. Berruti et al. (1995), Dry and Beeby (1997), Avidan (1997) and Matsen (1997) discuss a large number of industrial processes that utilize CFB technology, as well as processes still under development. These processes can be divided into: gas-solids reaction processes and gas-phase catalytic reaction processes. The former, which include such processes as combustion of low-grade fuels (e.g. coal) and alumina calcination, usually have low reaction rates and therefore do not necessarily require high gas velocities or high solids circulation rates. Catalytic gas-phase reactions, which include

fluid catalytic cracking of petroleum, Fischer-Tropsch synthesis and oxidation of butane, require a relatively high gas velocity in the riser to promote plug flow, thus avoiding gas backmixing. Their high reaction rates also call for higher gas velocities because of the desired short contact times between the gas and solids.

Figure 1.5 shows typical configurations of the two principal applications of CFB technology: circulating fluidized bed combustion (CFBC) and fluid catalytic cracking (FCC). CFBC is carried out by continuously feeding fuel particles (e.g. coal) to a riser containing an inert material such as sand fluidized by air. Limestone or dolomite is commonly added to the riser in order to remove sulphur dioxide resulting from the oxidation of sulphur compounds present in the coal during combustion. Heat is removed through the reactor wall and from the circulating solids, by means of heat exchangers placed in the recycle loop. The cracking of crude petroleum into lighter fractions is an endothermic process accompanied by carbon (also called coke) deposition on the catalyst surface. In the FCC unit feed oil is sprayed into the upflowing suspension of hot catalyst particles in the riser where heat absorption, reaction and coke deposition take place. After disengagement from the catalyst, the vapour stream is fed into a distillation column for fractionation into products. The spent catalyst is passed through a baffled stripping zone where hydrocarbons are removed by steam. The catalyst then flows into an air fluidized bed regenerator in the return loop where the deposited coke and any unstripped hydrocarbons are burnt off. The regenerated catalyst then re-enters the riser at the base and the cycle repeated.

Key features of the two CFB operations (Grace, 1990; Bi and Zhu, 1993; Werther, 1994; Berruti et al., 1995) are compared in Table 1.1. Significant differences exist in their design and operating characteristics. For example, the solids circulation rates in combustors are generally less than 100 kg/m^{2}s and the gas velocity is typically 5 to 9 m/s,

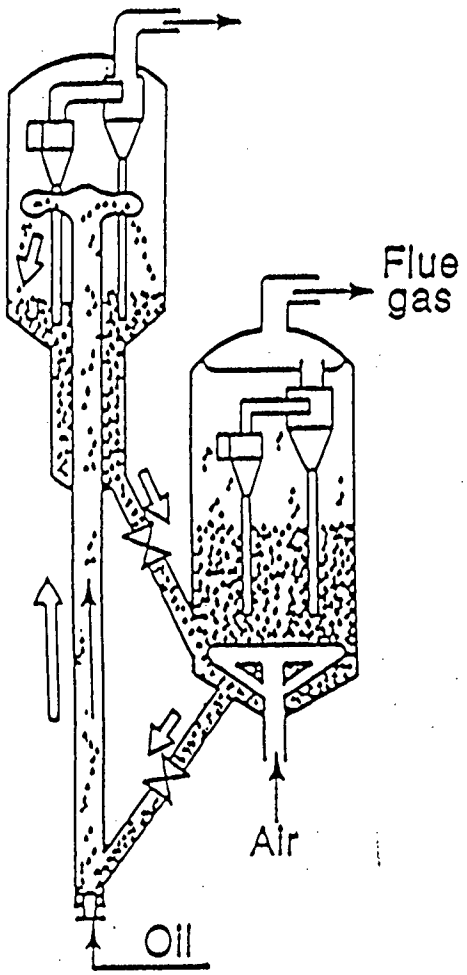

FCC (Marcia, 1992)

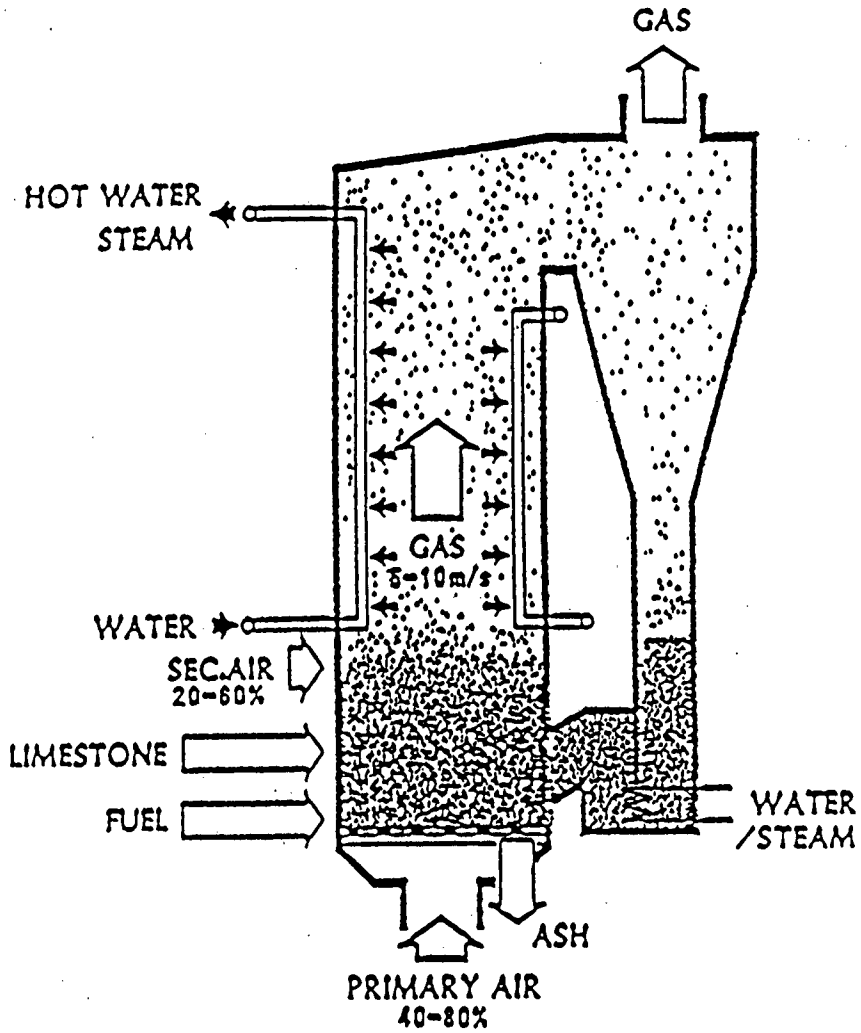

CFBC (Kullendorf and Andersson, 1985)

Fig. 1.5 Schematic of typical fluid catalytic cracking (FCC) and circulating fluidized bed combustion (CFBC) systems.

Table 1.1: Typical design and operating parameters for the two principal applications of fast fluidization: - fluid catalytic cracking and circulating fluidized bed combustion ([1]Grace, 1990; [2]Bi and Zhu, 1993; [3]Werther, 1994; [4]Berruti et al., 1995).

Parameter	Ref.	FCC Riser Reactor	CFB Combustor
Particle density, kg/m^3	1	1100 - 1500	1800 - 2600
Mean particle diameter, μm	1	60 - 70	150 - 250
	2	40 - 80	100 - 300
	4	50 - 150	250 - 500
	3	~ 60	~ 200
Particle size distribution	1	Quite broad	Broad
Geldart powder group	1,2,4	A	B
Superficial gas velocity, m/s	1	8 - 18 increasing with height	5 - 9
	4	4 - 10	2 - 6
	2	6 - 28 increasing with height	5 - 9
	3	4 - 20 increasing with height	5 - 8
Net solids flux, kg/m^2s	1	400 - 1400	10 - 100
	4	> 250	5 - 100
	2	400 - 1200	10 - 100
	3	>300	<10 - 15 (40)
Apparent solids concentration	2	3 - 12%	< 1%
in the developed region	3	1 - 10%	0.1 - 0.3
Average solids residence time	2	2 - 4	20 - 40
per single pass, s	3	~ 4	~ 20 - 40
Riser cross section geometry	3	circular	usually rectangular or square
Riser diameter, m	2,3	0.7 - 1.5	4 - 8 (hydraulic)
	4	1 - 2	8 - 10
Height-to-diameter ratio	2,3	> 20	< 5 - 10
Solids return column diameter-to-riser diameter ratio	2	>> 1	< 1
Solids inventory	2	high	low
Solids exit configuration	1,2,4	smooth, abrupt	abrupt
Solids feeding control device	2,4	mechanical devices	non-mechanical devices
Exit temperature, °C	1	500 - 550	850 - 900
	4	250 - 650	> 800
Pressure, kPa	1	150 - 300	110 - 120
	4	≥ 100	100

conditions which result in low solids holdups in the riser, usually less than 1% in the developed upper part. For FCC units solids mass fluxes above 250 kg/m^{2}s are typical, superficial gas velocities are as high as 20 m/s, and mean solids hold-ups range between 3 and 12%. Fine Geldart group A powders are used in FCC, while coarse group B particles are employed in CFBC. In addition, there are significant differences in column geometry, solids feeding devices and solids inventory. Zhu and Bi (1995) referred to circulating fluidized beds operating under high solids flux and/or high solids holdup conditions as high density circulating fluidized beds (HDCFB), while those operating at low solids flux (< 200 kg/m^{2}s) and low suspension densities (< 3% in the developed region) were called low density circulating fluidized beds (LDCFB). While this terminology is generally adopted in this thesis, a cross-sectional mean solids hold-up of 0.2 ± 0.05 (determined as explained in Chapter 3) is specified to indicate the lower limit of HDCFB operation.

Although extensive studies have been conducted of CFB systems (Yerushalmi and Avidan, 1985; Reh, 1985; Grace, 1990, Contractor and Chaouki, 1991, Berruti, et al., 1995), almost all reported CFB data are for systems operating at relatively low suspension densities (rarely above 2% solids by volume in the developed region), low gas velocities (< 10 m/s) and modest solids circulation rates (< 100 kg/m^{2}s), conditions typical of CFB combustors. CFB risers consist of a dilute region towards the top and a relatively dense region near the bottom, with the height of the dense region depending on the gas superficial velocity and solids circulation rates. The top dilute region has been subjected to much wider investigation than the bottom zone. The top region has a dilute core in which solids flow rapidly upward surrounded by a descending dense annulus.

Very few systematic measurements of local parameters are available for high-flux dense systems. Studies conducted in the lower dense zone of CFB risers at relatively low circulation rates (< 100 kg/m^{2}s) indicate differing observations. Some (e.g. Bolton and

Davidson, 1988; Werther, 1994; Bai et al., 1995) indicate the lower dense region to be in the turbulent bed regime, while others (e.g. Ishii and Horio, 1991; Johnsson et al., 1992; Svensson et al., 1996) suggest the region to be a bubbling fluidized bed. Except for some recent work by Wei et al. (1997) in the bottom region of a CFB riser, no measurements of local solids flux under high density conditions are available in the literature. Although previous studies give some insight into the flow structure of the dense zone in CFB risers, the solids circulation rates and gas velocity employed are well below those in commercial fluid catalytic cracking installations (see Table 1.1). Table 1.2 summarizes hydrodynamics studies with solids circulation rates in excess of 200 kg/m^2s. There is clearly a need for more fundamental research to study both global and local flow characteristics of CFB systems operated at high solids fluxes and suspension densities:

Flow regimes and the associated suspension flow behaviour must be considered in CFB reactor modelling. Reactor models are idealized human constructs that attempt to capture the essence of the behaviour of the flow, mixing and contacting of reacting species and phases in order to be able to predict reactor conversions, yields and dynamic responses. The principles involved are simple mass and energy balances once the flow behaviour in the riser has been modelled and adequate representation of the chemical kinetics and, to some extent, heat transfer and thermodynamics have been made. Several CFB reactor model representations of flow dynamics in CFB risers have been proposed in the literature. The major ones have been classified into two groups (Grace and Lim, 1997).

(1) Single-region one-dimensional models that ignore lateral or radial gradients, thereby treating the entire cross-section of the riser as if it were uniform.

(2) While the models in (1) can be used to provide a first approximation of reactor characteristics, they ignore lateral gradients. The core-annular flow structure observed in

Table 1.2: Hydrodynamic studies in circulating fluidized beds for which the solids circulation rate, G_S, exceeds 200 kg/m^{2}s.

Author	Riser (D x H) mm x m	Solids feed device	Particles	U_{max} m/s	$G_{s,max}$ kg/m^{2}s	Measurement technique
Yerushalmi et al. (1976, 1978)	76 x 7.2 152 x 8.2	J-valve J-valve	FCC FCC	7 5	213 220	Differential pressure
Arena et al. (1988, 1991)	41 x 6.4 400 x 10.5	Slide valve Loop seal	Sand Sand	7 6	600 260	Differential pressure
Galtier and Pontier (1989)	300 x 22	Mech. valve	FCC	20	400	Gamma-ray absorption
Patience et al. (1991)	82.8 x 5	L-valve	Sand	8	240	Differential pressure
Azzi et al. (1991)	750, 950 mm dia.	NA	FCC	15	1000	Momentum probe Gamma-ray absorption
Contractor et al. (1991)	150 x 27.4	NA	FCC	4.4	230	Differential pressure Radioactive tracer
Mori et al. (1991)	50 x 4.55		FCC	7	400	Differential pressure
Dry and Christensen (1989)	90 x 7.2	NA	FCC	8	200	Differential pressure
Martin et al. (1992)	190 x 11.7 940 x 27	Slide valve	FCC FCC	6	216	Gamma ray absorption Radioactive tracer
Donsi and Osseo (1994)	57* x 4.6	Butterfly valve	Glass	30	500	Differential press. Laser Doppler anemometry
Pugsley et al. (1993)	50 x 5.0		Sand	7	400	Differential pressure
Wei et al. (1994)	186 x 8	Slide valve	FCC	8.5	215	Differential press. Optical fiber imaging
Karri and Knowlton (1996)	300 x 13	L-valve	Catalyst	8.1	586	Differential pressure

* hydraulic diameter of a column of 40 mm x 100 mm cross-section

LDCFB risers led to several core-annulus two-region models. The gas and solids are assumed to behave quite differently in the outer annular region and in the inner core, with mass transfer between the two regions. The flow in each of these regions is commonly (but not always) assumed to be one-dimensional.

Understanding the fluid and particle dynamics is clearly critical to successful modelling of CFB reactors. Flow dynamics also influence the pressure drop across the riser, heat transfer rates between the suspension and the riser wall or other heat transfer surfaces (Grace et al., 1986) as well as erosion rates of surfaces (Zhu et al., 1989). In short improved understanding of the flow dynamics in high density circulating fluidized bed systems should enable better comprehension of the advantages and limitations of HDCFB reactors, in turn leading to more reliable scale-up and more cost-effective units.

The present project was initiated to provide improved understanding of high density/high flux CFB systems, where the dense and dilute zones coexist in the riser as well as for conditions where the dense region occupies the whole column. From the industrial application point of view this study is important because:

(1) FCC is still by far the major industrial CFB system and improvements may lead to substantial returns.

(2) Better understanding of the fundamentals of high density/high flux systems could improve the design and increase the applicability and capacity of other CFB processes.

(3) Increasing the suspension density even beyond that presently used in FCC reactors may lead to new applications requiring high solid/gas feed ratios and high solids hold-up (e.g. Shohji et al., 1983; Shaheen, 1983; Stripinis, 1991; Leuenberger and Wilbert, 1987; Park and Gau, 1986; Martin et al., 1992).

(4) The development of HDCFB should lead to high solids process capacity while maintaining good gas-solids contacting.

Objectives of this study

The objective of this work is to characterize the flow dynamics of high density/high solids flux CFBs. The work is limited to the study of solids distribution and flow behavior. Specifically, the main objectives were:

(a) To conceptualize, design and build a circulating fluidized bed apparatus capable of achieving high density and high solids flux in the riser.

(b) To obtain experimental data and establish the upper limit of suspension density and solids circulation rates achievable in the unit.

(c) To obtain experimental longitudinal cross-sectional solids hold-up profiles, local voidages and solids fluxes and characterize how they are affected by operating variables.

(d) To determine the local flow structure in circulating fluidized bed risers at high suspension densities and solids fluxes and to establish the flow regime.

Structure of thesis

To make this thesis easier to read, a general review of circulating fluidized beds is presented in Chapter 1 while leaving detailed reviews of previous work on specific topics to later chapters. For the same reason, except for the general instrumentation covered in Chapter 2, information on measurement techniques is presented in individual chapters as needed. Chapter 2 describes in detail the choice, design, construction and operation of the HDCFB facility designed and used in this study.

Chapter 3 discusses longitudinal solids hold-up profiles and the influence of operating conditions. The data are used to distinguish between LDCFB and HDCFB. Using the data of this study and those of other studies in the literature, correlations are formulated for the riser bottom and exit mean solids hold-ups. Pressure and inventory balance simulations are in turn conducted incorporating these correlations, and results are compared to experimental results.

Local voidage measurements from an optical fibre probe are presented in Chapter 4. Time-mean point average voidage profiles are used to describe the solids distribution and, with the instantaneous values, to explain the flow dynamics in high density risers, while also providing comparisons with low density risers. A correlation for predicting local time-mean voidage is formulated from the data and compared to correlations in the literature.

Chapter 5 discusses local solids flux profiles in the riser measured by an inverted U-tube for upflow and an inclined tube for descending particles. Comparisons are made between fluxes in LDCFB and HDCFB. Measurements of the local particle flow direction from a momentum probe are also presented. The probe was initially used to check visual observations regarding particle flow direction near the wall.

Chapter 6 compares the flow dynamics of HDCFB with those of the standard flow regimes. Differential pressure and local voidage measurements obtained in a separate experiment under bubbling and turbulent fluidized bed conditions are compared with HDCFB and LDCFB data.

Previous experimental methods for determining the lower and upper boundaries of fast fluidization are tedious and time consuming. A novel simple method for determining those boundaries is presented in Chapter 7, and results are compared to recommended correlations in the literature.

Chapter 8 gives conclusions of this work and lists recommendations for future work on CFB hydrodynamics.

CHAPTER 2

APPARATUS

2.1 Achieving high density/high flux conditions in risers

The suspension density in a circulating fluidized bed riser can be raised either by increasing the solids flux at a fixed superficial gas velocity or by lowering the superficial gas velocity while holding the solids flowrate constant. To maintain steady operation in the fast fluidization regime, there are, however, limits on the circulation rate for a given gas velocity and on the velocity for a fixed solids circulation flux. The limitations are imposed by either of two modes of instability which may take place in the riser. These are discussed next, together with methods of avoiding them.

2.1.1 Classical choking

Increasing gradually the solids circulation rate in a CFB riser operating at a fixed superficial gas velocity eventually leads to a point at which the upflowing gas can no longer support the particle suspension causing it to collapse. On the other hand, when the superficial gas velocity is reduced at a fixed solids flux, a similar phenomenon may also occur. This operational instability is generally referred to as choking (Zenz and Othmer, 1960) or Type C (Classical) choking (Bi et al., 1993). It becomes impossible to operate the riser in fast fluidization mode at a superficial gas velocity lower than that corresponding to choking at a fixed solids flux, and/or to operate at a higher solids flux than that at the choking point for a given superficial gas velocity because severe slugging appears for slugging systems, or the bed switches directly into the bubbling regime for

non-slugging systems. The onset of classical choking is dependent on gas and solids properties as well as on the size and geometry of the column. If suitable choices of these variables are made e.g. small particles and a riser of sufficiently large diameter, the unit can be operated in the fast fluidization flow regime over a wide range of solid circulation rates. Choking investigations have led to a number of correlations to determine the onset of the instability. An equation proposed by Yousfi and Gau (1974)

$$\frac{U_{ch}}{\sqrt{gd_p}} = 32\,Re_t^{-0.06}\left(\frac{G_s}{\rho_g U_{ch}}\right)^{0.28} \qquad (2.1)$$

has been found to be most accurate in predicting the classical choking velocity in Group A particles (Teo and Leung, 1984; Bi et al., 1993).

2.1.2 Equipment-induced instabilities

Two other forms of instability may also occur in a CFB system when attempting to increase the riser solids hold-up, before the classical transition point is reached. One occurs if the gas blower is unable to provide a sufficient pressure head to overcome the pressure drop in the riser and maintain the particles in suspension (Zenz and Othmer, 1960; Doig and Roper, 1963; Leung et al., 1971). The second results from pressure imbalance between the riser and the solids return leg making steady state operation impossible (Knowlton and Bachovchin, 1976; Takeuchi et al., 1986; Bader et al., 1988; Hirama et al., 1992).

The downcomer-riser loop pressure balance has been a subject of several theoretical analyses (Weinstein et al., 1983; Kwauk et al., 1986; Arena et al., 1987; Rhodes and Geldart, 1987; Rhodes and Laussmann, 1992; Yang, 1988; Breault and Mathur, 1989; Horio and Takei, 1991; Bi and Zhu, 1993). These have provided useful

information on improving CFB design and operation. Bi and Zhu (1993) proposed that high suspension densities and high solids fluxes could be achieved by a combination of high solids inventories, large downcomer-to-riser diameter ratio, a low pressure drop solid feeder, and minimizing pressure drops in solids separation devices and fittings along the loop, in addition to requiring a proper blower and suitable particle size/riser diameter combinations. The conceptual design of a laboratory scale high density CFB proposed by Bi and Zhu (1993) is shown in Fig. 2.1. The special feature in this design is the addition of a second riser to lift the solids from the first riser to a higher level, facilitating a taller downcomer, which, in addition to holding a high inventory of solids, provides a high pressure head, enabling high solids fluxes and high density to be achieved in the first riser. The diameter of the second riser needs to be larger than that of the first in order to reduce the overall pressure drop in raising the particles to the top of the tall downcomer.

Other methods, which do not rely on the downcomer pressure head, have been used previously for feeding solids to high-density risers. Yousfi and Gau (1974) superimposed pressure on a fluidized bed feeder installed in the solids return leg and adjusted the pressure in the feeder with an exhaust valve. Screw feeders have also been used (Drahos et al., 1988; Mori et al., 1991; Hirama et al., 1992). While these alternatives may overcome the disadvantages of gravity feeding, they are cumbersome from an industrial point of view and may not be able to supply the high solids rates required in commercial units. The dual-loop concept of Bi and Zhu (1993) was therefore adopted in this work.

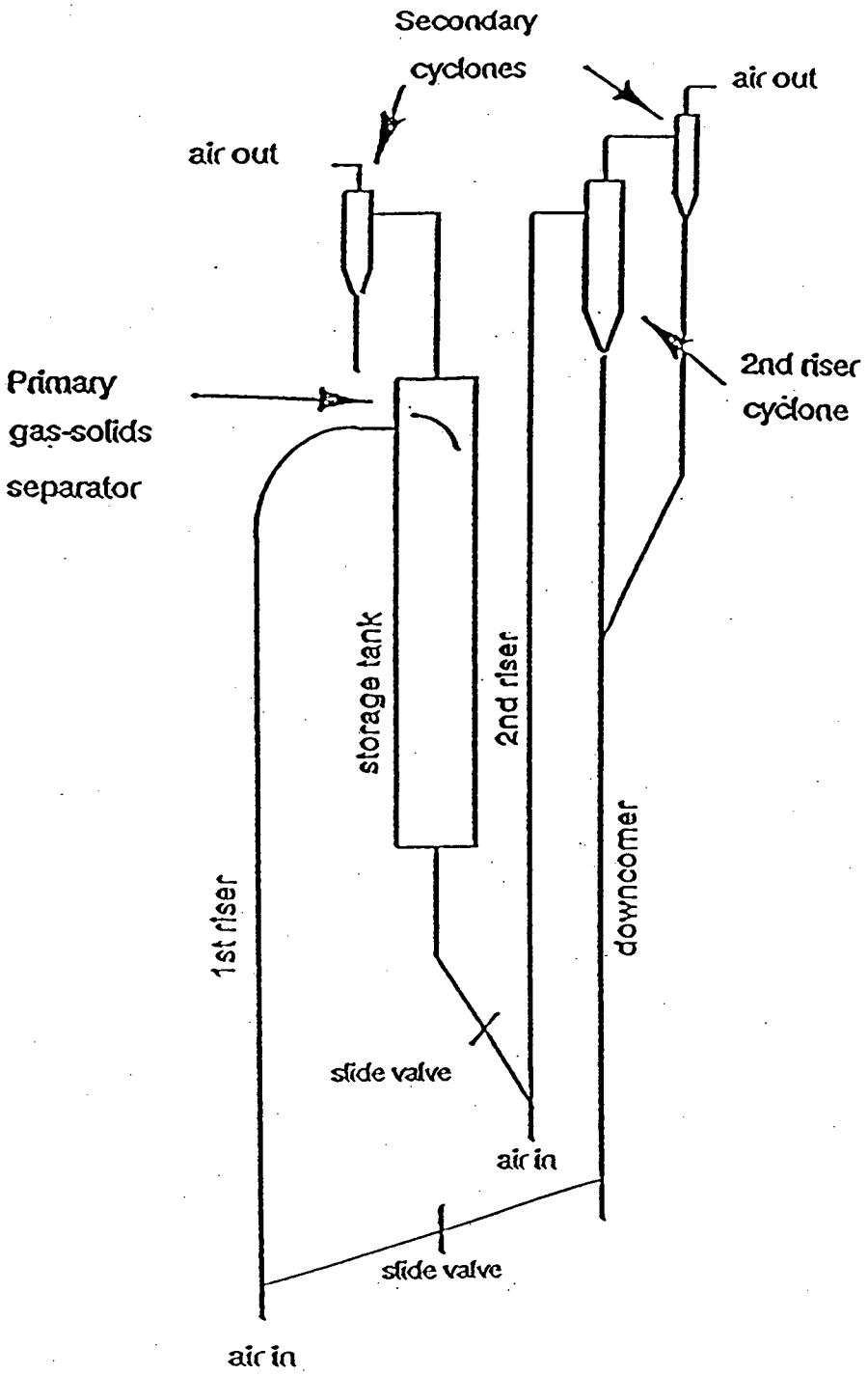

Fig. 2.1: Conceptual depiction of a high density CFB unit (Bi and Zhu, 1993).

2.2 Experimental Apparatus

Some of the main considerations in the design were:

(i) The unit should be capable of operating at superficial gas velocities and solids fluxes in the riser which are of interest to this study, i.e. which are representative of conditions in FCC reactors and other high density reactors as discussed in Chapter 1. The air velocity in the riser should be between 3 and 12 m/s, and the solids flux should exceed 200 kg/m^{2}s extending if possible to at least 500 kg/m^{2}s.

(ii) The riser should be tall enough that a substantial portion of it operates beyond the acceleration region. It should have as large a diameter as possible to make the results credible and useful for scale-up.

(iii) The unit should be modular and flexible in construction to allow insertion or exchange of column sections, permitting for example, variations in inlet and exit configurations, height and even column diameter.

(iv) The unit should be transparent to permit visual observation of the flow phenomena.

The design of the apparatus was constrained by several factors:

(i) A maximum overall height of about 10 m, dictated by the headroom in the laboratory.

(ii) The available air supply consisted of a shared building compressor rated at a capacity of 0.03 Nm^3/s at 200 kPag (64 SCFM at 30 psig), an electric Root's blower (Sutorbilt model 7 HV) providing 0.15 Nm^3/s at 34 kPag (324 SCFM at 5 psig) and a diesel-run Root's blower (Mitsubishi model 4D3) which gives 0.08 Nm^3/s at 40 kPag (172 SCFM at 5.6 psig).

The final set-up of the high density circulating fluidized bed unit is shown schematically in Fig. 2.2. The dual-loop CFB unit consists of two plexiglas risers, two PVC downcomers, a curved plate impingement separator, cyclones and an air filter baghouse. The first riser has a diameter of 76.2 mm and a height of 6.096 m. From this riser the suspension is directed onto a curved plate installed in a 0.91 m x 0.46 m x 0.61 m box by a 400 mm long vertical piece of pipe with a 33.1 mm nozzle at its end inclined at 30° from the vertical. This impingement-type separator has a low pressure drop and a reasonably high separation efficiency (Wei et. al., 1997) and was able to handle the high density suspension before further separation in a conventional cyclone. The design of the geometry and sizing of the impingement separator was assisted and guided by the Fluidization Laboratory at Tsinghua University.

From the impingement separator solids fall into the first downcomer, a 304.8 mm diameter column 4.24 m tall. The downcomer, which acts as a storage or buffer tank, was maintained at minimum fluidization conditions. A 101.6 mm diameter cyclone is used as a secondary separator returning the solids via a flapper valve to the storage tank. Solids from the storage tank are then fed via a 76.5 mm gate valve into the second riser which has a diameter of 101.6 mm and a height of 9.14 m. A smooth exit bend then guides the suspension into the primary cyclone, a conventional cyclone without a conical base. This design (also successfully used previously by Yerushalmi et al., 1978 and Brereton, 1987 among others) can handle large fluxes of solids, which might choke the conical exit of a conventional cyclone, and also allows aeration air, provided to the downcomer, to pass upward and outward through the cyclone without unduly affecting the solids discharge. Finally, the solids fall into the second downcomer, a 304.8 mm diameter, 8.33 m tall column, completing the loop via a second 76.2 mm gate valve installed in a pipe inclined at approximately 40° to the horizontal. This downcomer was also maintained at U_{mf}. A secondary cyclone (152.4 mm ID) returns the solids via a flapper valve to the downcomer.

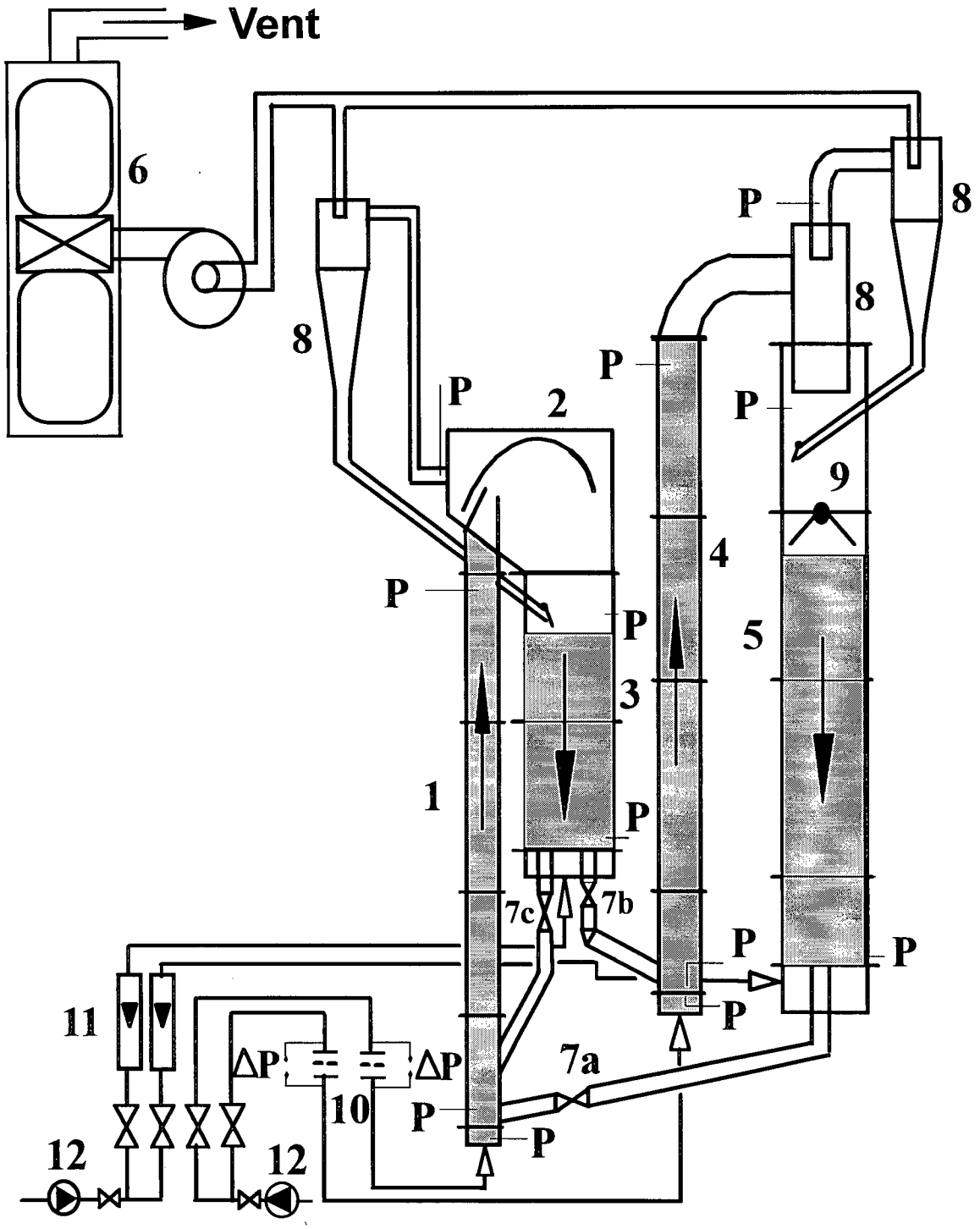

Fig. 2.2: Schematic diagram of high density CFB unit.

1. 1st Riser, 2. Impingement separator, 3. Storage tank, 4. 2nd Riser, 5. Downcomer, 6. Baghouse, 7. Gate valve, 8. Cyclones, 9. Butterfly valve, 10. Orificemeter, 11. Rotameter, 12. Root's Blower, P Absolute pressure transducer port, ΔP Manometer.

The air from both secondary cyclones passes through a filter baghouse before being discharged to the atmosphere. The cyclones were sized according to the classical high-efficiency geometry of Stairmand (Svarovsky, 1986). There is not much information on the influence of particle loading on cyclone efficiency, especially for high hold-ups typical of circulating fluidized beds. King (1992) indicated that commercial FCC cyclones improve in efficiency with solids loading probably due to particle agglomeration into clusters, enabling them to be more easily collected. However, Tuzla and Chen (1992) using sand particles of mean size 300 μm, found cyclone efficiency to deteriorate with increasing solid loadings at loadings 15 - 40 times higher than encountered in conventional applications of cyclones. Further work is therefore required in this area.

For start-up and control purposes, as well as to allow the system to operate as a conventional single loop CFB, a bypass recycle loop was installed from the storage tank to the bottom of the first riser. Valves were aerated to avoid clogging. Air entered the risers through perforated distributor plates with 19% free area. The air supplied to the downcomers and that used for aeration of valves came from the compressor, while riser 1 utilized air from the electric Root's blower and riser 2 from the diesel-driven Root's blower. To minimize transmitted vibrations, the columns were connected to the air-supply lines through rubber bellows and flexible hoses. On occasion the two Root's blowers were interchanged depending on the anticipated pressure drops in the two risers.

The equipment could be operated steadily with solids inventories up to 700 kg. The particles used in all experiments were FCC particles of mean surface/volume diameter (Geldart, 1986) of 70 μm and density 1600 kg/m^3. These catalyst particles have a minimum fluidization velocity, U_{mf}, of 0.0032 m/s (Grace, 1982) and a loosely packed bed voidage, ε_{mf}, of 0.45. Their size distribution is given in Table 2.1. A disadvantage of most transparent materials is that they promote considerable electrostatic charging,

Table 2.1: Size distribution of FCC particles determined by screening.

Mesh size [μm]	Mass fraction [%]
125 - 150	5.2
90 - 125	39.1
61 - 90	28.8
53 - 61	16.1
45 - 53	4.9
38 - 45	2.5
0 - 38	3.4

manifested by particles adhering to the wall. Various methods have been used to minimize this effect. For example, Glicksman (1994) coated the riser wall with a clear conductive wax, Myler et al. (1986) and Sobocinski et al. (1995) introduced polar vapor molecules (ammonia), Wei et al. (1995, 1997) stuck cellophane tapes on the inside wall of the riser, while Chang and Louge (1992) and Bergougnou et al. (1994) added small amounts of Larostat 519 powder (a quartenary salt of ammonium ethosulfate from Mazer Chemicals). In this study electrostatic charging was eliminated by a combination of proper earthing and addition of 0.5% by weight of Larostat 519 powder. During each experiment, the downcomers were first brought to minimum fluidization. Air was then introduced to the risers. Then the solids feed valves were opened and the air flows and solids circulation rate were set. The system was deemed to have reached steady state when the solids levels in the downcomers remained unchanged.

To allow measurement of pressures at different points along the CFB loop and to permit insertion of various intrusive probes, access ports and pressure taps are located at 0.3 m (12") and 0.6 m (24") intervals in risers 1 and 2, respectively, while aeration ports are located at 1 m intervals along the downcomers. The columns are supported structurally at the base by brackets attached to 50 mm x 50 mm square steel pillars. The brackets fix the columns rigidly in a horizontal plane while permitting vertical movement due to thermal expansion or vibrations. The principal dimensions of the risers and the downcomers and their elevations (at the air distributor level) from the building floor are given in Fig. 2.3. Drawings of the various components of the high-density CFB facility are given in Appendices A-1 to A-7.

2.3 Measurement and Data Acquisition Techniques

This section describes only the general all-purpose instrumentation, in particular measurements which characterize the overall operation and structure (macrostructure) of the high density circulating fluidized bed. Probes used to make local measurements are presented in later chapters.

2.3.1 Riser superficial gas velocity

Superficial gas velocities were measured in both risers using orifice meters, fabricated to ASME standards, with three interchangeable stainless steel orifice plates of bore diameter 41.1, 47.0 and 52.3 mm. Rotameters were used to measure low gas flowrates in the downcomer and the buffer tank, and to determine the valve aeration flowrate.

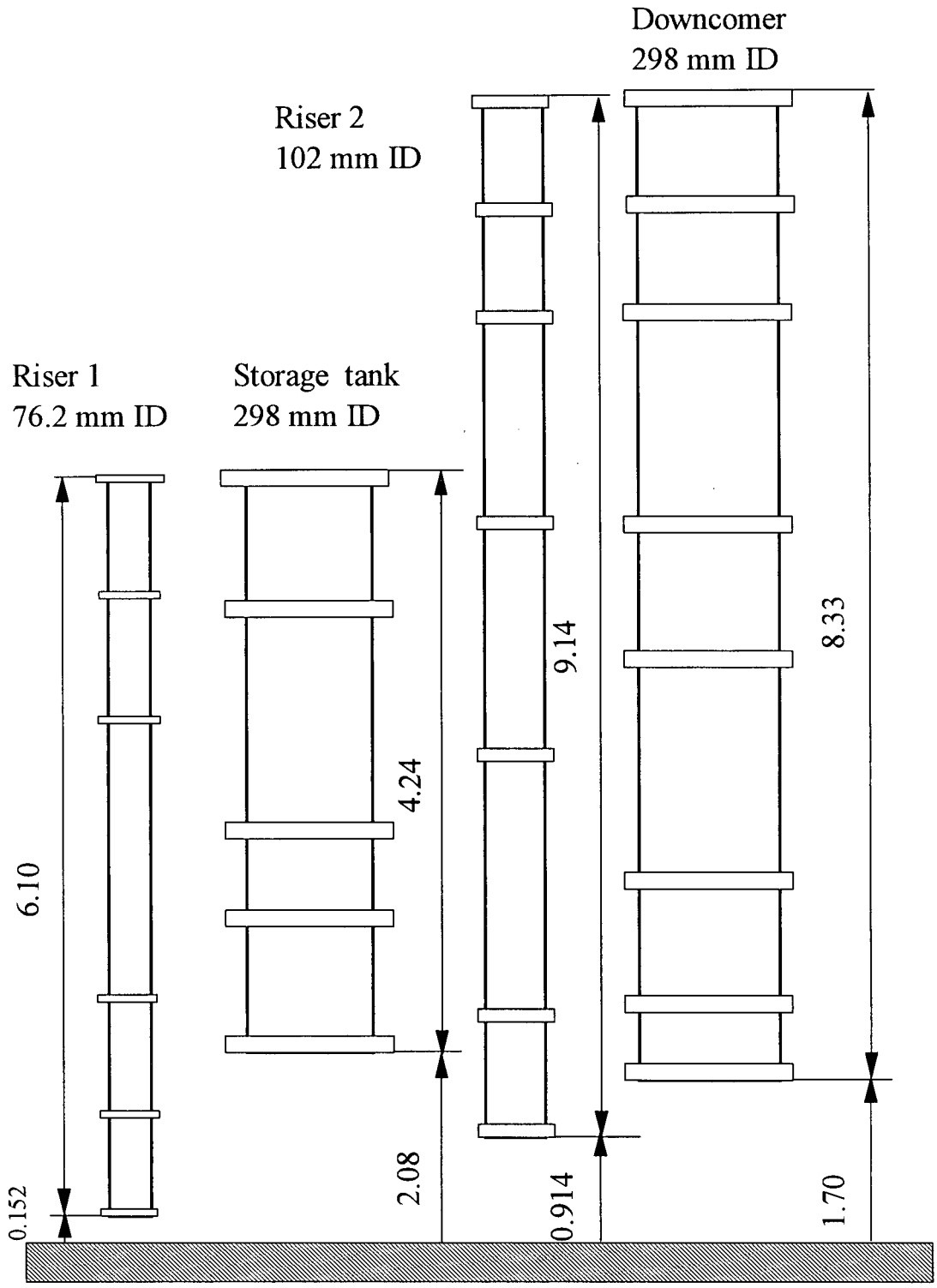

Fig. 2.3: Principal dimensions of the columns of the high density CFB unit. (All heights are in m.)

2.3.2 Solids inventory

Weighed quantities of FCC material were charged to the downcomers. The steady state solids levels in the downcomers could be measured with the system in operation since the Plexiglas columns are transparent. Solids were added or removed via feed and withdrawal points if the solids inventory was to be changed before a run.

2.3.3 Solids circulation rate

Burkell et al. (1988) assessed different solids flow measurement methods. Assuming negligible escape of solids from the cyclones, the flux is generally inferred from the solids flow traversing the downcomer. The method of timing the descent of an identifiable particle along the downcomer wall and the butterfly valve technique were found to work well for laboratory experiments. The former assumes the suspension to travel as a homogeneous plug of solids, with negligible radial velocity gradients, and the flux is then calculated from the packing solids volumetric fraction and the observed velocity. The method has, however, been noted (Patience and Chaouki, 1991) to underestimate the flowrate. Due to this drawback and the difficulty in visually tracing the small FCC particles, the butterfly valve method was adopted in this work. This method involves a sintered or drilled plate installed in the downcomer. When closed, the valve acts as a distributor onto which the solids returning to the downcomer form an incipiently fluidized bed. There are several variants of this technique. The solid rate can be calculated by measuring the time to accumulate a known volume of solids on top of the valve (Herb et al., 1992), from the time for a given pressure difference in the fluidized bed above the butterfly valve to be reached (Brereton, 1987; Li et al., 1991) or from the rate of descent

of the solids bed level in the downcomer (Weinstein et al., 1986) once the valve is closed. The first of these procedures was chosen in the current work due to its simplicity.

The butterfly valve, installed in the upper part of the downcomer, consisted of two semicircular drilled-plates covered with wire mesh which rotate downward on their axes. During measurements the two halves are rapidly rotated upward to the horizontal position, thus trapping the downflowing solids. Apart from the small pressure drop due to the valve itself, the total solids head in the downcomer remained practically constant throughout this procedure. Also due to the buffering action of the large downcomer the riser feedrate remained almost unaltered.

2.3.4 Pressure profiles

Pressure measurements have been widely used in fluidized bed studies. In circulating fluidized beds, differential pressure is often used as a mean of determining average cross-sectional solids hold-ups in risers, whereas its fluctuations are used in regime transition studies (e.g. Perales, et al., 1991; Brereton and Grace, 1992; Chehbouni et al., 1994; Bi and Grace, 1995; Bai et al., 1996) and for diagnostic purposes. Absolute pressure data are useful in CFB pressure balance studies. In this work differential pressure was measured by differential pressure transducers (Omega PX162). The risers were equipped with 7.9 mm diameter ports, covered with fine screen, purged regularly with air to avoid blockage by the FCC powder, and connected to the transducers by 300 mm lengths of 6 mm diameter plastic tubing. The length of the connecting plastic tubing was sufficiently short to minimize signal attenuation, essential in transient measurements (Clark and Atkinson, 1988; van der Stappen, 1993). To establish pressure profiles around the CFB loop, absolute pressure transducers (Omega PX142) were located at the entrances

and exits of each column. Differential and absolute pressure signals were fed to a PC computer via a Metrabyte DAS8-EXP16 A/D converter, and the output voltage signals were then converted into convenient pressure units using transducer calibration curves. The data acquisition software used was LABTECH Notebook.

CHAPTER 3

LONGITUDINAL DISTRIBUTION OF SOLIDS

3.1 Introduction

This chapter examines the global voidage and slip characteristics in the riser deduced from profiles of cross-sectional average solids concentration. As noted in Chapter 1, knowledge of the solids distribution and flow behaviour is vital for successful design and operation of CFB reactors. Longitudinal voidage correlations have often been used in one-region one-dimensional reactor models (Pogliolico et al., 1992; Li and Chang, 1994) as well as in CFB loop pressure and inventory balance calculations (Rhodes and Geldart, 1987) to establish necessary blower capacities and system solids inventories for maintaining steady operation. Gas and particle residence time distributions in the riser and heat transfer rates have also been found to be dependent on solids hold-up distributions.

The vertical variation of cross-sectional average solids hold-up in circulating fluidized bed risers is usually inferred from the gradient of absolute pressure profiles or from direct measurements of differential pressures over equal intervals along the riser height. The pressure drop per unit length is then equated to the weight of the solids and fluid per unit area, assuming that the combined effects of gas and solids-wall friction, and acceleration are negligible. Therefore, the apparent voidage, ε, is usually estimated from

$$\frac{\Delta P}{\Delta z} \approx [\rho_p (1-\varepsilon) + \rho\varepsilon]g \qquad (3.1)$$

In normal CFB operations $\rho_p >> \rho$ so that the gas weight term is usually neglected too. This method has been accepted by many workers, especially since it is non-intrusive,

inexpensive and simple. It is also adopted in this study, but only after evaluation of the acceleration contribution. Other methods which have also been used, but to a limited extent, include twin quick-closing slide valves (Arena et al., 1988; Pagliolico, et al. 1992; van der Ham, 1993, Venderbosch et al., 1996) and γ-ray and x-ray attenuation methods (Weinstein et al., 1984; Galtier et al., 1989; Azzi et al., 1991; Martin et al., 1992).

Upon entering the riser, particles usually initially travel horizontally or downwards due to horizontal or downwards inclined solids feeding. Significant vertical solids acceleration is therefore needed near the riser bottom. To determine the extent of particle-wall friction, comparisons have been made of voidages measured by γ-ray absorption to those from differential pressure. van Swaaij et al. (1970) found the solids frictional pressure drop to be 20 - 40 % of the total pressure drop in dilute flows, falling to about 25% under high density conditions. Wirth et al. (1991) found the deviation between the two methods to be ± 20%. Hartge et al. (1986) found satisfactory agreement between the two methods at low superficial gas velocities, but wall friction was significant at high velocities. Using x-ray techniques, Weinstein et al. (1983) found the solids frictional pressure drop to be less than 10% of the total pressure drop. Arena et al. (1986) observed significant differences at heights well away from the entrance region between solids hold-ups measured by a quick-closing valve technique and those inferred from pressure gradients. They attributed the discrepancies to frictional losses at the wall, but Louge and Chang (1990) explained the discrepancy as being due to the rapid solids acceleration during the transition from dense phase to dilute phase flow. These observations suggest that the contribution of solids friction to the total pressure drop should be low for the high-density and moderate-velocity conditions of this work.

Weinstein and Li (1989) proposed a method to evaluate voidages from differential pressure in the bottom region of a CFB riser, provided the length of the acceleration

section is known. Assuming the flow away from the inlet to be one-dimensional and neglecting solid and gas-to-wall friction, Louge and Chang (1990) calculated actual voidages from measured pressure gradients by solving continuity and momentum balance equations. This method has been adopted here, but with a modification to include friction terms (Appendix B-1). It is found from this method that the deviation between the apparent and the calculated solids hold-ups is always less than 20%. The influence of frictional and other losses to pressure drop data is also examined in Fig. 3.1 which compares solids hold-up measurements from Eq. (3.1) to those obtained by integrating local solids hold-ups (see Chapter 4). There is a deviation of about – 6% to +10% between the two methods. This deviation is small enough that it does not affect the findings of this work very significantly. Therefore, data are presented throughout this chapter as apparent solids concentrations or voidages.

Vertical solids hold-up distributions based on pressure gradients have been reported frequently for circulating fluidized bed risers. The studies of Yerushalmi et al. (1976) and Li and Kwauk (1980) show that a CFB riser contains a dilute region towards the top and a relatively dense region near the bottom with an inflection point inbetween giving a sigmoidal (or S-shape) profile. This type of profile has also been observed by many other workers (e.g. Arena et al., 1986; Rhodes and Geldart, 1986; Herb et al., 1989; Hartge et al. 1986, 1988; Schnitzlein and Weinstein, 1988; Bai et al., 1992) with a number of factors affecting the distribution. For example, increasing the gas velocity at a constant solids flowrate reduces the height of the dense phase region (e.g. Li and Kwauk, 1980), whereas an increase in solids flux at a fixed gas velocity increases the solids hold-up and causes the dense phase to expand (e.g. Bai et al., 1992). Operating at much higher solids circulation rates in a 6 m tall riser, Arena et. al. (1988) found that while the dilute phase voidage remained almost constant at values above 0.95, that of the dense phase changed between 0.75 and 0.85 and its height extended further upward with increasing solids

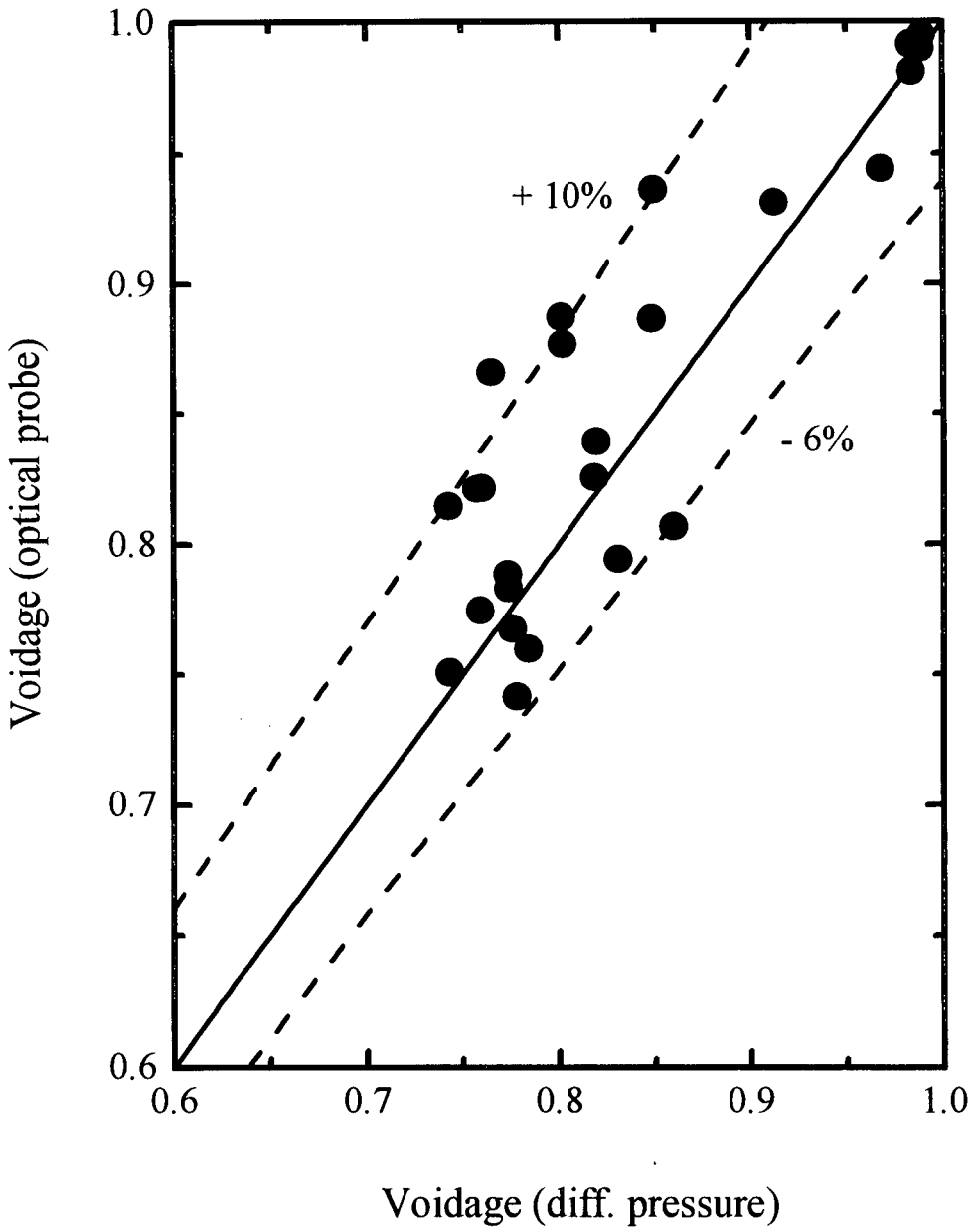

Fig. 3. 1: Comparison of apparent cross-sectional average voidages determined in this work from differential pressure measurements with integrated average voidages measured using optical fiber probe. For details of the latter, see Chapter 4.

circulation rate. At G_S = 190 kg/m^{2}s and U = 3 m/s the dense phase filled the whole riser. The phenomenon is not limited to small units. Contractor et. al. (1994) achieved solids holdups approaching 0.2 over the entire riser of a pilot scale CFB unit (0.15 ID, height 27.4 m) utilizing FCC particles for solids fluxes ranging between 250 and 1100 kg/m^{2}s and gas velocities of 4 to 10 m/s. Typical results of Contractor et al. are shown in Fig. 3.2. Depending on the combination of superficial velocity and solids circulation rate, the inflection point can move upward or downward. It may eventually pass beyond the top of the riser, leading to a wholly dense-phase riser operation, or reach the bottom making the riser operate in a dilute-phase transport mode (Hartge et al., 1986; Mori et al., 1991; Yang, 1993). Note that the inflection point is used here to represent the interface between the bottom dense zone and the upper dilute region since the dense zone in CFB risers has no clear surface as such. There are indications that the solids hold-up in the dense region is not very sensitive to the operating gas and solids flowrates. For example, Adanez et al. (1994) using group B particles found that the voidage in the dense phase varied only from 0.80 to 0.83 and was independent of the operating conditions. Based on data from many studies, Ouyang and Potter (1993) found that the average dense phase solids holdup was 0.18, not appreciably affected by the gas velocity or particle characteristics. Kunii and Levenspiel (1991) proposed that the solids hold-up in the dense region was between 0.16 and 0.22.

The longitudinal suspension density distribution in the riser is also influenced by geometric parameters. Strongly restricted riser exits cause substantial internal separation of entrained solids from the gas due to particle rebounding, leading to increased solids hold-up in the top region (Jin et al. 1988; Brereton and Grace, 1994; Harris et al., 1994, Zhou et al., 1994). The axial location and configuration of solids feeding (Brereton and Grace, 1994), secondary air injection (Wang and Gibbs, 1991), the presence of internals

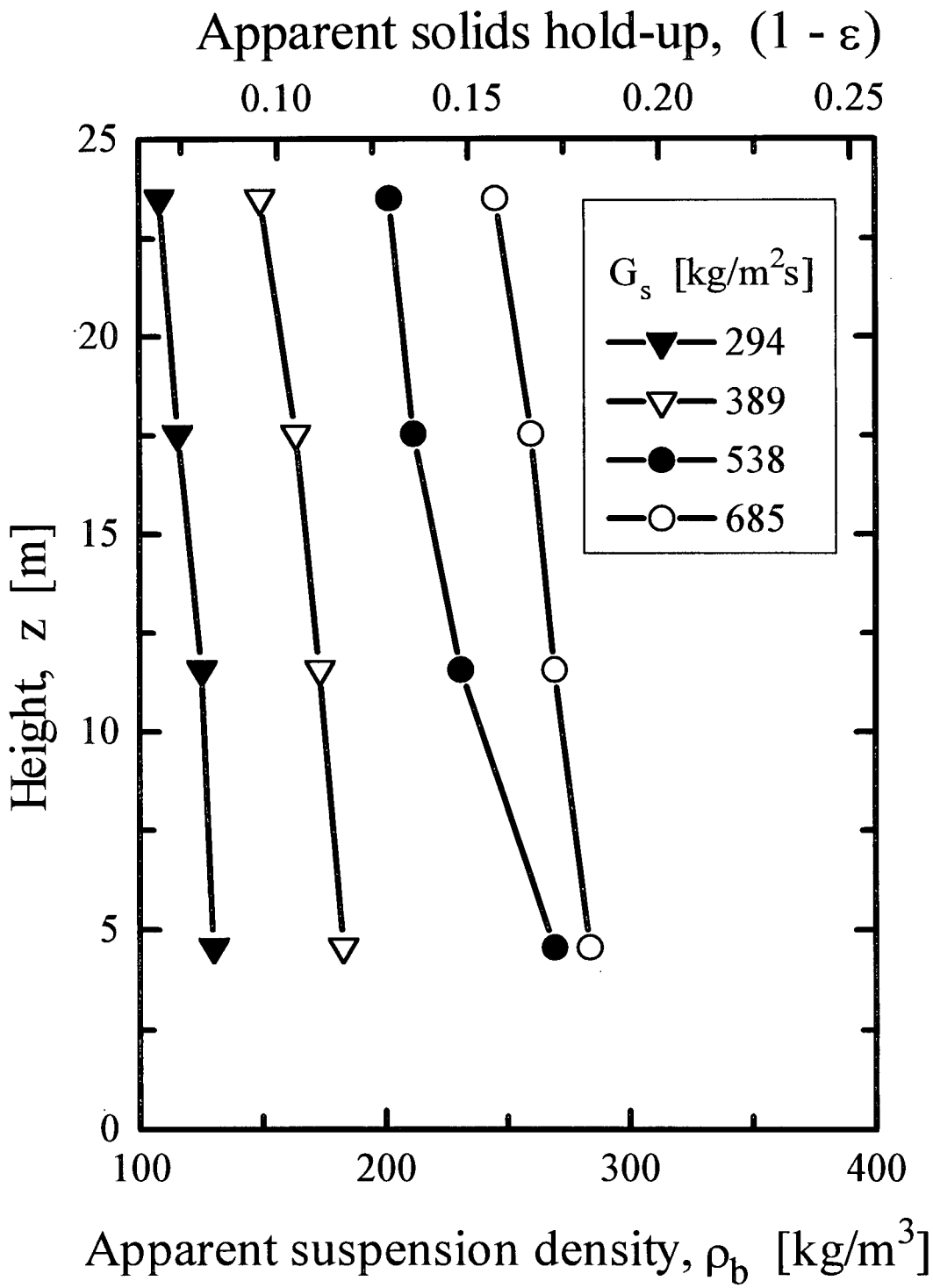

Fig. 3.2: Apparent suspension density profiles in a 0.15 m dia. riser for four solids circulation rates at U ≈ 5.7 m/s measured at exit (replotted from Contractor et al., 1993).

(Jiang et al., 1991) and particle size and density (Adanez et al., 1994) also affect voidage profiles.

3.2 Measurement procedure

Differential pressures were measured by ten pressure transducers installed over 300 mm intervals along the height of the 76 mm dia. riser, while two absolute pressure transducers determined the pressure at the inlet and exit of the riser. Except where otherwise stated, all results presented in this work were obtained from this riser. The data acquisition system was programmed to sample the differential and absolute pressure signals at frequencies of 100 Hz and 2 Hz, respectively, for periods of 100s. The lower sampling rate was sufficient for the absolute pressure signals where only the average value was needed, while the higher rate was necessary for the differential pressure signals because the fluctuations were also of interest. The average differential and absolute pressures and the standard deviation of the differential pressure were calculated from instantaneous differential and absolute pressures, respectively, as

$$\frac{\overline{\Delta P}}{\Delta z} = \frac{1}{N}\sum_{i=1}^{N}\left(\frac{\Delta P}{\Delta z}\right)_i \tag{3.2}$$

$$\overline{P} = \frac{1}{N}\sum_{i=1}^{N} P_i \tag{3.3}$$

$$\sigma_{\Delta P} = \sqrt{\frac{1}{N}\sum_{i=1}^{N}\left[\left(\frac{\Delta P}{\Delta z}\right)_i - \frac{\overline{\Delta P}}{\Delta z}\right]^2} \tag{3.4}$$

where N is the number of data points collected over each sampling period. The reliability of the sampling was verified by comparing data obtained at a series of acquisition frequencies and durations.

3.3. Results and Discussion

3.3.1 Solids hold-up profiles

Figures 3.3, 3.4 and 3.5 show the vertical profiles of solids hold-up in the riser at superficial air velocities of 4, 6 and 8 m/s, respectively, for a wide range of solids circulation rates. The extremely high apparent hold-ups recorded near the riser bottom are significantly affected by particle acceleration as well as by the solids entry configuration. Beyond this region the solids hold-up, depending on the air velocity and solids circulation rate, decreases exponentially, eventually reaching a constant value higher up the riser, or follows an S-shaped profile, with a dense phase at the bottom and a dilute region at the top or a relatively dense bed covering the entire column height. In all cases the solids hold-up increases with the solids circulation rate, while for a constant solids circulation rate the hold-up decreases with increasing air superficial velocity. These trends are consistent with earlier results in the literature (e.g. Li and Kwauk, 1980; Arena et al., 1986; Brereton, 1987; Bai et al., 1992). The smooth exit bend used in our equipment has little influence on the riser flow structure because internal solids separation is minimized. Due to limitations of the available blower, steady state operation of the unit was not possible for solids circulation rates beyond about 425 kg/m^{2}s.

Figure 3.6 is a plot of apparent solids hold-up at various heights along the riser as a function of solids flux for U = 6 m/s. A dense phase starts to form at the bottom when G_s exceeds about 75 kg/m^{2}s, as shown by a sharp jump in the solids holdup recorded by the bottom transducer, working its way upward until it fills the whole riser when the circulation flux exceeds about 275 kg/m^{2}s. At a circulation flux of about 325 kg/m^{2}s the whole riser is filled by dense phase having a solids hold-up of about 0.15 - 0.2. Similarly,

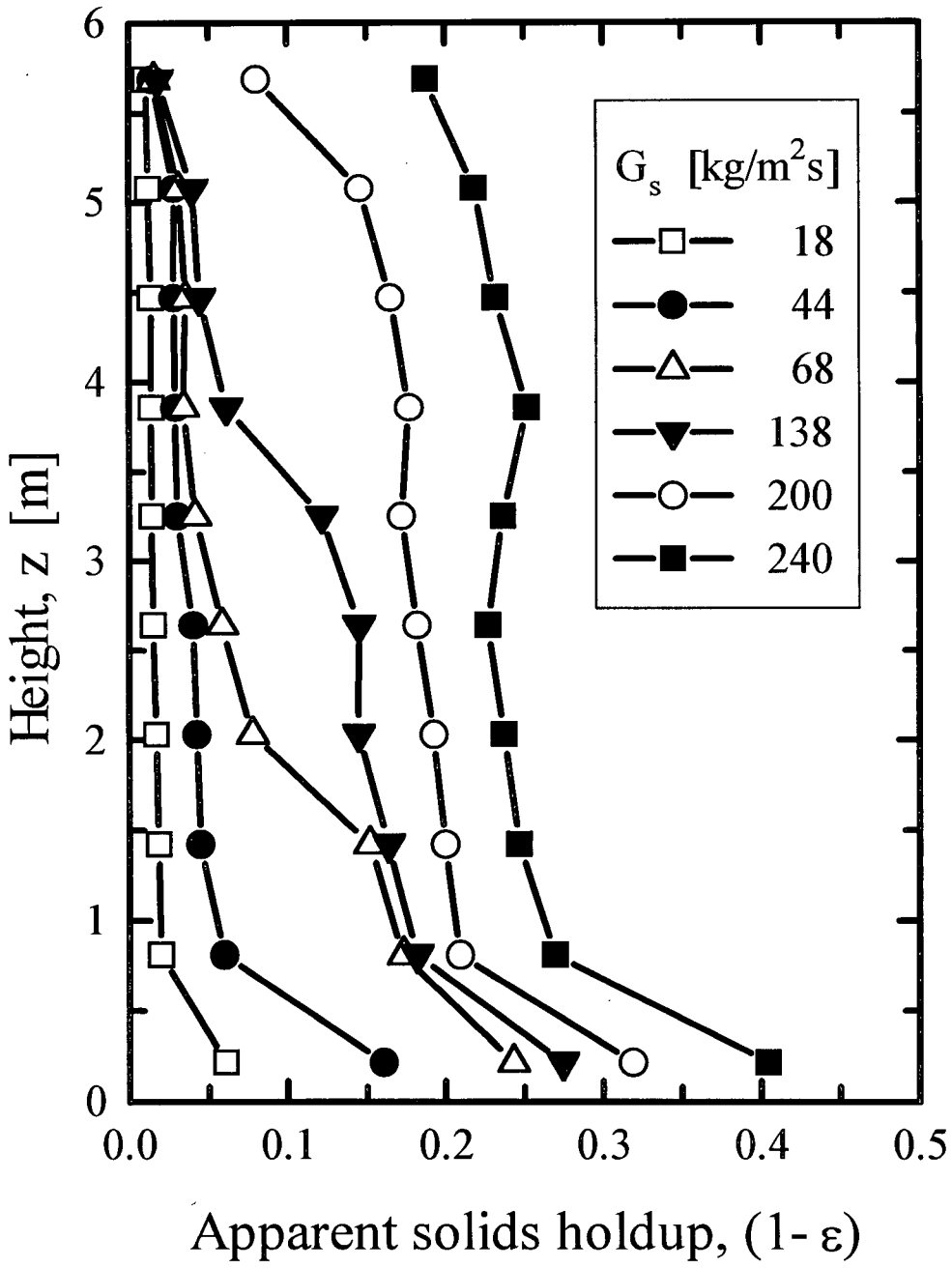

Fig. 3.3: Longitudinal profiles of apparent solids hold-up at U = 4 m/s for various solids circulation rates.

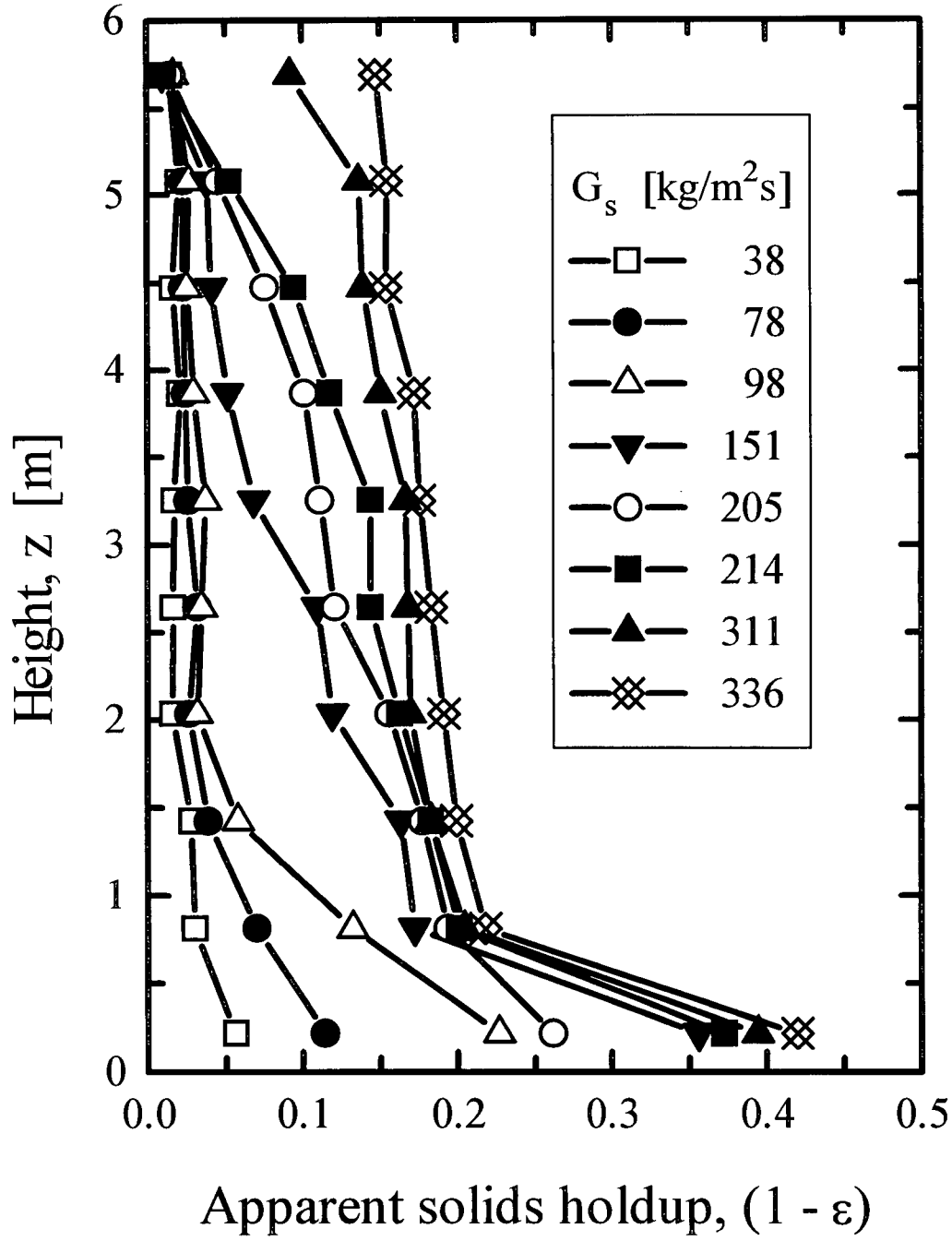

Fig. 3.4: Longitudinal profiles of solids hold-up at U = 6 m/s for various solids circulation rates.

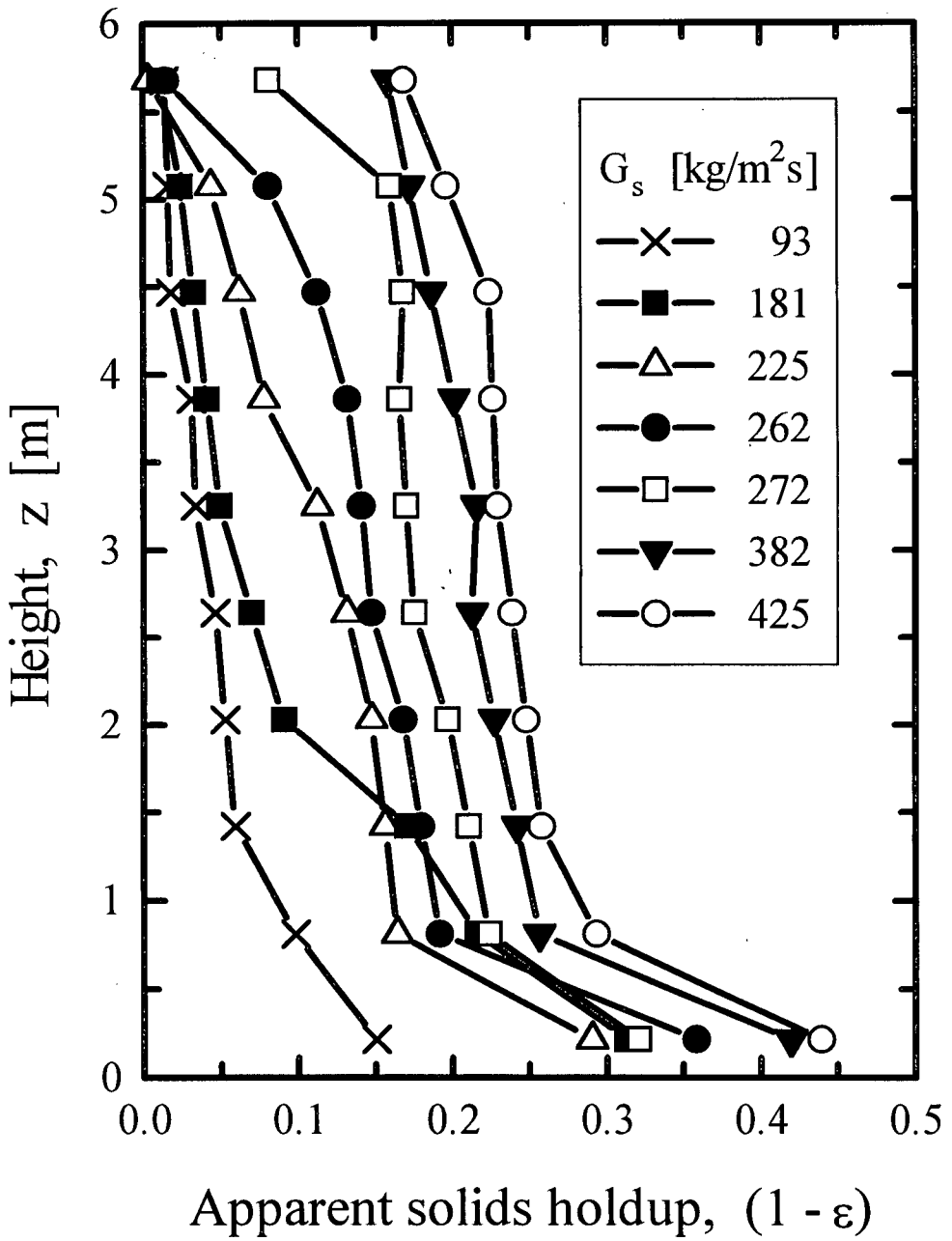

Fig. 3.5: Longitudinal profiles of apparent solids hold-up at U = 8 m/s for various solids circulation rates.

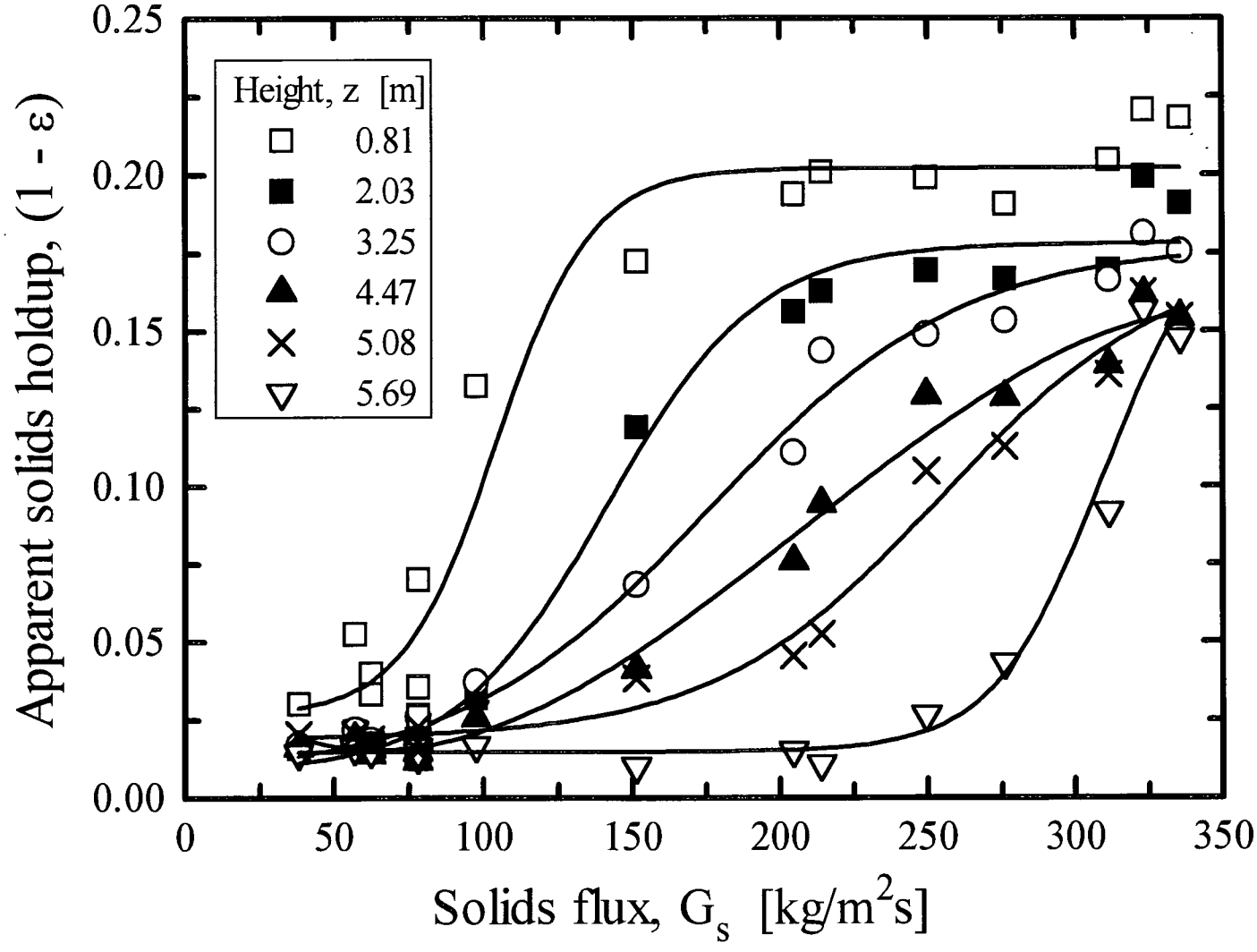

Fig. 3.6: Solids hold-up as a function of solids flux at various heights for U = 6 m/s.

as shown in Fig. 3.7 which plots apparent solids hold-up near the exit for air velocities of 4, 6 and 8 m/s, solids fluxes of about 240 to 360 kg/m^{2}s lead to high density conditions in the whole riser, with apparent solids hold-up exceeding 0.15. The influence of superficial gas velocity can be further observed in Fig. 3.8 where the solids hold-up at z = 2.03 m is plotted against the superficial air velocity with the solids circulation flux as the parameter. At the lowest G_S of 50 kg/m^{2}s, the flow pattern approaches pneumatic transport with voidages approaching unity, and the decrease in solids hold-up with increasing gas velocity is relatively small. The dense phase starts to build up in the riser at low gas velocities, with a higher solids circulation rate needed to achieve high density conditions at higher gas velocities. The variation of the solids hold-up with gas velocity is again small once high density conditions have been established.

Figure 3.9 plots the variation of apparent solids hold-up with solids circulation rate for a fixed superficial air velocity. At very low circulation rate the solids hold-up is low and all the particles are observed to be carried upward in pneumatic transport. As the solids circulation flux is increased, their concentration also rises. Further increase in G_S leads to a point beyond which the solids can no longer be suspended individually, and the suspension collapses starting the formation of a relatively dense suspension of voidage $\approx$ 0.8. This corresponds to type A or accumulative choking (Bi et al., 1993). In the dilute section above the dense zone, particles start to move down at the wall; as the feed rate is raised further, more solids refluxing occurs. This refluxing is only observed above the dense region. The sharp rise in the solids hold-up as more solids are fed to the bottom of the riser corresponds to the condition where the dense region has spread to the whole section between the two measurement points of the differential pressure transducer. Thereafter, the solids concentration remains 0.2 ± 0.05 over a considerably wide range of solids circulation rates as the dense suspension continues to encroach further and further up the riser. The dense region is observed to exhibit an almost homogeneous flow

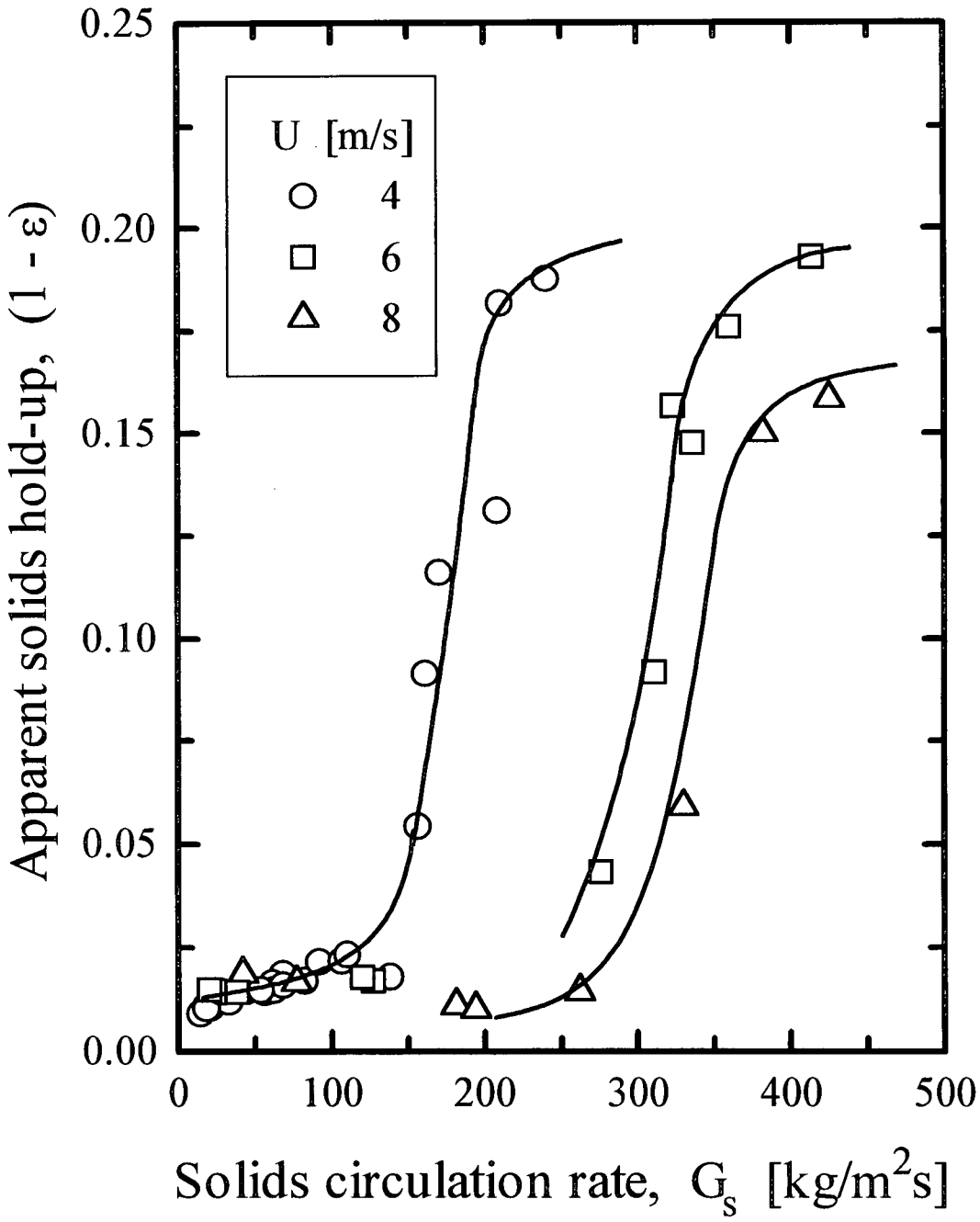

Fig. 3.7: Apparent solids hold-up as a function of solids circulation rate at z = 5.68 m for three superficial air velocities.

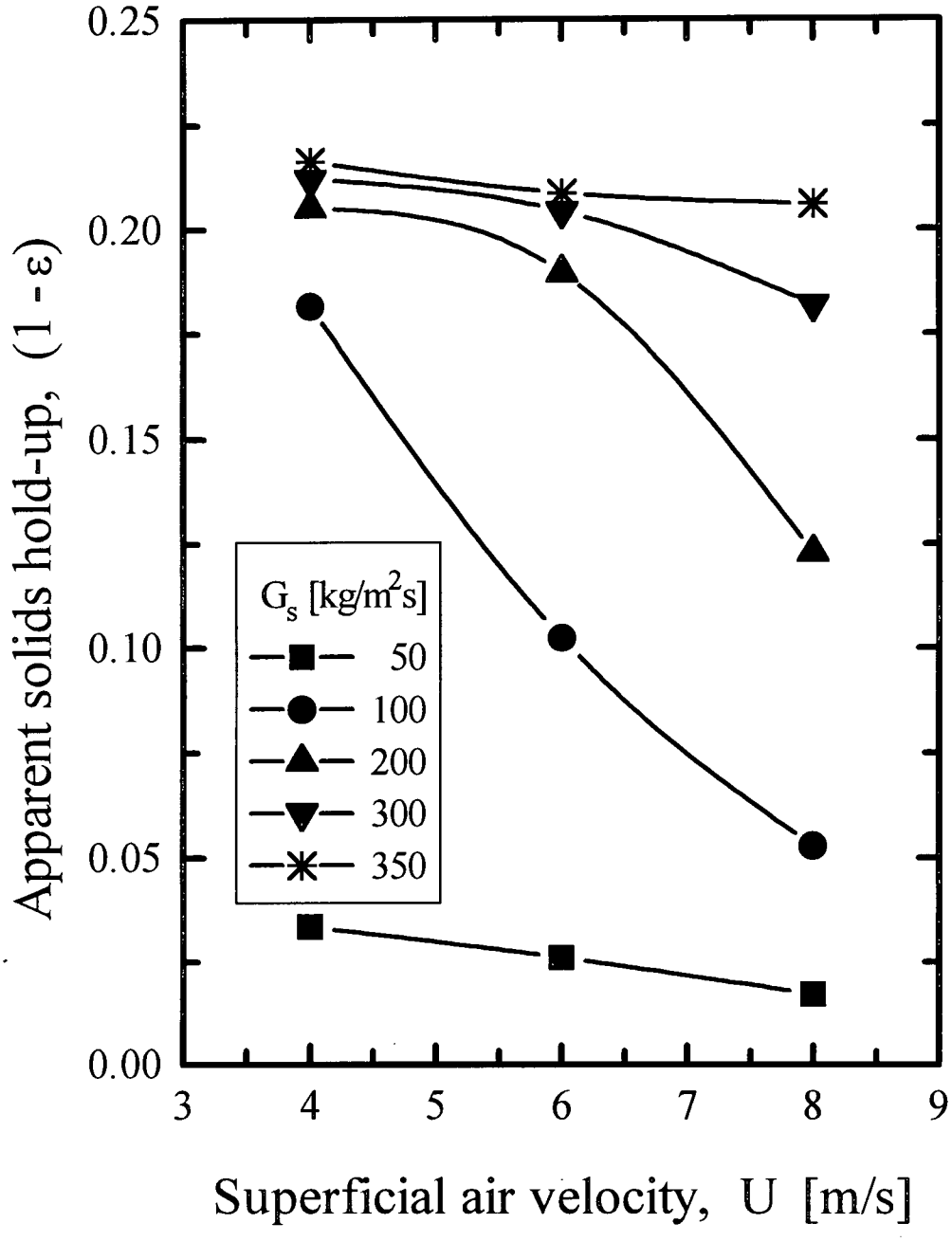

Fig. 3.8: Influence of superficial air velocity on the apparent solids hold-up at z = 2.03 m for various solids circulation rates.

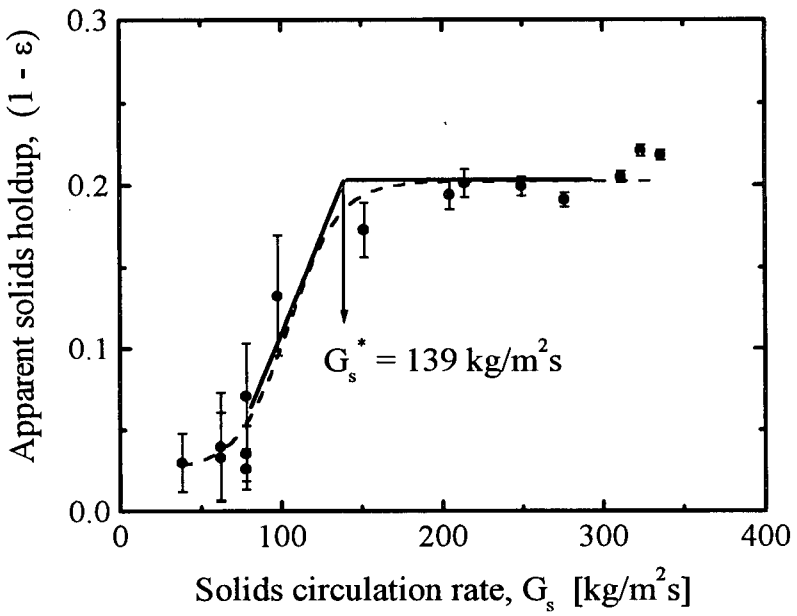

Fig. 3.9: Apparent solids hold-up as a function of solids circulation rate at z = 0.82 m for U = 6 m/s. The high density transition point is taken at the junction of the two linear portions.

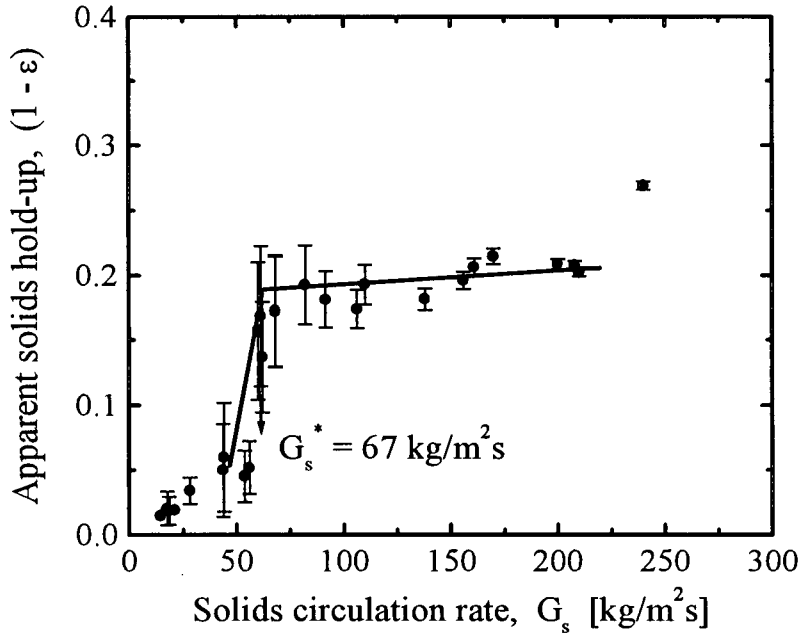

Fig. 3.10: Apparent solids hold-up as a function of solids circulation rate at z = 0.82 m for U = 4 m/s. High density transition point defined as in Fig. 3.9.

structure. Visual observation at the wall of the dense region indicates that solids refluxing, usually observed near the wall of dilute CFB risers, no longer exists; instead the whole suspension appears to be relatively homogeneous with moderate up and down fluctuations in the flow. It was impossible to visually determine the net direction of solids flow near the wall. Measurements of the local (vertical) solids flux (Chapter 6) indicate that the net solids flow is, on average, upwards both in the central region and adjacent to the wall.

We consider in this work the point at which the sharp rise in the solids hold-up ends, i.e. where the hold-up levels off, to be the starting point of high-density conditions. This transition point is defined as the intersection of the two linear portions of the solids hold-up vs. G_S plot when extrapolated towards each other, as illustrated in Fig. 3.9. Since the dense region expands with increasing solids circulation rate, there will be such intersection points for each value of z and, therefore, different vertical locations in the riser (and risers of different heights) attain fully dense conditions at different solids circulation rates for a given superficial gas velocity. Since the cross-sectional average solids concentration, an important parameter in regime transition studies, is not uniform over the riser height, and is a function of the solids circulation rate, it is appropriate to make measurements near the bottom. The transition point in this work was determined at a height of 0.82 m which allows, as shown in Chapter 7, meaningful comparisons with the characteristics of other flow regimes. For sufficiently tall CFB risers, the riser height has little influence on phenomena near the bottom.

It is only above the solids circulation rate corresponding to the junction of the two linear portions of the plot that there is a relatively dense suspension with no net solids downflow observed at the wall. Bai and Kato (1996) refer to the solids flux at this point as the saturation carrying capacity (SCC) of the gas stream. This term has, however, also been used to describe the limiting solids entrainment above the transport disengagement

height (TDH) in non-circulating fluidized beds (Zenz and Othmer, 1960), as well as in (accumulative) choking in CFB risers (Geldart, 1986), cases which do not have the same meaning. Therefore this point is referred to in the rest of this work as the "high-density transition point".

High-density transition points were also determined in Figs. 3.10 and 3.11 for superficial velocities of 4 and 8 m/s, respectively. Figure 3.12 plots the solids circulation rate at the transition point as a function of the superficial air velocity. A correlation for SCC by Bai and Kato (1996) gives

$$\frac{G_s^* d_p}{\mu} = 0.125 Fr^{1.85} Ar^{0.63} \left(\frac{\rho_p - \rho}{\rho} \right)^{-0.44} \tag{3.5}$$

Bi et al. (1993) recommended the accumulative choking correlation of Bi and Fan (1991) for estimating G_s^*, i.e.

$$\frac{U}{\sqrt{g d_p}} = 21.6 \left(\frac{G_s^*}{\rho U} \right)^{0.542} Ar^{0.105} \tag{3.6}$$

Equations 3.5 and 3.6 are plotted in Fig. 3.12. The data fall within the ±10% accuracy range reported for Eq. 3.5, while Eq. 3.6 appears to predict well only at low gas velocities. Note from the above discussion that Eqs. 3.5 and 3.6 can only be used to predict the circulation rate at commencement of high density conditions at the riser bottom. In Figs. 3.9 and 3.10 it can be noted that, after a range of solids fluxes where the suspension density remains relatively constant, the solids hold-up appears to start increasing again. This most likely indicates the start of a transition towards a much denser suspension, probably the moving bed type of flow.

Figure 3.13 plots the total riser pressure drop against the solids-to-air mass flow

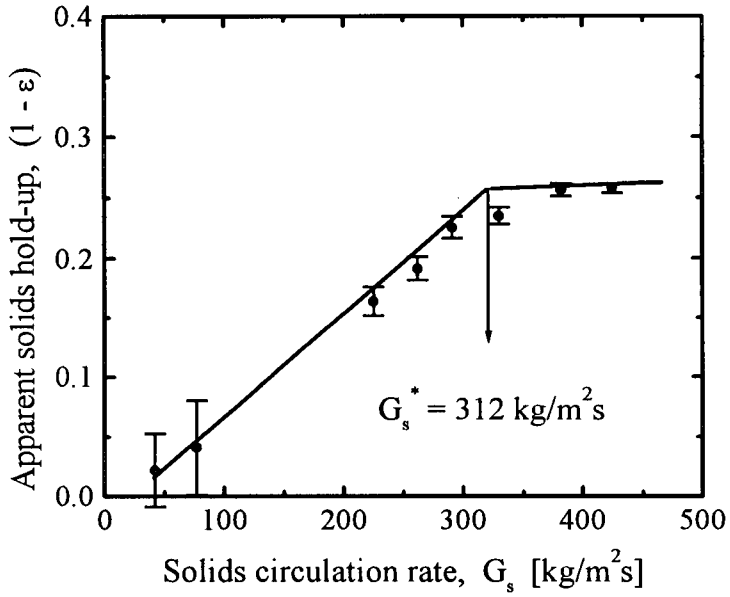

Fig. 3.11: Apparent solids hold-up as a function of solids circulation rate at z = 0.82 for U = 8 m/s. High density transition point defined as in Fig. 3.9.

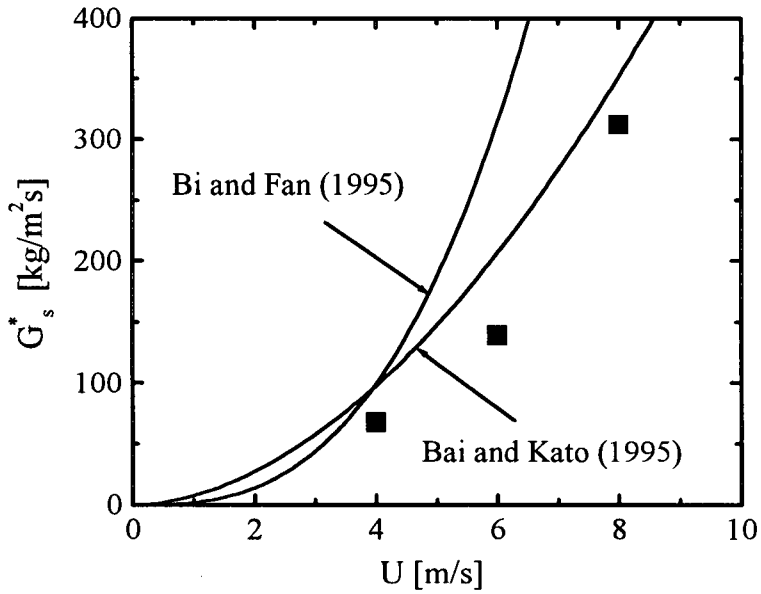

Fig. 3.12: Minimum solids circulation rates needed to initiate high density conditions at various superficial air velocities. Experimental points correspond to high-density transition points determined in this work.

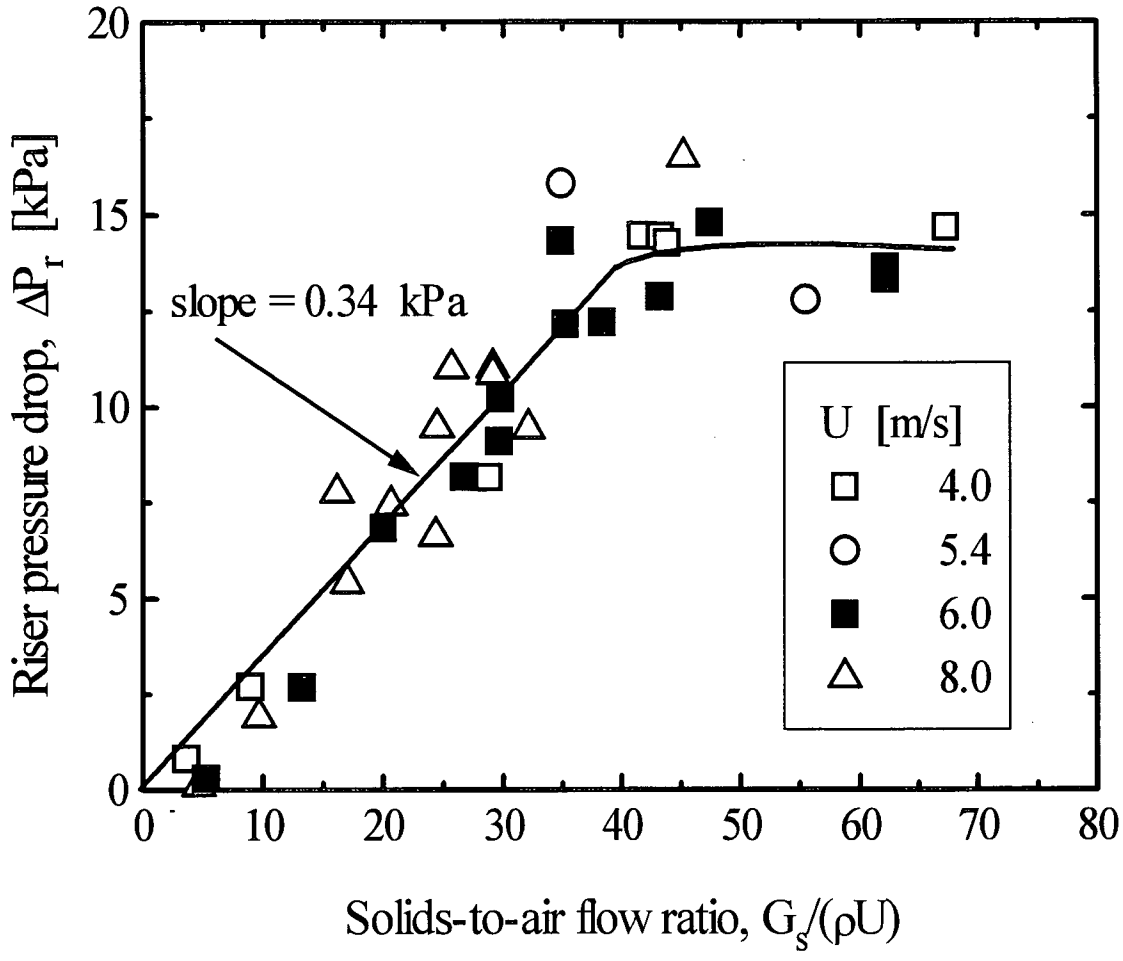

Fig. 3.13: Total pressure drop across riser, i.e. between z = 0.025 m and z = 5.84 m, as a function of solids-to-air mass flow ratio.

ratio ($G_S/\rho U$) for different superficial air velocities. The total pressure drop is the difference between the absolute pressure just above the distributor (z = 0.025 m) and that at the riser exit (z = 5.84 m). An approximately linear relationship is obtained for a wide range of flow ratios up to about 40, above which the total pressure drop levels off indicating that the whole riser is under high density conditions. Note that the G_S values calculated from $G_S/\rho U = 40$ corresponding to U = 4, 6 and 8 m/s are 192, 288 and 384 kg/m^2s, respectively. These are the solids circulation rates at which the riser is wholly dense and they are nearly the same as those estimated from the vertical apparent solids hold-up profiles in Figs. 3.3 to 3.5. The initial linear portion is consistent with results presented by Rhodes and Laussmann (1992).

The influence of solids inventory on the solids holdup profile in the riser was determined by setting different solids levels in the downcomer feeding riser 1, while adjusting the solids feed valve to maintain the same solids circulation rate at a fixed air superficial velocity. The results are presented in Fig. 3.14 where it is observed that the profiles remain almost unchanged with increasing solids inventories in the downcomer. Similar observations have been made by Chang and Louge (1992), Hirama et al. (1992), Rhodes and Laussmann (1992) and Issangya et al. (1996), although some studies (Weinstein et al., 1983; Li et al., 1988) reported an appreciable influence. The effect of increasing the solids inventory in the downcomer is to increase the solids flowrate. However, for CFB units utilizing mechanical valves, the valve opening has to be reduced to maintain a constant solids feed rate for a given air velocity. This leads to a higher pressure drop across the valve, counteracting the added downcomer pressure head so that there is almost no net influence on the riser. It is, however, possible for systems where the solids flow control valves are not sized properly and are operating almost fully open, that the change in solids inventory affects the operation of the riser since it would be difficult in

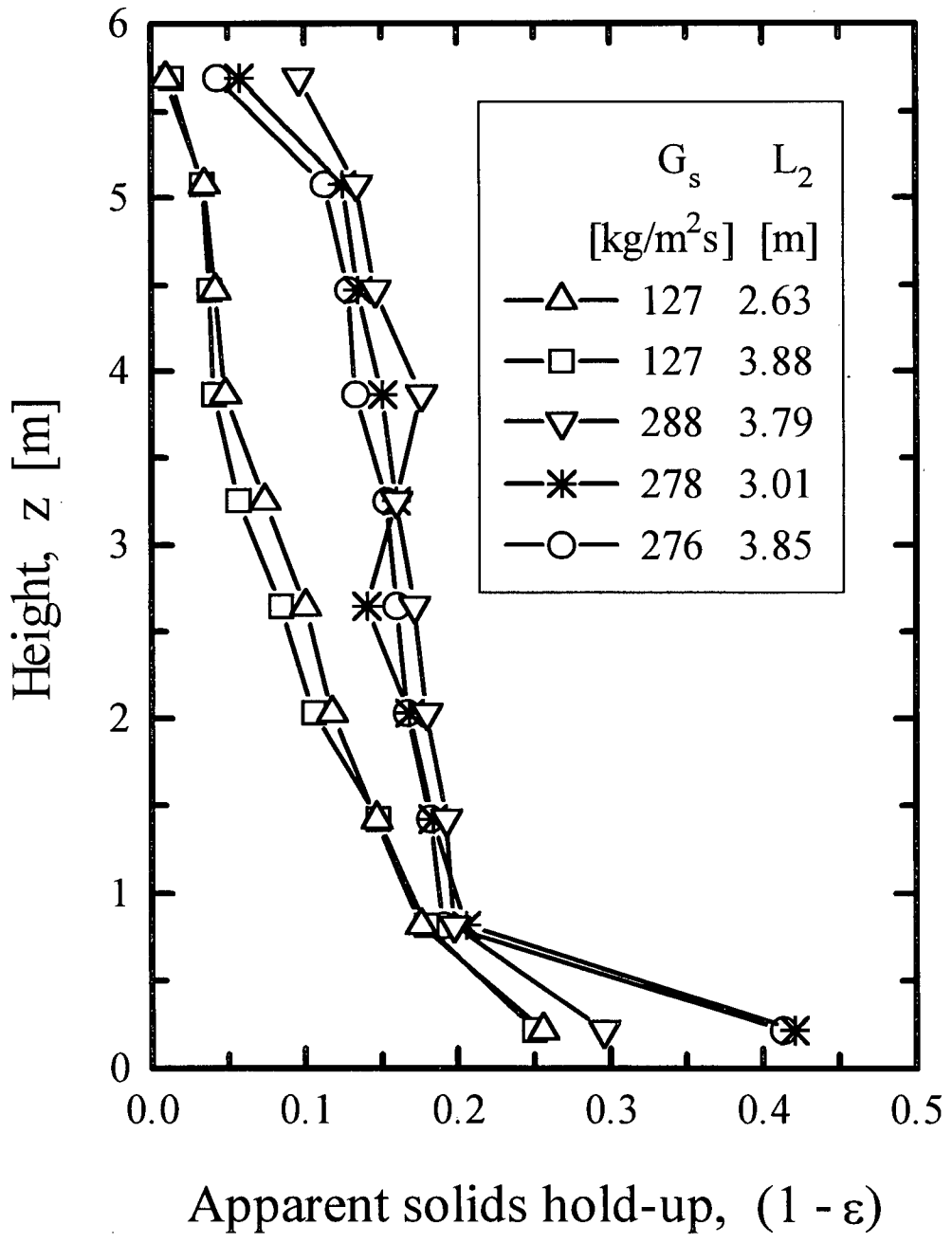

Fig. 3.14: Influence of solids inventory in downcomer 2 on longitudinal profiles of apparent solids hold-up for U = 5.5 m/s and two nearly constant solids circulation rates.

such circumstances to control the solids circulation rate effectively. A similar difficulty could also be experienced with non-mechanical valves.

3.3.2 Average slip velocity and slip factor

The average slip velocity in a circulating fluidized bed riser is defined as the mean relative velocity between the gas and a solid particle given by

$$\overline{V}_{slip} = V_g - V_p = \frac{U}{\varepsilon} - \frac{G_s}{\rho_p(1-\varepsilon)} \tag{3.7}$$

The ratio of the average (interstitial) gas velocity to the average particle velocity has been called (Matsen, 1976) the slip factor,

$$\Phi = \frac{U}{\varepsilon} / \frac{G_s}{\rho_p(1-\varepsilon)} \tag{3.8}$$

In very dilute suspensions, where particles are well dispersed and the particle motion is not significantly influenced by neighboring particles, the slip velocity is approximately equal to the single particle terminal velocity. Figure 3.15 shows the apparent voidage, slip velocity and slip factor at z = 2.03 m for U = 4 m/s at various solids circulation rates. As explained above, once dense conditions are established, any further increase in solids circulation rate is accompanied by only a small rise in solids concentration. Initially both the slip velocity and slip factor increase with increasing solids circulation rate, reaching maximum values around the high-density transition point. Thereafter, the slip velocity decreases very slowly and the slip factor falls gradually to a value of about 5 as more solids are added. The same trend is seen for U = 6 and 8 m/s as shown in Fig. 3.16 where the ratio of average slip velocity to the terminal velocity of particles of mean size is plotted against solids circulation rate. Slip velocities as high as 40 times the terminal velocity are observed. While high slip velocities are consistent with other studies (e.g. Yerushalmi et al., 1978; Yerushalmi and Cankurt, 1979), the present work reports data at much higher solids

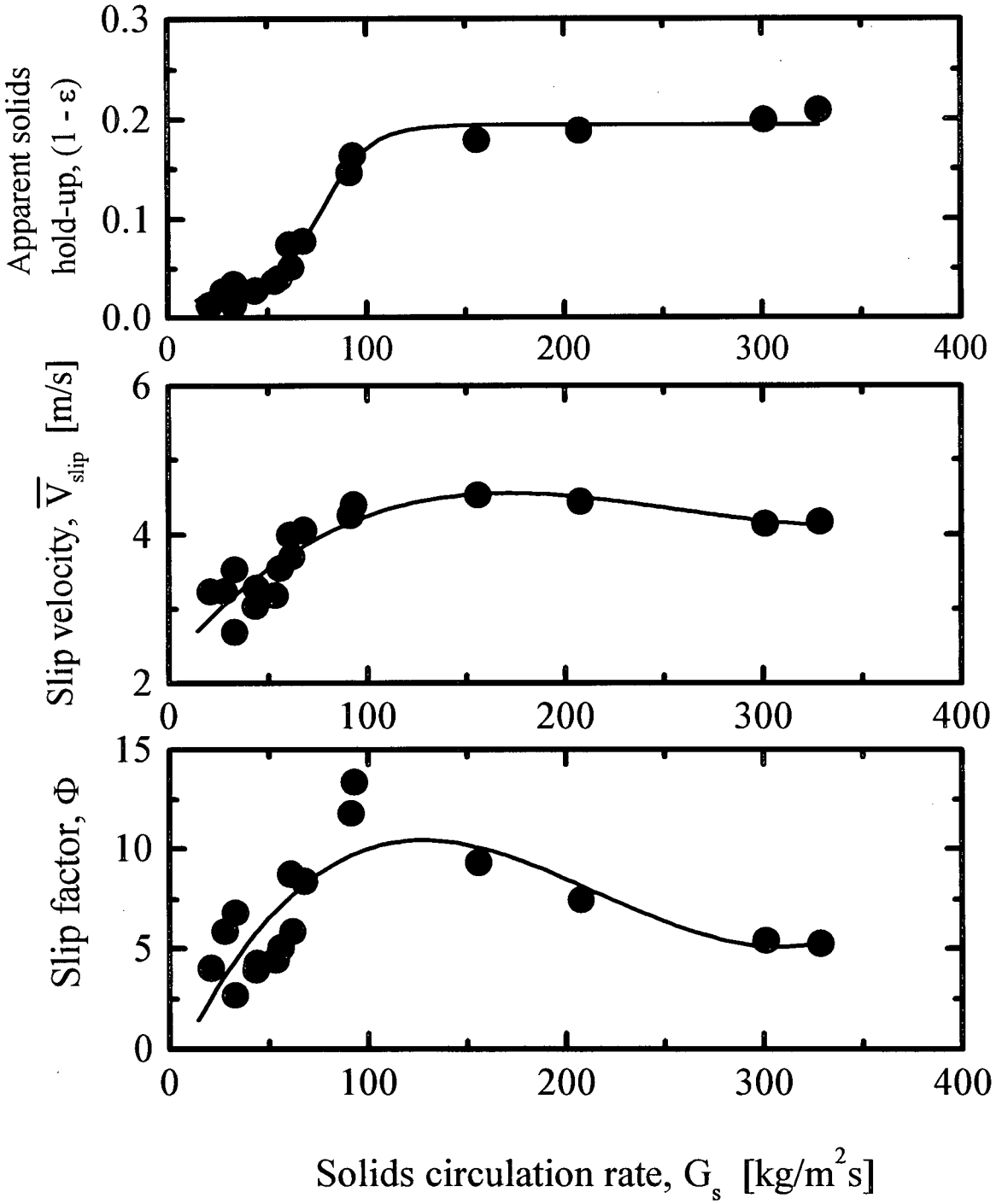

Fig. 3.15: Influence of solids circulation rate on (a) apparent solids hold-up, (b) slip velocity and (c) slip factor at height 2.03 m for a superficial velocity of 4 m/s: $d_p = 70$ μm, $\rho_p = 1600$ kg/m^3, $v_T \approx 0.24$ m/s.

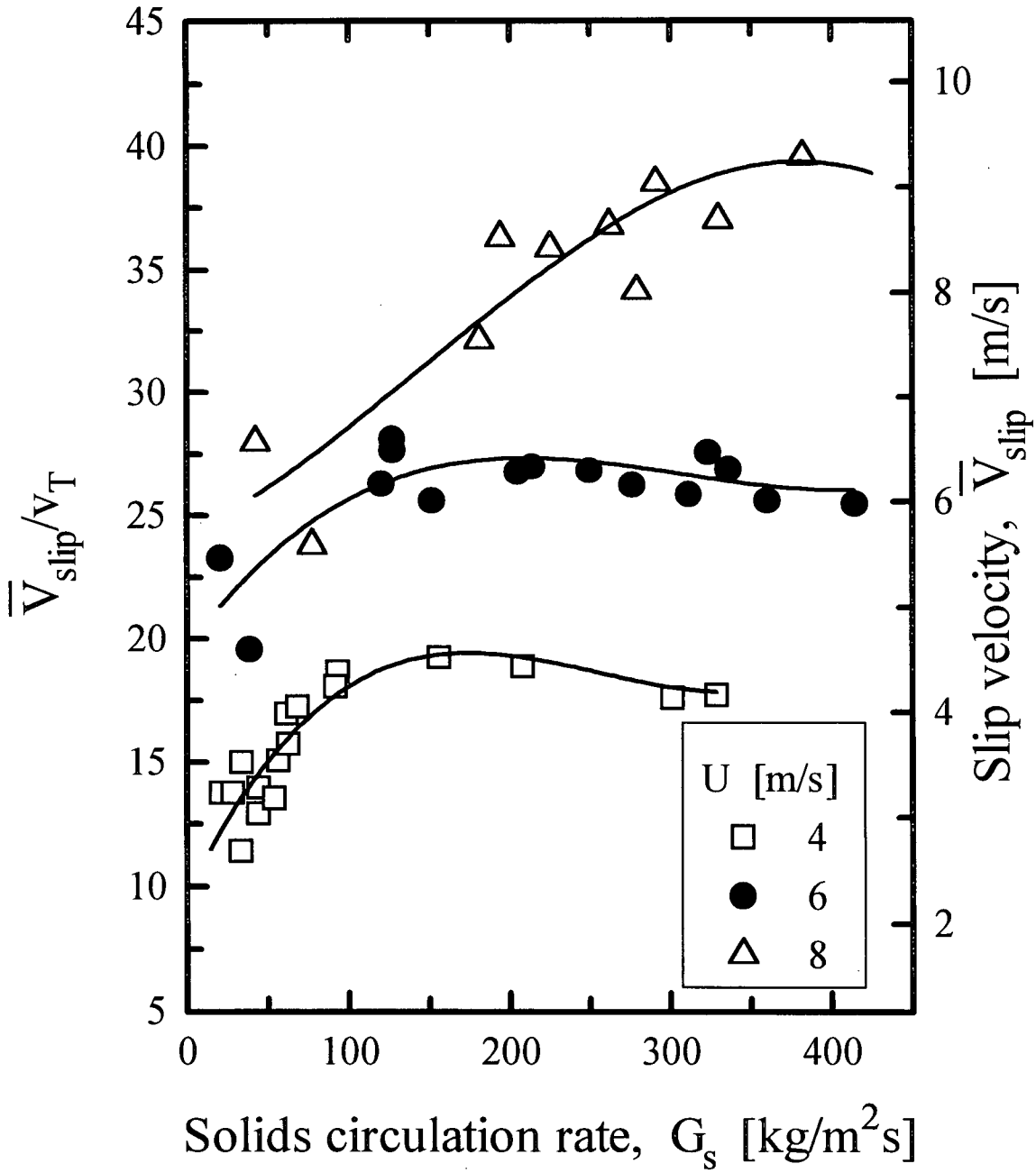

Fig. 3.16: Variation of dimensionless average slip velocity with solids circulation rate at z = 2.03 m for three superficial air velocities.

circulation rates, greater superficial air velocities and higher solids concentrations than earlier studies. The high values of slip velocity are probably due to particle-particle interaction, leading to the formation of clusters or other particle structures as reported in earlier studies (Yerushalmi and Cankurt, 1979; Grace and Tuot, 1979; Gidaspow et al., 1989; Li et al., 1991; Brereton and Grace, 1993; Horio and Kuroki, 1994; Lints and Glicksman, 1993; Bai et al., 1996; Glicksman and Noymer, 1997; Issangya et al., 1997). The high slip between the gas and particles can also be partly caused by radial heterogeneity in the riser, in which a dilute core region is surrounded by a relatively dense region near the wall (see Chapter 4). Yang et al. (1992, 1993) measured local particle and gas velocities in a dilute riser ($\varepsilon > 0.95$) and found that the integrated cross-sectional mean slip velocity was always smaller than the average slip velocity determined from differential pressure measurements. They attributed the difference to the core-annular flow structure in the riser. Estimation of local flow parameters, e.g. cluster size, from average slip velocity data, therefore, needs to be done with caution.

The variation of the average slip velocity and slip factor can be further examined by looking at how the interstitial gas velocity, V_g, and average particle velocity, V_p, change with the solids circulation rate. This is shown in Fig. 3.17 where, for convenience, the apparent solids hold-up, $(1 - \varepsilon)$, is also plotted. Variations are considered at two heights, $z = 2.03$ m and $z = 5.69$ m. Consider first the conditions near the bottom ($z = 2.03$ m). Initially the solids hold-up increases with the solids circulation rate, but once G_s is beyond the high density transition point (approximately 80 kg/m^{2}s), the increase in the suspension density is only slight. The interstitial gas velocity (V_g) remains around its superficial value before rising to a higher value on transition to high density conditions. Thereafter V_g remains more or less the same with increasing G_s. The particle velocity (V_p), first decreases when the solids hold-up rises sharply at the transition point, then rises with increasing G_s. The magnitude of V_p is, however, much smaller than the interstitial

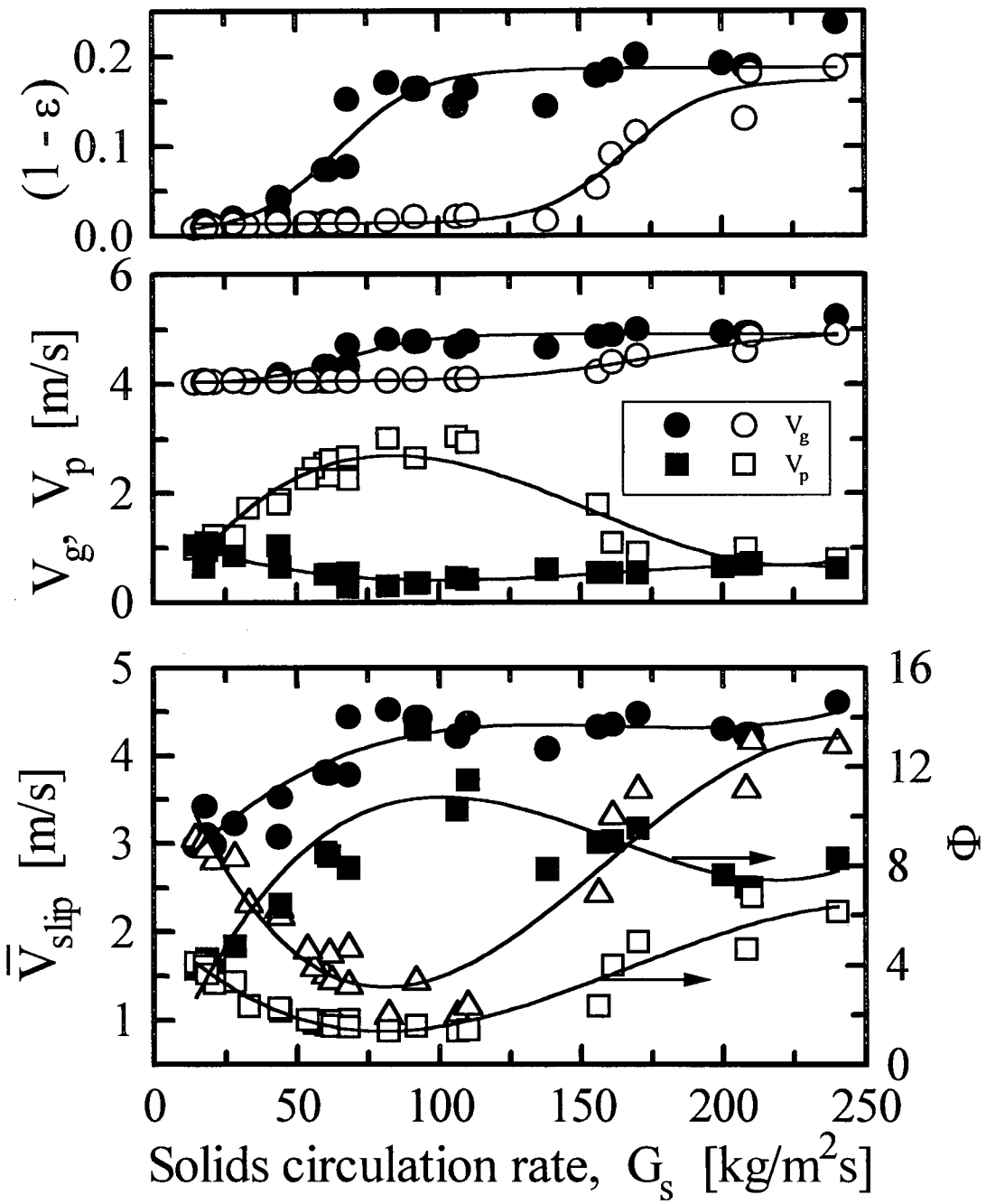

Fig. 3.17: Influence of solids circulation rate on apparent solids hold-up, interstitial gas velocity, average particle velocity, average slip velocity and slip factor at z = 2.03 (solid symbols) and z = 5.69 m (open symbols) for U = 4 m/s.

gas velocity at these dense conditions (< 1 m/s) and its increase with G_S is relatively small. The net result is that the average slip velocity changes very little with increasing solids circulation rate. On the other hand, at the higher level (z = 5.69 m) the high density condition is reached at a much higher solids circulation rate (approximately 200 kg/m^{2}s). Prior to this point, because the solids hold-up is low, the gas velocity changes only slightly remaining close to its superficial value. At the same time, because of the increasing solids circulation rate, the particle velocity also increases. The jump in the apparent solids hold-up at the high-density transition results in a significant increase in the interstitial gas velocity while causing the particle velocity to drop. A further increase in G_S alters these parameters only slightly. The change of the slip factor with G_S can be explained similarly. Note that under high density conditions the various quantities at the two levels converge. Also if the solids circulation rate were raised in much smaller steps, the variation trends of V_g, V_p, $\overline{V}_{slip}$ and Φ at the higher level could also have been seen at the lower level.

Yousfi and Gau (1974) correlated slip velocity data from experiments with particles of mean diameter 20 to 183 μm in risers of diameter 38 to 50 mm for volumetric solids concentrations up to 22% as

$$\frac{\overline{V}_{slip}}{v_T} = 1 + 0.0032 Re^{0.5} (1-\varepsilon)^{0.25} \left(\frac{d_p}{D}\right)^{-1.8} \left(\frac{\rho}{\rho_p}\right) \qquad (3.9)$$

where $Re = \rho DU/\mu$ is the gas Reynolds number. This correlation overestimates our results by a factor of up to about 10. The high dimensionless slip velocities (as high as 300) in their work may have been influenced by electrostatic charging. Matsen (1982) proposed a correlation in which the dimensionless slip velocity is only a function of solids concentration, while Ravisankar and Smith (1986) presented a correlation for group B and D particles. Such larger particles have less tendency to agglomerate because there is less particle-particle adhesion. Both these correlations underpredict our data.

Figure 3.18 plots the slip velocity against the apparent solids hold-up for the same conditions as in Figs. 3.3, 3.4 and 3.5, but with measurements near the solids inlet excluded, to minimize acceleration and entry effects. The data are for U = 4, 6 and 8 m/s and cover a wide range of solids circulation rates. For a given superficial air velocity, it appears that the slip velocity, except for some scatter at low hold-ups, is a function of solids hold-up only. Yerushalmi and Avidan (1985) indicated from their studies with FCC particles in a 152 mm dia. riser, that the slip velocity is a strong function of solids circulation rate at any given superficial gas velocity. They argue that the hydrodynamic behaviour of the suspension is mainly characterized by the interaction of the gas with clusters rather than with individual particles. Therefore, any change in the gas velocity or solids circulation rate should influence the spectrum of cluster sizes leading to non-uniqueness of the slip velocity - voidage relationship. While this may be true for dilute risers, our data do not show such a strong dependence of voidage or slip velocity on solids circulation rate, especially at apparent solids hold-ups exceeding about 0.15. It is likely that clustering is, therefore, not the only phenomenon determining the flow behaviour under such conditions. The data in Fig. 3.18 are well represented by

$$\frac{\overline{V}_{slip}}{U} = 1.67(1-\varepsilon)^{0.25} \qquad (3.10)$$

for $0.05 < (1-\varepsilon) < 0.3$ and U = 4 to 8 m/s.

Matsen (1976) reported that the slip factor in industrial FCC risers is approximately 2, whereas Ouyang and Potter (1993) obtained an average value of 2.6 from a pool of experimental data. Patience et al. (1992) correlated data for group A and B particles in risers of diameters from 0.04 to 0.15 m with the equation

$$\Phi = 1 + \frac{5.6}{U/\sqrt{gD}} + 0.47\left(\frac{v_T}{\sqrt{gD}}\right)^{0.41} \qquad (3.11)$$

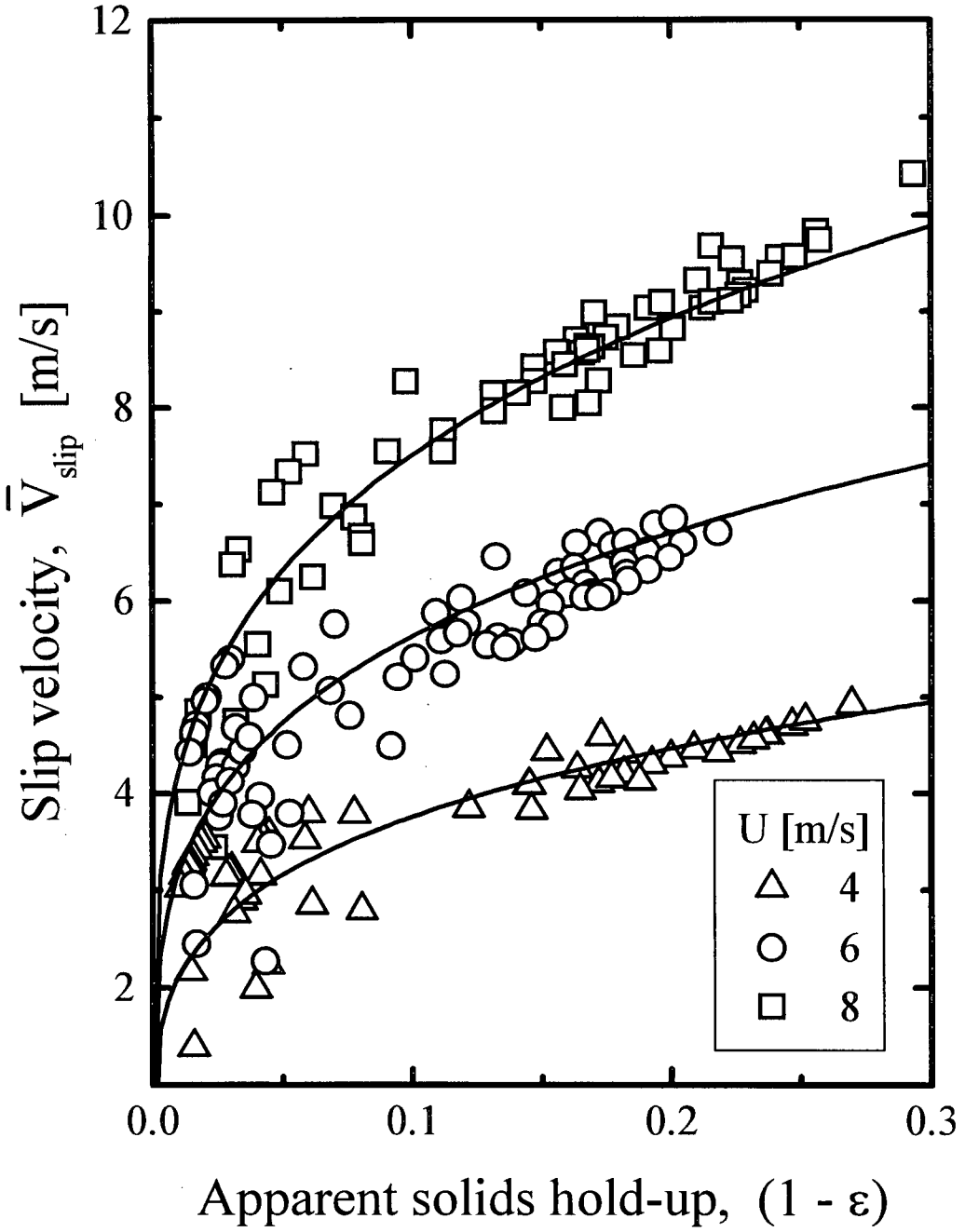

Fig. 3.18: Variation of average slip velocity with apparent solids hold-up at nine axial locations (excluding z = 0.216 m) for same conditions as in Figs. 3.3, 3.4 and 3.5. Lines are calculated using Eq. (3.10).

This equation predicts slip factors of about 2 at high superficial gas velocities (> 8 m/s), in good agreement with their experimental data. Most of their Φ data lie between 1.5 and 5. Figure 3.19 plots slip factors obtained in this study at z = 4.47 m for U = 4, 6 and 8 m/s. All the points appear to be for fully developed conditions, with constant differential pressure gradient. Predictions of Eq. (3.11) appear to be consistently lower than the measured values. Fig. 3.20 shows longitudinal profiles of solids hold-up, slip velocity and slip factor at a superficial air velocity of 6 m/s for solids circulation rates of 78, 151 and 336 kg/m^{2}s. At the lowest solids flux the suspension is dilute, and the slip velocity and slip factor are low and vary relatively little with height. Similarly at the highest circulation rate the whole riser is dense and the two parameters are relatively uniform over the riser height. At intermediate solids flowrate, on the other hand, a dense zone exists at the bottom while the suspension is dilute towards the top, causing substantial variation of slip velocity and slip factor over the height of the riser.

3.3.3 Voidage correlations and pressure balance analysis

In the design of circulating fluidized bed systems it is desirable to have reliable estimates of the overall riser pressure drop, solids hold-up and solids inventory to maintain stable operation at a given gas velocity and solids circulation rate (King, 1989; Jazayeri, 1991). The solids hold-up is related to the pressure drop across the riser, which in turn depends on the pressure drop across the downcomer and on pressure drops in other parts of the system (Bi and Zhu, 1993). The overall pressure balance therefore establishes the pressure driving force needed for solids circulation, as well as the required blower capacity. Theoretical analyses of the pressure balance around single-loop circulating fluidized bed systems have been carried out by several investigators (e.g. Weinstein et al., 1983; Kwauk et al., 1986; Arena et al., 1987; Rhodes and Geldart, 1987; Yang, 1988;

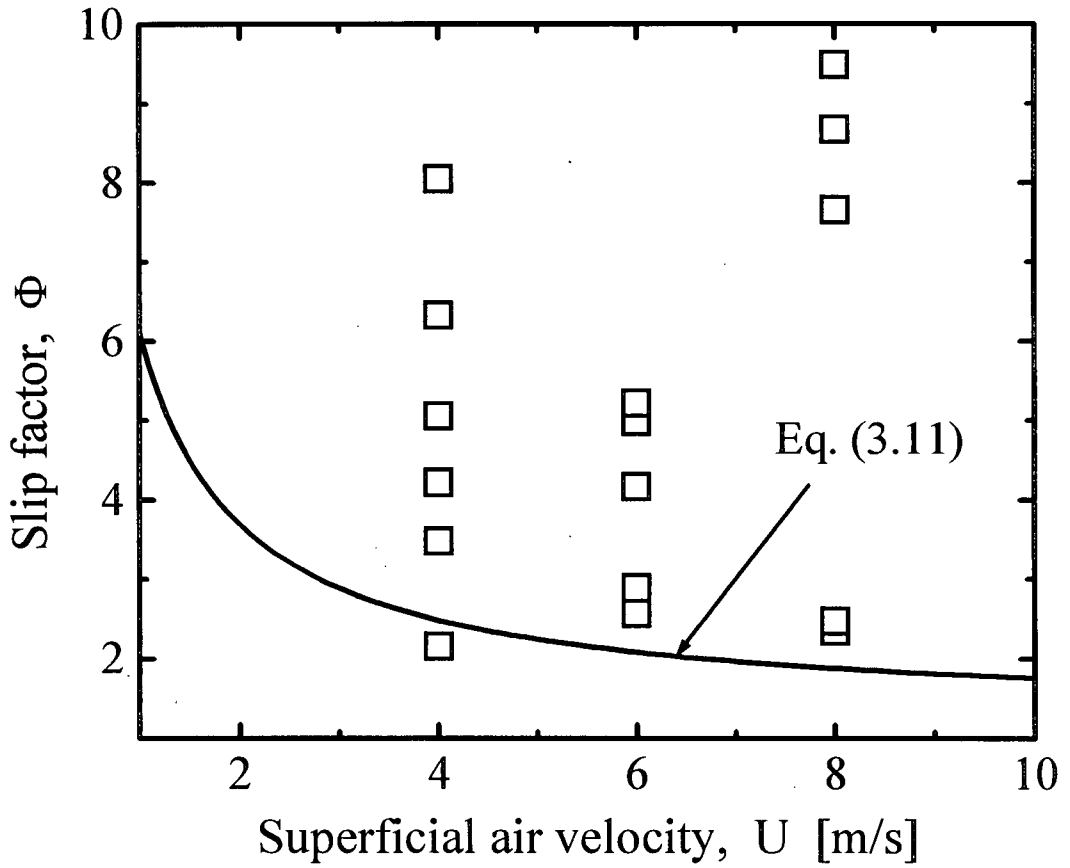

Fig. 3.19: Slip factors in fully developed flow at z = 4.47 m for U = 4, 6 and 8 m/s and various solids circulation rates.

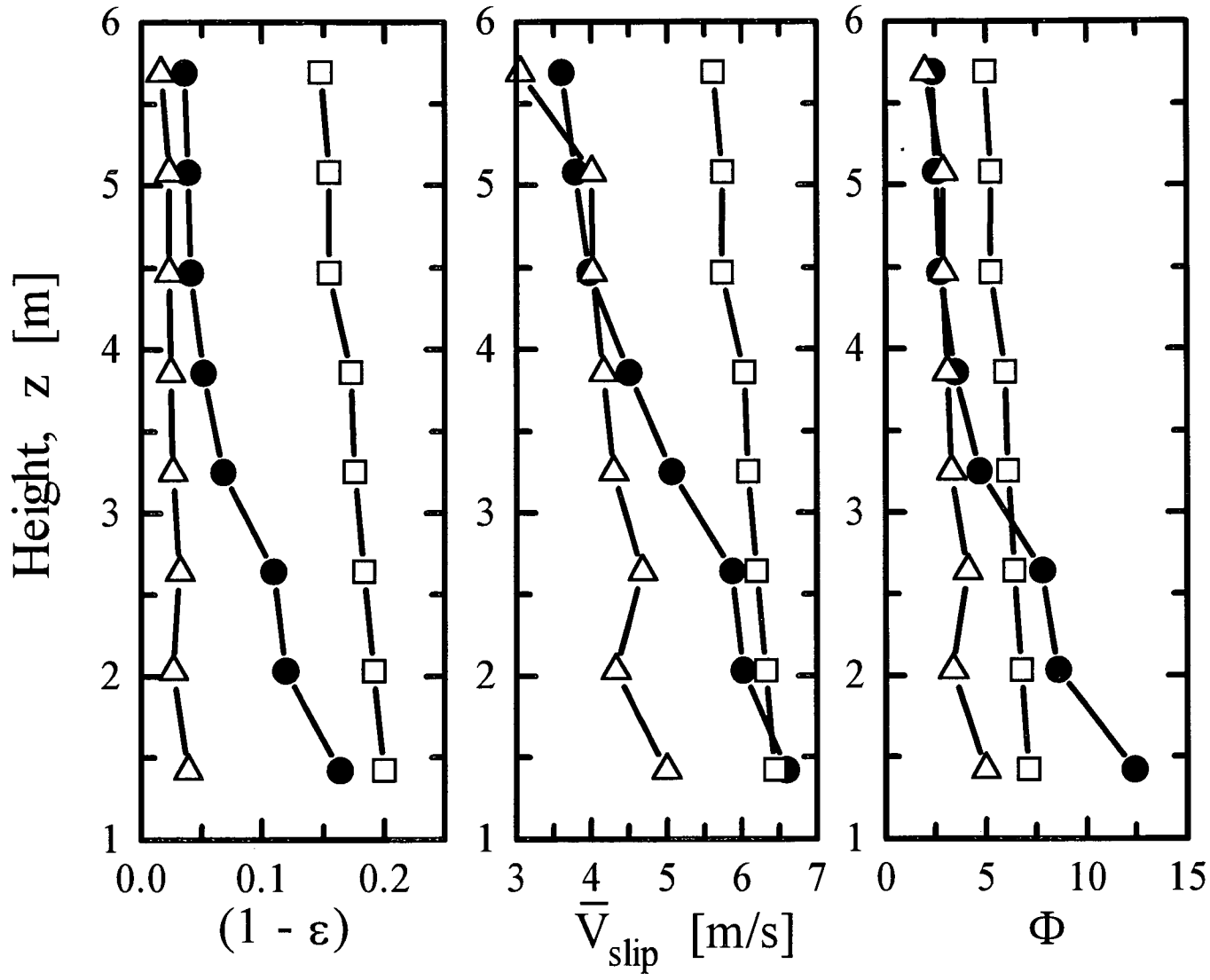

Fig. 3.20: Axial profiles of apparent solids hold-up, slip velocity and slip factor at U = 6 m/s for three solids circulation rates (Δ : 78; ●: 151; □ : 336 kg/m^{2}s).

Breault and Mathur, 1989b; Rhodes and Laussmann, 1991; Horio and Takei, 1991; Bi and Zhu, 1993). The analysis involves setting up a model to predict the system pressure balance and material balance, thus allowing evaluation of the effects of operating conditions and design parameters on the overall steady state riser hydrodynamics. Bai et al. (1997) used a similar approach to analyze the pressure balance in our dual-loop high density circulating fluidized bed (HDCFB) unit.

3.3.3.1 Axial solids hold-up profile correlations

Harris and Davidson (1994) classified riser flow models into three broad groups: those that predict only axial profiles of voidage without considering radial variations (e.g. Li and Kwauk, 1980; Arena et al., 1987; Rhodes and Geldart, 1987; Kunii and Levenspiel, 1991). Such radial variations have been observed experimentally as presented in Chapter 4. Next are models that predict both the longitudinal and radial variation by assuming two or more regions, e.g. core-annulus or clustering-annular flow models (Berutti and Kalogerakis, 1989; Rhodes, 1990; Senior and Brereton, 1992; Harris and Davidson, 1994). Finally there are models that employ the fundamental equations of fluid dynamics - continuity, momentum and pseudo-thermal energy balances, to predict the two-phase gas-solid flow behavior (Sinclair and Jackson, 1989; Tsuo and Gidaspow, 1991; Pita and Sundaresan, 1991; Sinclair, 1997). The first two types of model require correlations based on experimental data or a combination of correlations and fundamental relationships, and they have had some success in predicting overall behavior. The third type allows investigation of the riser local flow structure, but the models are often too numerically complex to allow wide application.

Under the operating conditions of this work, S-shape voidage profiles were observed as proposed by Li and Kwauk (1980). It was also possible to operate the unit at

high enough solids flux that the dense zone could be extended to cover the whole riser or at relatively low solids fluxes such that no dense zone was established in the riser. Most previous models have never been tested at the high density/high solids flux conditions achieved in this work. A form of equation similar to that of Li and Kwauk (1980) is adopted in this work to model vertical profiles of cross-sectional mean solids hold-up in the riser. The equation assumes an S-shape voidage profile and gives the mean voidage $\bar{\varepsilon}$ at a height z as,

$$\frac{\varepsilon - \varepsilon_a}{\varepsilon^* - \varepsilon} = \exp\left(\frac{z - z_i}{z_o}\right) \tag{3.12}$$

ε^* and ε_a are the limiting dilute and dense phase voidages, while z_i is the height of the inflection point above the distributor and z_o is a fitting parameter. Kwauk et al. (1986) proposed empirical equations for ε_a, $\varepsilon^*$and z_o. Their equations for ε_a and ε^*, however, require an iterative solution. In addition, the predictions of Eq. (3.12) using empirical correlations for ε_a, $\varepsilon^*$and z_o have not always agreed well with experimental findings (e.g. Hartge et al., 1986; Louge et al., 1990; Yang, 1993). This could result from the limited number of data used to obtain the correlations. Bai et al. (1997) approximated the dilute phase limiting voidage by assuming the average slip velocity to be equal to the single particle terminal velocity and the limiting dense phase voidage to be that at minimum fluidization, ε_{mf}. While the first assumption has support from experimental results (Kunii and Levenspiel, 1996), the latter sets the limiting voidage at the bottom too low, causing errors in predicting the longitudinal profiles. A different approach is taken in this work.

Substituting z = 0 and z = H in Eq. (3.12) the voidages ε_D and ε_e at the riser bottom and exit can be expressed, respectively as

$$\frac{\varepsilon_D - \varepsilon_a}{\varepsilon^* - \varepsilon_D} = \exp\left(-\frac{z_i}{z_0}\right) \tag{3.13}$$

and

$$\frac{\varepsilon_e - \varepsilon_a}{\varepsilon^* - \varepsilon_e} = \exp\left(\frac{H - z_i}{z_0}\right) \tag{3.14}$$

The approach here is to first establish correlations of ε_D, ε_e and z_i from the voidage data available in the literature summarized in Table 3.1, together with the high density data obtained in this work. ε_e was obtained by extending the hold-up profile to z = H, whereas, in order to exclude acceleration and entry effects, the linear portion of the profile in the dense region was extrapolated to z = 0 to get ε_D. Figures 3.21 and 3.22 present the solids hold-up at riser bottom and exit, respectively. The riser exit data used in the analysis were only from studies where no significant increase in solids concentration occurred near the exit, i.e. where there were no significant exit constriction effects. These data are tabulated in Appendix B-2. It is worth pointing out, as can be noted from Figs. 3.21 and 3.22, that slip factors in the exit region are about 5 at most, whereas those in the dense zone extend to about 50. Several dimensionless groups were tested in correlating the data, and the following equations were found to best fit the data:

$$1 - \varepsilon_D = 1.59\left[\frac{G_s}{\rho_p(U - v_T)}\right]^{0.50} U^{*-0.46}\left(\frac{D}{d_p}\right)^{0.11} \tag{3.15}$$

where

$$U^* = U\left[\frac{\rho^2}{g(\rho_p - \rho)\mu}\right]^{1/3} \tag{3.16}$$

and

$$1 - \varepsilon_e = 5.06\left[\frac{G_s}{\rho_p(U - v_T)}\right]^{1.19} Ar^{-0.05} \tag{3.17}$$

Table 3.1: References and experimental conditions for data of Figs. 3.22 to 3.25.

Symbol	Reference	D [m]	d_p [μm]	ρ_p [kg/m^3]	U [m/s]	G_s [kg/m^{2}s]
⊡	Contractor et al. (1993)	0.1500	70	1570	5.7	294 - 685
▼	Ouyang and Porter (1993)	0.2540	65	1380	2.3 - 7.5	54 - 206
✳	Li and Kwauk (1980)	0.0900	105 81 56	4510 3090 3050	4.0 - 5.5 2.2 - 5.6 1.5	135 73 129
▲	Li et al. (1988)	0.0900	54	930	1.5 - 2.1	14 - 96
■	Yerushalmi et al.(1979)	0.0760	60	881	2.4 - 4.5	50 - 212
+	Yerushalmi and Avidan (1985)	0.1520	49	1450	1.9 - 4.1	113 - 173
◇	Rhodes and Geldart (1986)	0.1520	64 270	1800 2600	2.5 - 4.5 6.0 - 8.0	41 - 107 70 - 160
✦	Hartge et al. (1986)	0.050 0.400	56 56	2600	3.4 - 4.0 4.2 - 5.0	72 - 90 64 - 118
⊖	Louge and Chang (1990)	0.2030	72	1300	2.0	40
⊠	Bi et al. (1989)	0.1860	280	706	3.7, 6.0	34 - 84
▽	Yang et al. (1984)	0.1150	220	794	5.3	132 - 160
⊞	Arena et al. (1991)	0.1200 0.4000	90 90	2543 2543 2600	5.0 5.0 7.0	92 115 251 382 - 600
⊠	Bader et al. (1988)	0.3050	76	1714	4.3	147
O	Weinstein et al. (1984)	0.1520	49	1450	2.9 - 3.4	71 - 140
⊖	Gao (1990)	0.09	62 205 82	1020 760 1780	1.2 - 1.4 2.7 - 4.3 2.5	12 - 18 37 - 82 35
▽	Nishino (1990)	0.0970	69	1690	4.0	107 - 200
✕	Schnitzlein (1987)	0.152	59	1450	3.0 - 4.0	68 - 145
□	Bai and Kato (1995)	0.15 0.097 0.066	59.1 59.1 59.1	1623 1623 1623	1.5 - 2.5 1.5 - 3.0 1.5 - 3.0	18 - 88 10 - 64 8 - 38
⊽	Pugsley (1990)	0.05	150	2500	6.5	270 - 385
⊼	Patience (1990)	0.0828	275	2630	6.0	102 - 198
⊞	Vergel (1990)	0.3	70	1400	11.1	147
⊕	Horio, et al. (1988)	0.0500	60	1000	1.17 - 1.29	11 - 14
●	This work	0.0762	70	1600	4.0 - 8.0	30 - 425

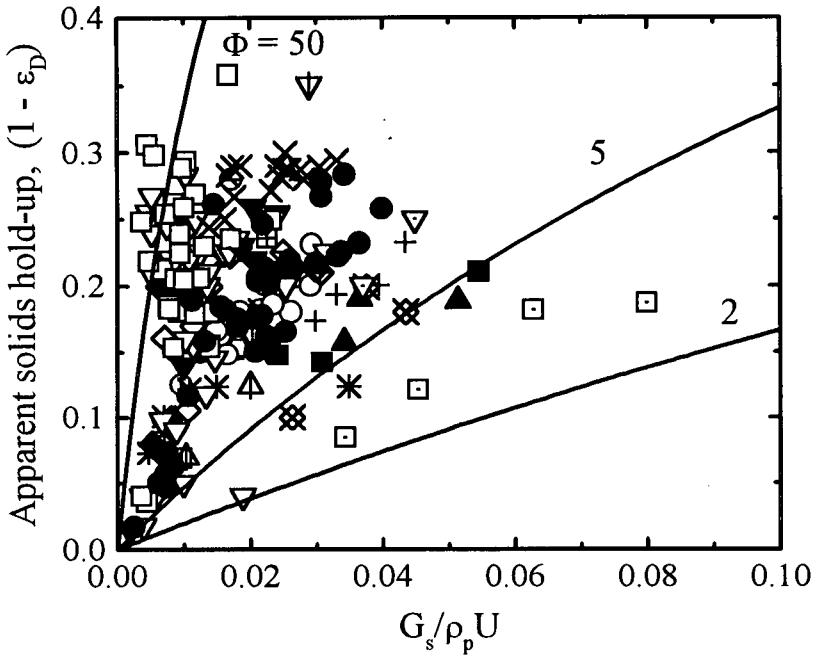

Fig. 3.21: Apparent solids hold-ups at riser bottom for different operating conditions and riser sizes (● - this work; for other symbols see Table 3.1).

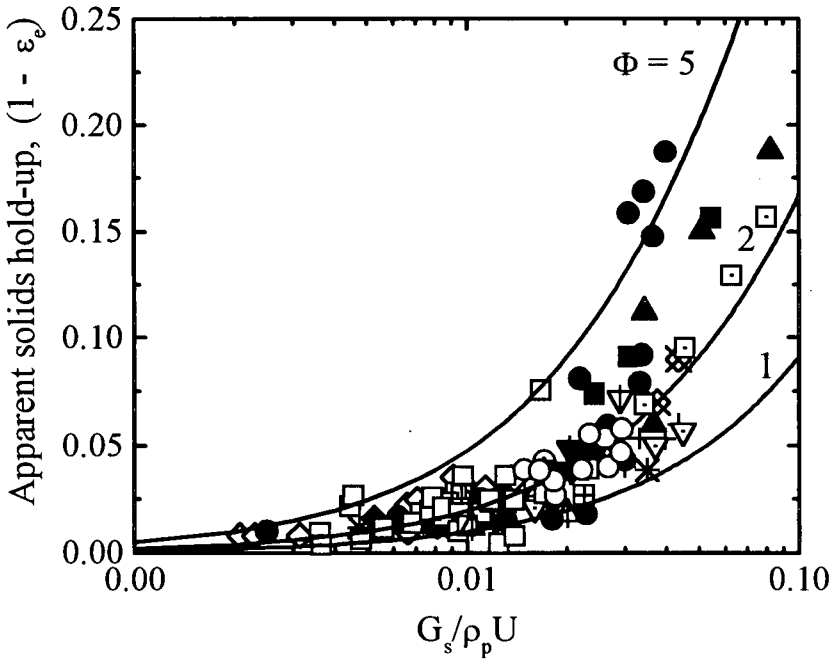

Fig. 3.22: Apparent solids hold-up at riser exit for different operating conditions and riser sizes (● - this work; for other symbols see Table 3.1).

The range of the variables used to obtain these correlations were:

$$1.17 < U < 11.1 \text{ m/s}$$

$$7.85 < G_s < 425 \text{ kg/m}^2\text{s}$$

$$0.05 < D < 0.4 \text{ m}$$

$$2.79 < H < 15.8 \text{ m}$$

$$49 < d_p < 280 \text{ } \mu\text{m}$$

$$706 < \rho_p < 4510 \text{ kg/m}^3$$

All data were obtained from cold units with air as the fluidizing gas so that the density, ρ, and viscosity, μ, were not varied. They are only introduced in the correlations to make the equations dimensionless. Their inclusion needs to be confirmed. Stemerding (1962) found that the pressure drop in a pipe was independent of gas properties for $0.33 < \rho < 5.0$ kg/m^3 and $1.4\ 10^{-7} < \mu < 3.7\ 10^{-7}$ Pa s. Therefore it seems unlikely that small variations of ρ and μ will have much influence on the validity of Eqs. (3.15) to (3.17). Predictions of the correlations are compared to experimental data in Figs. 3.23 and 3.24. In both cases the predictions are within ±15% of most of the data. Tables 3.2 and 3.3 compare Eqs. (3.15) and (3.17) with other equations in the literature by showing their relative mean square deviation (RMSD) for all the data in Fig. 3.21 (185 points) and Fig. 3.22 (135 points). Both equations offer superior predictions.

The literature data for z_i show so much scatter, probably due to the influence of solids inventory and the use of different solids feed devices, that regression was performed only on the data from this work giving

$$\frac{z_i}{H} = 1.32 - \frac{3.24}{1 + \exp(0.05 \frac{G_s}{\rho U})} \qquad (3.18)$$

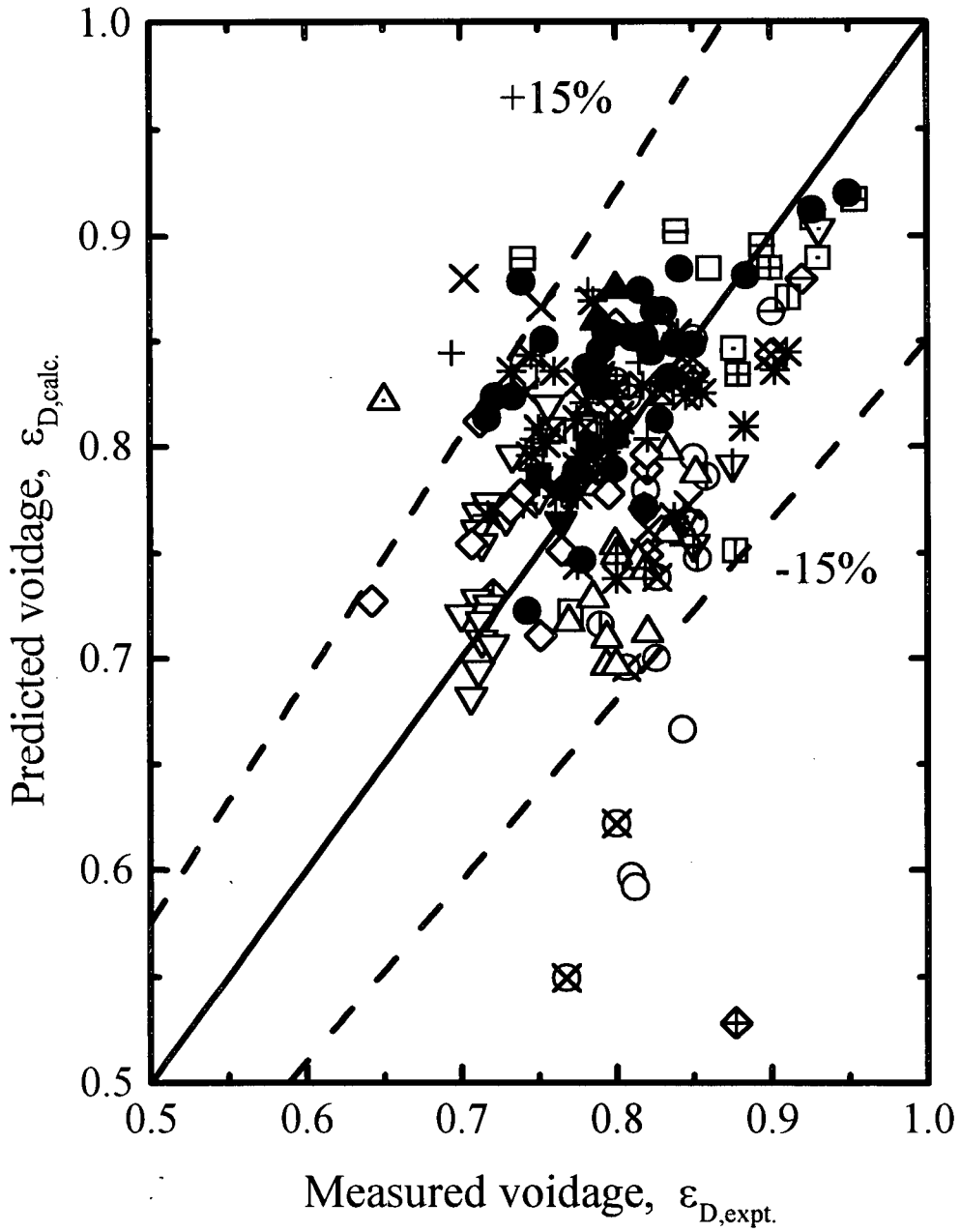

Fig. 3.23: Comparison between riser bottom apparent voidages predicted by Eq. (3.15) and experimental values (●- this work; for other symbols see Table 3.1.)

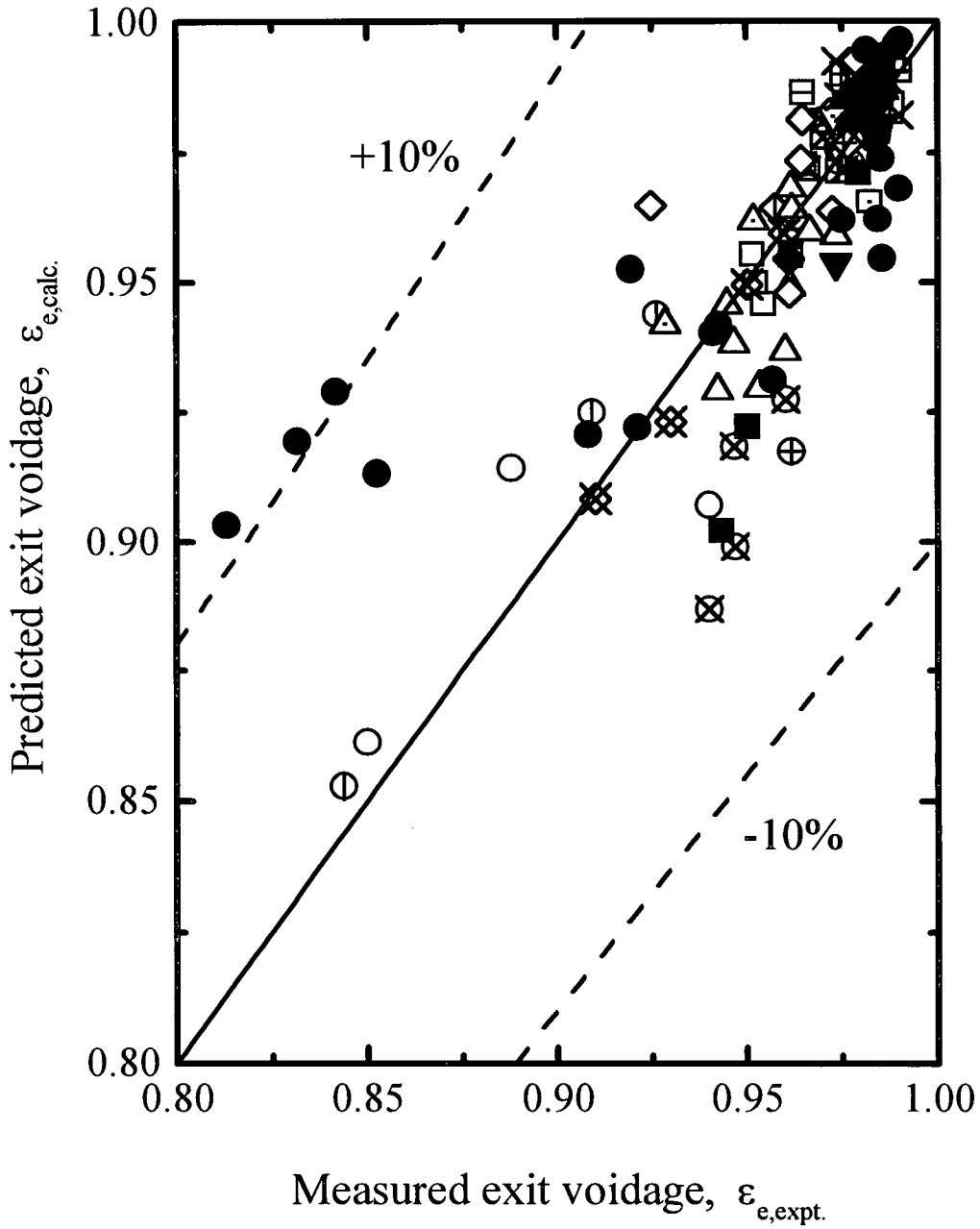

Fig. 3.24: Comparison between riser exit apparent voidages predicted by Eq. (3.17) and experimental values. (● this work; for other symbols see Table 3.1.)

Table 3.2: Comparison of correlations for dense region voidage

No.	Author	Correlation	RMS deviation
1.	Pugsley et al. (1994)	$\varepsilon_D = 1.0 - 8\times10^{-4} G_s$	0.1789
2.	King (1989)	$\varepsilon_D = \dfrac{U+1}{U+2}$	0.1057
3.	Wong et al. (1992)	$\varepsilon_D = 0.71\left(\dfrac{G_s}{\rho_p U}\right)^{-0.03} D^{-0.08}\,\mathrm{Re}_p^{-0.12}$ for Group A $\varepsilon_D = 0.25\left(\dfrac{G_s}{\rho_p U}\right)^{-0.11} D^{-0.23}\,\mathrm{Re}_p^{-0.02}$ for Group B	0.1161
4.	Bai and Kato (1994)	$\dfrac{1-\varepsilon_D}{1-\varepsilon^*} = 1 + 6.14\times10^{-3}\left(\dfrac{U\rho_p}{G_s}\right)^{-0.23}\left(\dfrac{\rho_p-\rho}{\rho}\right)^{1.21}\left(\dfrac{U}{\sqrt{gD}}\right)^{-0.383}$ for $G_S > G_S^*$ $\dfrac{1-\varepsilon_D}{1-\varepsilon^*} = 1 + 0.103\left(\dfrac{U\rho_p}{G_s}\right)^{1.13}\left(\dfrac{\rho_p-\rho}{\rho}\right)^{-0.013}$ for $G_S \le G_S^*$ $\dfrac{G_s^* d_p}{\mu} = 0.125\left(\dfrac{U}{\sqrt{gd_p}}\right)^{1.85} \mathrm{Ar}^{0.63}\left(\dfrac{\rho_p-\rho}{\rho}\right)^{-0.44}$	0.1043
5.	This work	$1-\varepsilon_D = 1.59\left[\dfrac{G_s}{\rho_p(U-v_T)}\right]^{0.50}\left[U\left(\dfrac{\rho^2}{\mu(\rho_p-\rho)}\right)^{1/3}\right]^{-0.46}\left(\dfrac{D}{d_p}\right)^{0.11}$	0.0938

Table 3.3: Comparison of correlations for riser exit voidage

	Author	Correlation	RMS deviation
1.	Wong et al. (1992)	$\frac{\varepsilon_e}{1-\varepsilon_e} = 130.93\left[U\left(\frac{\rho^2}{\mu(\rho_p-\rho)}\right)^{1/3}\right]^{-0.86} D^{-0.54}\,Re_p^{-0.10}\,z^{-0.34}$	0.0474
2.	Patience et al. (1992)	$\varepsilon_e = \frac{1}{1+\Phi\left(\frac{G_s}{\rho_p U}\right)}$ where $\Phi = 1 + \frac{5.6}{\left(\frac{U}{\sqrt{gD}}\right)} + 0.47\left(\frac{v_T}{\sqrt{gD}}\right)^{0.41}$	0.0340
3.	Bai and Kato (1994)	$1-\varepsilon_e = 4.04\left[\frac{G_s}{\rho_p(U-v_T)}\right]^{1.214}$	0.0275
4.	This work	$1-\varepsilon_e = 5.06\left[\frac{G_s}{\rho_p(U-v_T)}\right]^{1.19} Ar^{-0.05}$	0.0252

Figure 3.25 shows that this equation fits our data well. The limiting dilute phase voidage, ε^*, can be approximated by assuming that the slip velocity between gas and solids approaches the terminal velocity of a single particle of diameter equal to the mean size and also taking $U/\varepsilon \approx U$, i.e.

$$\varepsilon^* = 1 - \frac{G_s}{\rho_p (U - v_T)} \tag{3.18}$$

Once ε_D, ε_e, ε^* and z_i are known, Eqs. (3.13) and (3.14) can be solved simultaneously to determine ε_a and z_o and the voidage profiles calculated by Eq. (3.12). The overall mean solids hold-up, $\bar{\varepsilon}_m$, is then obtained by integration over the entire riser height giving

$$\frac{\bar{\varepsilon}_m - \varepsilon_a}{\varepsilon^* - \varepsilon_a} = \frac{z_0}{H} \ln\left[\frac{1 + \exp[(H - z_i)/z_0]}{1 + \exp(-z_i/z_0)}\right] \tag{3.20}$$

3.3.3.2 Pressure and inventory balances

The major components in the dual-loop CFB unit which influence this analysis are risers, downcomers, gas-solids separators and solids flow control valves. Bends and other such restrictions are not considered.

1. Pressure drop across risers. The energy of gas entering the base of a riser is partially transferred to the solids through gas-solids interactions, and partially dissipated due to friction. For most operating conditions, gravitational effects are much larger than the frictional energy dissipation. However, friction effects may become significant, for

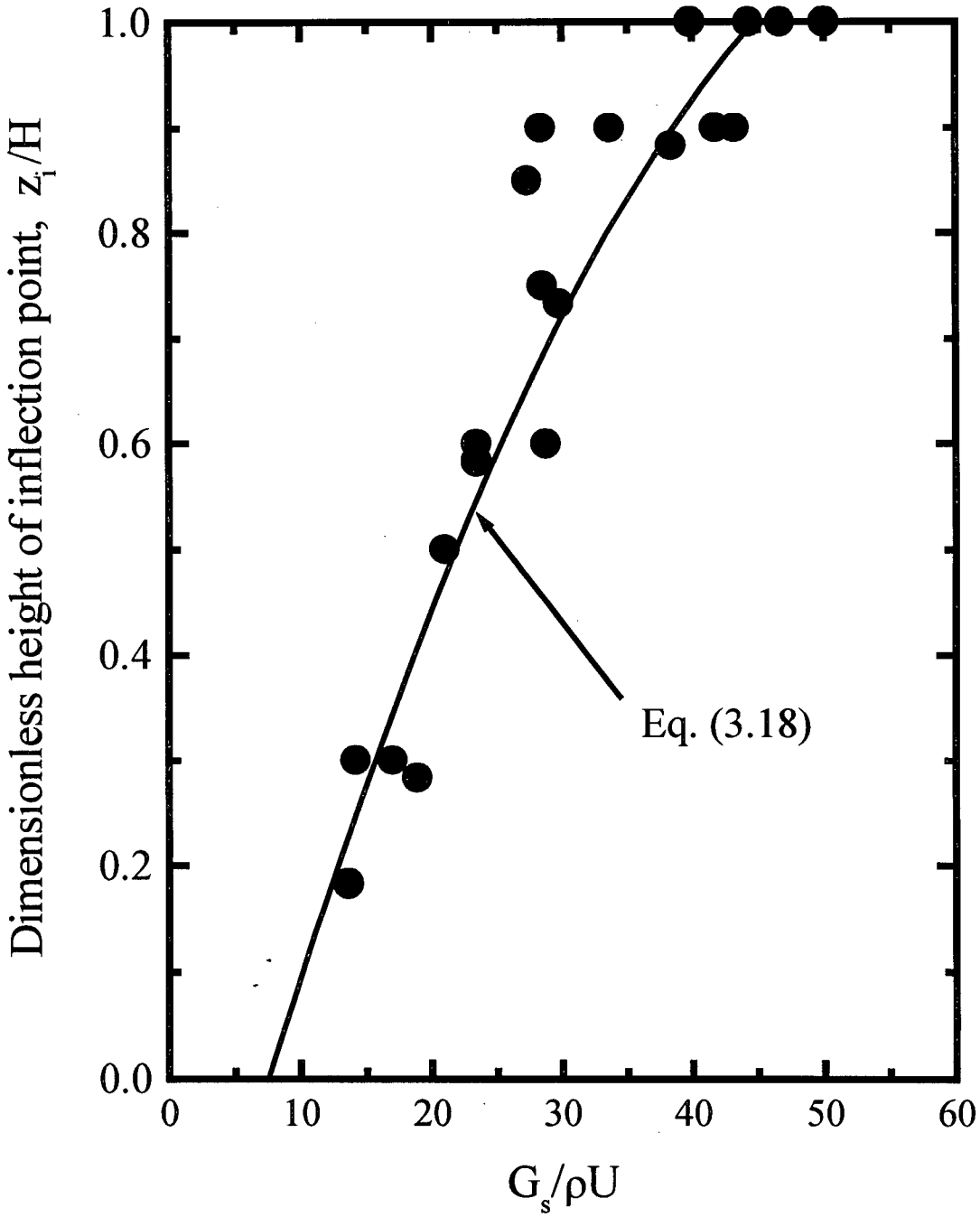

Fig. 3.25: Dimensionless height of inflection point as a function of solids-to-gas mass flow ratio compared with predictions of Eq. (3.18).

example, at high gas velocities and high solids circulation rates. If the pressures at the outlets of the two secondary cyclones are assumed to be equal to the same reference pressure, P_{ref}, then the pressure at the bottom of each riser can be expressed as

$$P_r = P_{ref} + \rho\bar{\varepsilon}_m gH + \rho_p(1-\bar{\varepsilon}_m)gH + \Delta P_{ac} + \Delta P_{fg} + \Delta P_{fs} + \Delta P_{cy,p} + \Delta P_{cy,s} \qquad (3.21)$$

The pressure drop in the riser is assumed to be composed of the sum of components due to gas and solids weight, solids acceleration, friction from both gas and solids, and losses across primary and secondary cyclones or other gas-solids separators. The pressure drop due to solids acceleration is insignificant at low solids circulation rates but needs to be considered at high G_S. Particles can be considered to accelerate from zero velocity at the riser bottom to $G_s/(\rho_p(1-\varepsilon))$ in the developed region within the riser, requiring a pressure drop (Breault and Mathur, 1989a) of:

$$\Delta P_{ac} = \frac{G_s^{\,2}}{\rho_p(1-\bar{\varepsilon}_m)} \qquad (3.22)$$

For the gas-wall friction, the Fanning equation (see Bird et al., 1960) is used:

$$\Delta P_{fg} = \frac{2f_g\rho U^2}{D}H \qquad (3.23)$$

with the Fanning friction coefficient, f_g, estimated by

$$f_g = \begin{cases} \dfrac{16}{Re} & Re \le 2.1\times10^3 \\ \dfrac{0.0791}{Re^{0.313}} & 2.1\times10^3 < Re < 10^5 \end{cases} \qquad (3.24)$$

While a large number of correlations are available for solids-wall friction in vertical dilute phase conveying (e.g. Leung and Wiles, 1976; Leung, 1980), there are very few equations applicable to the dense suspension flows encountered in CFB risers, probably because the pressure drop due to solids-wall friction is generally small compared to the weight of solids for such conditions. The correlation by Geldart and Ling (1990) is adopted here

since it was obtained for a wider range of solids and gas flows and for voidages as low as 0.55. Thus

$$\Delta P_{fs} = K\left(\frac{G_s}{D}\right)^m \left(\frac{\mu}{\rho}\right)^{0.4} \frac{1}{U} H \qquad (3.25)$$

where $K = 106$ and $m = 0.83$ for $G_s/D < 4.7 \times 10^4$ $kgm^{-3}s^{-1}$ while $K = 0.838$ and $m = 1.28$ for $G_s/D > 4.7 \times 10^4$ $kgm^{-3}s^{-1}$. The units of K are $kg^{(1-m)} m^{(3m-1.8)} s^{(m-2.6)}$.

2. **Pressure drop across cyclones.** As a first approximation, the pressure drop across the impingement solids-gas separator can be ignored (Wei et al. 1997). For simplicity, it is also assumed that the pressure drop across the "coneless" separator installed on the second downcomer is the same as that of a full cyclone subject to the same duty. The pressures at the outlets of the secondary cyclones are assumed to be equal to the same reference pressure, P_{ref}. In industrial units, separators may be arranged differently, and that would need to be taken into consideration in the pressure balance analysis. The pressure drop across a cyclone is often expressed (Perry and Green, 1984) as

$$\Delta P_{cy} = k\rho U_{cy}^2 \qquad (3.26)$$

where k is typically 1 to 20 depending on the cyclone geometry (Perry et al., 1984). Rhodes and Geldart (1987) proposed that this relationship be used for circulating fluidized bed cyclones with U_{cy} taken as the superficial gas velocity in the riser and k=25. Given that the cyclone pressure drop is a relatively minor component in the pressure balance and that it has been found (e.g. Comas, et al., 1991; Hoffmann et al., 1992; Trefz and Muschelknautz, 1993) to decrease with increasing solids concentration, we adopt this simple approach here.

3. **Pressure drop across downcomers.** The downcomers in our unit were supplied with air to maintain them at minimum fluidization conditions. This provides a smooth

downflow of solids while allowing a high pressure head. For such cases, the solids acceleration and friction in the downcomer can reasonably be neglected. Thus the pressure at the bottom of the downcomer can be expressed by

$$P_d \approx P_{ref} + L(1-\varepsilon_{mf})\rho_p g \tag{3.27}$$

4. **Pressure drop across solids flow control valve.** The solids flow control devices used in circulating fluidized bed systems can be mechanical or non-mechanical valves, typically L-valves. Yang and Knowlton (1993) modelled an L-valve by visualizing it as a pneumatically-actuated pseudo-mechanical valve and then related the valve opening, A_O, to the total aeration. It is thus possible to express the pressure drop across the two types of valve by the following equation due to Jones and Davidson (1965):

$$\Delta P_v = \frac{1}{2\rho_p(1-\varepsilon_{mf})}\left(\frac{W_s}{C_d A_{dis}\phi}\right)^2 \tag{3.28}$$

where ϕ is the valve fractional opening (= A_O/A_{dis}). The discharge coefficient, C_d, varies from about 0.7 to 0.8 (Rudolph et al., 1991). $C_d = 0.75$ is assumed in this analysis.

5. **Conditions for steady HDCFB operation.** The operation of the HDCFB is initiated by causing air to flow into risers 1 and 2 at superficial velocities U_1 and U_2, respectively. The solids inventory in the whole system is M_{inv}, and there is no addition to, and negligible removal from, the system. Upon adjusting the openings, ϕ_1 and ϕ_2, of the two gate valves, the system attains steady operation after a transient period where the solids flowrates through the two valves differ. When steady operation is achieved, the solids flowrate anywhere in the system (ignoring losses through the gas-solids separators) is designated as W_S and the solids levels in downcomers 1 and 2 remain steady at heights L_1 and L_2 measured from their respective distributors. For simplicity the solids inventories in parts of the system other than the downcomers and risers are ignored in the overall

solids inventory balance. Under steady operation, the pressure and solids material balances around the dual-loop unit can then be written:

$$\Delta P_{v1} = P_{d2} - P_{r1} \tag{3.29}$$

$$\Delta P_{v2} = P_{d1} - P_{r2} \tag{3.30}$$

$$M_{inv} = A_{r1}\rho_p(1-\bar{\varepsilon}_{m1})H_1 + A_{r2}\rho_p(1-\bar{\varepsilon}_{m2})H_2 + (A_{d1}L_1 + A_{d2}L_2)\rho_p(1-\varepsilon_{mf}) \tag{3.31}$$

If the riser dimensions (D_1, H_1, D_2, H_2), valve fractional openings (ϕ_1, ϕ_2), superficial gas velocities in the risers (U_1 and U_2) and the total solids inventory (M_{inv}) are specified, then equations (3.12), (3.20) and (3.29) to (3.31) can be solved to give the solids circulation rate W_S, axial voidage profiles ($\varepsilon_1(z)$, $\varepsilon_2(z)$), mean voidages in the risers ($\bar{\varepsilon}_{m1}$, $\bar{\varepsilon}_{m2}$) and the steady state heights of solids in the downcomers (L_1, L_2). Alternatively, the solids circulation rate can be specified instead of the total solids inventory. Influences of various parameters can be estimated based on any realistic combination of the input variables.

3.3.3.3 Comparison with experimental data

Figure 3.26 compares the axial solids hold-up profiles predicted using Eqs. (3.12) to (3.19) in the riser to our experimental data at U = 4 m/s for G_S = 44, 138 and 240 kg/m^{2}s. Considering that the correlations were obtained from a wide range of data sources, not only from this work, there is reasonable agreement between the model predictions and the experimental data. Figure 3.27 plots measured average solids hold-ups, obtained by integrating the experimental (1 - ε) vz. z data over the riser height, for U = 4,

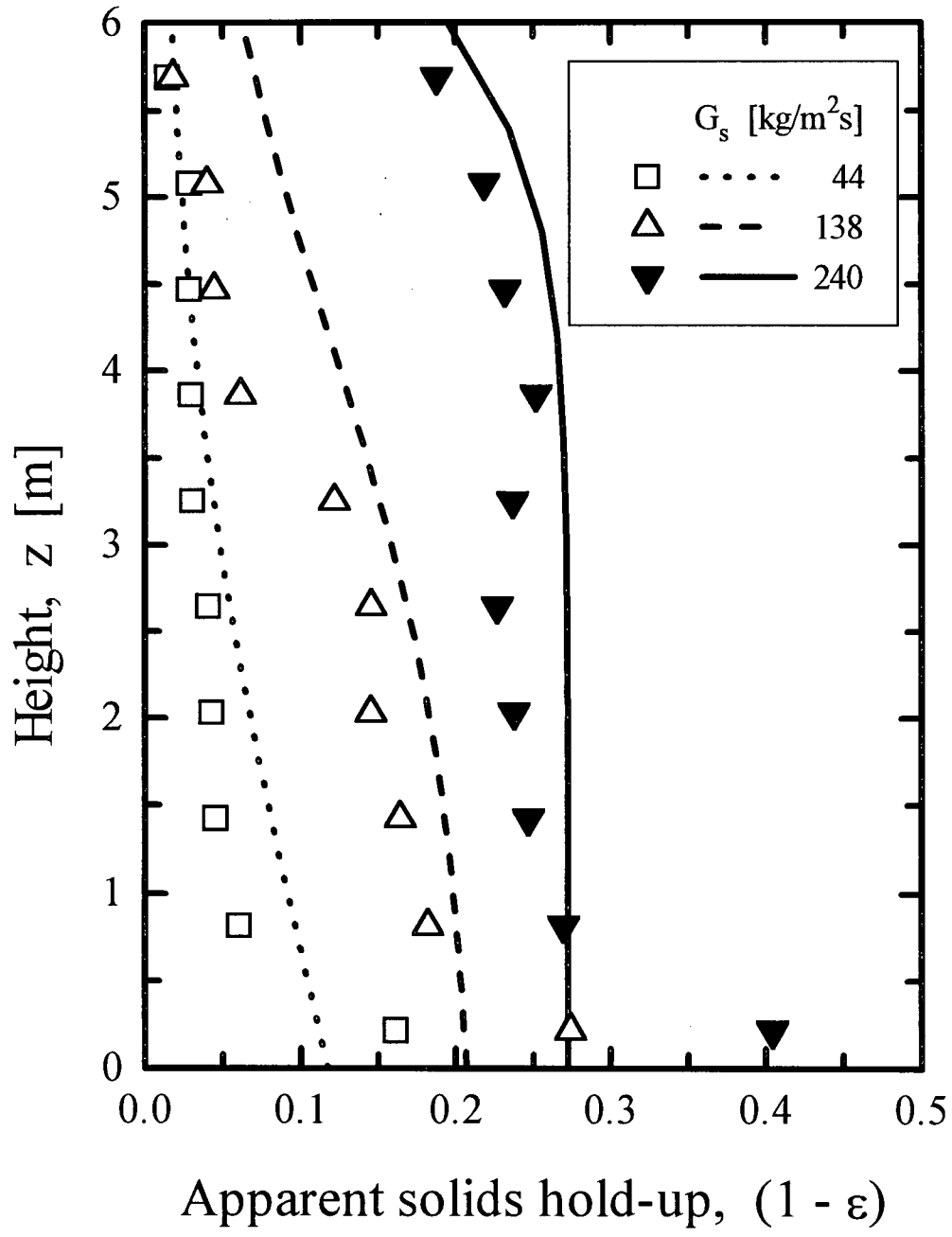

Fig. 3.26: Comparison between longitudinal apparent solids hold-up profiles predicted by Eq. 3.12 (shown by lines) and experimental values (shown by points) for U = 4 m/s and three solids circulation rates.

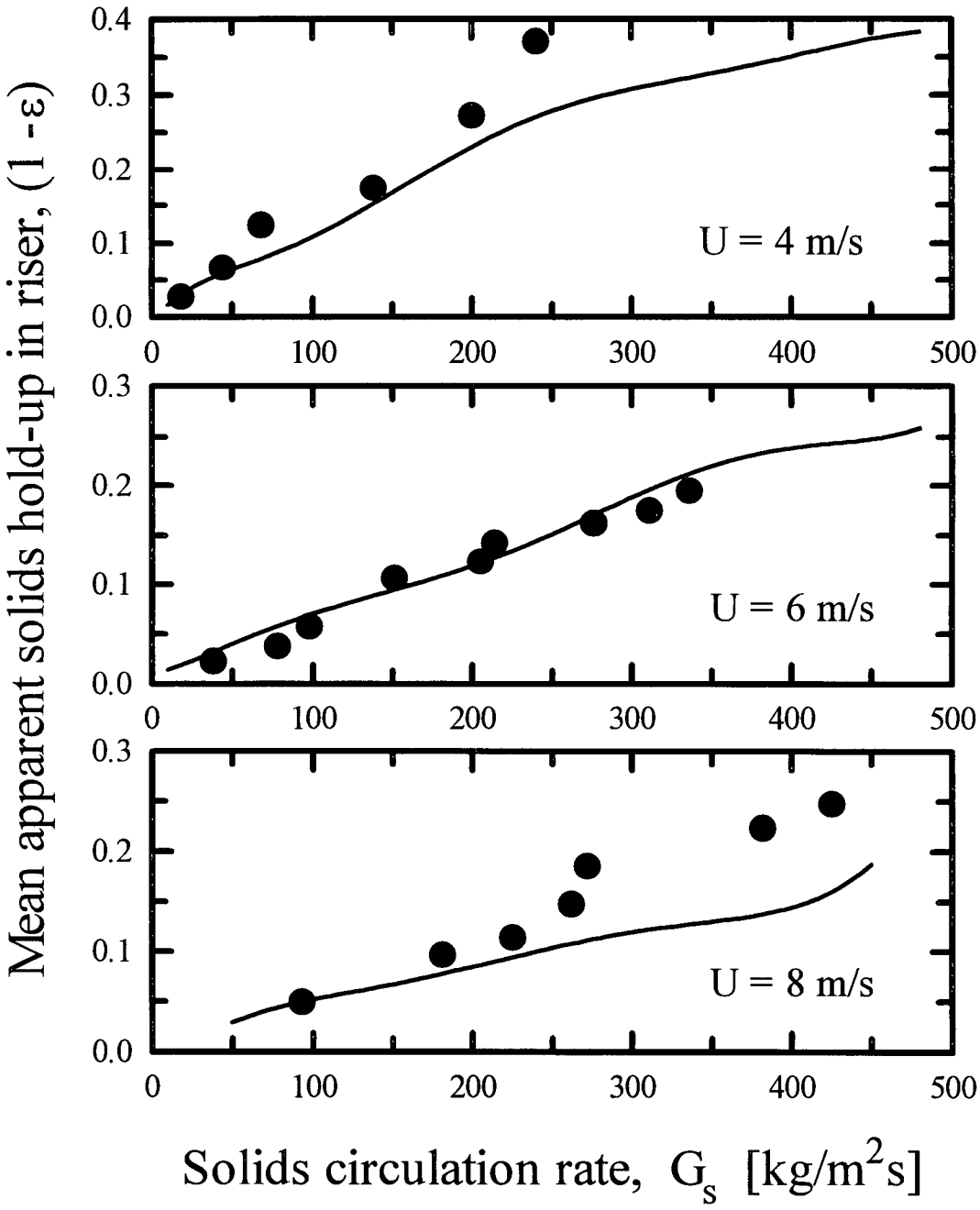

Fig. 3.27: Mean apparent solids hold-ups in riser at U = 4, 6 and 8 m/s for various solids circulation rates (• expt., —— model).

6 and 8 m/s and various solids circulation rates. Again the model predictions are seen to be quite reasonable. Appendix B.2 tabulates the operating superficial air velocity, solids circulation rate and mean solids hold-ups in both risers, together with solids inventories in the downcomers. Also included in Appendix B.2 are the corresponding calculated mean solids hold-ups, total solids inventory and solids levels in the downcomers. For this wide range of operating conditions a plot of actual solids levels in the downcomers against the predicted values is given in Fig. 3.28. The experimental solids levels are equal to, or higher than, the calculated values. This suggests that for any given operating U and G_S, there is a corresponding minimum pressure head, reflected by the levels of particles in the downcomers, required to feed solids in the riser. Additional solids in the downcomer do not influence significantly the conditions in the riser provided the feed valve is regulated to maintain the same solids flux. The additional inventory will, of course, increase the solids circulation rate if the valve is left wide open. This was observed in our measurements (Fig. 3.14) and in other studies as discussed above.

3.4 Summary

The dual-loop circulating fluidized bed unit was capable of achieving solids hold-ups as high as 0.15 to 0.25 averaged over the entire riser and solids circulation rates of 400 kg/m^{2}s and beyond. The influence of air velocity and solids circulation rate on the solids hold-up is small once high density conditions are attained. Visual observations indicate that the commonly observed net downflow of solids near the riser wall in low density CFB risers disappears at high solids flux and high density conditions, starting from the bottom and working progressively upwards, being replaced by a more homogeneous flow structure. Except for some scatter at high voidages, the slip velocity increases with solids hold-up and for any given superficial velocity there appears to be a unique

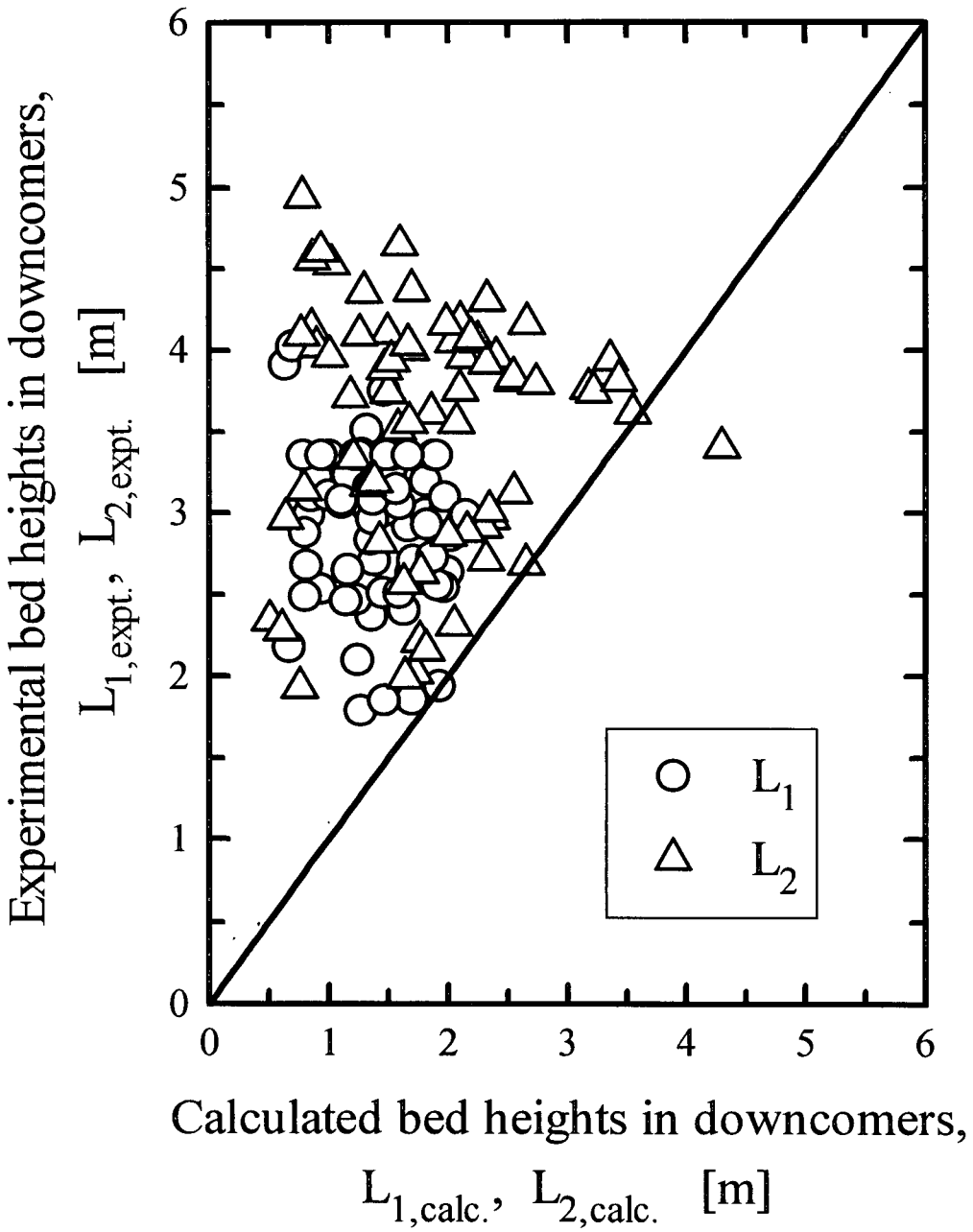

Fig. 3.28: Comparison of minimum bed heights required in downcomers to actual values used.

relationship between the two. Slip factors as high as 15 were obtained, compared to about 2 to 5 reported in the literature for the developed region of dilute risers. The values are, however, within the range of values for the dense region of risers reported in other studies. The total pressure drop across the riser was found to be directly proportional to the solids-to-air mass flow ratio over a wide range, but levels off at higher solids flowrates when the riser is wholly under high density conditions.

Correlations of literature data and data obtained in this work give reasonable predictions of longitudinal profiles of mean voidage. A pressure and overall material inventory balance analysis gives the minimum solids inventories needed to maintain steady operation for fixed G_S and U. The analysis supports observation from this work and the literature which suggest that, at a fixed solids circulation rate and air velocity, increasing solids inventories in the downcomers have a negligible effect on solids hold-ups in risers.

This chapter has described the overall flow behaviour in a CFB risers in terms of cross-sectionally averaged solids distribution along the whole riser and how it varied with experimental variables. The high average slip velocities found between the gas and solids have been attributed to the existence of particles in the suspension as dense particle clusters or other structures. The flow behaviour is not significantly influenced by solids inventories in the return loop if solids fluxes are held constant. To further understand this global behaviour, there is need for studying the flow characteristics at the local level. The combination of macro- and microstructure studies would then lead to a more realistic conceptual understanding of the flow dynamics of high density CFB risers. The next chapter deals with radial profiles of local solids concentration in the riser.

CHAPTER 4

LOCAL VOIDAGE PROFILES

4.1 Introduction

Local voidage is an important parameter in circulating fluidized bed reactors. Time-averaged local voidage profiles indicate the local solids distribution in the riser while instantaneous local voidage data aid the understanding of the local flow structure. Since it is not yet possible to predict the complex fluid dynamics, transport and chemical behaviour in CFB risers from fundamental equations, most presently available models require empirical inputs, which can only be obtained through experimentation.

Many experimental techniques have been developed for measuring various parameters in fluidized beds as reviewed by Grace and Baeyens (1986), Cheremisinoff (1986), Williams, et al. (1991), Werther, et al., 1993; Yates and Simons (1994) and Louge (1997). The most commonly used methods for measuring local voidages in circulating fluidized bed risers are X-ray and γ-ray attenuation, capacitance probes and optical fiber probes.

In X-ray and γ-ray densitometers, a radioactive source emits a beam of X-rays or γ-rays across the column through its wall to a detector. The photons interact with the detector material to produce charge pulses (ionization type detector), or light pulses (scintillation type detectors) which are then transformed into DC signals proportional to the radiation received. Plate or movie film exposures can also be taken to give snapshots

of the solids distribution (e.g. Weinstein et al., 1992). With calibration, the concentration of particles along a chord can then be determined from the attenuation of the measured X-ray or γ-ray signal. In many cases, the calibration has been based on comparison of the signals with voidages calculated from differential pressure profiles. It is, therefore, questionable whether the measurement volumes in the two instances are identical. Weimer et al. (1985) examined several practical issues involving γ-ray measurements and noted that the technique is too slow for time-dependent measurements in fluidized suspensions. The technique can therefore be considered to give length-averaged time-averaged densities, rather than localized instantaneous measurements.

Tomographic images and 3-D density maps can be obtained if the radiation source and detector are moved or if several sources and detectors are employed together to scan the riser along a number of chords (e.g. Galtier, et al., 1989; Martin et al., 1992; Simons et al., 1993). Other studies have been intrusive (e.g. Schuurmans, 1980; Wirth et al., 1991; Miller and Gidaspow, 1992) in which a detector is placed externally and the radiation source traverses the riser internally. X-ray and γ-ray equipment requires a large space around the riser, and safety precautions are necessary to avoid radiation exposure. In addition, the equipment is expensive, virtually limiting its use to pilot and industrial installations (Bartholomew and Casagrande, 1957; Saxton and Worley, 1970; Schuurmans, 1980; Martin et al., 1992).

Capacitance transducers work on the principle that solids inside a sensing volume alter the effective dielectric constant (permittivity) of the gas/solid mixture. Therefore the capacitance can be used to indicate the concentration of solid particles. Since fluidized bed particles are typically non-conducting materials (silica, silica-alumina, etc.), capacitance is usually a more appropriate property to measure than electrical resistance or conductivity. Various probe configurations have been used, ranging from parallel plates to needle-

shaped probes. The instrumentation is simple, inexpensive and relatively easy to construct. The system, however, requires calibration for each bed material. Problems associated with the technique include drift of the probe signal, e.g. due to capacitance change caused by humidity or temperature variations. Other problems include the possibility of powder build-up on the probe and difficulty in delineating the exact measuring volume.

In optical fiber probes a bundle of fibers projects light onto a swarm of particles and the solids concentration is inferred from the intensity of either the reflected light (reflective-type probes) or the transmitted light (transmission probes). The transmission method is restricted to relatively low solids volume fractions because the emitted light is totally attenuated by the particles at higher concentrations (Yang et al., 1987; Wether et al., 1993). Reflective probes, on the other hand, may be used over the entire range of particle concentrations up to the fixed bed state, once they have been suitably calibrated. Some advantages of optical fiber probes include insensitivity to high voltages, parasitic electrical effects and magnetic fields, very low signal loss along the fiber, low weight, small dimensions, high flexibility of geometric configuration, high sensitivity and low cost. They have a disadvantage of perturbing the flow, but the extent of interference can be minimal if the probe is sufficiently small. A reflective-type optical fiber probe was chosen for this work after considering such factors as cost, availability, suitability for our particles and operating conditions, together with the fact that considerable experience had been gathered using optical probes in previous studies in our department (e.g. Bi, 1994; Zhou, 1995; He, 1995).

Local voidage profiles in vertical suspension flows have been studied for many years both in industry and in academia. Bartholomew and Casagrande (1957), Hunt et al. (1957), Saxton and Worley (1970) and Schuurmans (1980) used γ-ray absorption to establish solids concentration profiles in commercial scale catalytic cracking riser reactors.

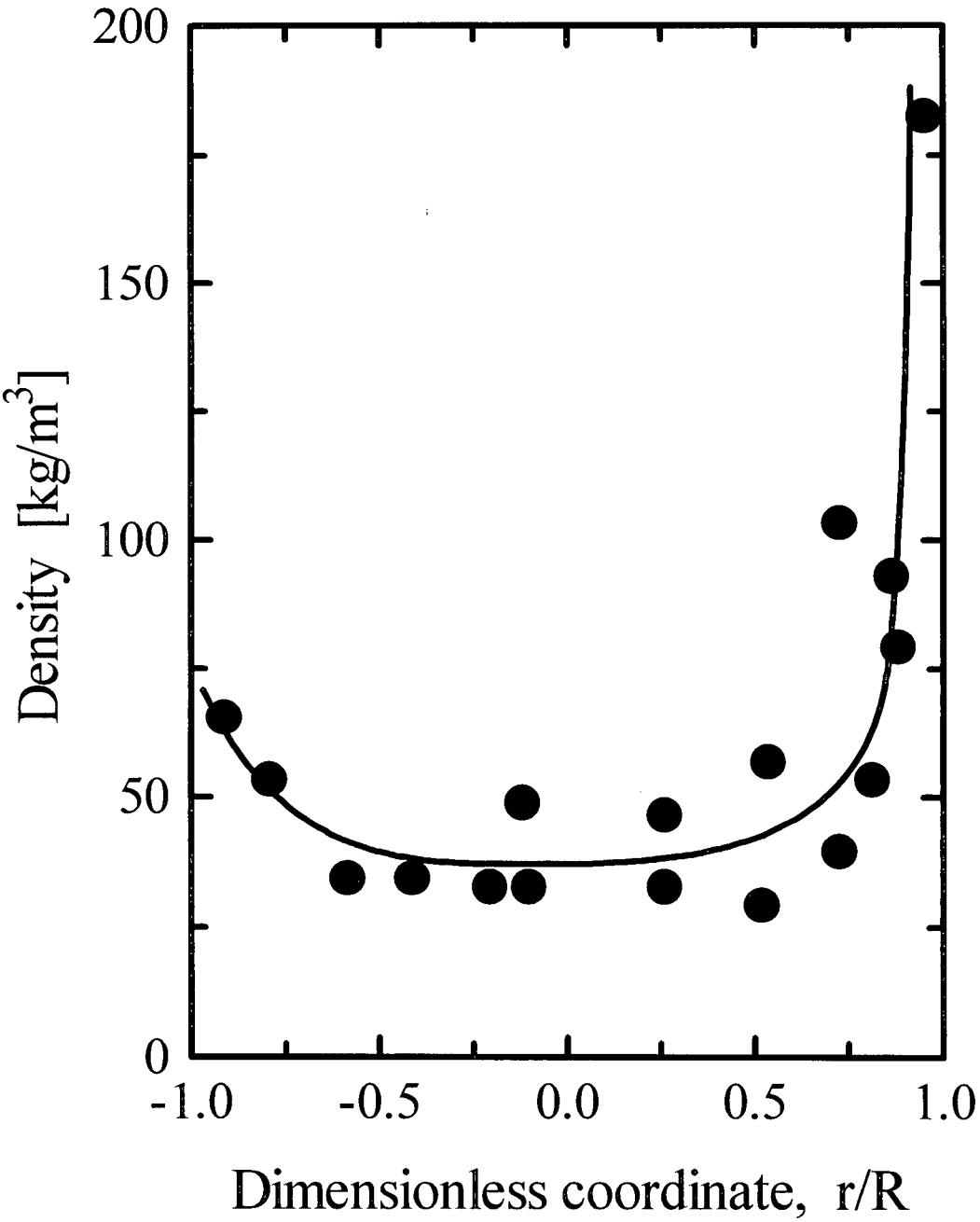

Fig. 4.1: Sample radial profile of catalyst density in a fluid catalytic cracking riser (D ≈ 0.7 m, H ≈ 30 m, Oil feed rate = 3000 t/day). Replotted from Schuurmans (1980).

Strong segregation of catalyst toward the wall was found. Figure 4.1 shows a sample of radial catalyst profile obtained by Schuurmanns (1980). The same kind of radial segregation of solids into a dilute core region surrounded by a relatively dense annulus was later found in the upper dilute region of circulating fluidized bed risers. Some examples of studies on radial voidage profiles, listed according to measurement technique, are: γ-ray absorption (e.g. Hartge, 1989; Azzi et al., 1991; Martin et al., 1992), X-ray absorption (e.g. Weinstein et al., 1986; Miller and Gidaspow, 1992), optical fiber probes (e.g. Hartge et al., 1988; Kato et al., 1991; Reh and Li, 1991; Zhang et al., 1991; Zhou et al., 1994; Nieuwland et al., 1996), and capacitance probes (e.g. Hartge et al., 1986; Herb et al., 1989; Riley and Louge, 1989, Louge et al., 1990; Brereton and Grace, 1993). Visual observation and measurements of particle velocity or solids flux (e.g. Bader et al., 1988; Herb et al., 1992) have also revealed that the core region is dominated by an upflowing solids suspension while solids travel downwards in the annulus, mostly in forms of clusters, strands, swarms or particle sheets (e.g. Brereton, 1987; Horio and Kuroki, 1994). Zhang et al. (1991) found that decreasing the superficial gas velocity or increasing the solids circulation rate increases the overall solids concentration and steepens the voidage profile. The profiles become more uniform with increasing height (Kato et al., 1991; Yang et al., 1991; Brereton and Grace, 1993), although this could be due to the decrease of solids hold-up with increasing height.

Most attention has so far been focussed on the top dilute region. The bottom dense region, as well as fully dense CFB risers, have received relatively little attention. Very few systematic measurements of local parameters have been conducted to determine the flow behaviour in high-flux dense systems. Bolton and Davidson (1988) and Bai et al. (1995b) indicated that the lower dense bed region is in the turbulent bed regime, while others (e.g. Johnsson et al., 1992; Svensson et al., 1996) have treated the lower region as a bubbling fluidized bed. Werther (1994) suggested that the lower dense region may be turbulent in a

laboratory riser, but bubbling for larger risers. Weinstein et al. (1984) using X-ray photography in a 0.152 mm ID riser with 59 μm particles appear to have presented the first radial voidage profiles in the dense region of a CFB riser. Nearly parabolic voidage profiles were observed for U = 3.1 m/s and G_S = 90 kg/m^{2}s with a voidage of about 0.65 near the wall and about 0.92 in the center. Hartge et al. (1986) used an optical fiber probe to measure radial voidage profiles in risers of diameters 0.05 and 0.40 m with quartz particles of mean size 58 μm for U = 3.9 and 5.0 m/s and G_S = 100 and 75 kg/m^{2}s, in the respective risers. The profiles in the dilute region appeared relatively flat, with a slight increase close to the wall. On the other hand, the profiles in the dense zone were much steeper with solids concentration in the central region between 5 and 10%, reaching 30 to 40% near the wall. Louge et al. (1990), using a capacitance probe in a riser of diameter 0.2 m with 61 μm FCC particles for U = 2 m/s and G_S up to 40 kg/m^{2}s, found that the voidage near the wall was always lower than the average voidage across the riser. Although these studies give some insight into the flow structure of the dense zone in CFB risers, the solids circulation rates and gas velocities employed are well below those in commercial fluid catalytic cracking installations (see Table 1.1). In Chapter 3, solids fluxes exceeding 400 kg/m^{2}s were attained at gas velocities reaching 8 m/s, and it was observed that the dense region, with average solids holdup of about 0.2, extended over the entire riser height. The riser then exhibited an almost homogeneous longitudinal flow structure with negligible downflow of solids at the wall. This chapter explores further the flow structure in risers under high density conditions based on measurements of radial voidage profiles.

4.2 Measurement method

4.2.1. Principle of operation of optical fiber probe

Optical fiber probes were initially used in conventional fluidized beds to measure particle and bubble velocities (Okhi and Shirai, 1976; Ishida and Shirai., 1980; Ishida et al., 1980) through cross-correlation of the reflected light signals from two probes arranged one above the other, separated by a known distance. Morooka et al., (1980) and Matsuno et al. (1983) extended their use to measure particle concentration in the freeboard region. Okhi et al. (1975) used optical fibers to estimate particle sizes in flowing suspensions. Their application to solids concentration in CFB risers was pioneered by Qin and Liu (1982). Many later studies have adopted this method (e.g. Horio, et al., 1988; Hartge et al., 1986, 1988; Kato et al., 1991; Nowak et al., 1990; Zhang et al., 1991; Reh and Li, 1991; Werther, et al., 1993; Herbert, et al., 1994; Zhou et al., 1994).

Depending on the relative size of the particles and the probe, two types of probes can be identified for particle concentration measurement, as shown in Fig. 4.2. If the particle diameter is larger than the fibre core diameter (Type 1) single particles are detected. The output signals from the light receiver are converted to pulses at any threshold level, V_c and the pulse count corresponds to the number of particles. It is necessary to know the particle velocity in order to convert the number of pulses in a given time interval to particle concentration. The method requires a long time to measure particle concentration with high accuracy, and gives only average concentrations. On the other hand, if the particle diameter is much smaller than the probe core diameter (Type 2), the reflected light comes from many particles in the measurement volume. Instantaneous solids volume concentration can then be inferred from the output voltage if a suitable calibration is available. A type 2 method was used in this study. The penetration of light

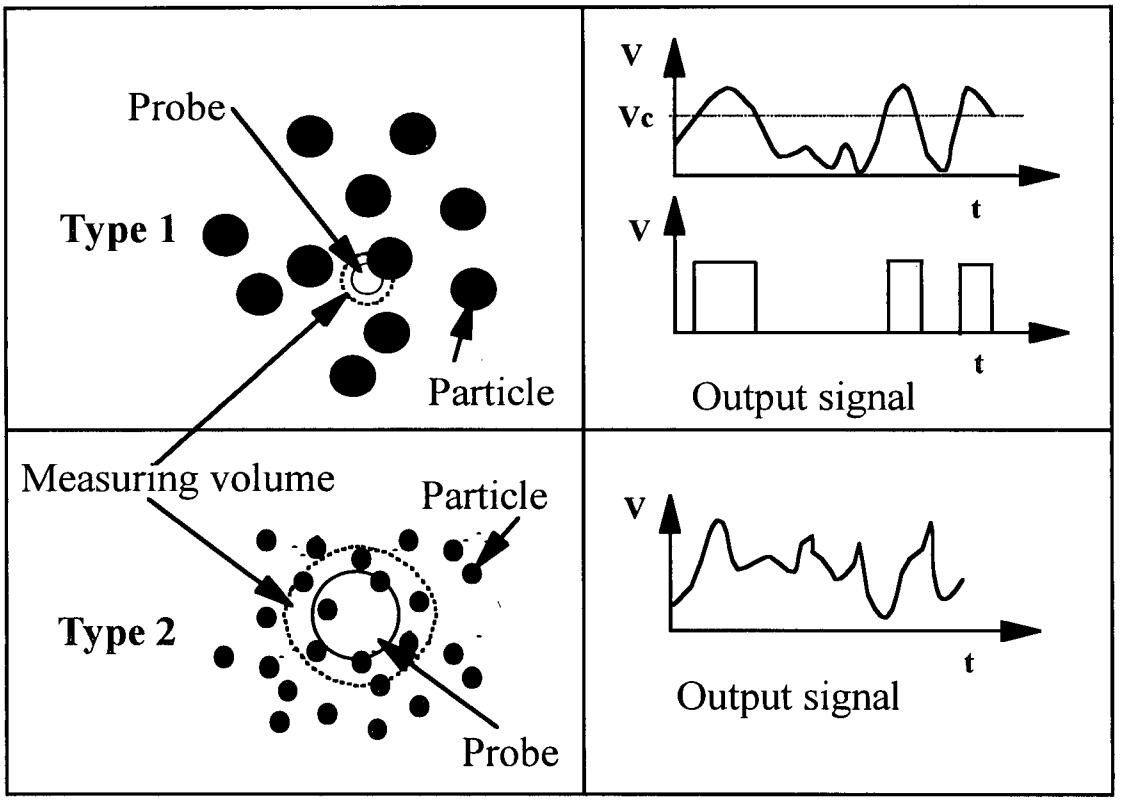

Fig. 4.2: Optical fibre probes for measuring local particle concentrations: Type 1 - Detection of single particle; Type 2 - Detection of swarm of particles (Matsuno et al., 1983).

into the suspension and, consequently, the size of the measuring volume depends on the local solids volumetric concentration (Lischer and Louge, 1992). Zhou (1995) using 213 μm sand particles found that the penetration length was about 7 mm for voidages approaching unity, decreasing to about 4 mm for a voidage of 0.6 and was even smaller near the wall where voidages were lower. Reh and Li (1991) attempted to minimize the measurement volume using a crossed-fiber arrangement, the two fiber bundles converging at an angle of 30 - 35°, while Turner et al. (1993) used a small lens to achieve convergence with a single fiber probe. To measure very low local solids hold-ups (0.2 to 0.7%), Sobocinski et al. (1995) used a probe with a rounded (hemispherical) tip. This was able to converge the light at a distance of approximately 500 μm. Voidages encountered in the present work tend to be relatively low so that the measurements are expected to be more localized on average than those reported previously.

Figure 4.3 shows schematically the fiber optic system used in this work. It is similar to that used by Zhou (1995). The optical fiber probe is made of two bundles of quartz fibers encased in a 3 mm ID stainless steel tube with a 2 x 2 mm square active tip area. The individual quartz fibers are 15 μm in diameter. One bundle of fibers carries light from a source and projects it onto the passing swarm of particles. The other interspersed bundle transmits the light reflected by the particles to a phototransistor which converts the light into an electrical signal. An amplifier raises the resulting signal to a voltage range of 0 - 5 V, after which the signal is fed to a PC computer via a DAS8-EXP16 A/D converter. Within the probe fibers are arranged in an array in which the fibers acting as light projectors alternate with fibers acting as light receivers. In any run, the HDCFB unit was brought to steady conditions, and then local voidages were measured at different radial positions by traversing the probe horizontally. Measurements were made at ten radial locations between the center and the wall: r = 0.0, 12.7, 18.0, 22.0, 25.4, 28.4, 31.1, 33.6, 35.9 and 38.1 mm. In early measurements, the probe was traversed from one wall to the

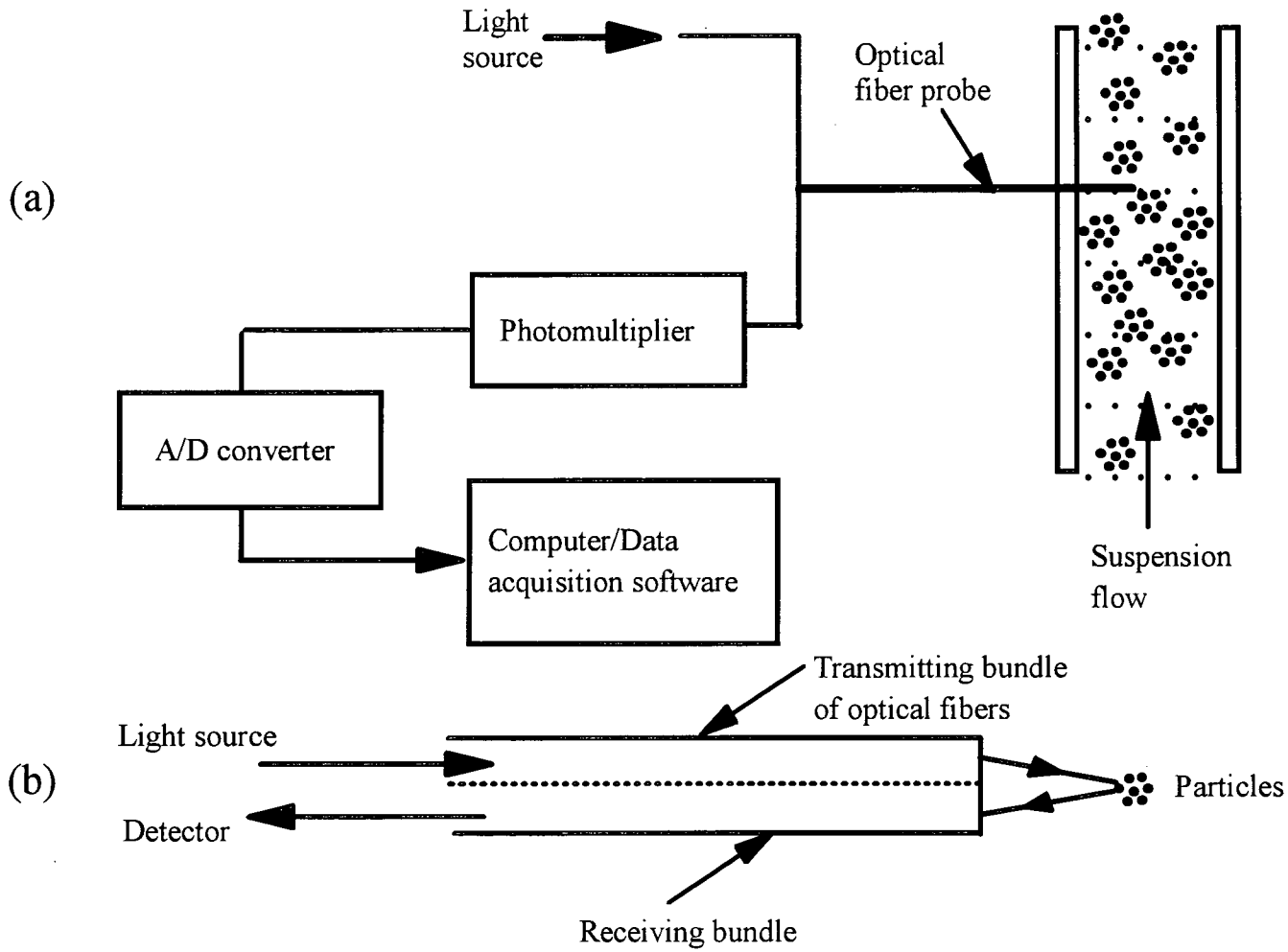

Fig. 4.3: Schematic diagram of local voidage measurement apparatus and configuration of reflective optical fiber probe: (a) overall set-up; (b) probe itself.

other and no significant asymmetry was found in the voidage profiles. The sampling frequency was 100 Hz and the duration of measurement 100 s. The same procedure was repeated for different solids circulation rates and superficial velocities at different levels. For each measurement location, the column, extending about 0.3 m above and below the probe, was wrapped with a black plastic sheet to prevent external light from penetrating into the riser and interfering with the measurements.

4.2.2 Calibration of optical fiber probe

The accuracy of optical fiber probe data relies upon the precision of the calibration. Various methods have been employed. Matsuno et al. (1983) calibrated their probe in a stream of glass beads falling from a vibrating sieve and inferred the concentration of the particles passing in front of the probe from the measured particle flux and particle velocity, assuming the latter to be equal to the single particle terminal falling velocity. This calibration method is, however, limited to dilute systems. Matsuno et al. (1983) calibrated their probe by allowing particles to fall through a stagnant liquid and assuming them to attain a velocity equal to the single particle terminal velocity. Hindered settling likely influenced their data. Zhang et al. (1991) used the cross-sectional average voidage inferred from static pressure drop measurements to calibrate their probe. Hartge et al. (1986) obtained a linear relationship for quartz particles in a water-fluidized bed for solids volume fractions up to 50%. They then assumed linearity in their gas-solid riser and calibrated their probe by comparing the optical signal to two concentration values obtained by γ-ray absorption in the actual measurements. A similar assumption has been made in other studies (e.g. Kato et al.; 1991; Zhou et al., 1994). Hartge et al. (1989) using solid-liquid suspensions with FCC and sand particles, suggested an empirical fit of the form $\Delta I = k(1-\varepsilon)^n$ and found that the exponent n was independent of the fluid properties. This implies that n can be determined from a calibration in a liquid-solid mixture, where a

homogeneous mixture can be readily obtained by agitation, and the constant k can then be established by measuring the output signal in a loose packed bed of particles of known voidage. Using sand in both water and polyethylene glycol, Nieuwland et al. (1996) obtained similar results. Lischer and Louge (1992) found a similar power law from an *in situ* calibration of their optical fiber using a capacitance probe. They, however, also noted the influence of refraction by the particles and by the suspending medium. A mathematical simulation of the output of a single fiber immersed in a suspension of spheres showed the output to be influenced by particle size and the ratio of the refractive indices of the particles and the suspending medium. Therefore immersing optical fibers in liquid may provide a misleading calibration for gas suspensions. Yamazaki et al (1992) reached similar conclusions from measurements in a stirred tank. A non-linear calibration curve was also obtained by Herbert et al. (1994) who placed the optical fiber flush with the inner wall of a square tube and recorded the output signal as FCC particles fell uniformly. The corresponding voidage was calculated from the mass of solids collected and the particle velocity, which was simultaneously measured by the probe. A potential disadvantage of this procedure is that the calibration takes place under non-obtrusive conditions, while in practice the measurements are almost always intrusive.

In view of the different calibration results discussed above and the probable dependence of the signal intensity on both the fluid and solids properties, a new calibration procedure was developed in this study. The equipment is shown in Fig. 4.4. FCC particles fall from an incipiently fluidized bed through a short piece of tube in the center of a punched plate distributor covered with fine wire mesh into a 12 mm ID tube, where they fall into a collection vessel. Once a steady flow was ensured, the signal from the optical fiber probe, inserted in the tube 1.5 m from the top, was recorded at 100 Hz for durations of 30 s. Then the two slide plates (32 mm apart) were closed quickly and simultaneously to trap the solids in a section of pipe surrounding the probe. Measurement of the mass of

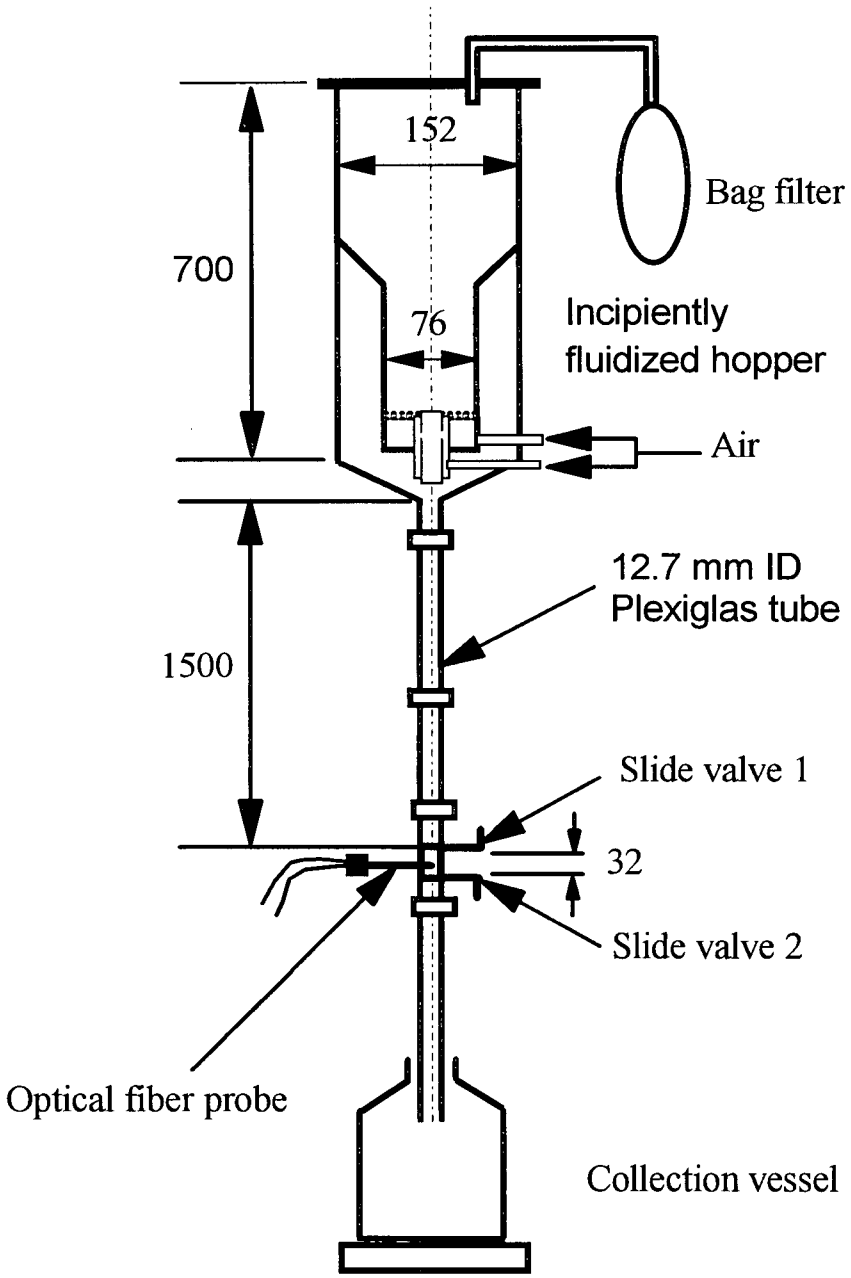

Fig. 4.4: Schematic diagram of equipment for calibrating optical fiber probe (dimensions in mm).

the trapped solids then allows the solids concentration to be calculated. By using different sizes of feeding tube and the flow of aeration air, different concentrations of solids up to nearly ε_{mf} could be obtained. A small concentration (0.5% by weight) of Larostat 519 powder was mixed with the FCC particles, to eliminate static electricity. The calibration data are presented in Fig. 4.5. Least squares fitting of the data gave the calibration

$$\frac{1-\bar{\varepsilon}}{1-\varepsilon_{mf}} = \left(\frac{V - V_0}{V_{mf} - V_0}\right)^{2.028} \tag{4.1}$$

where V_O (= 0) and V_{mf} are time-mean voltages recorded without solids and in a loose-packed bed, respectively. ε_{mf} = 0.45 for the FCC particles used in this study.

4.3 Results and Discussion

4.3.1 Time-mean local voidage profiles

Figure 4.6 shows a typical trace of the instantaneous local voidage, ε_t, against time obtained by the optical fiber probe. Rapid fluctuations with variable amplitudes are observed reflecting rapid local changes in suspension density. Averaging such data over the duration of measurement gives the time-mean local voidage, $\bar{\varepsilon}$

$$\bar{\varepsilon} = \frac{1}{T}\int_0^T \varepsilon_t dt = \frac{1}{N}\sum_{i=1}^{N} \varepsilon_{ti} \tag{4.2}$$

The cross-sectional mean voidage, ε_m, is obtained by integration of the local time-mean voidage, $\bar{\varepsilon}$, over the riser cross-section,

$$\varepsilon_m = \frac{1}{R^2}\int_0^R 2\bar{\varepsilon} r dr = \int_0^1 2\bar{\varepsilon}\varphi d\varphi \tag{4.3}$$

where φ = r/R.

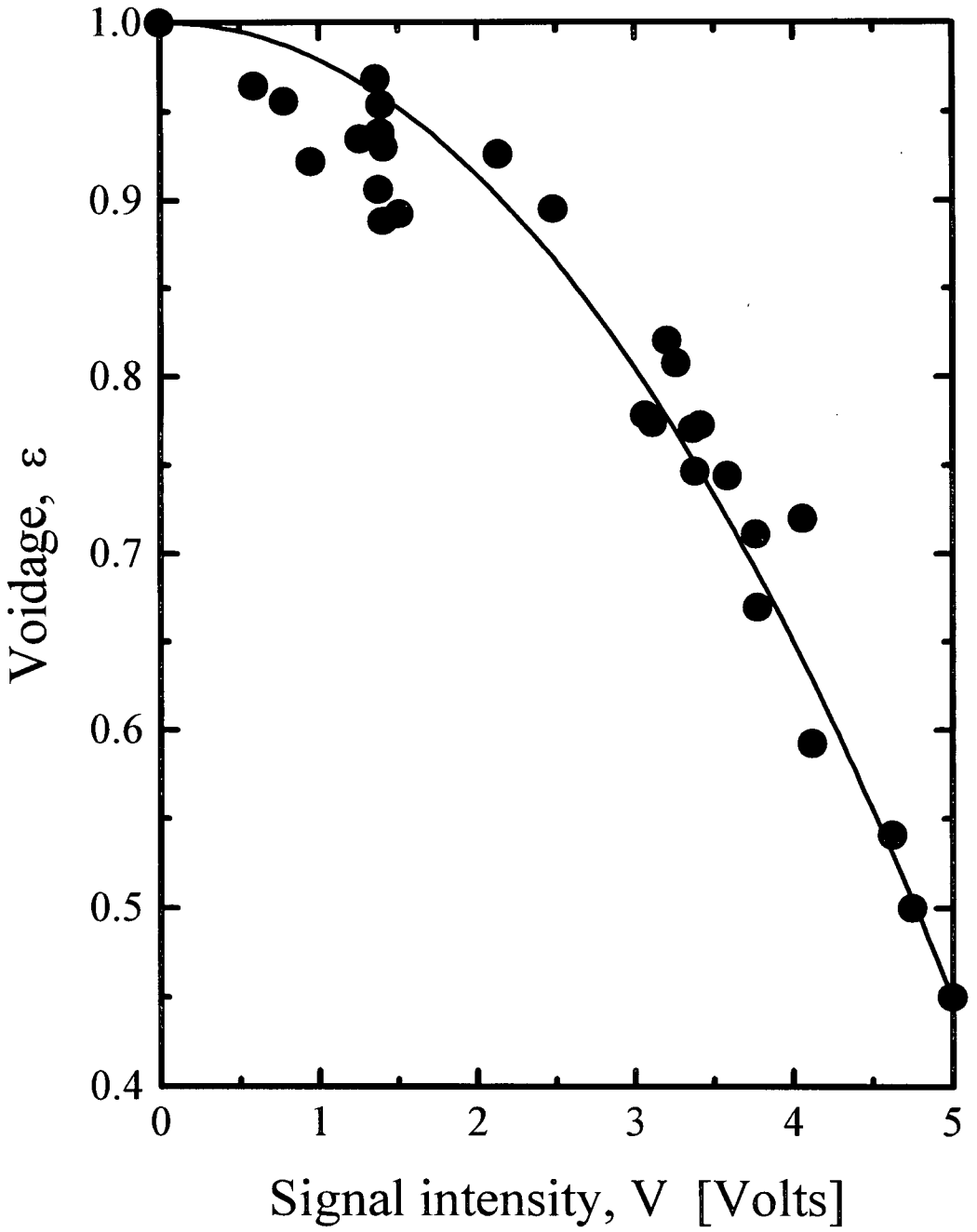

Fig. 4.5: Calibration plot for optical fiber probe. The line is a least squares fit given by Eq. (4.1).

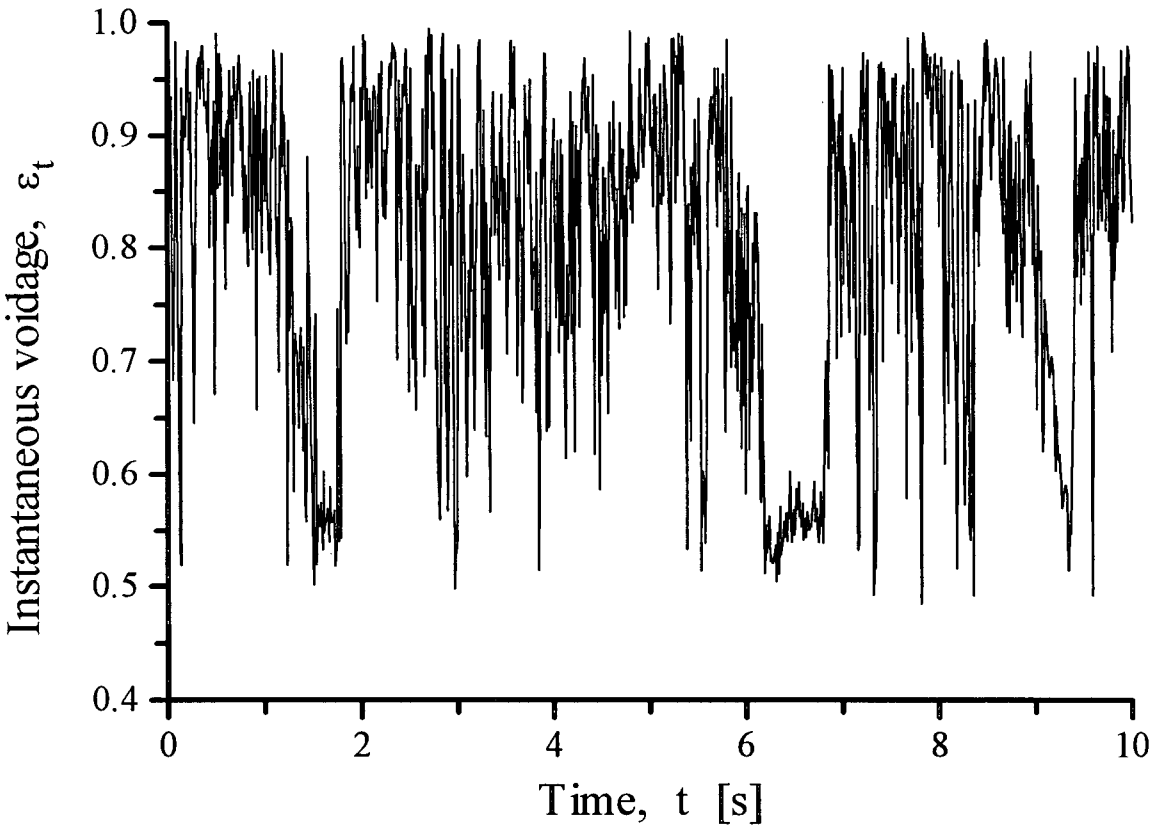

Fig. 4.6: Local instantaneous voidage versus time for radial position r/R = 0.75 at height of 3.4 m. (U = 8 m/s, G_s = 389 kg/m^{2}s).

Figure 4.7 plots the local time-mean radial voidage profiles at z = 1.57 m for U = 4.0 m/s and different solids circulation rates. For the very dilute condition at G_S = 14 kg/m^{2}s, the profile is nearly flat over the whole cross-section, corresponding to pneumatic transport conditions. The mean overall cross-sectional voidage is then 0.995. At G_S = 52 kg/m^{2}s, the overall cross-sectional mean voidage is about 0.9, and the local voidage profile remains relatively flat over a considerable radial distance before falling off sharply near the wall. Visually, solids were then observed to be moving downward at the wall, consistent with the results of the studies cited above on dilute CFB risers. Further increase of solids circulation rate to 196 and 246 kg/m^{2}s led to high density conditions in the riser with cross-sectional time-mean voidages of 0.81 and 0.76, respectively. As for low solids flux and dilute conditions, there was a dense annular region near the wall and a relatively dilute region in the core of the riser for these conditions. The voidage drops relatively gradually from a value of less than 0.95 at the center to as low as nearly 0.5 at the wall. There is no clear boundary between the dilute and dense zones.

Figure 4.8 gives radial voidage profiles for the same height as in Fig. 4.7 for a superficial air velocity of 8.0 m/s and solids circulation rates up to 425 kg/m^{2}s. The riser was under dense conditions at this height and radial segregation of solids into a dilute core and a relatively dense wall zone is again observed. Comparison of Figs. 4.7 and 4.8 shows that there is a small increase in local voidage with increasing superficial air velocity at similar G_S. Figure 4.9 shows the voidage profiles at z = 2.5 m for U = 6.0 m/s and different solids circulation rates. Except at the lowest solids flowrate, the local voidage profiles dropped off rather sharply near the wall. Figure 4.10 plots radial voidage profiles at four heights for U = 6.6 m/s and G_S = 234 kg/m^{2}s. Solids segregation into a relatively dilute core and a relatively dense outer region near the wall occurs at all heights. The local voidage increases with height, the increase being more significant towards the wall where

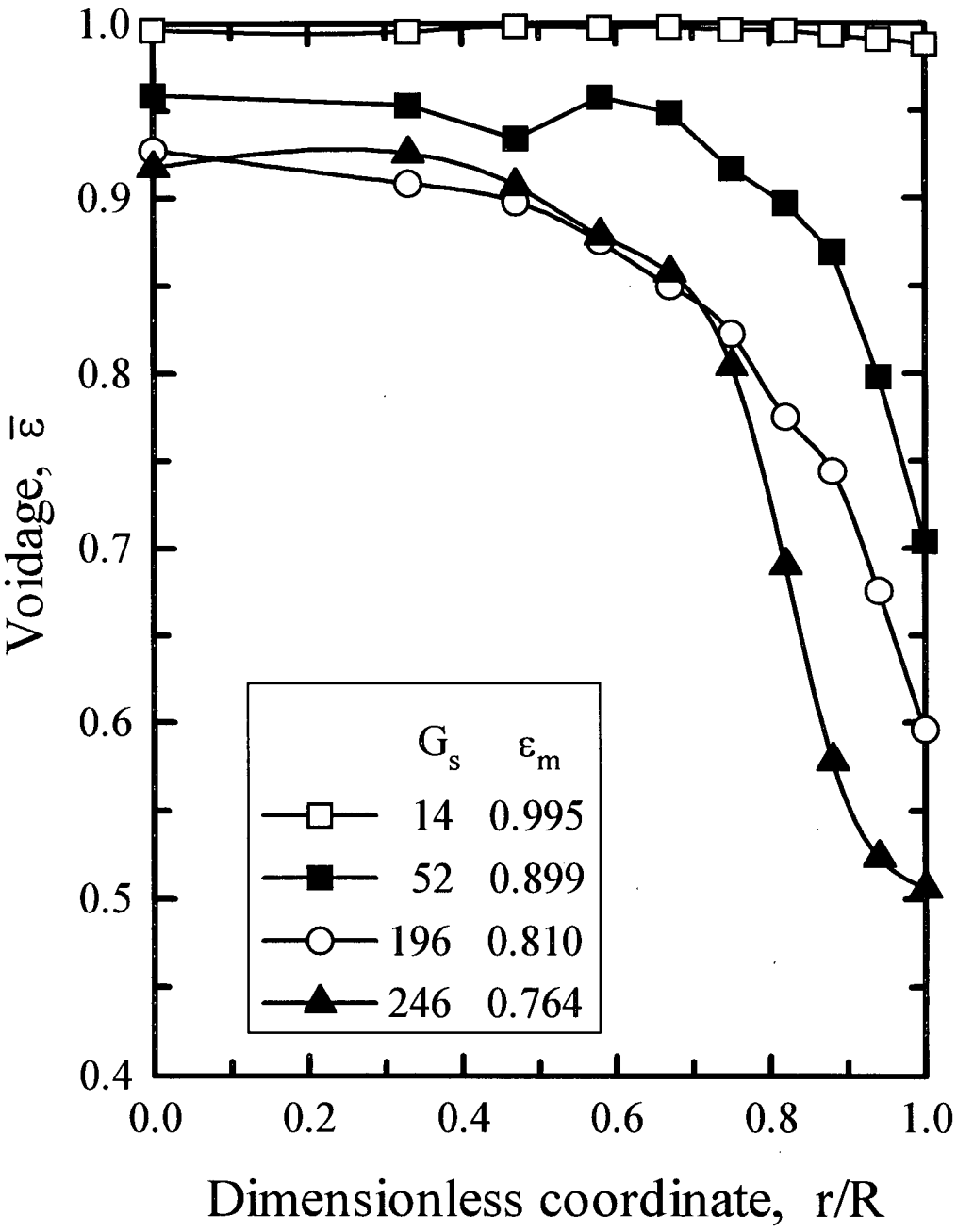

Fig. 4.7: Radial voidage profiles at U = 4.0 m/s for z = 1.57 m and various solids circulation rates.

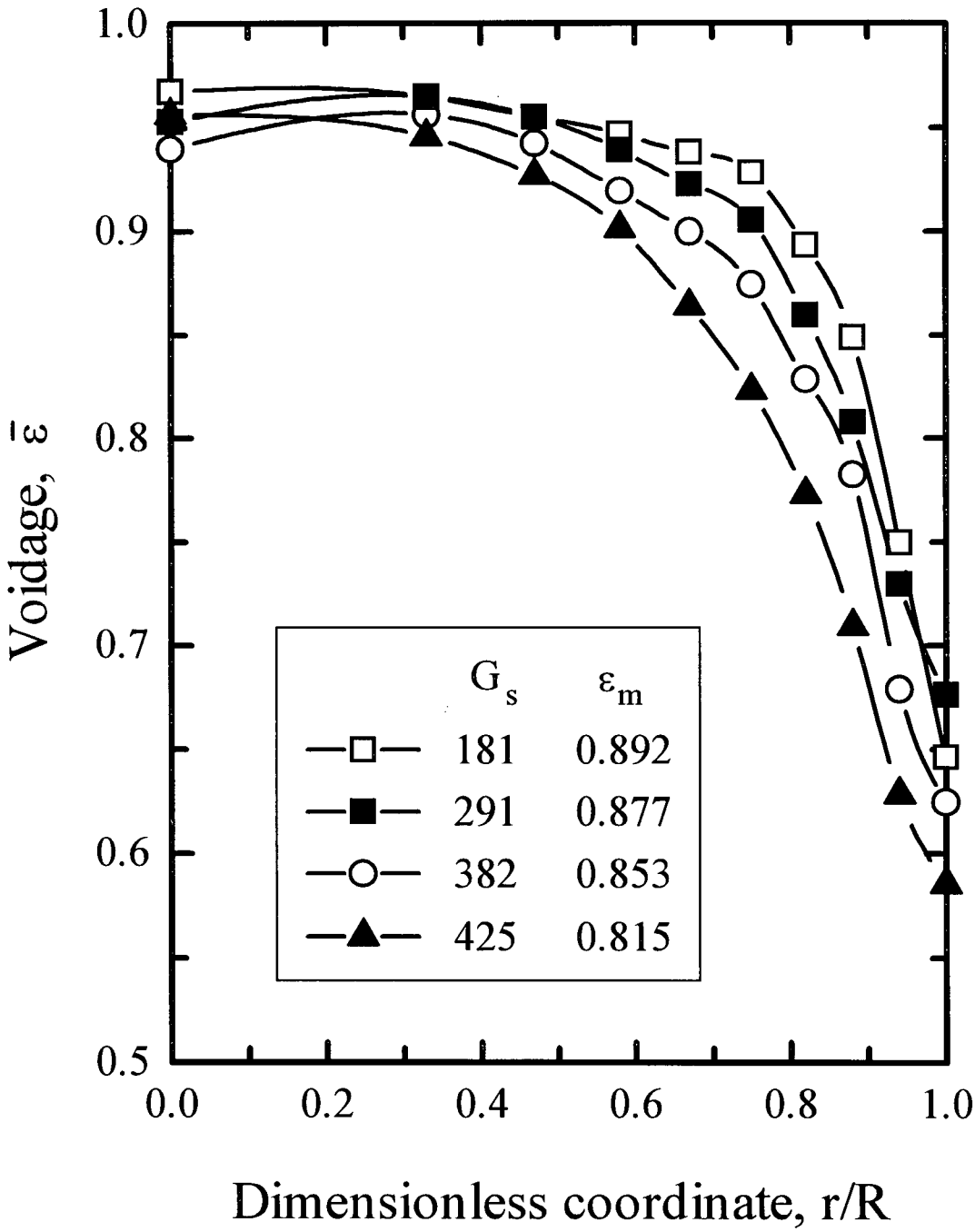

Fig. 4.8: Radial voidage profiles at U = 8.0 m/s for z = 1.57 m and various solids circulation rates.

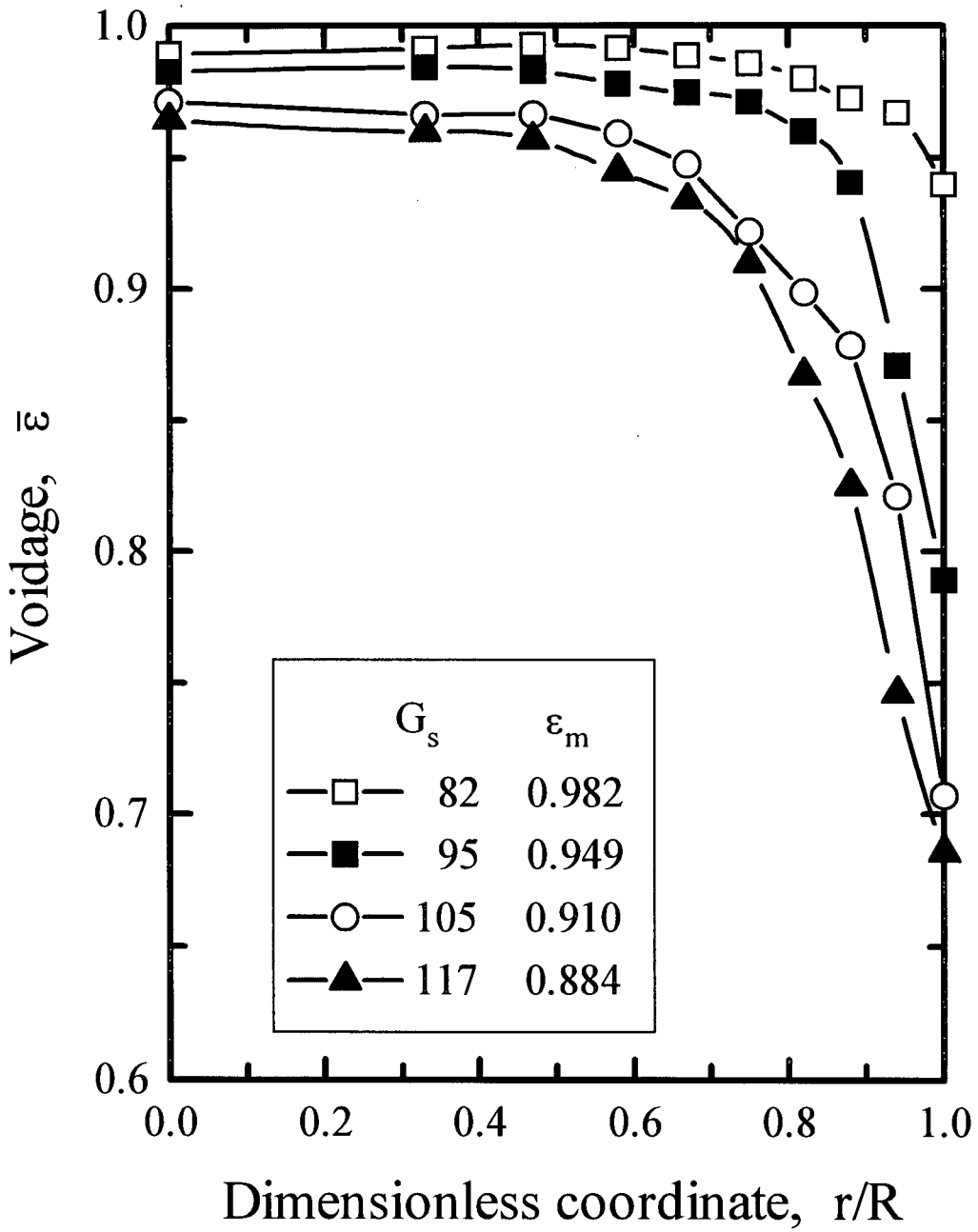

Fig. 4.9: Radial voidage profiles at U = 6.0 m/s for z = 2.5 m and various solids circulation rates.

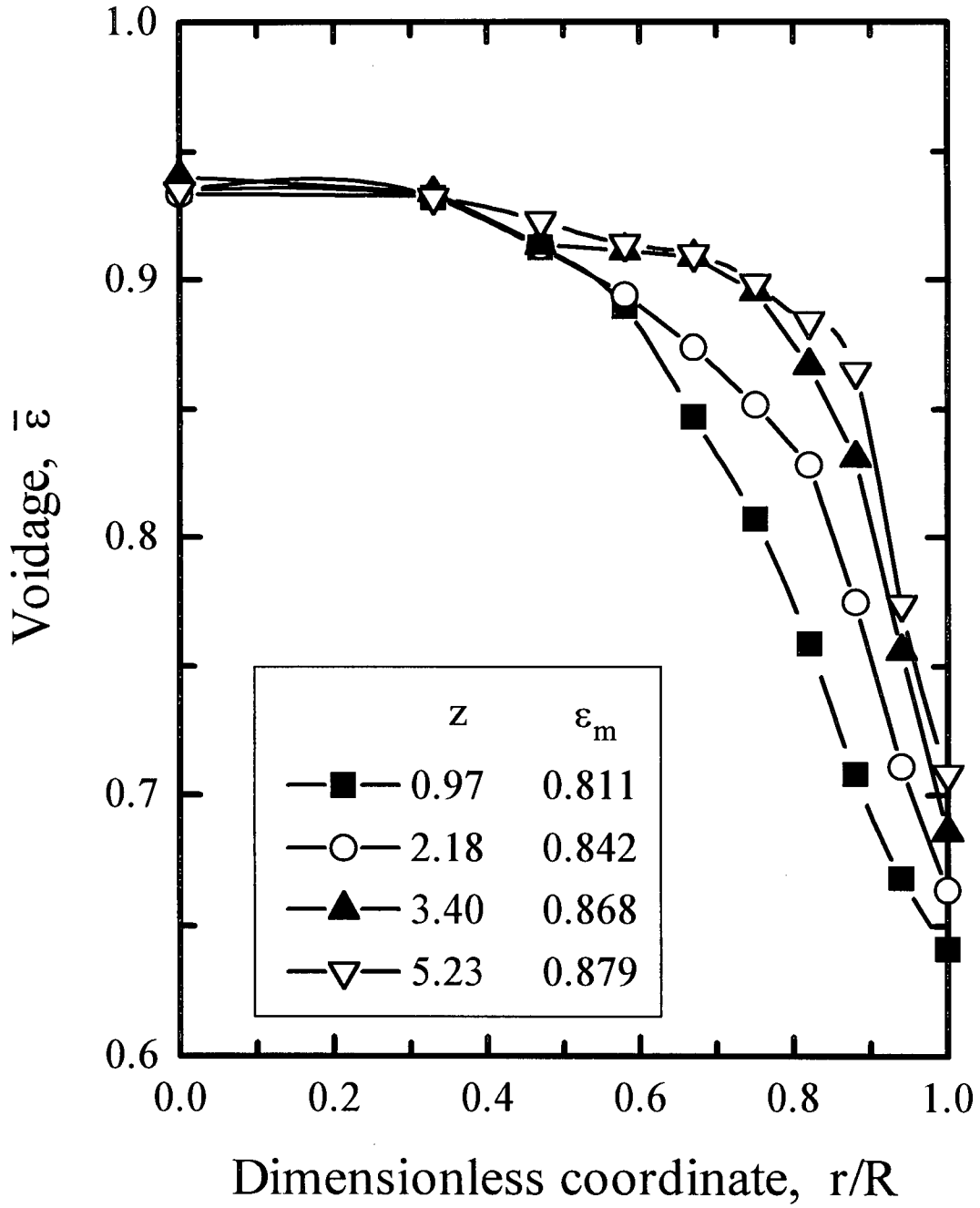

Fig. 4.10: Radial profiles of local voidage at different heights for $U = 6.6$ m/s and $G_S = 234$ kg/m^{2}s.

it changes from about 0.65 at z = 0.97 m to about 0.70 at z = 5.23 m. Along the axis of the column the voidage remained at about 0.94. Similar observations can be deduced from Figs. 4.11 and 4.12 where voidage profiles are given for three heights in the riser at U = 7.0 m/s, G_S = 246 kg/m^{2}s and U = 5.3 m/s, G_S = 222 kg/m^{2}s, respectively. The increase in the local voidage reflects the increase in the cross-sectional mean voidage which is about 6 to 10 % higher at the highest level compared to the lowest measurement elevation.

As shown in Fig. 4.13 for U = 6.0 m/s and z = 2.5 m/s, local voidage drops most towards the wall as the solids circulation rate is raised. For a wide range of operating conditions in this work, as shown in Fig. 4.14, the local voidage drops only to about 0.9 at the axis, whereas at the wall it nearly reaches ε_{mf}. The radial solids distribution profiles obtained here are consistent with those of previous studies (e.g. Hartge et al. 1986; Weinstein et al., 1984) in the dense region of CFB risers. The M-shaped voidage profiles noted by Zhou et al. (1994) were not, however, found in the present work. Cross-sectional non-uniformity of gas turbulence was suggested as the cause of such radial profiles. Given the high solids concentration, the dominant form of the solids crossflux from the core to the outer region is likely interparticle collision rather than turbulence diffusion in the present study.

4.3.2 Radial voidage correlations

Herb et al. (1989) using a capacitance probe with FCC particles in a riser of diameter 0.15 m observed similar local solids concentration profiles at different elevations, when normalized using the cross-sectional average voidage. They thus suggested that there may be a universal radial profile of bed voidage for any time-averaged cross-sectional mean solids concentration. This was supported by Tung et al. (1988) and

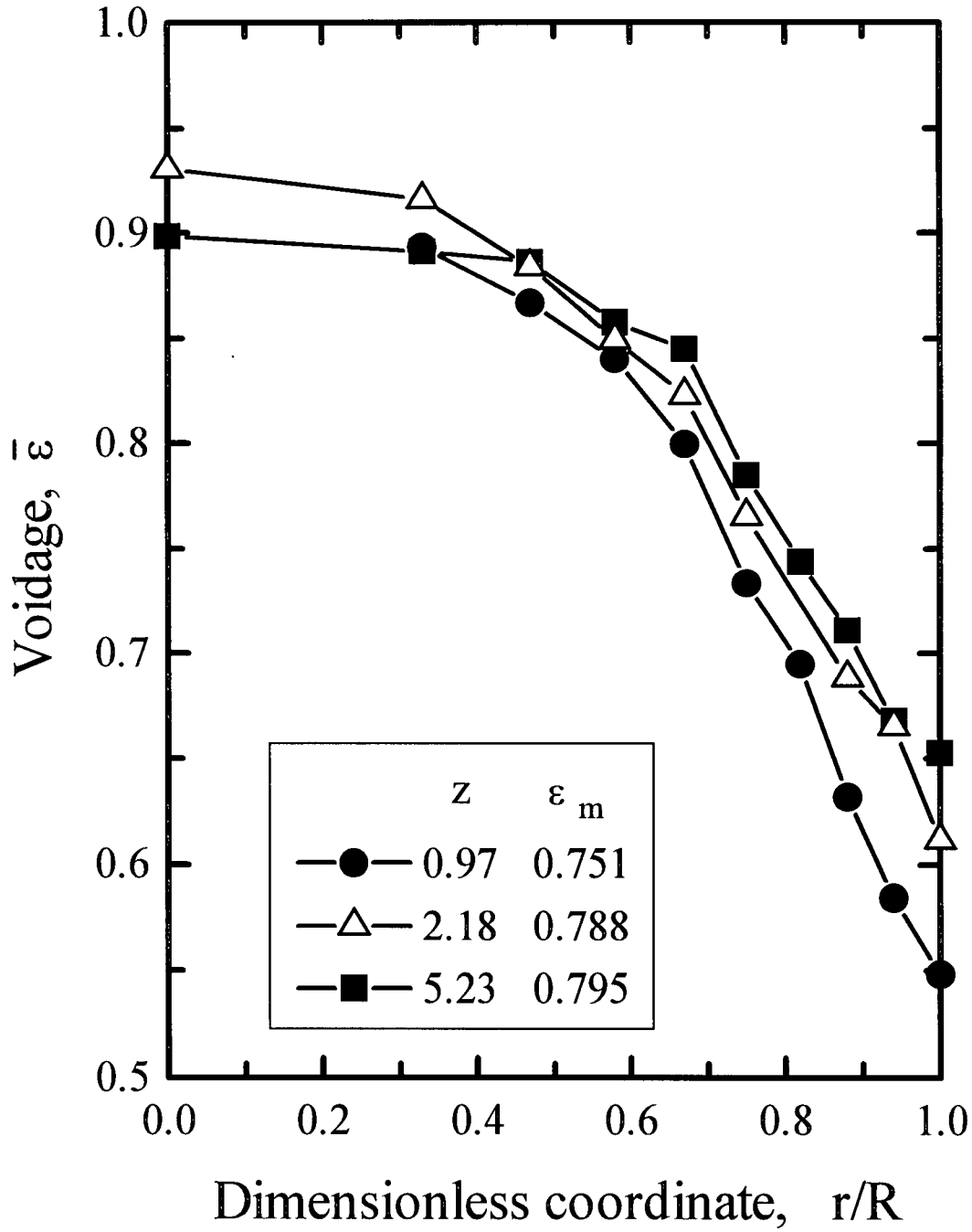

Fig. 4.11: Radial profiles of local voidage at different heights for U = 7.0 m/s and G_s = 246 kg/m^{2}s.

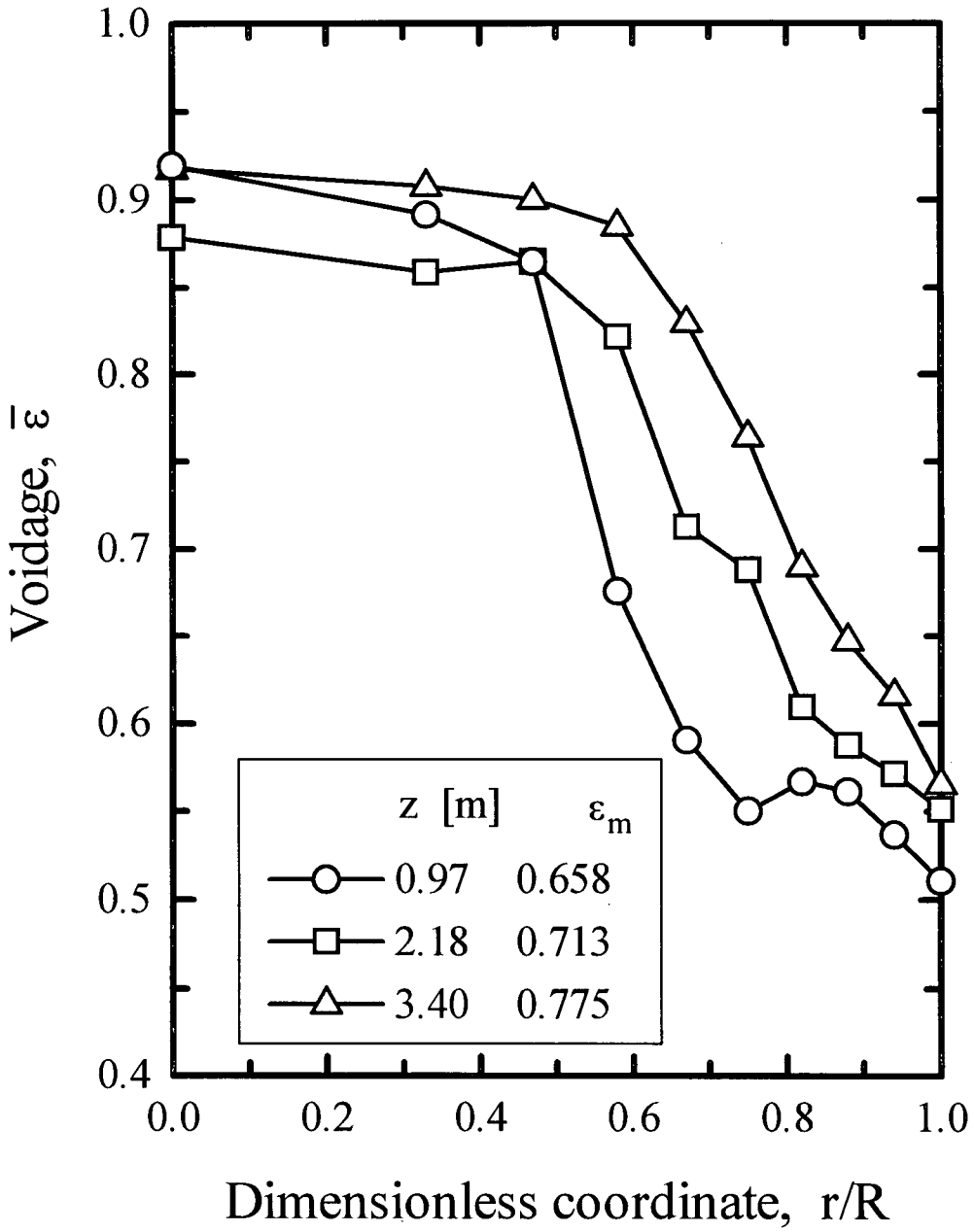

Fig. 4.12: Radial profiles of local voidage at three heights for U = 5.3 m/s and G_s = 222 kg/m^{2}s.

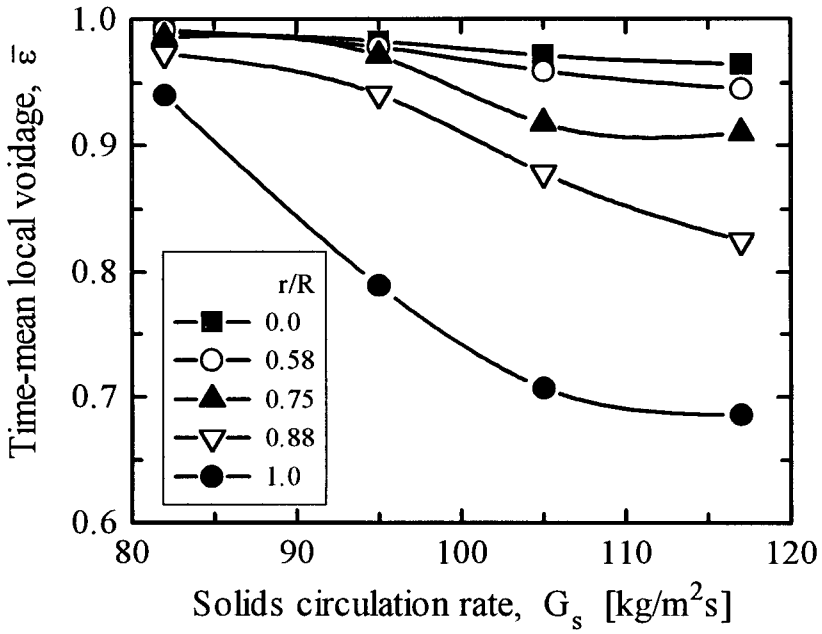

Fig. 4.13: Variation of time-mean local voidage with solids circulation rate at three radial locations for U = 6.0 m/s and z = 2.5 m.

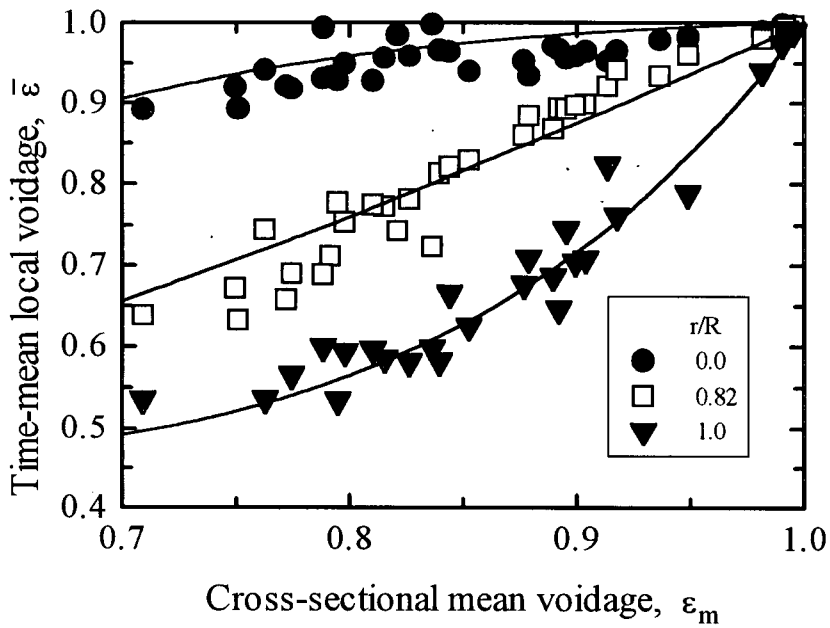

Fig. 4.14: Variation of time-mean local voidage with cross-sectional mean voidage at three radial locations. Data are for different operating conditions in this work (U = 4 - 8 m/s, G_s = 14 - 425 kg/m^{2}s and z = 0.97 - 5.23 m). Lines calculated from Eq. 4.9.

Zhang et al. (1991) for different particles at different superficial gas velocities and solids circulation rates in risers of different diameter. Zhang et al. (1991) proposed

$$\bar{\varepsilon} = \varepsilon_m^{\,0.191+\varphi^{2.5}+3\varphi^{11}} \tag{4.4}$$

relating time-mean local voidage, $\bar{\varepsilon}$, to the cross-sectional average voidage, ε_m and dimensionless radius, φ. Rhodes et al. (1992) observed from sets of voidage data that the solids concentration at the wall was on average about twice the cross-sectional mean. Aided by this simplification, they correlated the local voidage by means of

$$\frac{1-\bar{\varepsilon}}{1-\varepsilon_m} = 2\varphi^2 \tag{4.5}$$

Equation (4.5) is, however, flawed, since it always predicts the voidage at the axis to be unity contrary to many experimental findings. Goedicke and Reh (1993) correlated the local voidage at the wall, $\bar{\varepsilon}_w$, with the average voidage from differential pressure measurements for 62 μm particles and obtained

$$\bar{\varepsilon}_w = 0.322 + 0.196\varepsilon_m + 15.09(\varepsilon_m - 0.4)^{6.74} \tag{4.6}$$

A similar dependency of local voidage on average voidage was found by Patience and Chaouki (1995) and Wang et al (1996), who respectively proposed

$$\frac{\varepsilon_m^{\,0.4} - \bar{\varepsilon}}{\varepsilon_m^{\,0.4} - \varepsilon_m} = 4\varphi^6 \tag{4.7}$$

and

$$\frac{1-\bar{\varepsilon}}{1-\varepsilon_m} = 0.211 + 1.92\sin^{10}\left(\frac{\pi}{2}\varphi\right) \tag{4.8}$$

The local voidage in this work could also be correlated as a function of ε_m and φ at different superficial velocities, solids circulation rates and different heights giving

$$\bar{\varepsilon} = \varepsilon_{mf} + (\varepsilon_m - \varepsilon_{mf})\varepsilon_m^{\,-1.5+2.1\varphi^{3.1}+5.0\varphi^{8.8}} \tag{4.9}$$

Figure 4.15 compares predictions of Eq. (4.9) with our experimental data. The predictions are almost all within ±10% of the data. Figure 4.16 compares predictions of

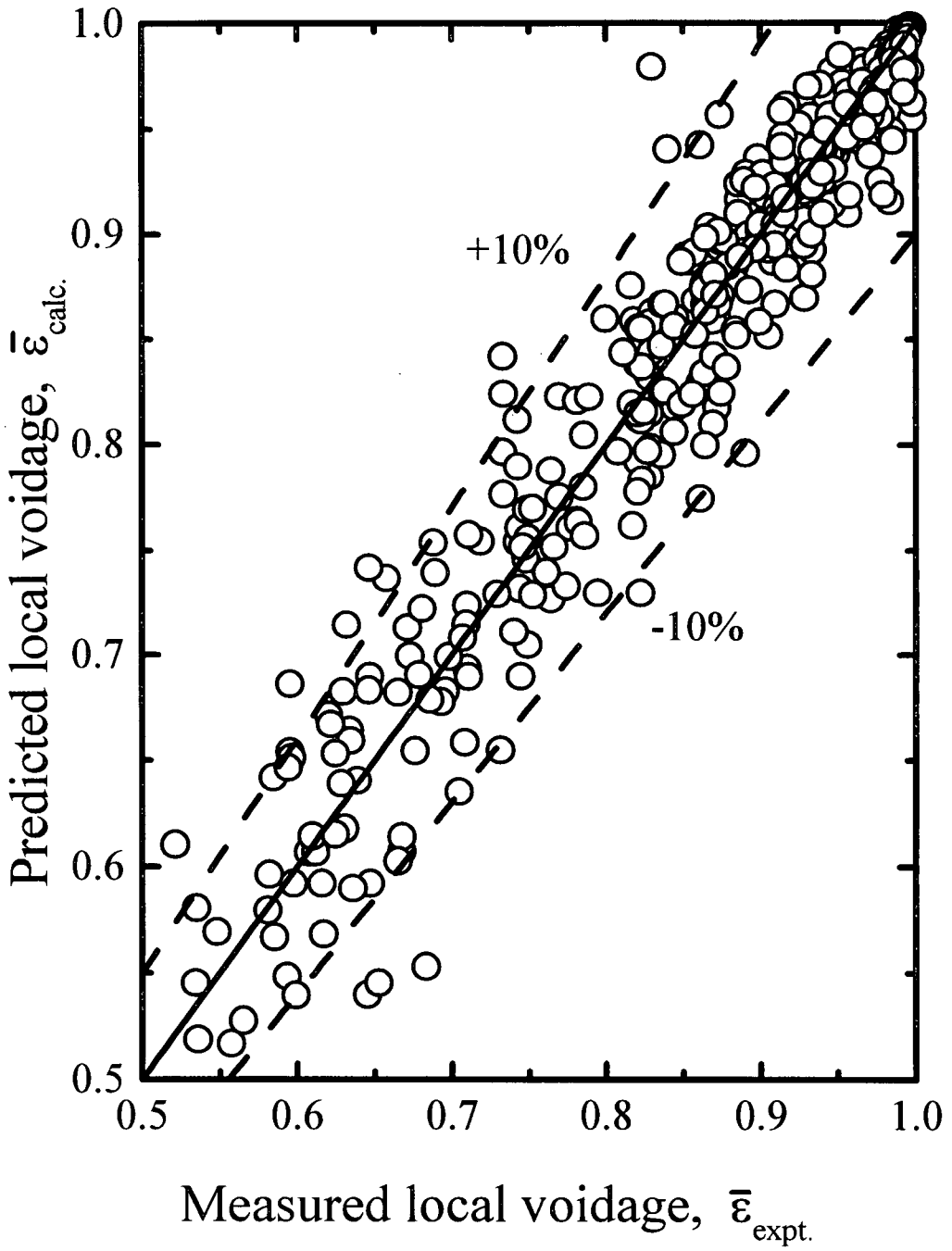

Fig. 4.15: Comparison between local voidage calculated by Eq. (4.9) and data measured in this study.

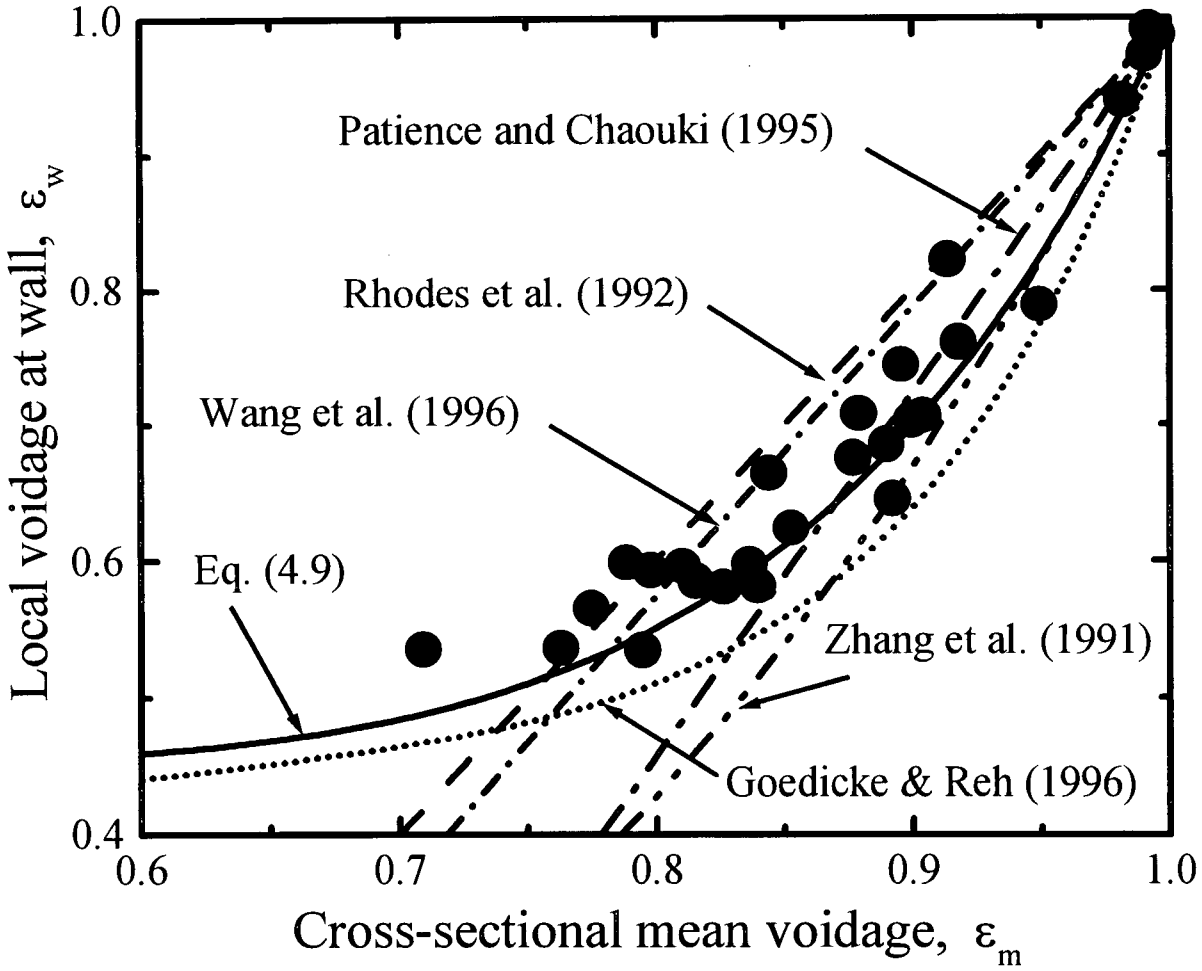

Fig. 4.16: Comparison between local voidage at the wall calculated by various correlations and values measured in this work.

the above correlations with local voidage at the wall, while Fig. 4.17 compares predictions of the same correlations, except Eq. (4.6), with experimental data for U = 8.0 m/s, G_S = 425 kg/m^{2}s and z = 1.57 m. In both cases Eq. (4.9) fits best. The same is observed when the correlations are compared by calculating their root mean square deviations (RMSD) for all local voidage data obtained in this work as summarized in Table 4.1. Figure 4.18 plots typical local voidage profiles at different operating conditions obtained in this study in comparison with lines calculated from Eq. (4.9). Again the correlation is in good agreement with experimental data. Equation (4.9) also appears to predict well the data of other studies as shown in Fig. 4.19. Using the same literature data plotted in Fig. 4.19, the above correlations are compared in Table 4.2 by evaluating their root mean square deviations. Overall, Eq. (4.9) offers superior predictions. The shortcomings of the literature correlations appear to result from the limited ranges of suspension density (mostly from the dilute zone of CFB risers) used in their formulation. Equation (4.9) predicts well local voidage in both the bottom dense zone and the upper dilute region of CFB risers. It therefore, when used in conjunction with the correlations for average longitudinal voidage profiles established in Chapter 3, offers a simple means of estimating the local voidage in CFB risers. It can also be used to estimate local voidage profiles in the dense zone of CFB risers, for which few experimental data are currently available.

4.3.3 Local voidage fluctuations

To gain a better understanding of the local flow behaviour, it is important to examine the instantaneous behaviour in addition to the time-averaged behaviour. Fluctuations are reflected in time-traces of voidage and more quantitatively in the standard deviation of the local voidage about its mean. Figure 4.20 shows 10 s traces describing the variation of instantaneous local voidage at six radial positions at z = 3.4 m for U = 7.5 m/s

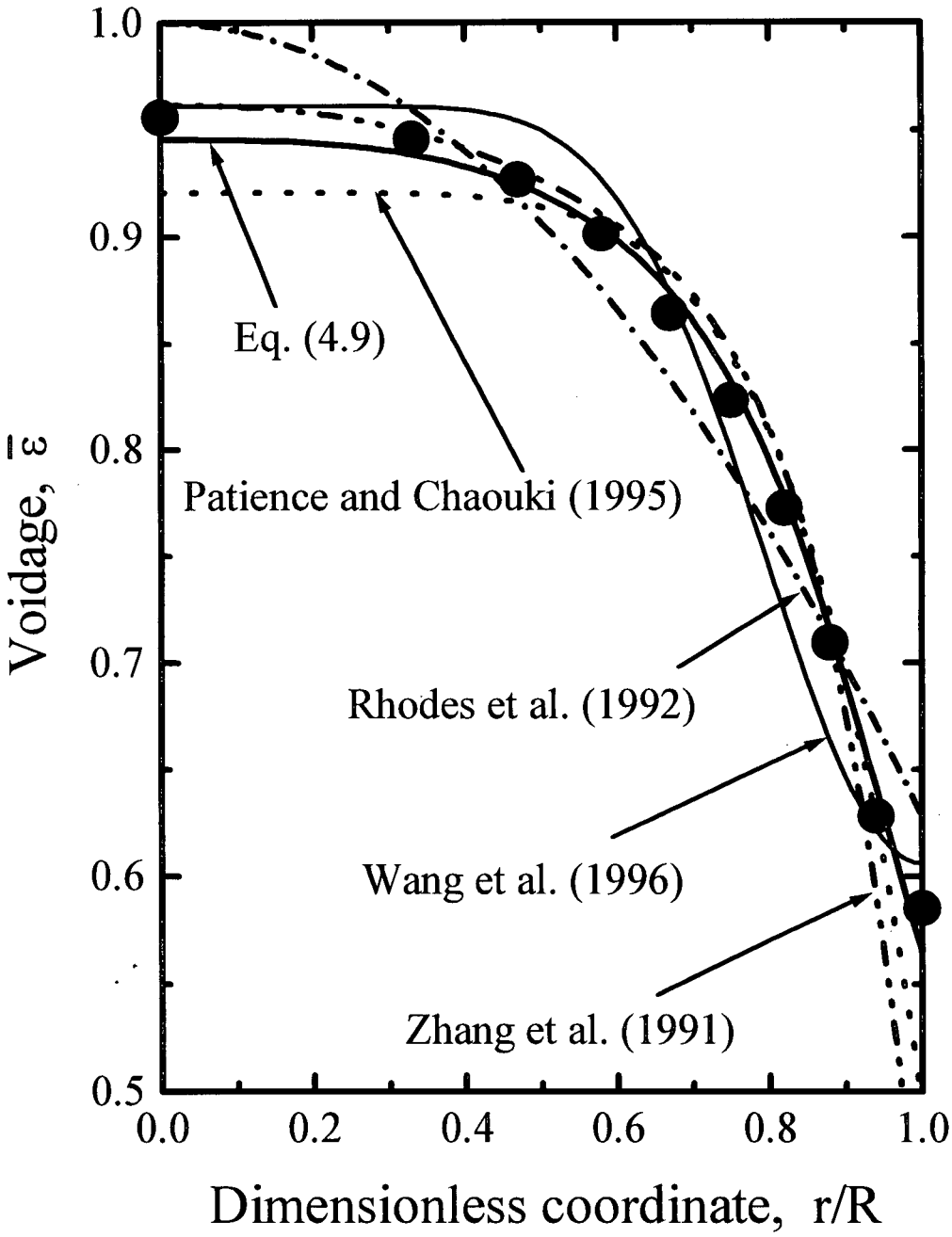

Fig. 4.17: Comparison between local voidage calculated by various correlations and data measured in this work for U = 8 m/s, G_S = 425 kg/m^{2}s and z = 1.57 m.

Table 4.1: Comparison of deviations from various radial voidage correlations for all experimental data obtained in this work: $4 < U < 8$ m/s; $14 < G_S < 425$ kg/m^{2}s; $0.658 < \varepsilon_m < 0.995$.

Author	Correlation	RMSD all data	RMSD at wall
Zhang et al. (1991)	$\bar{\varepsilon} = \varepsilon_m^{\,0.191+\varphi^{2.5}+3\varphi^{11}}$	0.0856	0.2533
Rhodes et al. (1992)	$\frac{1-\bar{\varepsilon}}{1-\varepsilon_m} = 2\varphi^2$	0.0550	0.0986
Goedicke and Reh (1993)	$\varepsilon_w = 0.322 + 0.196\varepsilon_m + 15.09(\varepsilon_m - 0.4)^{6.74}$	-	0.1309
Patience and Chaouki (1995)	$\frac{\varepsilon_m^{\,0.4} - \bar{\varepsilon}}{\varepsilon_m^{\,0.4} - \varepsilon_m} = 4\varphi^6$	0.0661	0.1790
Wang et al. (1996)	$\frac{1-\bar{\varepsilon}}{1-\varepsilon_m} = 0.211 + 1.92\sin^{10}\left(\frac{\pi}{2}\varphi\right)$	0.0604	0.0943
This work	$\bar{\varepsilon} = \varepsilon_{mf} + (\varepsilon_m - \varepsilon_{mf})\varepsilon_m^{\,-1.5+2.1\varphi^{3.1}+5.0\varphi^{8.8}}$	0.0452	0.0777

$$\text{RMSD} = \sqrt{\frac{1}{N}\sum_{1}^{N}\left(\frac{\varepsilon_{\text{calc.,i}} - \varepsilon_{\text{exp t.,i}}}{\varepsilon_{\text{exp t.,i}}}\right)^2}, \qquad \varphi = \frac{r}{R}, \qquad \varepsilon_W = \text{voidage at the wall.}$$

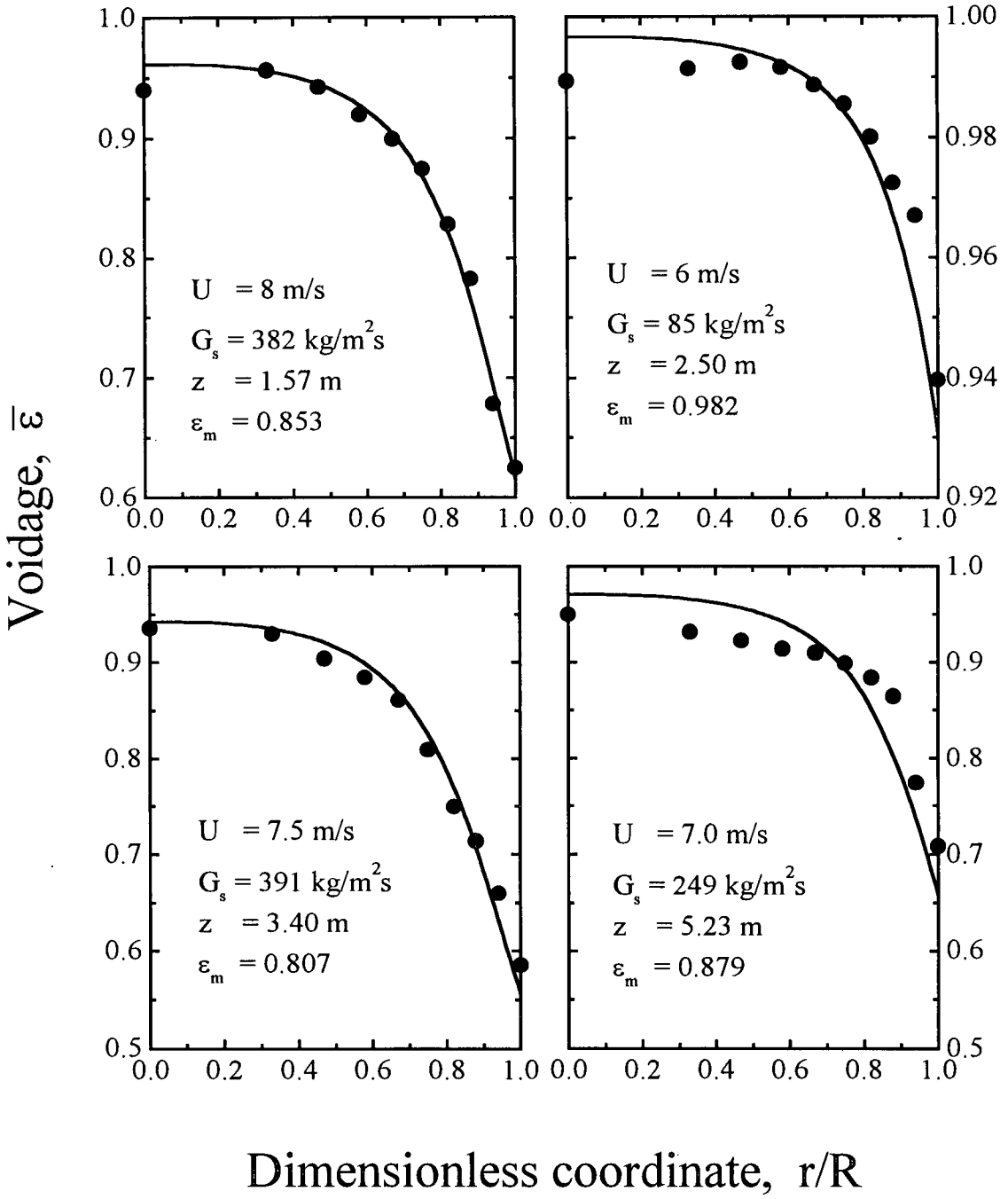

Fig. 4.18: Comparison between local voidages calculated from Eq. (4.9) (lines) and experimental values measured in this work for different operating conditions.

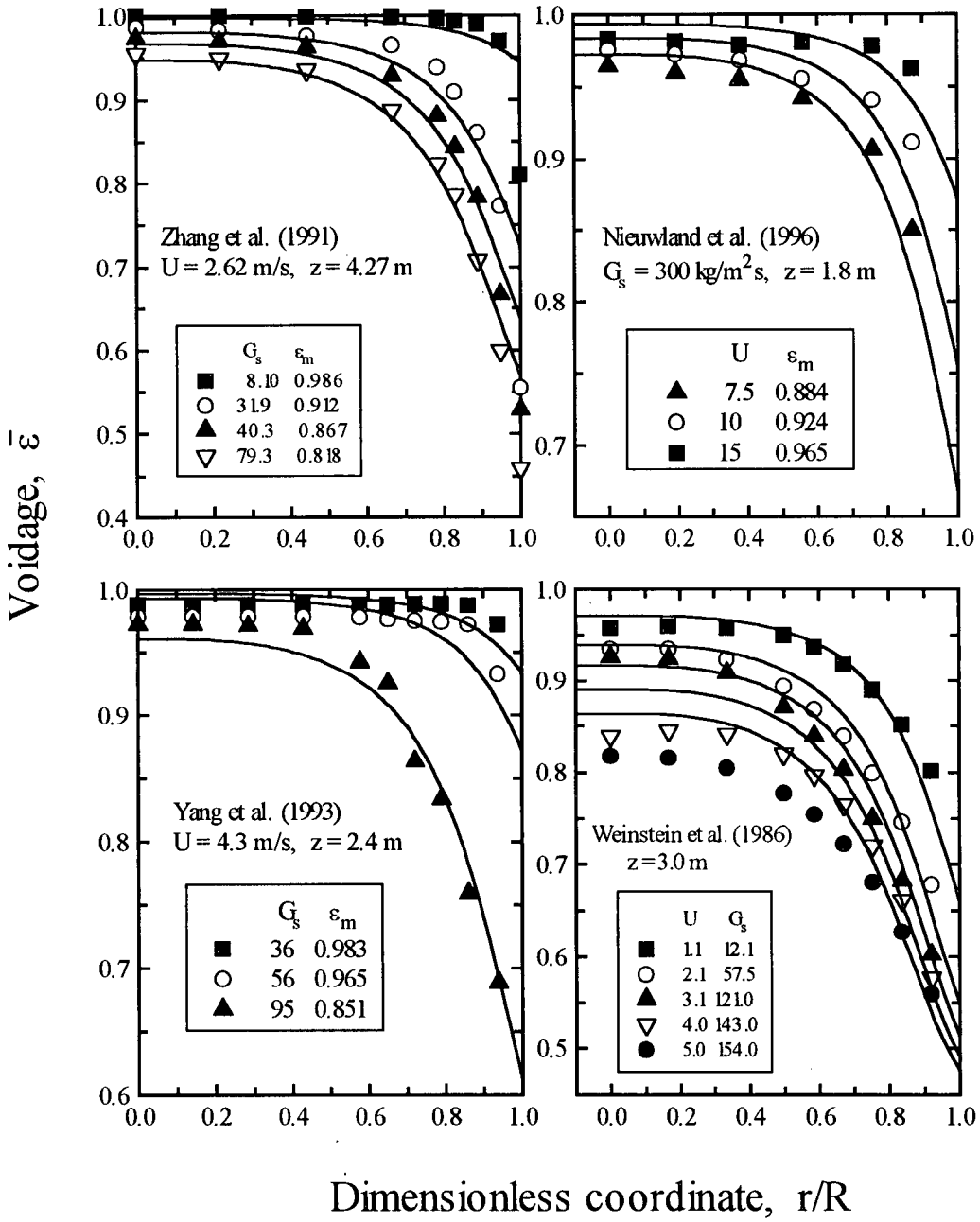

Fig. 4.19: Comparison between local voidages calculated rom Eq. (4.9) (lines) and experimental values from the literature.

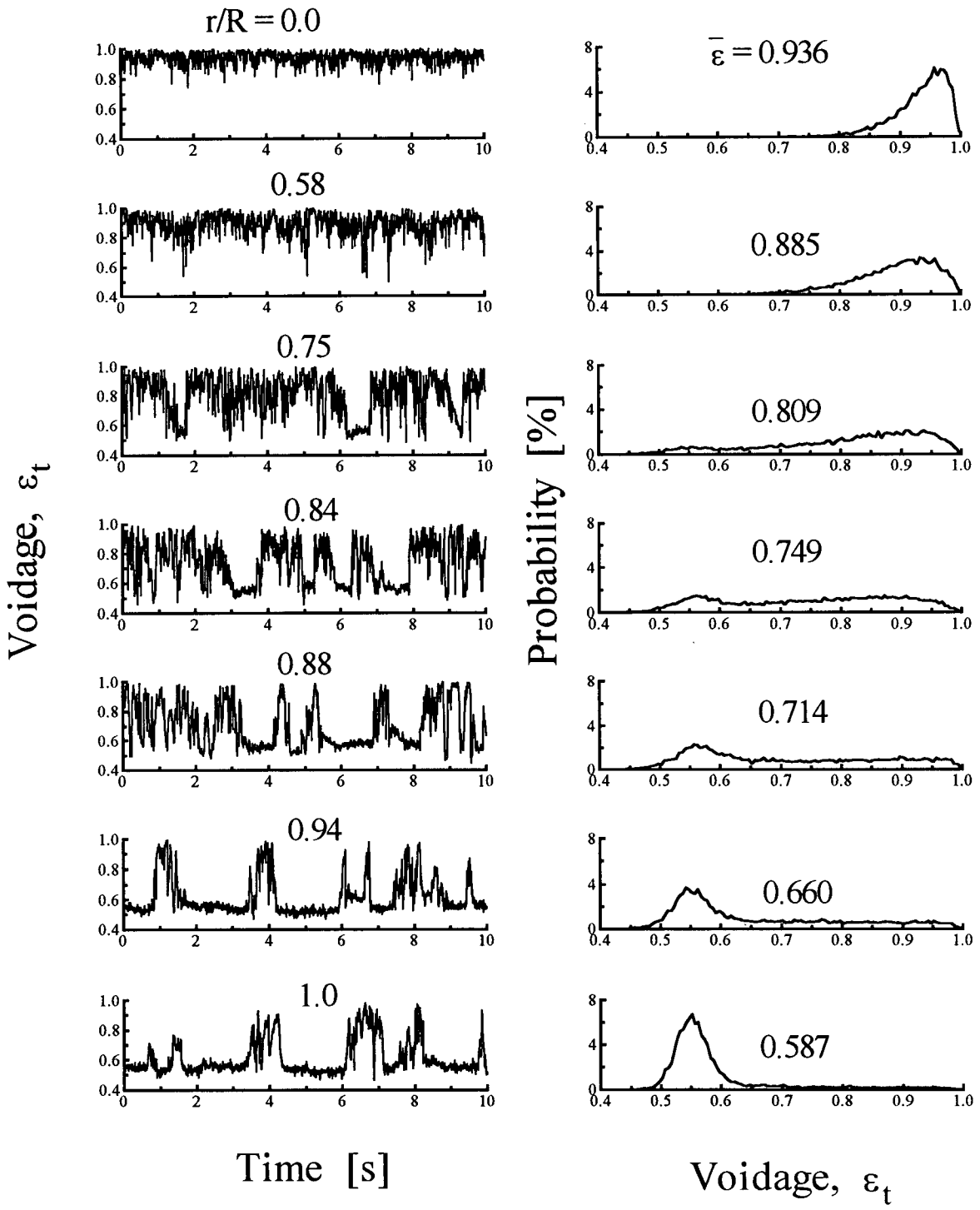

Fig. 4.20: Local voidage trace with the corresponding probability distribution plots for six radial locations at U = 7.5 m/s, G_S = 391 kg/m^{2}s and z = 3.4 m. Cross-sectional average voidage = 0.807.

Table 4.2: Comparison of root mean square relative deviations from various radial voidage correlations for literature data plotted in Fig. 4.13.

Data source	No. of data	RMS relative deviation from experimental data				
		Eq. (4.4)	Eq. (4.5)	Eq. (4.7)	Eq. (4.8)	Eq. (4.9)
Neuwland et al. (1996)	21	0.038	0.040	0.038	0.037	0.020
Zhang et al. (1991)	36	0.045	0.136	0.082	0.124	0.082
Weinstein et al. (1986)	50	0.151	0.090	0.144	0.118	0.032
Wang et al. (1993)	33	0.036	0.036	0.020	0.026	0.014
All data	140	0.095	0.089	0.095	0.095	0.046

and G_s = 391 kg/m^{2}s. The cross-sectional mean voidage was 0.807, a typical high density value. Also included in Fig. 4.20 are plots of probability distribution corresponding to the instantaneous voidages for sampling periods of 100 s at a frequency of 100 Hz. On the axis the voidage is high with low-amplitude fluctuations. The corresponding probability distribution plot shows a single high voidage peak indicating that the flow is predominantly a dilute suspension with $\varepsilon > 0.9$. Further outwards there is an increasing frequency of lower voidage fractions as the suspension becomes denser, leading to a wider voidage distribution. Close to the wall the fluctuations start to die down, the high voidage peaks become less frequent, and the flow becomes predominantly dense. A high voidage probability peak is no longer observed and is replaced by a high concentration peak at $\varepsilon \approx$

0.55. Figure 4.21 shows similar plots for typical dilute fast fluidization conditions (ε_m = 0.949). In this case the flow is predominantly dilute at all radial positions, as shown by the persistent high voidage peak in the probability distributions, although broadening occurs near the wall. The voidage fluctuations clearly influence transport processes, invalidating any simplistic view based solely on time-averaged behaviour.

Figure 4.22 plots the standard deviation of local voidage at different radial positions for the same conditions as in Fig. 4.20. The corresponding radial profile of time-mean voidage is also included, for completeness. The standard deviation increases from a low value at the center to a peak at r/R $\approx$ 0.9 before falling off towards the wall. The peak in the standard deviation profiles suggests vigorous solids interaction at that radial position. Figure 4.23 plots radial profiles of standard deviation for the same conditions as in Fig. 4.7. For pneumatic transport conditions (ε_m = 0.995 and G_s = 14 kg/m^{2}s), voidage fluctuations are of very small magnitude, and the increase in the standard deviation with increasing r is very small. This reflects the flow behaviour in the pneumatic transport regime, where there is very little particle-particle interaction. For dilute CFB conditions (G_s = 52 kg/m^{2}s, ε_m = 0.90) the standard deviation of local voidage increases outward, reaching its highest value at the wall. For high densities (G_s = 196 and 246 kg/m^{2}s) the standard deviation reaches a peak between the center and the wall. The location of the peak appears to move inwards with increasing solids circulation rate.

Figures 4.24 and 4.25 show the influence of solids circulation rate on the standard deviation of local voidage for the same conditions as in Figs. 4.8 and 4.9, respectively. For high density conditions the maximum standard deviation always occurs at some distance from the wall, an important distinguishing feature of high density CFB risers. In conventional dilute CFB risers, the boundary between the core region and the dense

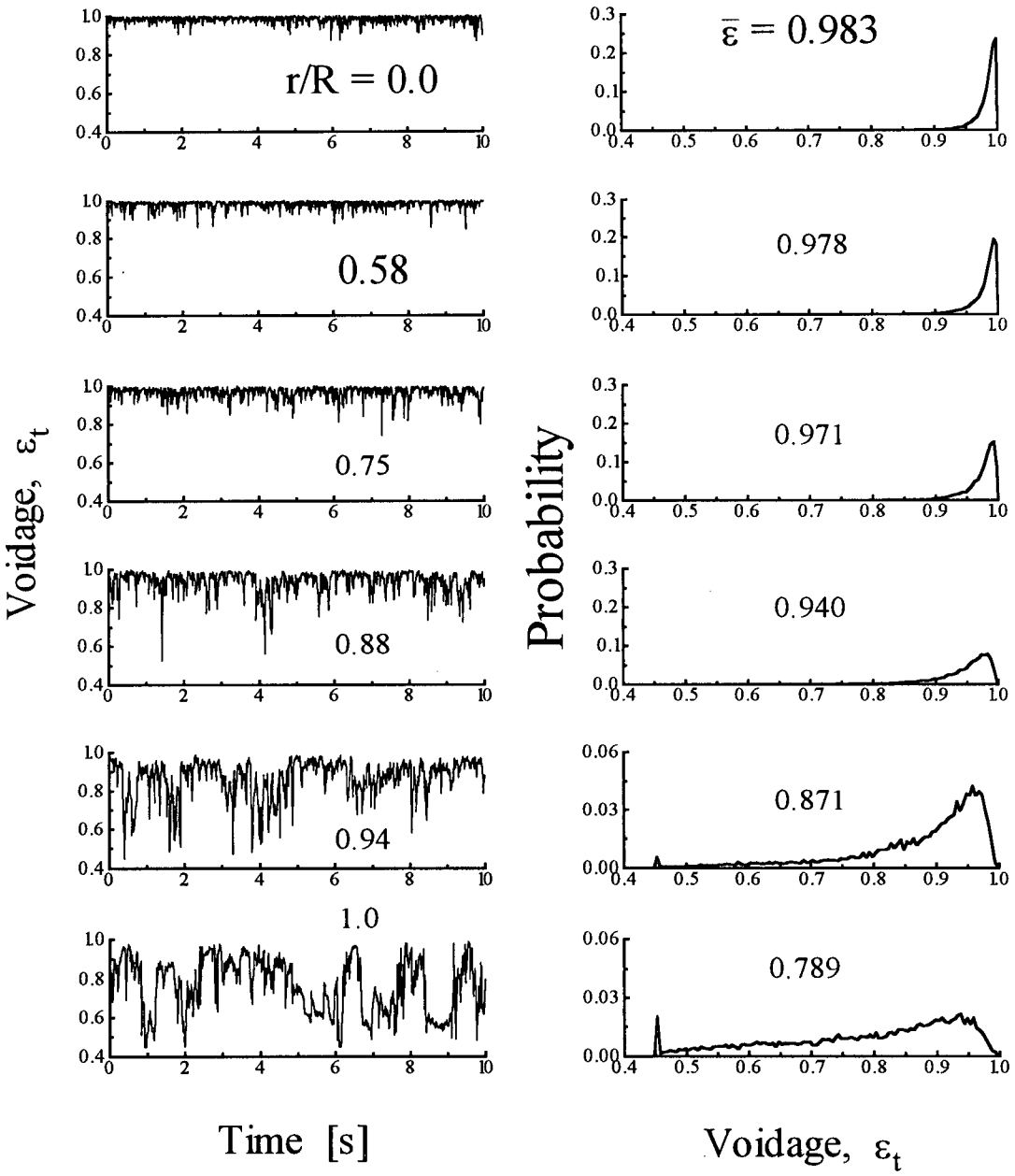

Fig. 4.21: Local voidage trace with the corresponding probability distribution plots for six radial locations at U = 6 m/s, G_s = 95 kg/m^{2}s and z = 2.5 m. Cross-sectional average voidage = 0.949.

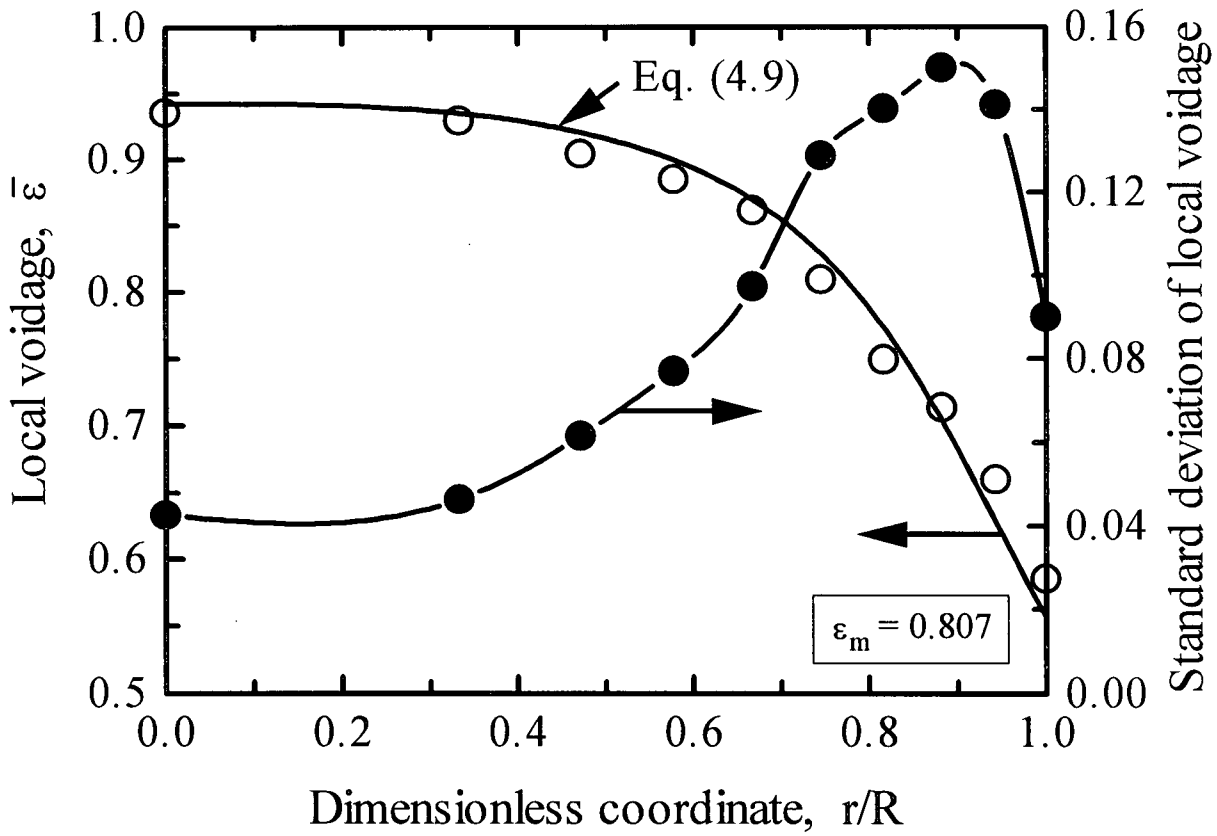

Fig. 4.22: Radial profiles of local voidage and its standard deviation for U = 7.5 m/s, G_s = 391 kg/m^{2}s and z = 3.4 m.

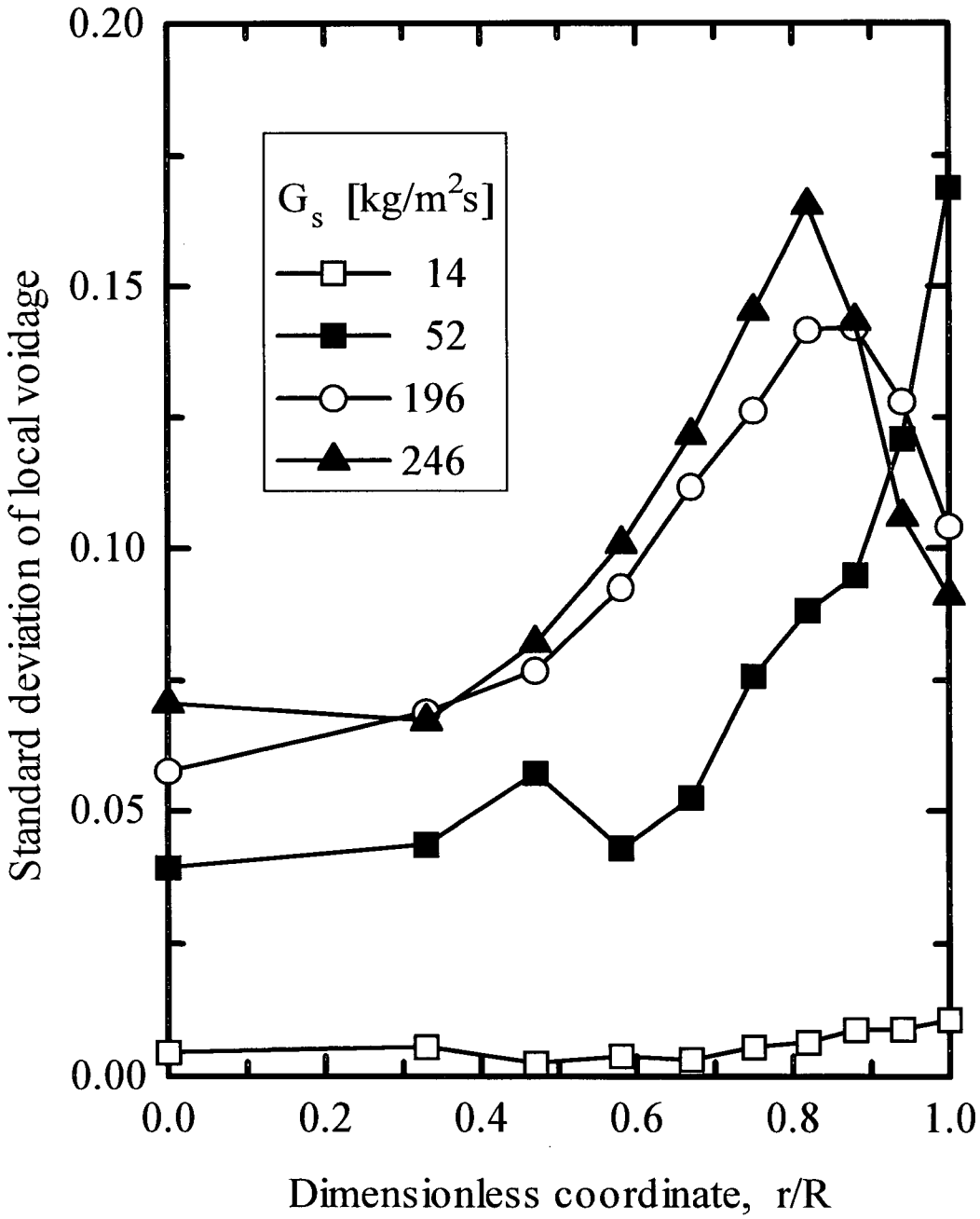

Fig. 4.23: Radial profiles of standard deviation of local voidage for U = 4.0 m/s and z = 1.57 m (same conditions as in Fig. 4.7).

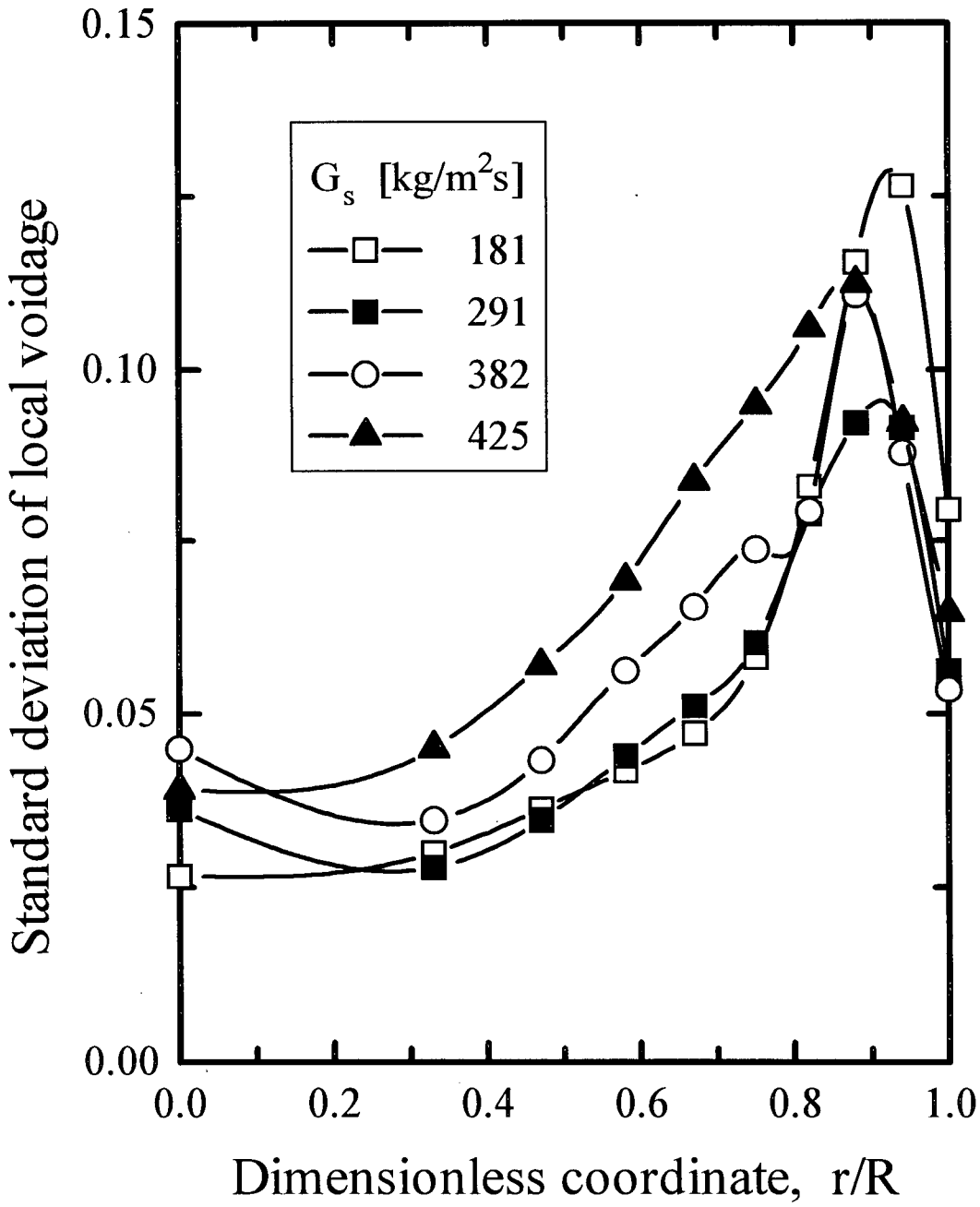

Fig. 4.24: Radial profiles of standard deviation of local voidage for U = 8.0 m/s and z = 1.57 m (same conditions as in Fig. 4.8).

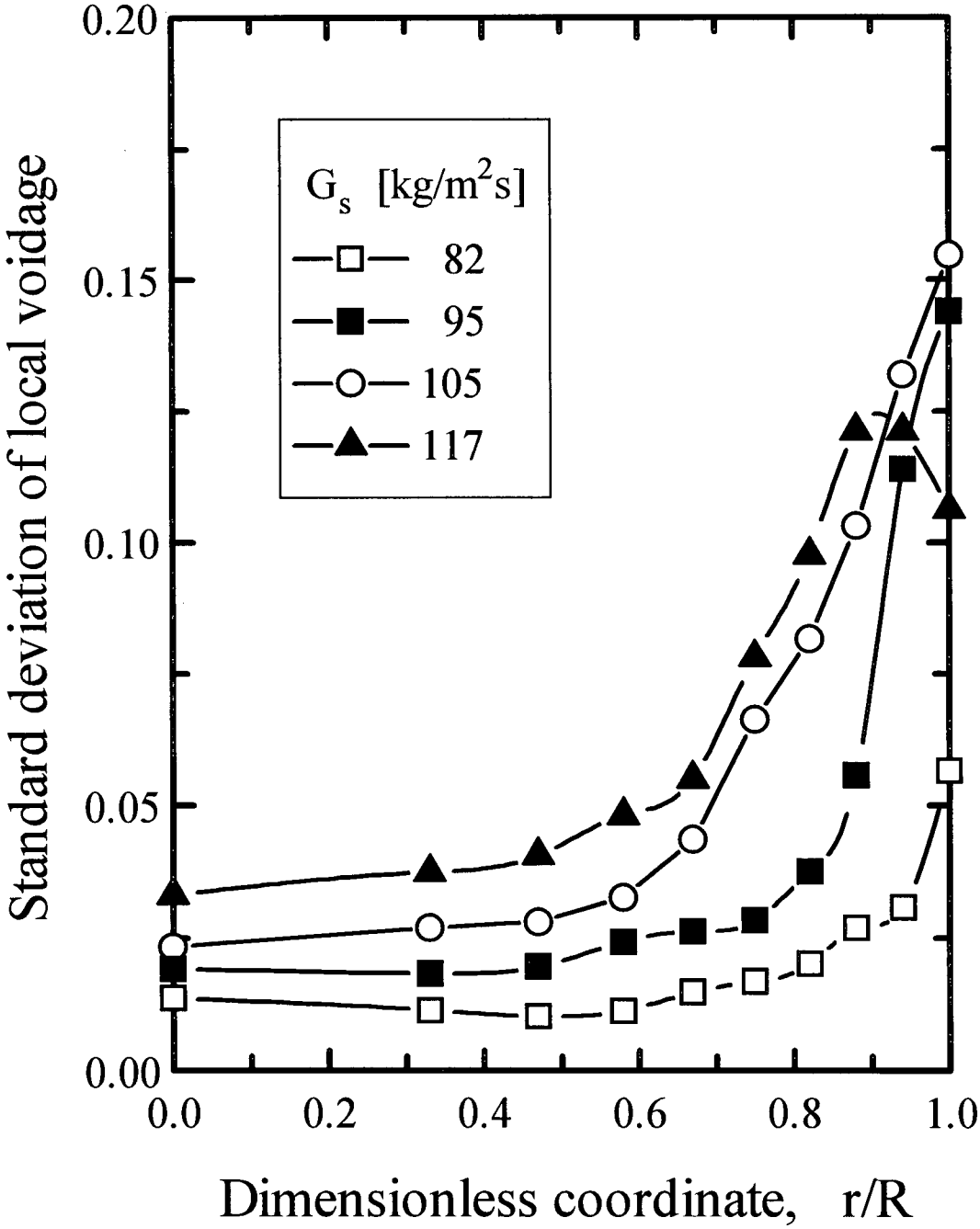

Fig. 4.25: Radial profiles of standard deviation of local voidage for U = 6.0 m/s and z = 2.5 m (same conditions as in Fig. 4.9).

annulus is normally taken at the point where average vertical particle velocity or net vertical solids flux is zero (e.g. Werther, 1994), the latter being preferred (Bi et al., 1996). In this study no net downflow of solids was observed at the wall for high density conditions. Measurements of local vertical solids flux presented in Chapter 5 found also that there was no net downflow at other radial positions. In the absence of an annular downflow layer, the location of the peak standard deviation, designated $r = R - \delta_\sigma$, may indicate a boundary between a more dilute inner core and a denser annular region. Figure 4.26 to 4.28 plot radial profiles of voidage standard deviation at different heights for the same conditions as in Figs. 4.10 to 4.12. The location of the maximum standard deviation moves slightly outwards with increasing height.

Several explanations have been offered as to the cause of voidage fluctuations in CFB risers (e.g. Sinclair and Jackson, 1989; Brereton and Grace, 1993; Dasgupta et al., 1994). They include particle-particle collisions, particle-wall collisions, as well as gas turbulence. These factors all depend on suspension density. While more studies are necessary for the high density conditions examined in this work, it is apparent that the standard deviation does not increase indefinitely with increasing solids concentration. The fluctuations become relatively small at both extremes, i.e. as the local time-mean voidage approaches ε_{mf} and as $\bar{\varepsilon}$ approaches 1. This is observed in Fig. 4.29 where the standard deviation is plotted against the time-mean local voidage for many different operating conditions. It appears that the highest fluctuations occur at $\bar{\varepsilon} \approx 0.75$. A quadratic fit of all the data in Fig. 4.29 gives

$$\sigma_\varepsilon = 1.584\left(1-\bar{\varepsilon}\right)\left(\bar{\varepsilon}-\varepsilon_{mf}\right) \qquad (4.10)$$

It is clear from Fig. 4.29 that there is considerable scatter around this equation, especially for local voidages below about 0.9. Data corresponding to $\bar{\varepsilon} \geq 0.9$ are for the inner dilute region where voidage fluctuations are most likely due to the interaction of the gas with

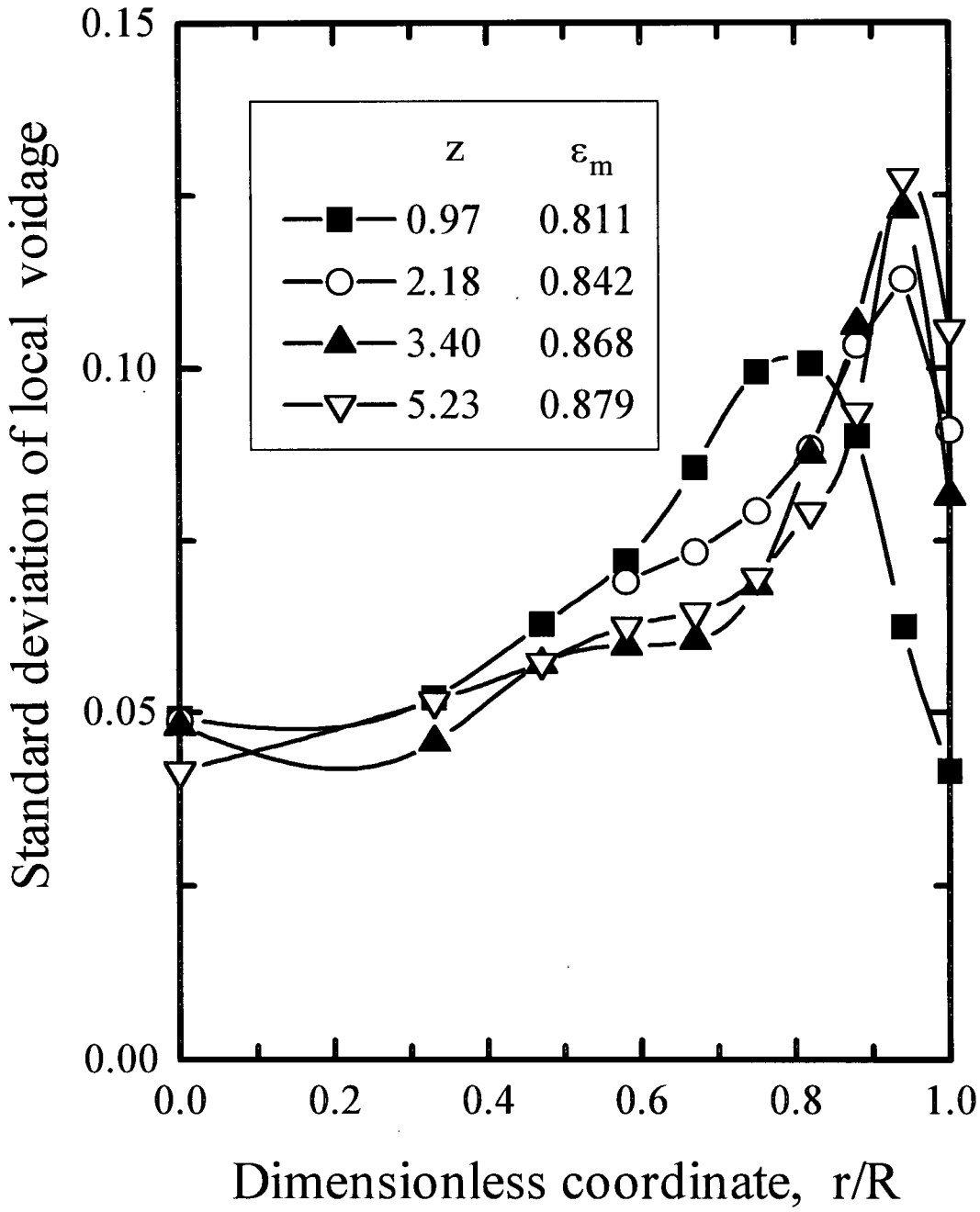

Fig. 4.26: Radial profiles of standard deviation of local voidage at different heights for U = 6.6 m/s and G_s = 234 kg/m²s (same conditions as in Fig. 4.10).

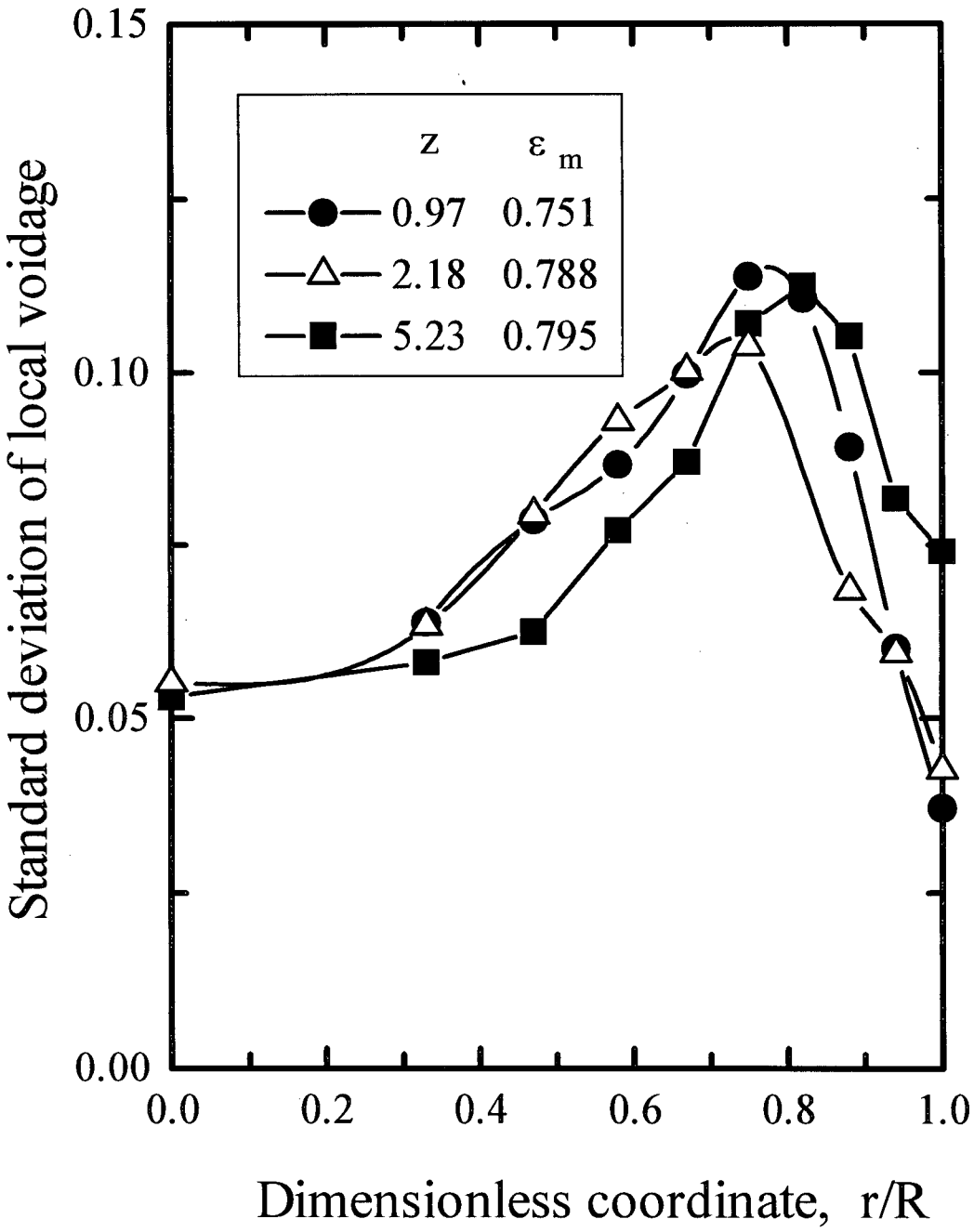

Fig. 4.27: Radial profiles of standard deviation of local voidage at different heights for U = 7.0 m/s and G_s = 246 kg/m²s (same conditions as in Fig. 4.11).

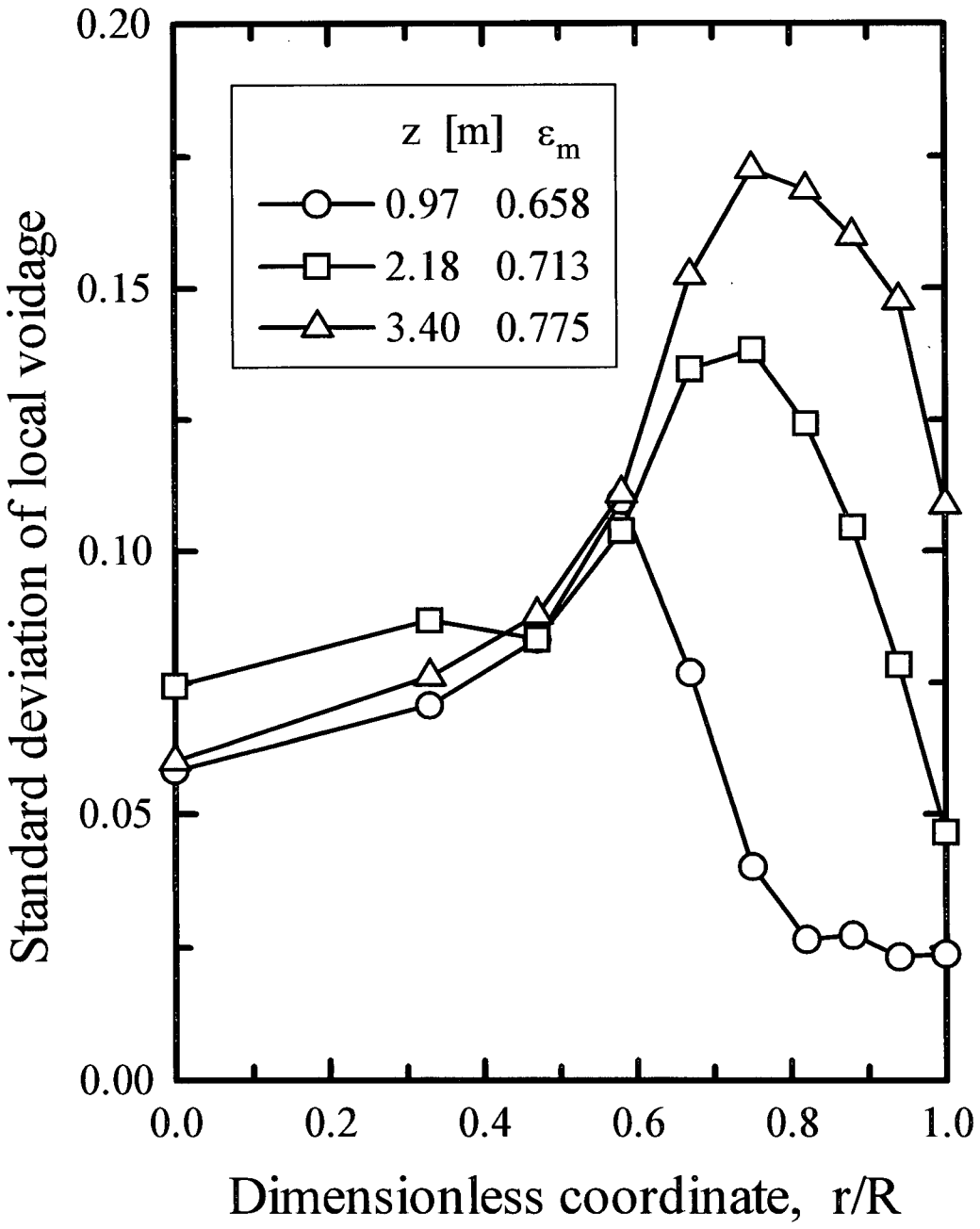

Fig. 4.28: Radial profiles of standard deviation of local voidage at three heights for U = 5.3 m/s and G_s = 222 kg/m^{2}s (same conditions as in Fig. 4.12).

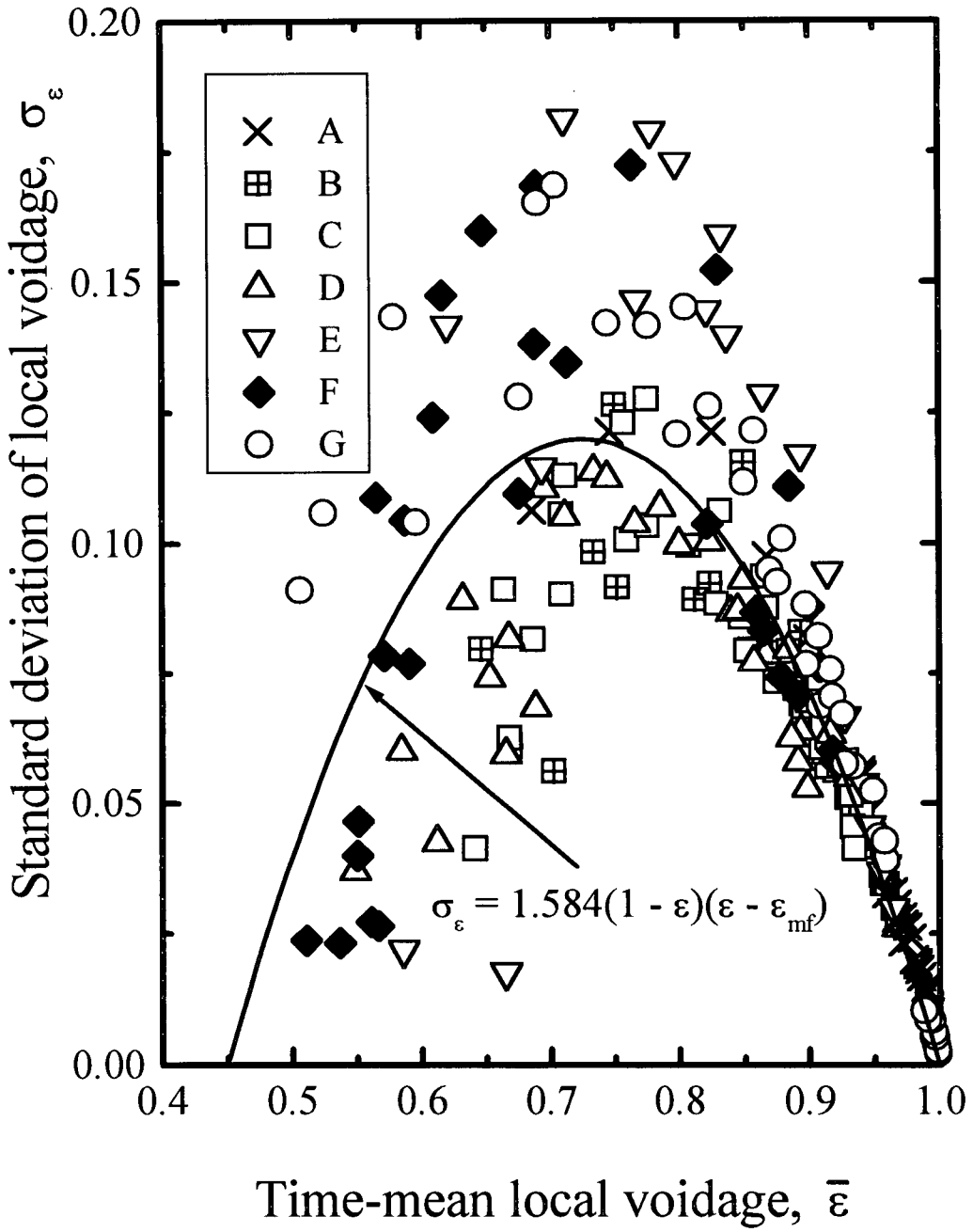

Fig. 4.29: Variation of standard deviation of local voidage fluctuations with time-mean local voidage for different operating conditions. [(A) z = 2.5 m, U = 6 m/s, various G_S; (B) z = 1.57 m, U = 8 m/s, various G_S; (C) U = 6.6 m/s, G_S = 234 kg/m^{2}s, various z; (D) U = 7 m/s, G_S = 249 kg/m^{2}s, various z; (E) z = 0.97 m, U = 4.9 m/s, G_S = 86 kg/m^{2}s; (F) U = 5.3 m/s, G_S = 222 kg/m^{2}s, various z; (G) z = 1.57 m, U = 4 m/s, various G_S)].

individual particles rather than with particle clusters or other structures as discussed below.

The position of the maximum standard deviation, normalized with riser diameter, i.e. δ_σ/D, is plotted as a function of the cross-sectional average solids concentration, $(1 - \varepsilon_m)$, in Fig. 4.30. It appears that δ_σ/D is a function of ε_m only. The two are well correlated by

$$\delta_\sigma / D = 1.03(1-\varepsilon_m)^{1.45} - 0.013 \qquad (4.11).$$

Note that D, the diameter of the column, was not varied and is simply included here as a normalizing parameter. The wall layer thickness is important in hydrodynamic models which assume a core/annular flow structure in the dilute region of CFB risers (e.g. Berruti and Kalogerakis, 1989; Harris and Davidson, 1994). The correlation of Patience and Chaouki (1993) relates the annulus thickness, δ_{Gs}, (defined as the distance from the wall to where net upwards solids flux begins) to the overall solids circulation rate, superficial gas velocity and particle density. Their correlation, however, fails to consider the variation of annulus thickness with elevation. The variation with elevation is accounted for in the correlation of Werther (1994), but it does not include the influence of solids circulation rate. In the correlations of Bai et al. (1995) and Bi et al. (1996)

$$\delta_{\Delta P,mo} / D = 0.403(1-\varepsilon_m)^{0.7} \qquad (4.12)$$

and

$$\delta_{Gs} / D = 0.5\left[1-\sqrt{1.34-1.30(1-\varepsilon_m)^{0.2}+(1-\varepsilon_m)^{1.4}}\right] \qquad (4.13)$$

respectively, the dimensionless wall layer thickness is a function of the mean voidage only. $\delta_{\Delta P,mo}$ is the wall layer thickness determined by a momentum probe technique (Bai et al., 1995). Wei et al. (1997) proposed the correlation

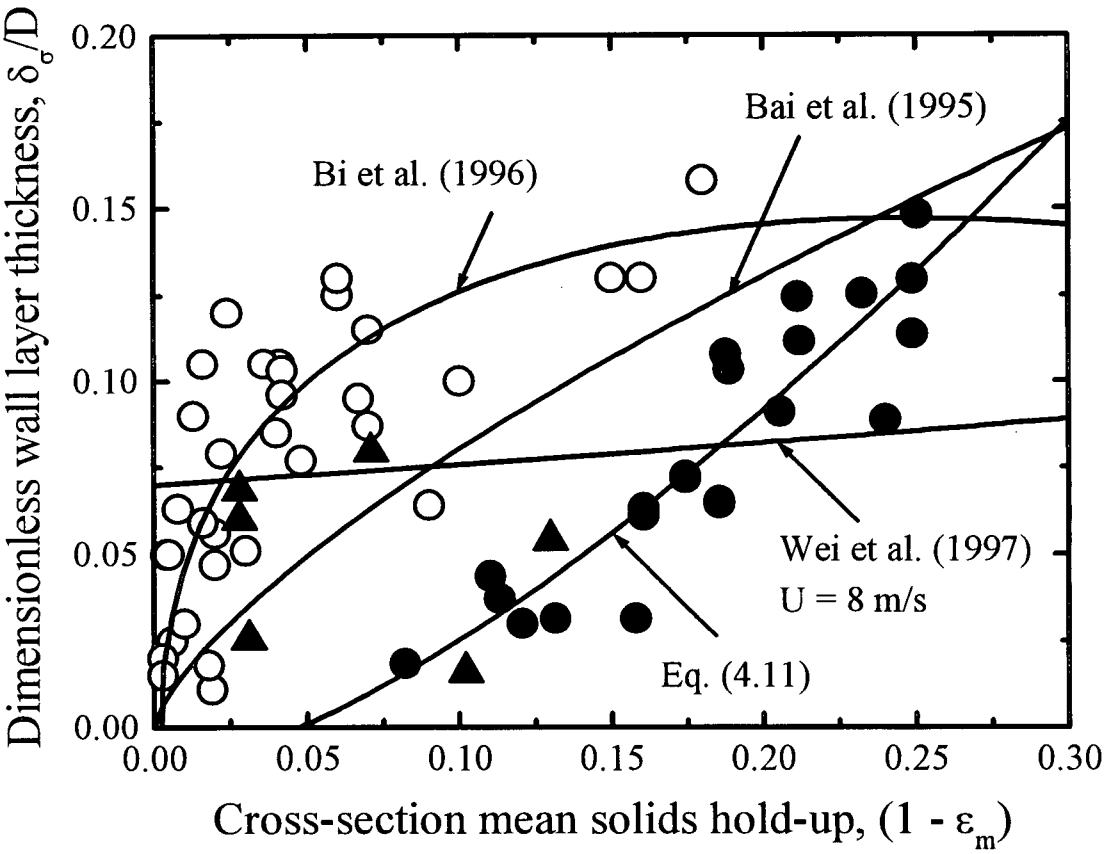

Fig. 4.30: Dimensionless wall layer thicknesses vs cross-sectional mean solids hold-up for O : literature data based on solids flux measurements (see Bi et al., 1996); ▲ : sampling probe measurements of this work (Chapter 5); and ● : distance from wall to position where standard deviation of voidage fluctuations reaches a maximum from this work.

$$\delta_{Gs}/D = 0.5\left(1 - 0.21 Re^{0.133} \varepsilon_m{}^{0.127}\right) \quad (4.14)$$

for $4.05 \times 10^4 < Re = \rho UD/\mu < 1.05 \times 10^5$.

Equations (4.12) to (4.14) as well as wall layer thickness, δ_{Gs}, data from the literature (Bi et al., 1996) are also included in Fig. 4.30. None of these correlations fits the δ_σ/D data well. δ_{Gs} is always larger than δ_σ. There is, however, reasonable agreement between most of the δ_{Gs} wall layer thickness values obtained by the sampling probe in Chapter 5 (solid upward triangles) and the literature data. Clearly the distance from the wall to the position of maximum standard deviation (δ_σ) is quite different from the wall layer thickness based on solids flux measurements (δ_{Gs}).

4.3.4 Intermittency index

Thus far our picture regarding the flow behaviour in high density CFB risers is that of a suspension whose local time-mean voidage falls gradually from about 0.9 to 0.95 at the axis to values approaching the minimum fluidization voidage, $\varepsilon_{mf} \approx 0.45$ at the wall. The standard deviation of local voidage fluctuations has provided a quantitative measure of the variability of the local voidage, from which a boundary between a denser annular region and a more dilute core has been deduced at the point of maximum standard deviation. It is, however, difficult to explain from the standard deviation of local voidage fluctuations the nature of the suspension flow because the time-mean voidage also varies from point to point. A better parameter is the intermittency index, γ, proposed by Brereton and Grace (1993) who normalized the point standard deviation as,

$$\gamma = \frac{\text{Standard deviation of voidage fluctuations at a given point}}{\text{Standard deviation of voidage fluctuations for fully segregated two-phase flow with identical mean voidage at the same point}} \quad (4.15)$$

The segregated two-phase flow of the denominator alternates between only two voidages, ε_{mf} and unity (realized in ideal bubbling beds). It can be shown that the denominator is

$$\sigma_{max} = \sqrt{(1-\bar{\varepsilon})(\bar{\varepsilon}-\varepsilon_{mf})} \qquad (4.16)$$

where $\bar{\varepsilon}$ is the time-mean point voidage and ε_{mf} is the minimum fluidization voidage. If the flow were an ideal cluster flow, with particles segregated into clusters with voidage equal to ε_{mf}, surrounded by solids-free gas, γ would be equal to unity. On the other hand, if there were to be a perfectly uniform local suspension, γ would be zero. The higher the value of γ, the more segregated the flow structure at the given location.

Radial profiles of intermittency index at z = 2.5 m for U = 6.0 m/s and different solids circulation rates are given in Fig. 4.31. At the lowest circulation rate, the suspension is relatively dilute at the measurement cross-section (see Fig. 4.9). The intermittency index remains relatively low, < 0.2, over most of the riser cross-section, rising sharply towards the wall. Similar observations can be made for the other two dilute conditions. At the highest solids circulation rate (G_s = 117 kg/m^{2}s) the intermittency index is higher at the center suggesting more particle clustering. It rises to a peak value of about 0.47 at r/R $\approx$ 0.82 before falling to about 0.4 at the wall, compared with ~ 0.25 at the axis. The location of the peak intermittency index is similar to that of the peak standard deviation.

Figure 4.32 plots the intermittency index as a function of radius for U = 7.5 m/s, G_s = 391 kg/m^{2}s and z = 3.4 m. See Fig. 4.20 for corresponding local voidage traces and probability distribution plots. The intermittency index at the axis is about 0.15. Though the suspension is relatively dilute there ($\bar{\varepsilon}$ = 0.936) the γ indicates the presence of particle agglomerates or clusters. These clusters may have a distribution of voidages, but their lowest voidage for the prevailing operating conditions at the axis is around 0.8 (see Fig. 4.20). Radial profiles are flat until r/R $\approx$ 0.33, but thereafter the intermittency index starts

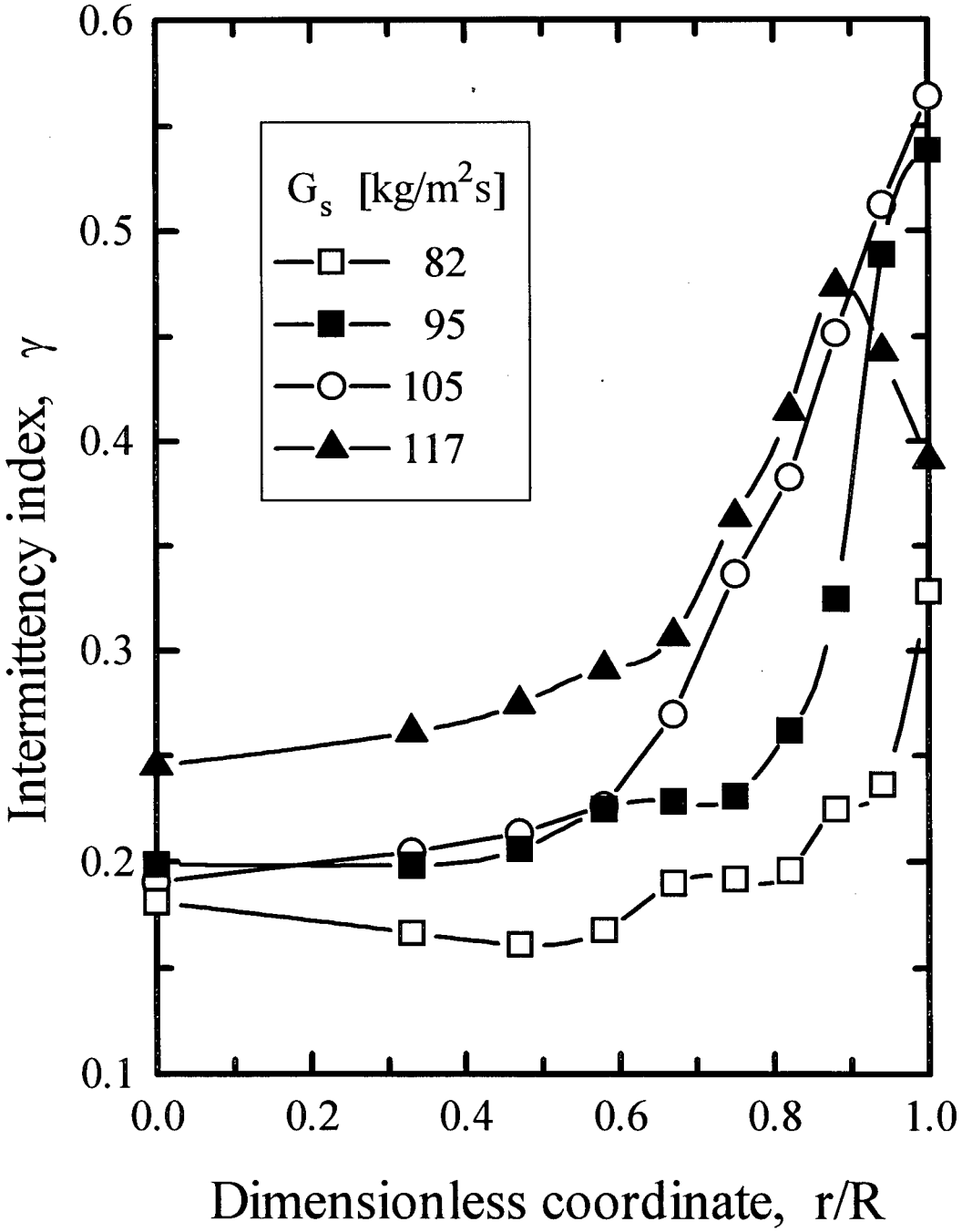

Fig. 4.31: Radial profiles of intermittency index for U = 6.0 m/s and z = 2.5 m (same conditions as in Fig. 4.9).

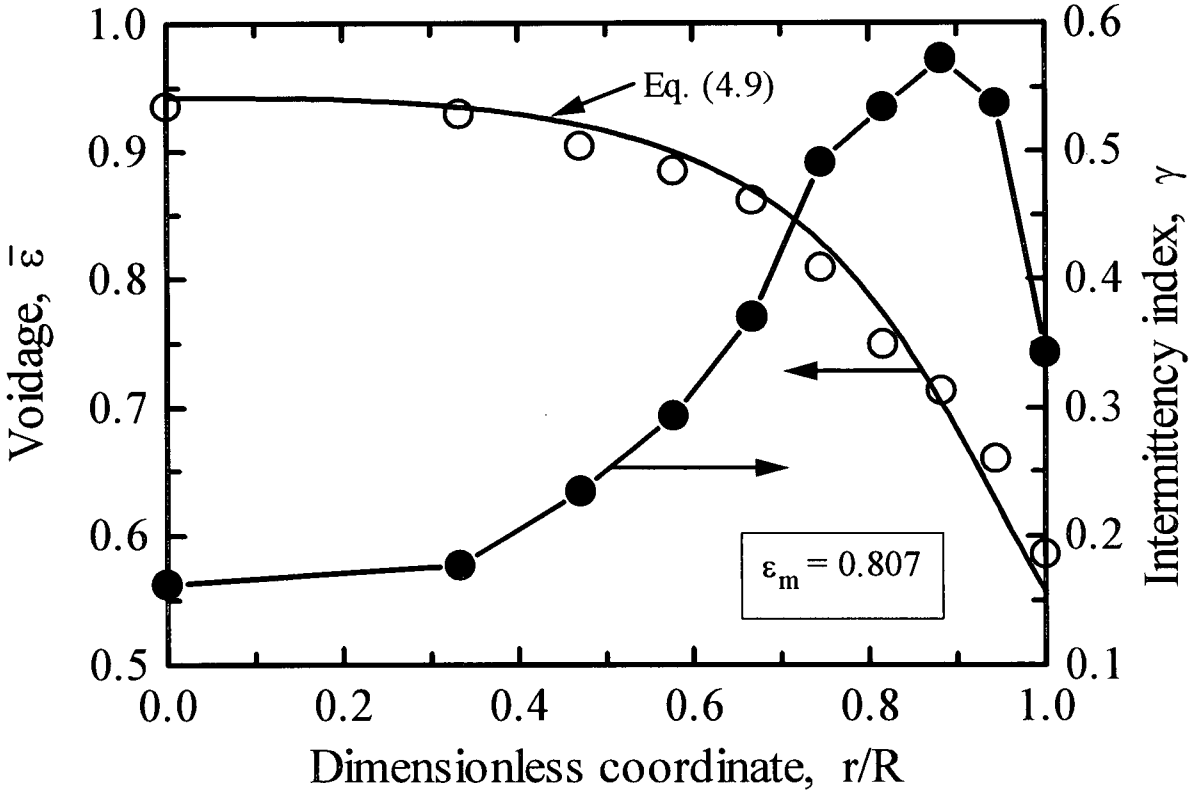

Fig. 4.32: Radial profile of intermittency index for U = 7.5 m/s, G_s = 391 kg/m^{2}s and z = 3.4 m (same conditions as in Fig. 4.20).

to rise rather sharply as the suspension becomes denser. The frequency of clusters or other structures, some with instantaneous voidages as low as 0.5, continues to rise leading to more inhomogeneity. The intermittency index rises to a maximum of nearly 0.6 at $r/R \approx 0.88$ where the voidage is widely distributed. Further outward the suspension becomes increasingly dense with the voidage nearing that of the clusters or other structures. This leads to a more homogeneous high density suspension, as reflected in the continual decrease of the intermittency index, reaching ~ 0.3 at the wall.

Figure 4.33 plots profiles of γ at $z = 1.57$ m and $U = 8.0$ m/s for various solids circulation rates. The intermittency indices rise from about 0.25 to peaks of between 0.3 and 0.45 before dropping to values nearly the same or below those at the axis. Similar trends are observed in Fig. 4.34 for a lower gas velocity. The intermittency index generally increases with G_s. Note from Fig. 4.34 that for dilute pneumatic transport, the index is much lower and nearly constant over the cross-section.

The evolution of the intermittency index with height is shown in Figs. 4.35 and 4.36(a). Although in Fig. 4.35 the intermittency index is higher at the higher elevation than near the bottom, this is not always the case in Fig. 4.36(a), due to the "bell-shape" nature of the intermittency index vs. local mean voidage relationship shown in Fig. 4.36(b). On one hand, if the local voidage is higher than about 0.75, as in dilute risers or in the top dilute zone of a HDCFB riser, the suspension homogeneity increases with elevation due to the decreasing quantity and density of particle clusters or other particle structures in the suspension. On the other hand the suspension becomes more homogeneous if the local solids concentration exceeds that corresponding to the peak intermittency index as explained above.

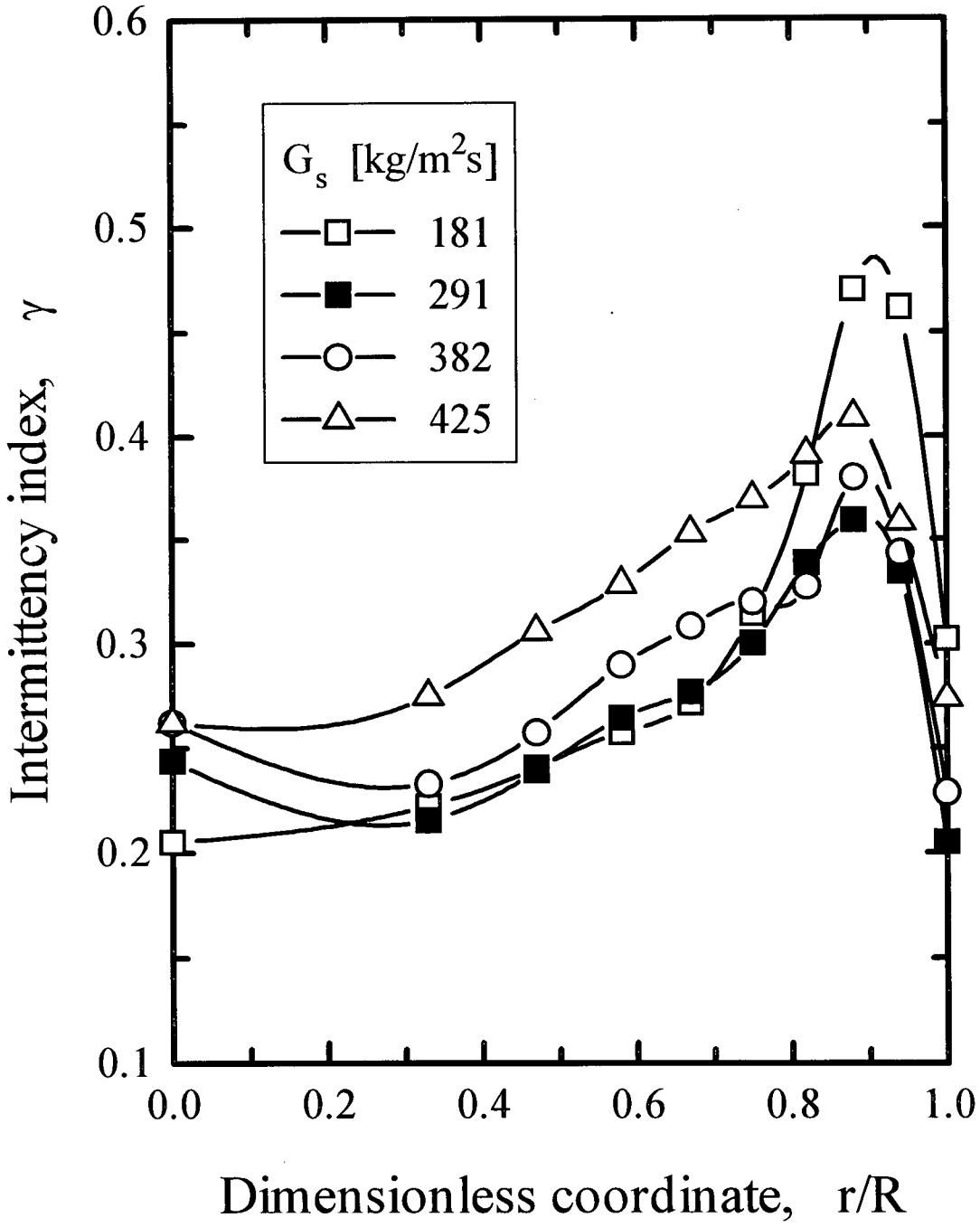

Fig. 4.33: Radial profiles of intermittency index for U = 8.0 m/s and z = 1.57 m (same conditions as in Fig. 4.8).

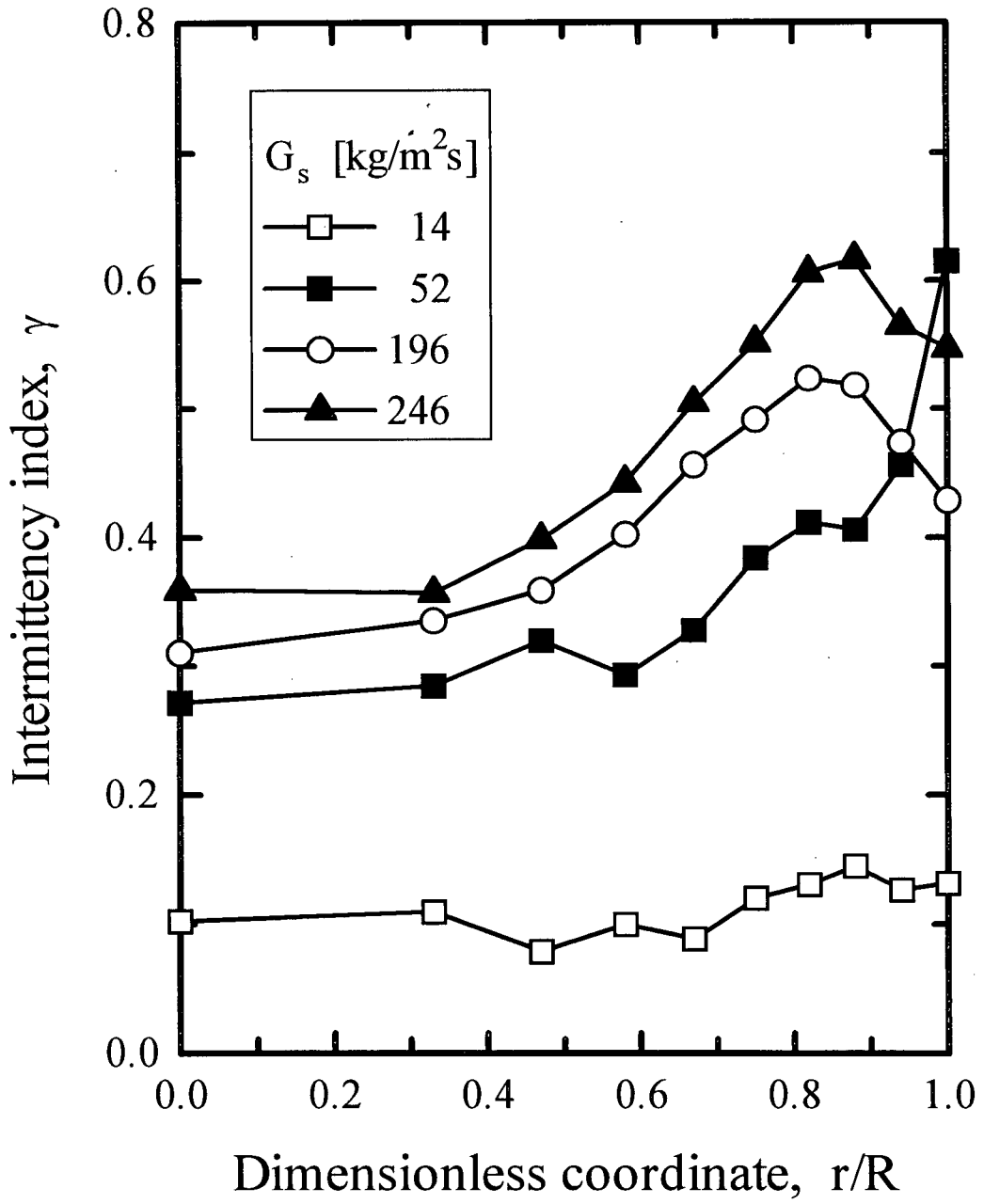

Fig. 4.34: Radial profiles of intermittency index for U = 4.0 m/s and z = 1.57 m (same conditions as in Fig. 4.7).

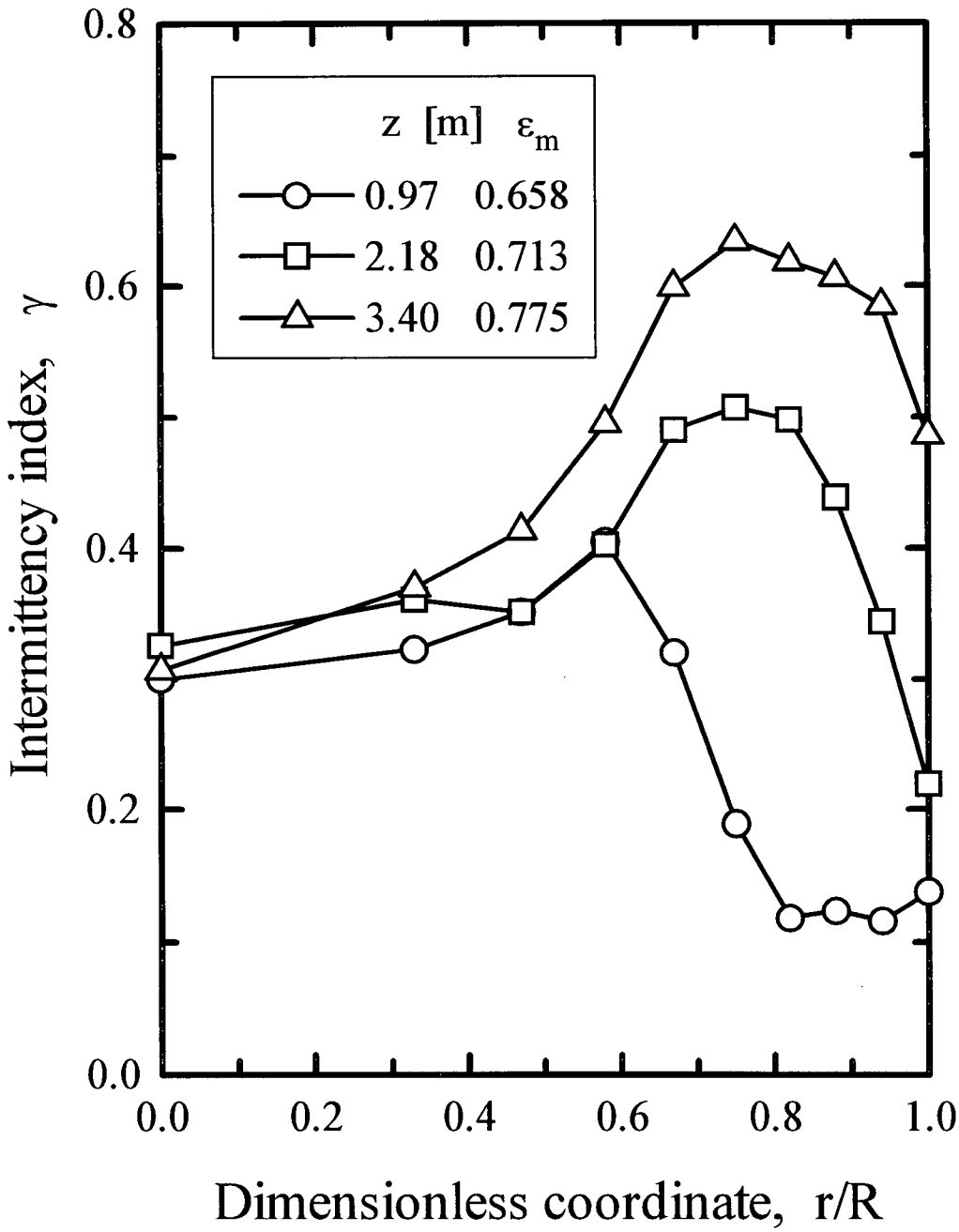

Fig. 4.35: Radial profiles of intermittency index at three heights for U = 5.3 m/s and G_s = 222 kg/m^{2}s (same conditions as in Fig. 4.12).

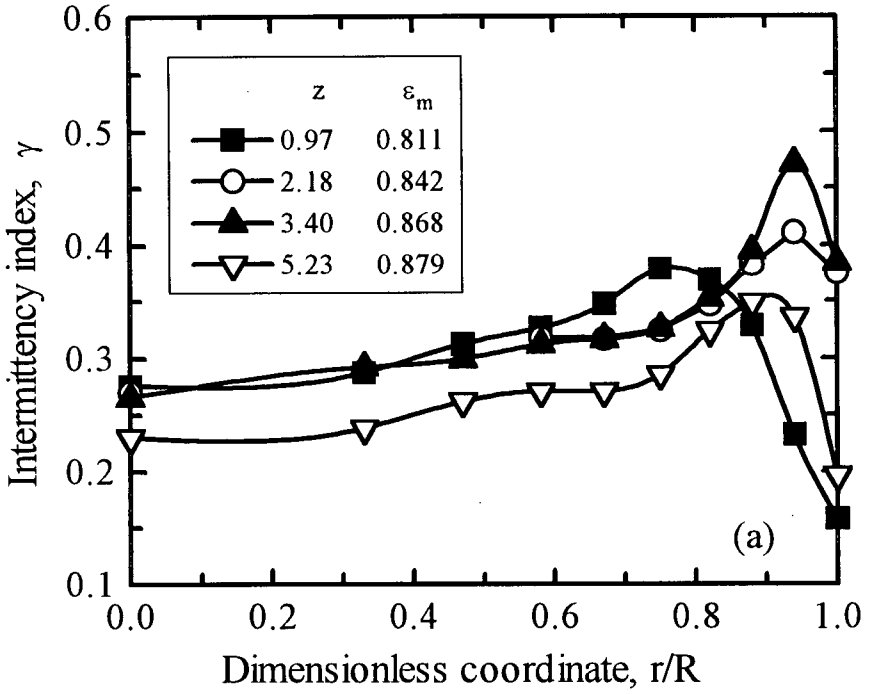

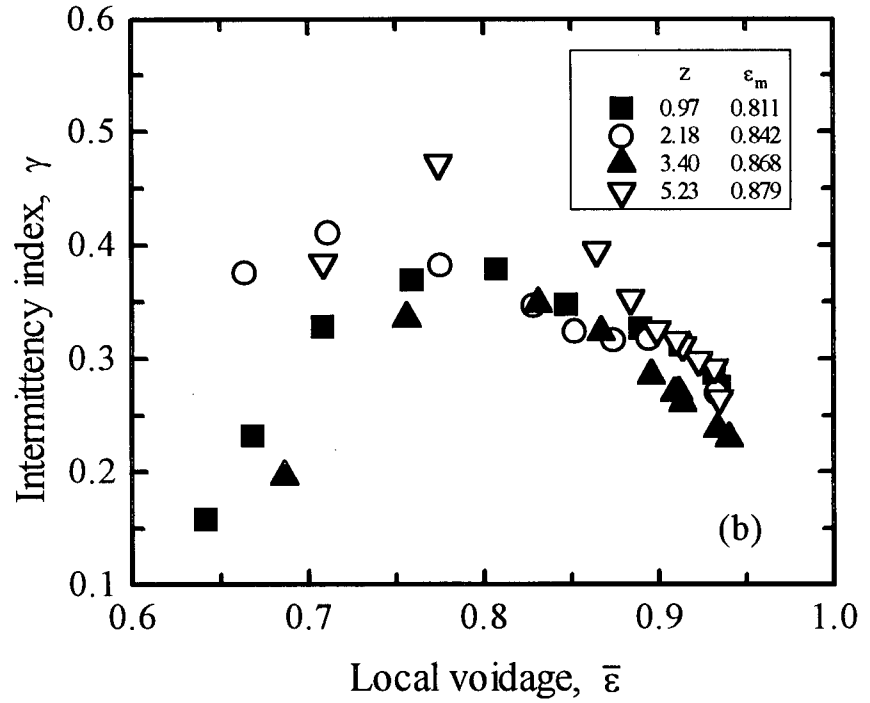

Fig. 4.36: Intermittency index as a function of (a) radial position and (b) local voidage at different heights for U = 6.6 m/s and G_s = 234 kg/m^{2}s (same conditions as in Fig. 4.10).

4.4 Summary

For the FCC particles used in this work, the intensity of the reflected light is not a linear function of the solids concentration as assumed in many previous studies. This necessitates that optical fiber probes be calibrated over a wide range of solids concentrations and not only at the two extremes of no solids and packed bed conditions. A new method of calibrating concentration optical fiber probes has been developed.

As for low solids flux and dilute conditions, voidages for high density conditions are lower near the wall than in the core, with time-mean voidages nearly as low as ε_{mf} at the wall and as high as 0.9 at the axis. The superficial air velocity and solids circulation rate have more influence on the voidage at the wall than in the core. The local voidage data were correlated as a function of the cross-sectional mean voidage; this correlation gives better predictions than previous correlations, formulated for more limited ranges of suspension density.

The radial profile of standard deviation of local voidage fluctuations shows a characteristic peak at some distance from the wall. This is an important feature of HDCFB risers not found in dilute risers. The location of the peak standard deviation can be used to delineate a boundary between a dilute core region and the relatively denser region at the wall. The wall layer thickness defined in this manner is, however, quite different from the wall layer thickness obtained from local solids flux measurements in dilute risers.

Local voidage traces, voidage frequency distribution plots and intermittency index profiles are used to characterize the local flow behaviour in the high density CFB riser. In the riser core voidage fluctuations are low, with a narrow high voidage peak in the frequency distribution. The intermittency index is low in the core suggesting a relatively

uniform predominantly dilute flow interspersed with small fractions of rather high voidage agglomerates. Further outwards, the frequency and density of the agglomerates increase, while the local time-mean voidage decreases. At the location corresponding to the peak standard deviation of voidage fluctuations, the flow has a widely distributed voidage, with no particular dominant fraction. The intermittency index is also highest near this point, showing maximum heterogeneity. Towards the wall, the high voidage peak in the voidage distribution plots disappears as the suspension becomes even denser. The clusters or other structures no longer exist individually, but join in the 'emulsion phase' causing the intermittency index to fall as the flow becomes more uniform. Eventually the suspension is very dense and relatively uniform near the wall.

The perfect homogeneity of the suspension at the two extremes of the voidage scale, i.e. packed bed and zero solids conditions, leads to a "bell-shaped" intermittency vs. local voidage plot, with peak heterogeneity occurring when the local time-mean voidage $\approx$ 0.75.

Having determined the spatial distribution of solid in this chapter, we turn next to the local flow behaviour in the riser based on measurements of the time-mean local particle flow direction and solids flux.

CHAPTER 5

LOCAL SOLIDS FLUX PROFILES

5.1 Introduction

Measurements of local solids mass flux have played an important role in forming our understanding of the flow behavior in circulating fluidized beds. Gadjos and Bierl (1978) and Bierl et al. (1980) presented early local solids flux data based on sampling probes suggesting the core-annulus flow structure in dilute CFB risers, a major departure from the cluster concept proposed earlier by Yerushalmi et al. (1976). Since then many others have studied local solids flux (e.g. Monceaux et al., 1986; Bader et al., 1988; Rhodes, et al., 1988; Bolton and Davidson, 1988; Rhodes, 1990; Herb et al., 1992). In addition to influencing chemical reactions, the local solids flux distribution affects heat transfer (Wu et al., 1990) as well as erosion patterns (Zhu et al., 1989).

Chapter 3 showed that high density conditions can be established in the entire CFB riser with apparent solid hold-ups up to 0.2 ± 0.05. No net solids downflow is observed; instead, the suspension adjacent to the wall appears to be relatively homogeneous. Measurements with a fiber optic probe (Chapter 4) revealed that, as in dilute risers, there is a dilute central region and denser wall region. Bai et al. (1995) inferred the local direction of FCC particles in the bottom dense region differential pressures measured between the tips of a momentum probe. The time-average net vertical direction of particle flow was found to be upward at all radial locations, and

the flow structure resembled that in the turbulent regime. Apart from some recent work by Wei et al. (1997) in the bottom region of a CFB riser, no measurements of local solids flux under high density conditions are available in the literature. This chapter presents local solids flux measurements in the high density circulating fluidized bed riser.

5.2 Measurement method

Solids sampling by applying suction to a tube inserted in a column and bent to face the flow has been most widely used for measuring local vertical solids fluxes in CFB risers. A less direct method is the electrostatic ball technique (Louge, 1997) in which a small metal ball is inserted into the riser. When particles of a different material contact the ball, the ball surface and the particles attain opposite charges. Each particle contact is detected as an individual pulse appearing at the output of a charge-to-voltage converter connected to the sphere. The pulse frequency is a function of the number of particles striking the sphere and therefore the solids flux. The probe cannot identify the direction of impacting particles. It also requires calibration, in most cases by a sampling probe. The sampling technique is simpler and was adopted in this study.

5.2.1 Sampling probes

Isokinetic sampling probes, commonly employed to sample steady, dilute aerosol flows, are superior to non-isokinetic sampling, but it is doubtful whether they can follow the large and rapid velocity changes in risers. Denser suspensions also

require high suction gas velocities to maintain particle transport through the line without blockage, making it unlikely that isokinetic conditions could be maintained even in a time-average sense. Harris et al. (1994) indicated that isokinetic sampling was impossible near the riser wall with their probe tip facing upwards. Their probe also choked at low air flows so that a minimum air flow was needed to maintain particle sampling. These limitations have led workers to adopt non-isokinetic sampling. Azzi et al. (1991) found that the particle flux remained nearly constant if the suction velocity was varied within ± 1.5 m/s of the superficial gas velocity. Suction velocities equal to the superficial gas velocity were reported (Aguillon et al., 1996) to give satisfactory results. Monceaux et al. (1986), using fine catalyst particles, observed that the solids collected first increased with suction rate, then stayed constant over a wide range, and then increased again. Bader et al. (1988) and Werther et al. (1993) observed no significant influence of the suction gas velocity. Rhodes et al. (1988), Rhodes (1990) and Miller and Gidaspow (1992) found that although the upward and downward mass fluxes were sensitive to the sampling gas flow rate, the net solids mass flux was virtually independent of the gas velocity at the tip, provided that the gas velocity in the sample line was sufficient to prevent blockage.

Bierl et al. (1980) found a significant effect of the suction velocity of their non-isokinetic probe on the solids mass flux when measuring solids downflow near the wall. They suggested that the true flux there should be obtained by extrapolating the solids flux to zero suction velocity. They also recommended that measurements near the wall be performed with a suction velocity that just keeps the probe free of blockage. de Diego et al. (1995) found that both the downward and upward solids flux in the dense region of their riser were greatly affected by the suction velocity.

Their attempt to measure solids fluxes at different suction velocities and extrapolate to zero suction failed to produce reasonable results. Herb et al. (1992) using an isokinetic probe, observed that measured solids fluxes in the core region were not strongly dependent on the suction velocity near the isokinetic operating point. Their sensitivity study showed that the downward component of the solids flux was sensitive to the suction velocity in the region near the wall where the downflow of solids was significant. To overcome the sampling problem at the wall, Bolton and Davidson (1988) used 5 mm ID acrylic tubes at different heights to collect particles falling near the wall; by assuming negligible solids upflow, they were able to estimate the solids flux in the wall region.

Louge (1997) explains that for conditions prevailing in dilute circulating fluidized bed risers, the Stokes numbers in the core region is often large (10 to 1000) so that the gas suction does not influence particle trajectories significantly. However, because of the no slip condition at the wall, the Stokes number is considerably smaller in the descending curtain of solids near the wall. Particles are more readily entrained by suction, and therefore collection becomes a strong function of the suction rate.

Two types of sampling probes were used in this study, one for upflow and the other for downflow. The upflowing solids flux was measured with an "inverted-U" suction tube (Rhodes, et al., 1988) made of 4 mm I.D. stainless tubing. Downflowing solids were sampled at four radial locations (r = 0.0, 19.1, 28.6 and 36.1 mm) using 45° inclined tubes, inserted one at a time to minimize disturbance. The inclination angle was sufficient to allow smooth solids flow without blockage. The ends of the tubes were cut flat at 45° to make the opening horizontal, with a portion of the orifice blocked as indicated in Fig. 5.1(b) to minimize solids reflection back into the

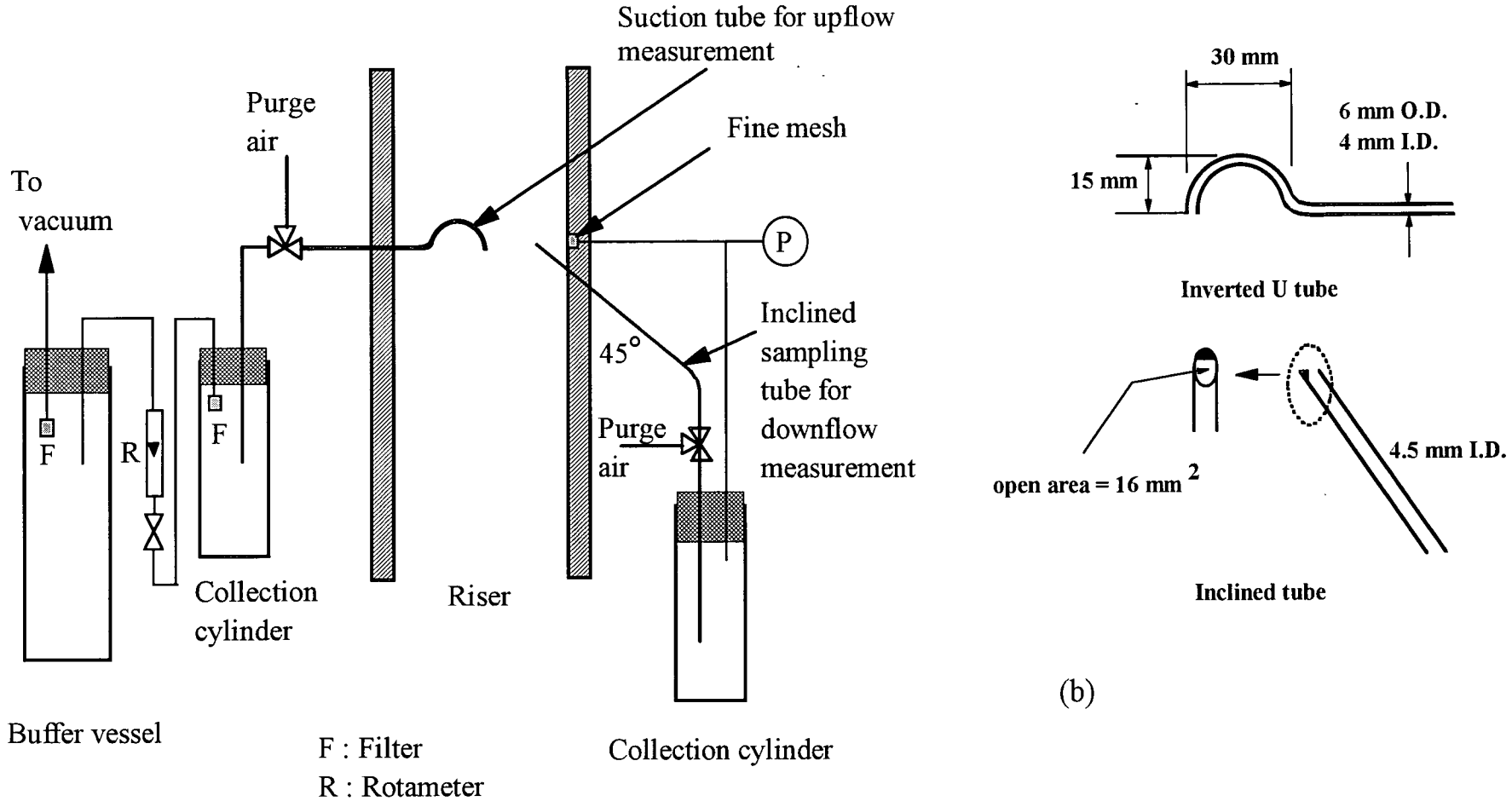

Fig. 5.1: Solids flux sampling system: (a) Schematic of system; (b) Details of sampling tube.

mainstream. The open area of each tube was 16 mm^2. To allow air displaced from the collection vessel by the accumulating particles to return to the column without obstructing the solids flow, a tube covered with wire mesh at its end connected the collection cylinder to the riser at the same level as the sampling position. Samples were collected over periods from 30 to 180 s. The solids flux in each direction is obtained by dividing the corresponding collected mass of solids by the sampling duration and the cross-sectional area of the probe tip. Figure 5.1 provides other details of the probes and a schematic of the sampling system, while Appendix A-8 gives more details.

5.3 Results and Discussion

Figure 5.2 shows local solids fluxes at two radial locations near the wall (r/R = 0.67 and 0.89) for different suction velocities. No significant influence of suction velocity is observed, so all experiments were performed with the suction velocity equal to the superficial air velocity in the riser.

Figures 5.3, 5.4 and 5.5 show radial profiles of upward, downward and net solids flux at a height of 2.8 m for superficial gas velocities of 4.5, 7.5 and 7.0 m/s and solids circulation fluxes of 210, 250 and 325 kg/m^2s, respectively. The upflow solids fluxes are highest at the center of the column, decreasing towards the wall, whereas the magnitudes of the measured downward fluxes are low at the center and increase toward the wall. The net profiles are roughly parabolic, with the net solids flux decreasing from the center, where it is about two to three times G_S, to low values near the wall. Measurements were only possible beyond 2 mm from the wall. The

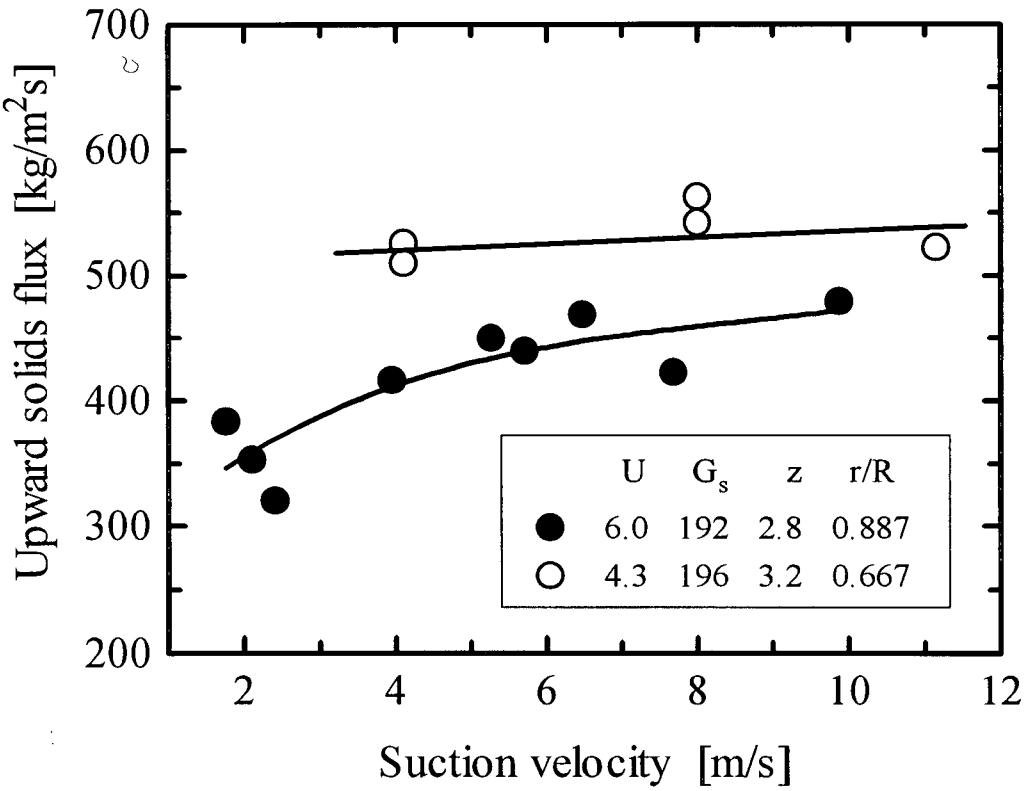

Fig. 5.2: Influence of suction velocity on upward local solids flux. U, G_s and z have units of m/s, kg/m^{2}s and m, respectively.

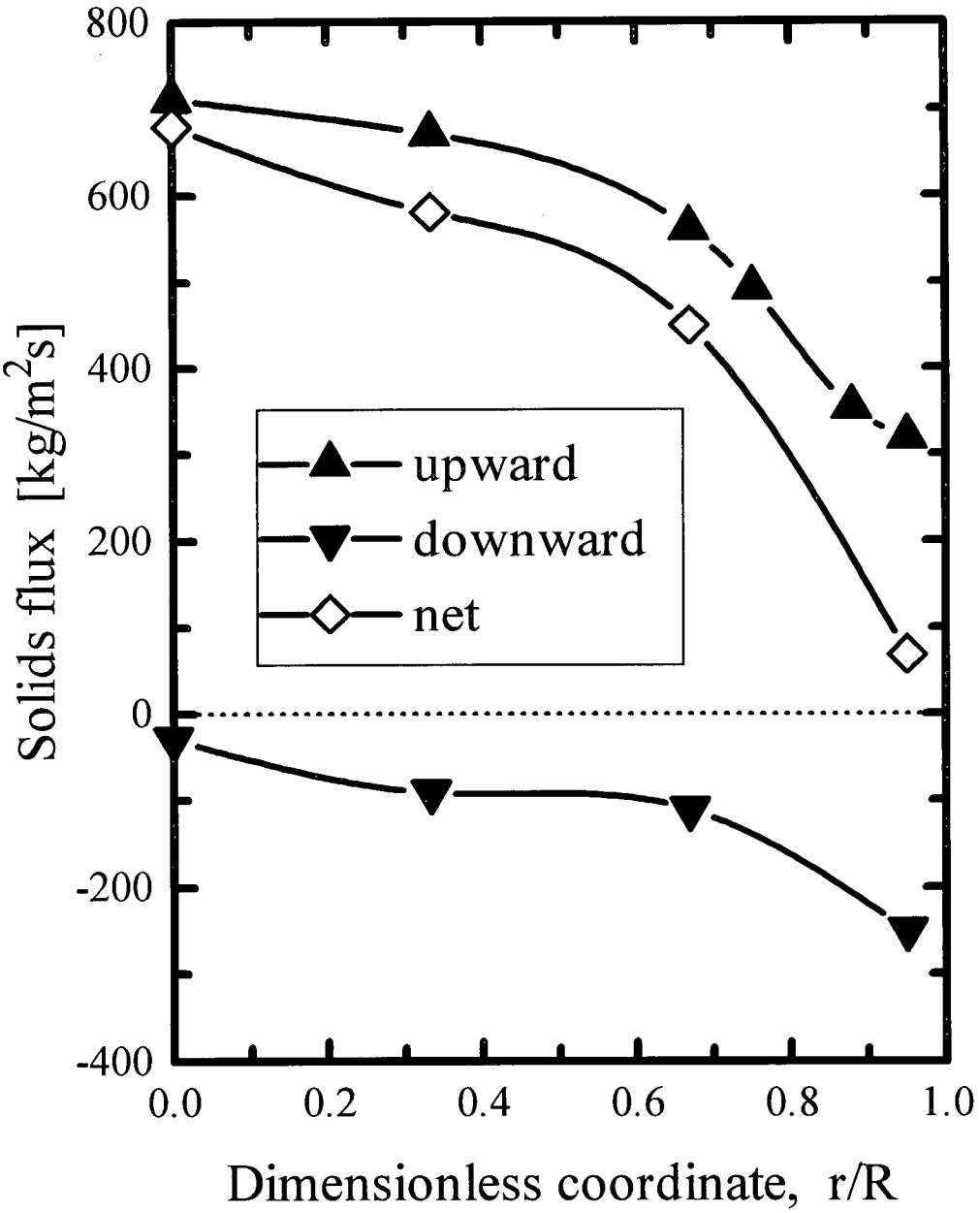

Fig. 5.3: Radial profiles of local solids mass flux profiles at U = 4.5 m/s, G_s = 210 kg/m^{2}s and z = 2.8 m.

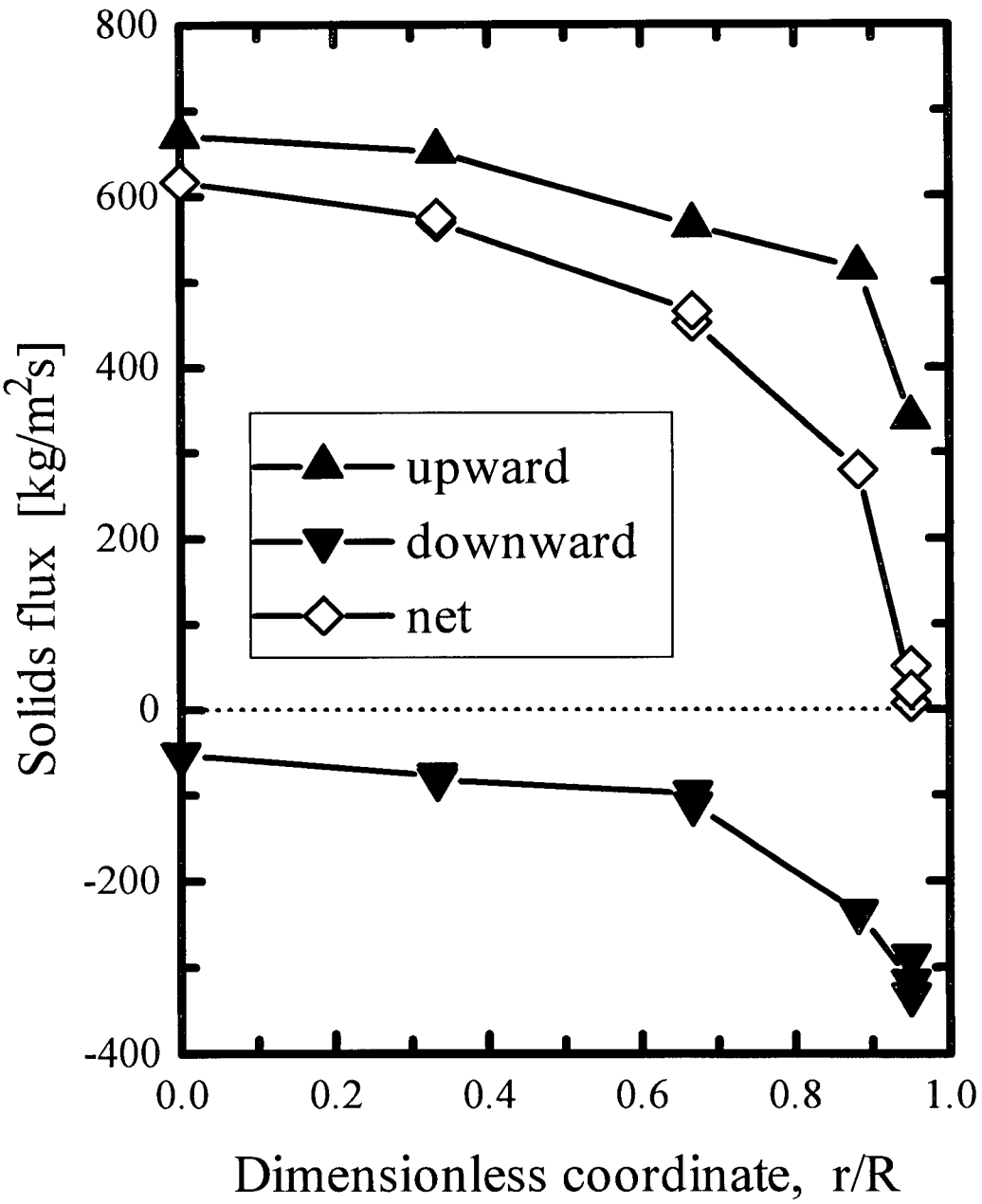

Fig. 5.4: Radial profiles of local solids mass flux profiles at U = 7.5 m/s, G_S = 250 kg/m^{2}s and z = 2.8 m.

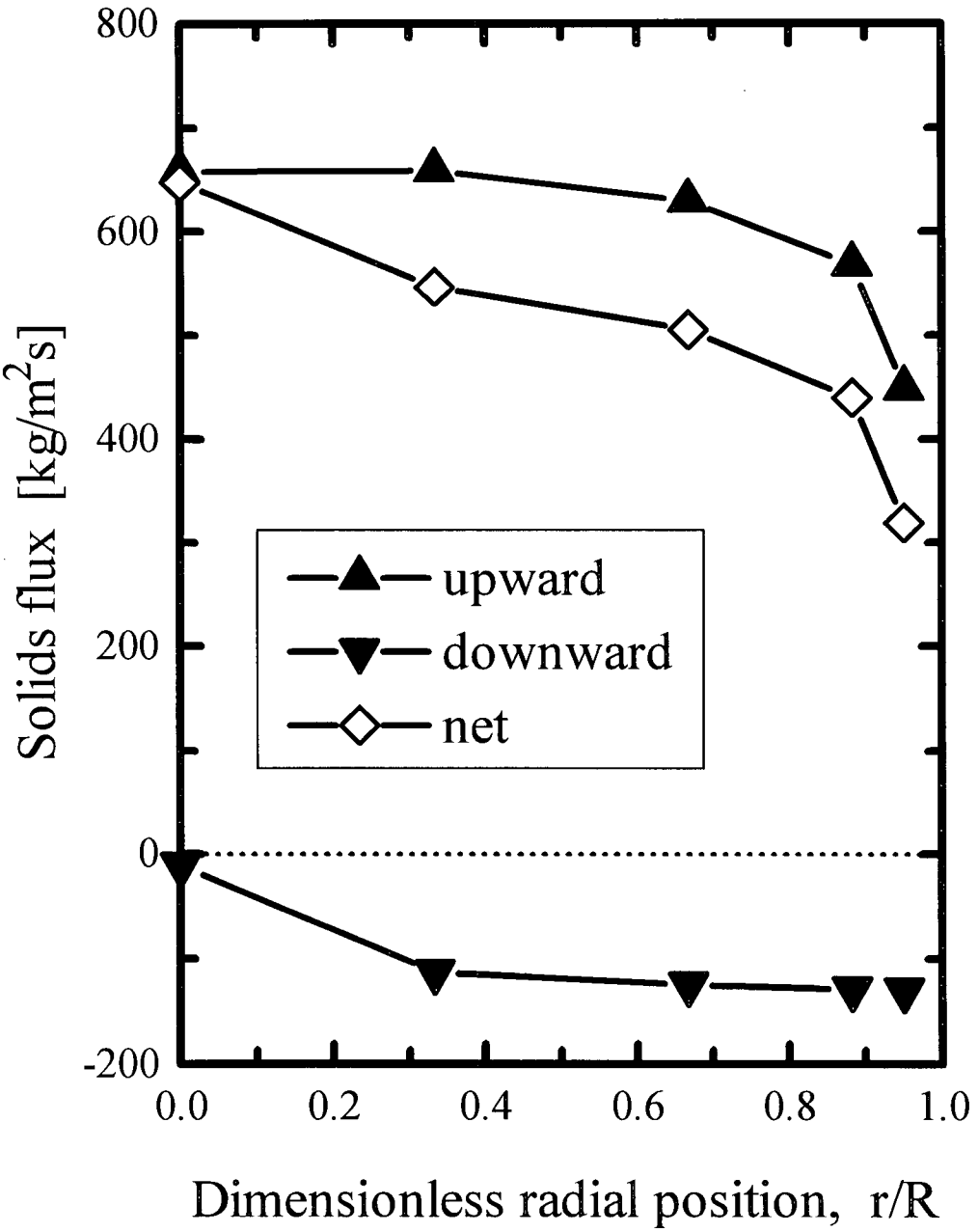

Fig. 5.5: Radial profiles of local solids mass flux profiles at U = 7.0 m/s, G_s = 325 kg/m^{2}s and z = 2.8 m.

profiles indicate that under high density conditions, on average, solids are moving rapidly upward in the central region, while they are nearly stagnant or moving slowly upwards near the wall. This accords with visual observations. For comparison, Fig. 5.6 shows similar measurements for a relatively dilute riser at the same height. While the shape of the profile is similar, there is a substantial downward flux near the wall, unlike the high-density case where there is little (if any) net downwards motion.

The influence of net solids circulation flux, G_S, on solids net flux profiles is shown in Figs. 5.7 and 5.8 for superficial gas velocities of 4.5 and 7.0 m/s, respectively. Comparison of the integrated solids fluxes obtained from the local measurements and the net solids fluxes determined by the butterfly valve closing method (see Chapter 2) shows that there is an average difference of about 15% between the two as shown in Table 5.1where % deviation = $(G_{s,expt.} - G_{s,calc.})/G_{s,expt.}$ x 100%. Given the error inherent in measuring the net solids circulation flux, the fact that the local values are obtained by subtraction of two larger magnitudes, and the occurrence of both positive and negative deviations, this range is acceptable. For $G_S > 170$ kg/m^{2}s the profiles are roughly parabolic and an increase in G_S is accompanied by an increase in solids flux in the central region. It has been observed previously for dilute conditions (e.g. Herb et al., 1992) that solids downflow increases near the wall as the solids flow is raised. On the other hand, Figs. 5.7 and 5.8 show that once the section is sufficiently concentrated ($\varepsilon_m \geq 0.15$) the net solids flux near the wall falls to close to zero, changes direction to upflow and continues to increase with increasing net solids circulation rate. The observed profiles are consistent with earlier results at lower G_S (e.g. Herb et al., 1992) and with measured radial voidage profiles (Chapter 4). The no-slip condition at the wall means that the gas velocity approaches zero in the outer part of the column. There is therefore a

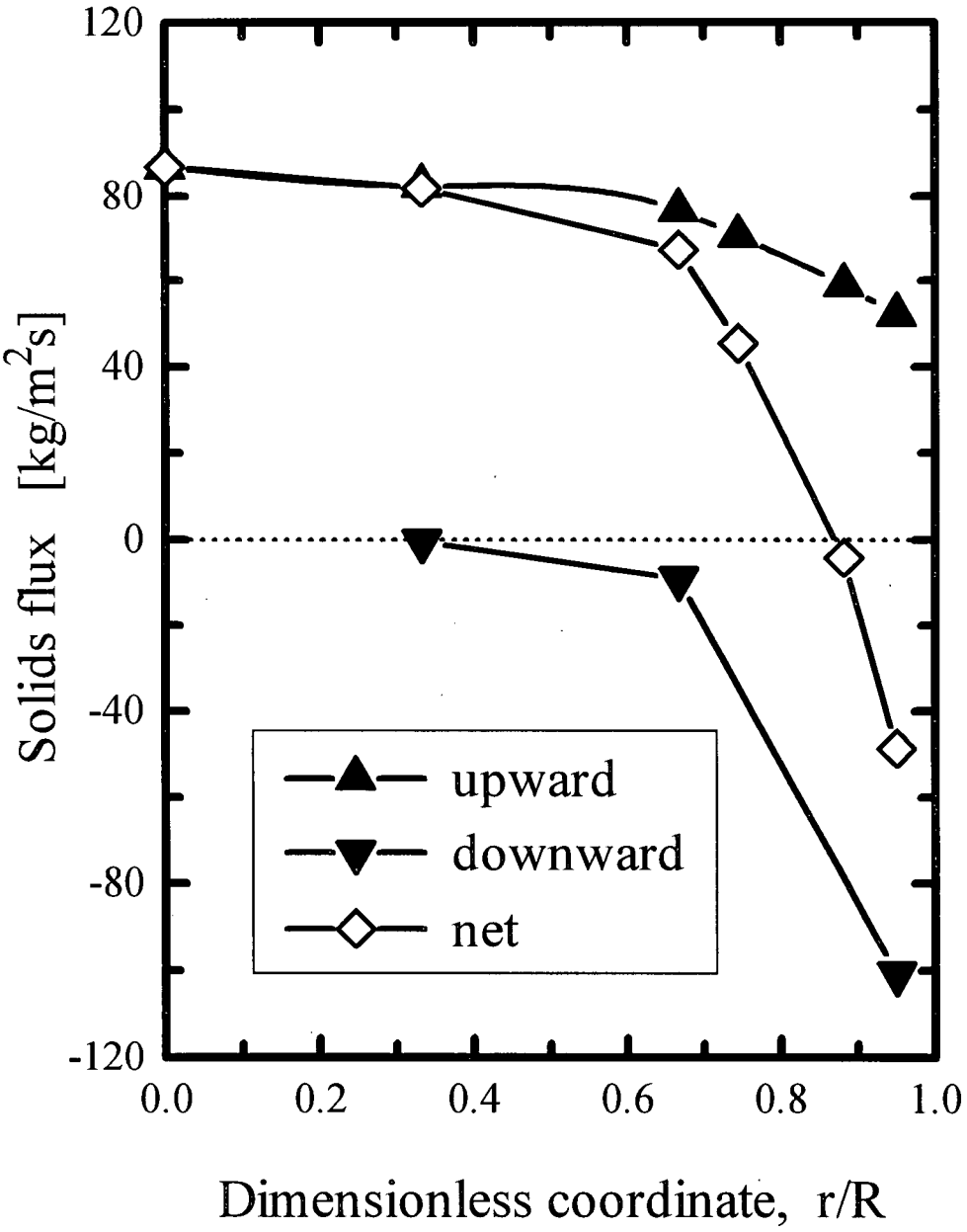

Fig. 5.6: Radial profiles of local solids mass flux profiles at U = 4.5 m/s, G_s = 38 kg/m^{2}s and z = 2.8 m.

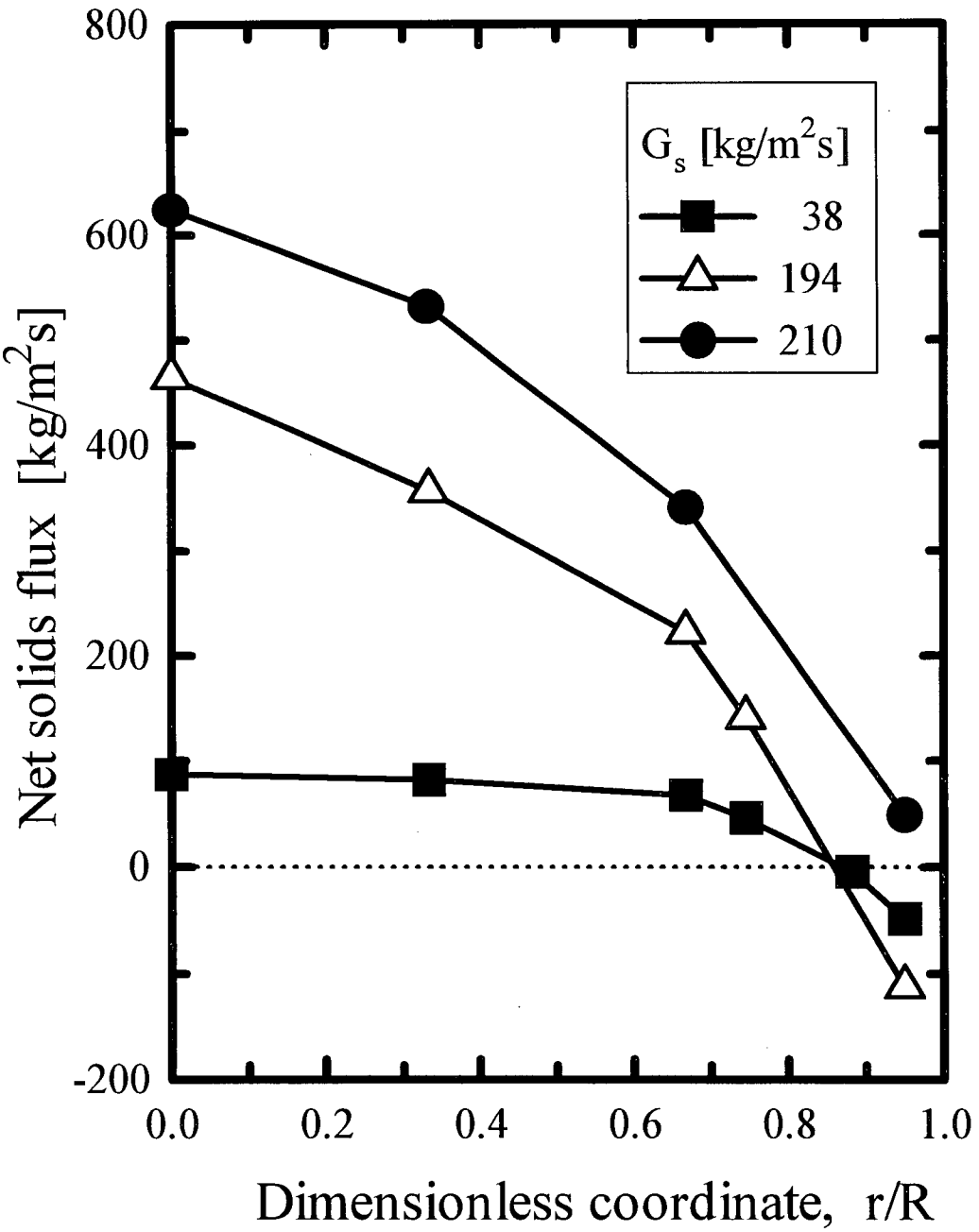

Fig. 5.7: Radial profiles of net solids mass flux profiles at U = 4.5 m/s and z = 2.8 m for different solids circulation fluxes.

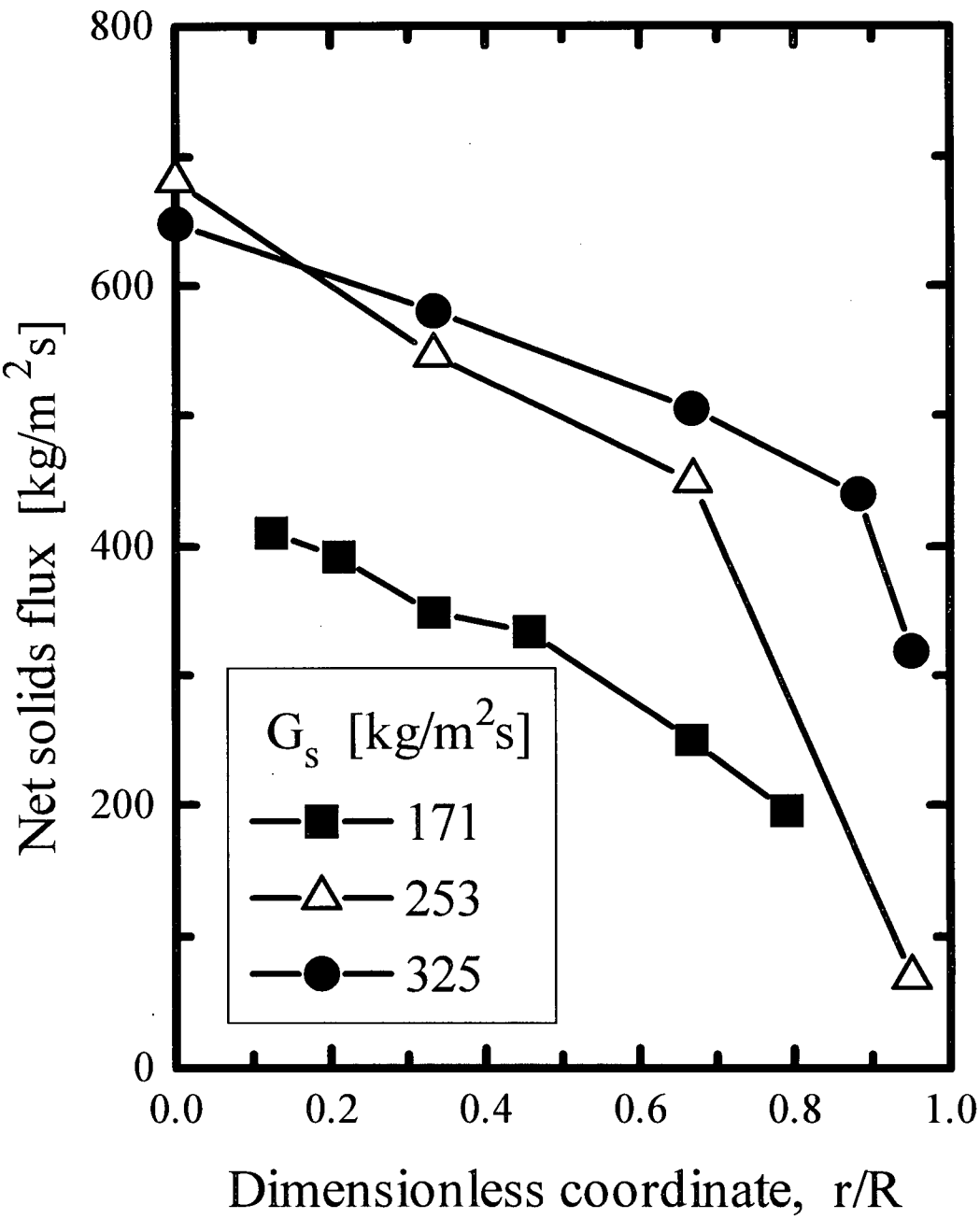

Fig. 5.8: Radial profiles of net solids mass flux profiles at U = 7.0 m/s and z = 2.8 m for different solids circulation fluxes.

Table 5.1: Comparison of integrated local solids fluxes with net circulation fluxes measured by butterfly valve closing method.

U [m/s]	z [m]	$G_{s,expt.}$ [kg/m^{2}s]	$G_{s,calc.}$ [kg/m^{2}s]	% deviation
4.5	2.8	38	37	+ 3
4.5	2.8	194	147	+24
4.5	2.8	210	271	-29
7.0	2.8	253	353	-40
7.0	2.8	325	436	-34
7.5	2.8	250	329	-32
7.5	4.6	246	189	+23

tendency for particles to fall near the wall, especially when they form clusters or streamers. However, the high concentration of particles near the wall for high-density conditions results in increased momentum transfer from the upflowing suspension in the interior of the column, meaning that there is relatively little downflow in the vicinity of the wall.

Figure 5.9 compares solids flux profiles 2.80 and 4.62 m above the distributor. The conditions at the higher elevation were relatively dilute, and therefore the net solids flux is downward near the wall; compensating for this downflow, a higher solids flux is measured at the centre compared to the lower elevation. For nearly constant G_s, the superficial gas velocity appears to have little influence on the solids flux, as shown in Fig. 5.10.

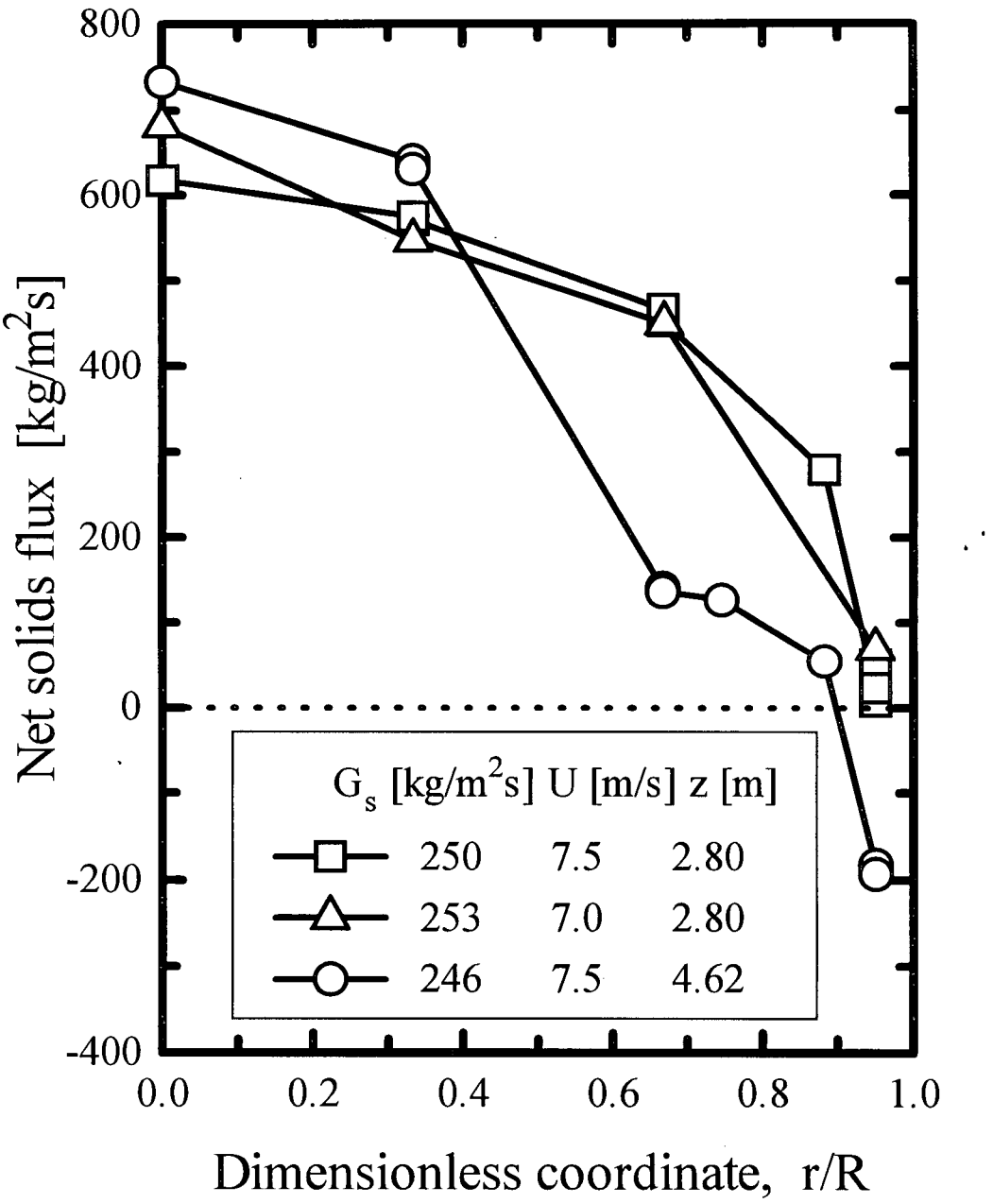

Fig. 5.9: Effect of elevation on radial profiles of net local solids mass flux.

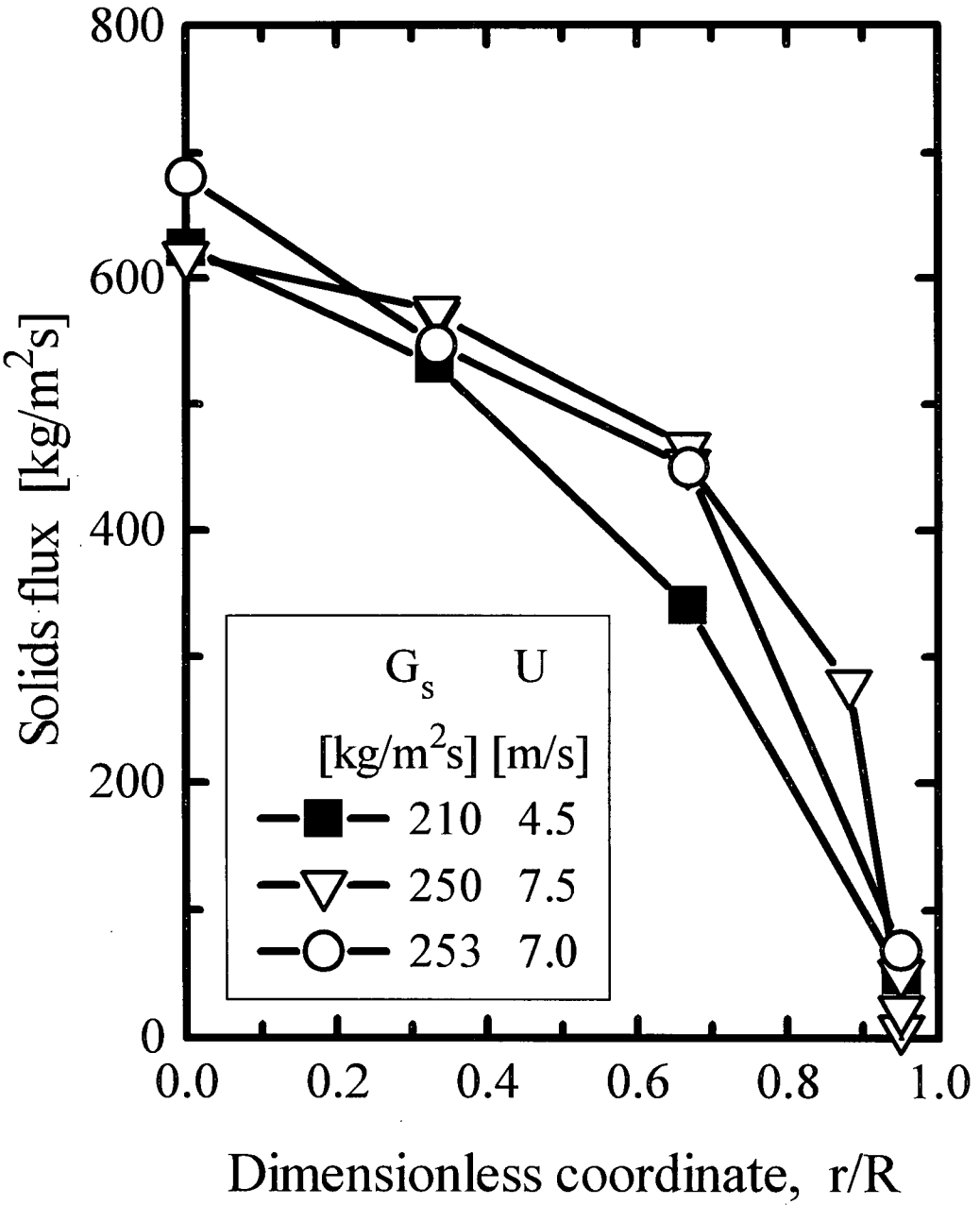

Fig. 5.10: Effect of superficial gas velocity on radial profiles of local solids mass flux at z = 2.8 m.

5.4 Local solids flow direction determined by momentum probe

Probes measuring the dynamic pressure have been utilized in some studies to indicate the local solids flow direction and to estimate the magnitude of the resultant particle velocity. Earlier forms of this type of probe consisted of a single tube bent into a right angle and inserted into the flow to measure the dynamic pressure. A small quantity of purge air is usually introduced to keep the tubes free of particles. If the flow is assumed to be uniform with negligible gradients, the tube is similar to a Pitot tube. The suspension momentum flux could then, neglecting the gas contribution, be expressed from Bernoulli's principle as,

$$\Delta P_{mo} = \alpha G_s V_p \qquad (5.1)$$

where ΔP_{mo} is the pressure drop caused by the deceleration of particles and α is a constant. Zoonen (1962) assumed $\alpha = 0.5$ as for single phase incompressible flow, while Gadjos and Bierl (1978) and Bader et al. (1988) found $\alpha = 0.81$ and 0.75, respectively, from their studies.

Because of the fluctuating nature of the flow under CFB conditions, two tubes side by side and bent into right angles to face in opposite directions, one up and the other down, were later used by Azzi et al. (1991), Zhang et al. (1994) and Bai et al. (1995). The tubes were connected to pressure transducers to measure the dynamic pressure on either end. Azzi et al. (1991) proposed

$$\Delta P_{mo} = K G_s V_p = K G_s^2 / [\rho_p (1 - \varepsilon)] \qquad (5.2)$$

by assuming the pressure drop between the two tube-ends to be proportional to the suspension momentum. Measurements of the solids flux by a sampling probe and local voidage by a γ - ray absorption technique gave $K \approx 1.39$ for FCC particles. Zhang et al. (1994) using sand particles in a CFB boiler proposed

$$\Delta P_{mo} = \alpha \frac{G_s^{\,2}}{\rho_p(1-\varepsilon)} + k \qquad (5.3)$$

for a probe with tubes of inner diameter 8 mm, where $\alpha = 1.19$ and $k = 81.25$ Pa.

The theoretical interpretation of the recorded pressure from momentum tubes is complicated by inhomogeneity as well as by intermittent reversal of the flow. For dense conditions gravity and particle-particle and particle-tube collisions are significant. Concentration gradients build up as the suspension is brought to rest, and the flow is neither irrotational nor inviscid (Louge, 1997). In this study, therefore, a momentum probe was used only as a simple preliminary tool to indicate the local particle flow direction. The Pitot-type momentum probe used here and shown in Fig. 5.11(a) consists of two brass tubes of inner diameter 2.5 mm attached to the optical fiber probe and bent into smooth right angles as in the designs of Azzi et al. (1991). The optical fibre probe was attached to facilitate simultaneous measurement of both pressure drop and local voidage. The distance between the tips is 15 mm. The pressure difference, ΔP_{mo}, was measured at ten radial positions. The pressure in each tube was measured by an absolute pressure transducer (Omega PX142) from which ΔP_{mo} was obtained by difference. Purge air was metered into both tubes using needle valves to prevent blockage. The purge air flowrate had no significant influence on the pressure difference, provided it was within the range of local air velocities anticipated in the riser (Fig. 5.11b). Neglecting the gas contribution and also the static pressure difference between the two ports, the following approximate equation can be written, since the upstream facing port measures a stagnation pressure while the downward facing port measures a lesser pressure in its own wake:

$$\Delta P_{mo} \approx K \frac{1}{2}[\rho_p(1-\bar{\varepsilon})V_p]|V_p| \qquad (5.4)$$

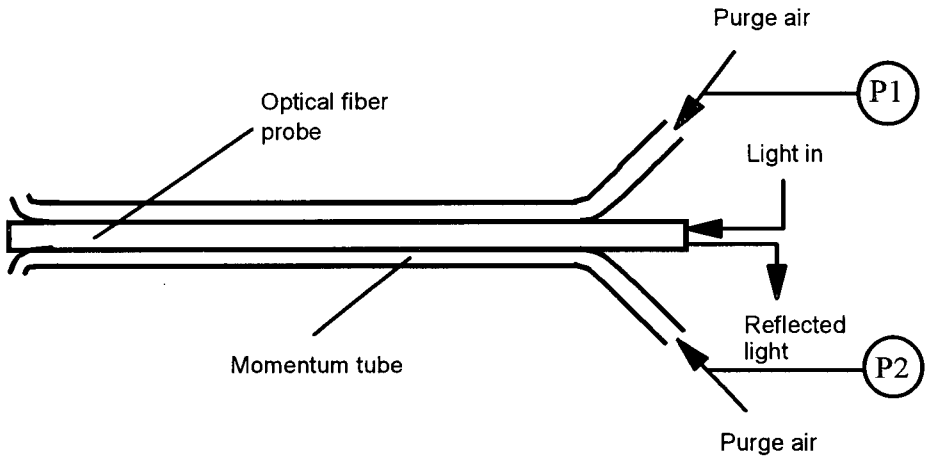

(a)

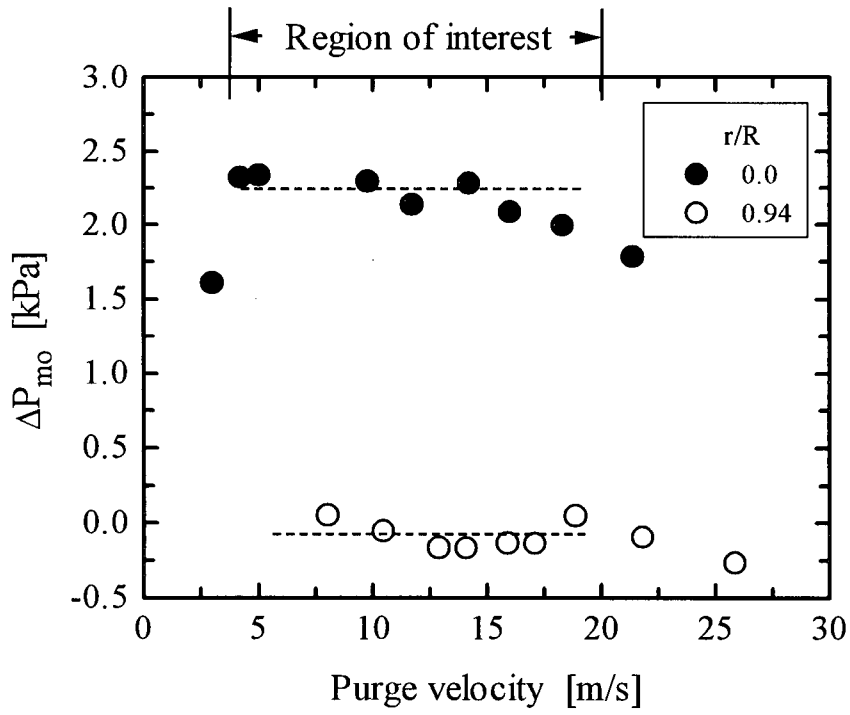

(b)

Fig.5.11: Combined optical fiber-momentum probe: (a) Probe; (c) Influence of purge velocity on momentum tube pressure drop (U = 8.0 m/s, G_s = 149 kg/m^{2}s, z = 2.16 m).

K is dependent on the probe design but is assumed to be independent of $\bar{\varepsilon}$ and V_p. The solids movement can then be characterized by recording ΔP_{mo} as a function of time. A positive pressure difference indicates net upward movement of particles while negative values indicate net downflow. Signals from both the optical fibre probe and the absolute pressure transducers were logged on a personal computer via an A/D converter for periods of 100 s at a sampling frequency of 100 Hz.

Figure 5.12 gives instantaneous ΔP_{mo} and local voidage traces at six radial locations 3.40 m above the distributor for U = 7.8 m/s and G_s = 272 kg/m^{2}s. The cross-sectional mean voidage is 0.794. On the axis the flow is wholly upwards as reflected by the high positive value of ΔP_{mo}. The fluctuations amplitude slowly decreases toward the wall and some particles appear to move downwards as reflected by brief periods of negative ΔP_{mo}. However, on average the net time-mean flow is always upward as shown in Fig. 5.13 which plots ΔP_{mo} for G_s = 272 kg/m^{2}s and 354 kg/m^{2}s for z = 3.4 and 1.57 m, respectively. Both locations are subject to high density conditions. The local voidage trace was discussed in Chapter 4. It is clear that the dynamic pressure decreases with increasing solids concentration, reflecting the low particle velocities associated with such dense suspensions. For comparison purposes, ΔP_{mo} for G_s = 126 kg/m^{2}s and z = 2.16 m, above the dense phase, is also plotted in Fig. 5.13. Here the flow is upward in the core region and downward at the wall. For the higher G_s values, the magnitude of the measured momentum probe pressure drop is consistent with the solids flux data in indicating that solids travel upwards rapidly in the central dilute region while remaining stagnant or rising much more slowly at the wall. Bai et al. (1995), using a similar probe, found that the time-average ΔP_{mo} was positive for all radial positions in the dense zone of their riser but negative near the wall in the upper dilute region. They defined the annular wall layer

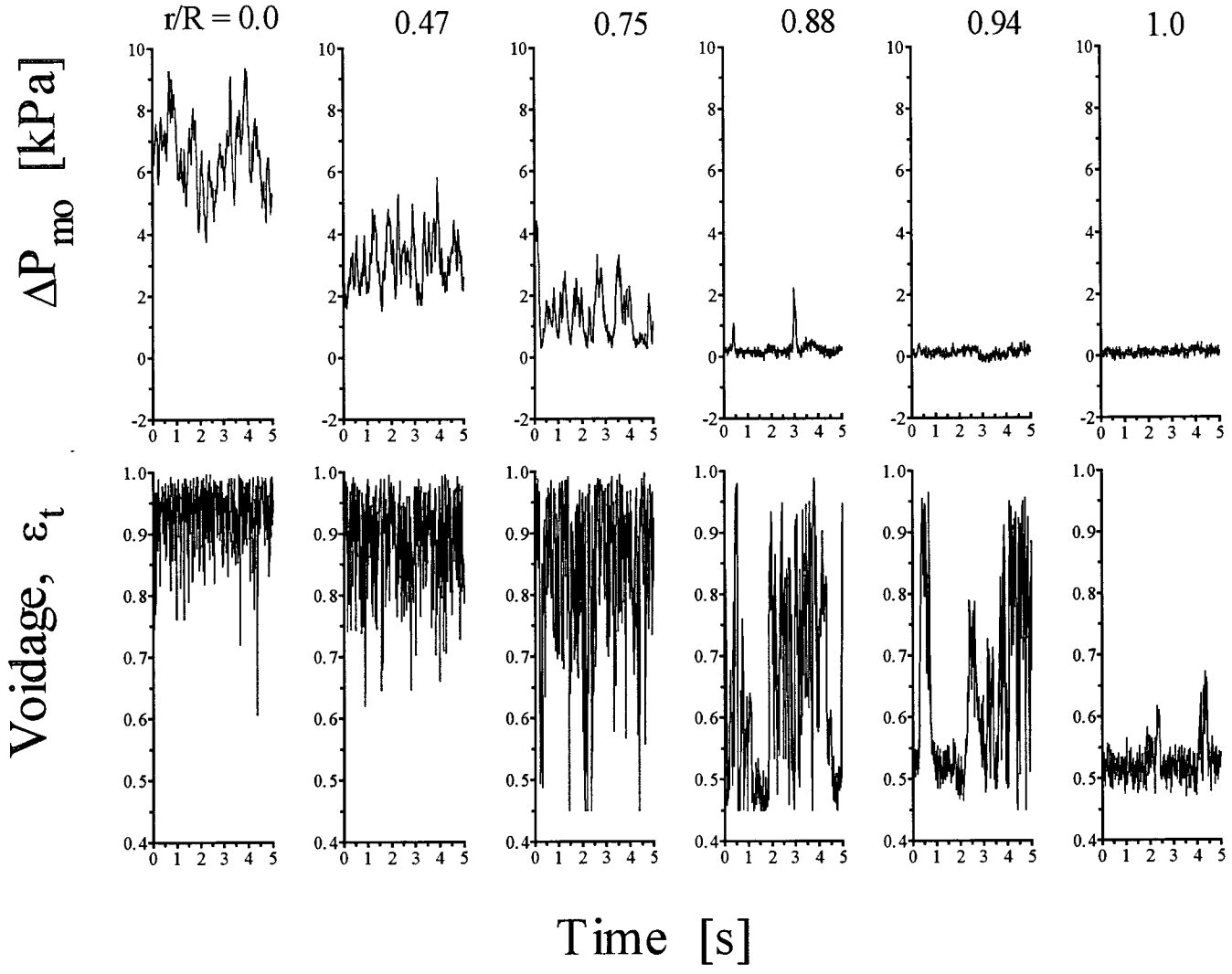

Fig. 5.12: Instantaneous momentum probe pressure drop and optical fibre voidage traces at six radial locations for U = 7.8 m/s, G_s = 272 kg/m^{2}s and z = 3.4 m.

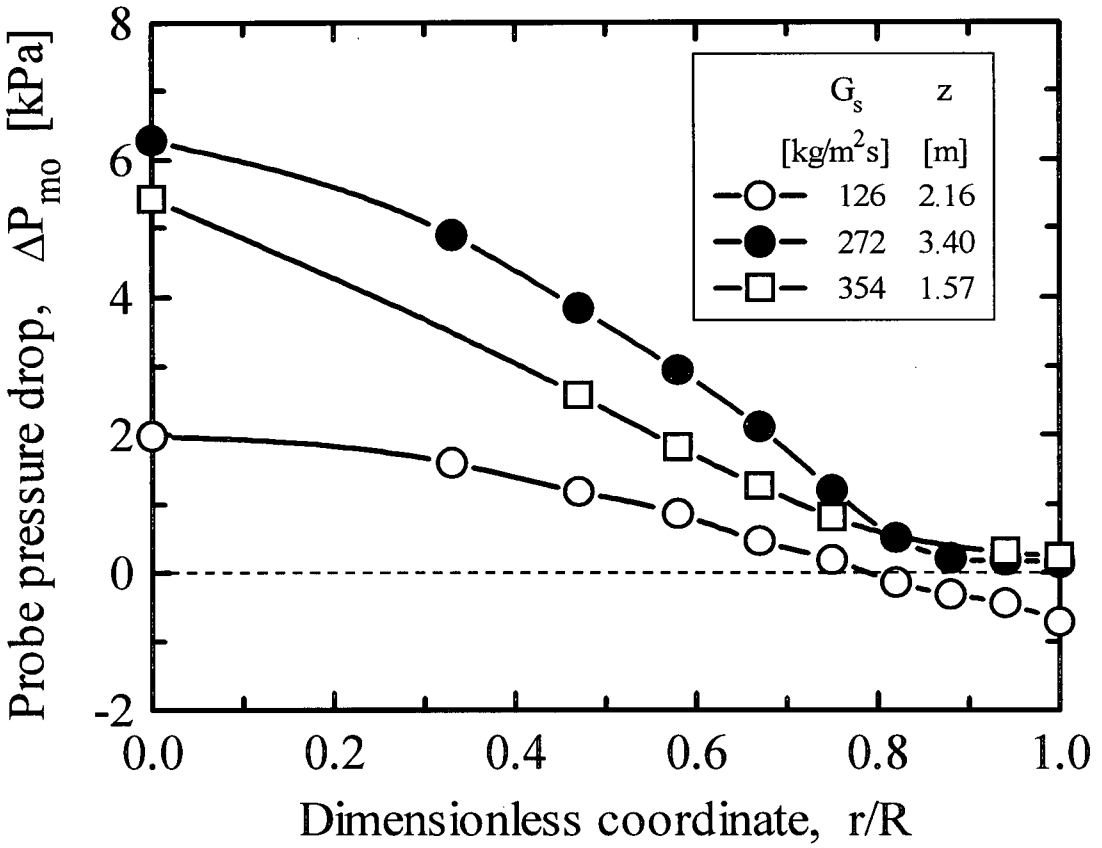

Fig. 5.13: Radial profiles of momentum probe pressure drop for U = 7.8 m/s.

thickness as the distance from the wall to the point where $\Delta P_{mo} = 0$, and correlated it to the cross-sectional mean voidage as given by Eq. (4.12). The present results are, however, not consistent with the data of Wei et al. (1997), who using a non-isokinetic sampling probe for both the upward and downward solids sampling, found that there was net solids downflow near the column wall both for dense and dilute regions.

5.4 Summary

Strong radial gradients of vertical solids flux exist in dense risers, as in dilute risers. While the high-density fast fluidized bed shows some features of low-density systems, in particular lower voidages towards the wall (Chapter 4) and increased upwards solids fluxes in the interior, there is a substantial difference in that there is no region of net downflow near the wall for high-density risers. As a result, the concept of distinct core and annular regions, commonly used in characterizing and modelling low-density CFB risers, appears to have little or no applicability under high-density conditions. Instead, it is important to consider continuous radial variation of both voidage and particle flux. Visual observations suggest absence of net solids downflow at the wall at both the top and bottom of the riser under HDCFB conditions, but further measurements are needed in these regions.

Now after determining the flow characteristics of HDCFB risers there is need to compare flow dynamics in HDCFB risers with those of standard gas-solid flow regimes, as well as find whether or how the operation treated in this thesis fits in the conventional classification of fluidized bed flow regimes. These items are dealt with in the next chapter.

CHAPTER 6

HDCFB FLOW DYNAMICS RELATIVE TO STANDARD GAS-SOLID FLOW REGIMES

6.1 Introduction

The flow characteristics and transition velocities of bubbling, turbulent, slugging and fast fluidization regimes were reviewed in Chapter 1. The objective of the present chapter is to compare the flow characteristics of high density circulating fluidized bed risers to those of the known flow regimes. We first recapitulate briefly the main features of these regimes. In the bubbling regime, bubbles form at the distributor and rise, coalescing and growing larger as they migrate upwards and simultaneously inducing mixing of particles in the bed. A slugging regime is formed if bubbles grow to sizes comparable with the column diameter. In general, slugging is not encountered for shallow beds, in columns of very large diameter or for fine particles ($d_p < 60$ μm) because bubbles are then unable to grow to be of comparable size to the column diameter (Grace and Bi, 1997). Transition from bubbling to turbulent fluidization occurs when the superficial velocity exceeds the velocity U_c at which the standard deviation of differential pressure fluctuations reaches a maximum. Although differing views have been presented about the nature of the turbulent regime, it is widely agreed that full-fledged bubbles no longer exist. The upper limit of turbulent fluidization is the onset of fast fluidization, and is marked by the velocity U_{se}, at which significant entrainment of bed particles starts to take place (Bi et al., 1995). Dilute circulating fluidized beds are operated in either the fast fluidization regime or in dilute transport.

A CFB riser operating under fast fluidization conditions has a bottom dense zone and an upper dilute zone, with a transition region inbetween. For dilute phase pneumatic transport, the solids feed rate is sufficiently low or the gas velocity high enough that all particles are conveyed up the column, leaving no accumulation at the bed bottom. Radially, the top dilute region of a CFB riser has a core-annulus structure, consisting of a dilute upward-flowing suspension in the core, with some entrained particle clusters or other structures (Bader et al., 1988; Horio, et al., 1988), and a descending dense annular layer, interspersed with dense clusters or other agglomerates. Clusters have varying sizes, densities, velocities and residence times (e.g. see Lim et al., 1995).

The few studies available in the literature prior to the present study have not offered a conclusive picture of the dense bottom region of CFB risers nor of the flow dynamics in the region. Yerushalmi and Cankurt (1979) suggested from measurements of differential pressures along the riser height, that a dense phase arises from the tendency of particles to aggregate. When the mean interparticle distance becomes smaller than a critical value corresponding to the saturation carrying capacity of the gas, the particles were said to aggregate in snowball fashion, and the suspension collapses to form a dense fluidized bed, which may be turbulent, bubbling or slugging depending on the difference between the gas velocity and the mean particle velocity. Louge et al. (1991) postulated that the suspension collapses when the particle weight overcomes gas shear.

Bolton and Davidson (1988) and Bai et al. (1995) indicated that the lower dense bed region for CFB risers is in the turbulent regime. Ishii and Horio (1991) found from optical fiber signals at the column axis and near the wall that bubbles were present in the bottom dense zone of a CFB operated at U = 0.8 m/s and G_S = 8.0 kg/m^{2}s (suggested by the authors to be under bubbling-turbulent fluidization). No voids were found for U = 1.4 m/s and G_S = 18.9 kg/m^{2}s, considered by the authors to be fast fluidization. Horio et al.

(1992) determined local voidages on the axis of a 50 mm diameter column with FCC and sand particles. They reported cluster lengths and voidages for both the turbulent regime and the dense zone of the CFB riser. Clusters in both cases had internal voidages which did not vary substantially with gas velocity. The clusters were, however, substantially larger in the turbulent regime than in the dense zone of the CFB riser. The authors concluded that the flow structures in the turbulent and fast fluidization regimes are intrinsically different, with clusters entrained by the gas flow in the latter but not in the former.

Some data from large CFB risers with relatively shallow dense regions (e.g. Johnsson et al., 1992; Svensson et al., 1996) have shown the lower region to be a bubbling fluidized bed. Werther (1994) suggested that the lower dense region may be turbulent in a laboratory riser, but bubbling for larger risers. This chapter first describes experiments conducted to determine apparent and local voidages under bubbling and turbulent conditions for comparison with the results obtained in the high density CFB. Features distinguishing high density CFB risers from conventional fluidized beds are then discussed.

6.2 Measurements in bubbling and turbulent flow regimes

Experiments for the bubbling and turbulent regimes required only partial operation of the HDCFB unit. To prevent backflow of solids at the relatively low superficial velocities needed for these tests, a 400 mesh stainless steel screen (width of opening = 0.038 mm) was laid on top of the distributor. After bringing the downcomer to incipient fluidization, the valve leading to riser 1 was slowly opened to allow a solids bed to build in the riser to a settled height of 0.46 m and then closed. Air was then introduced to the riser at superficial velocities up to 0.7 m/s. At each setting, differential pressure signals were recorded by a transducer between $z = 0.03$ and 0.38 m (i.e. $\Delta z = 0.35$ m). The tips of the

pressure probes were covered with fine screen to prevent entry of, or blockage by, fine particles. At low air velocities, bubbles were observed to form and rise through the bed and very few particles were carried out of the riser. At higher gas velocities, however, significant solids carry-over was observed, and the bed surface became increasingly diffuse. The solids feed valve was, therefore, carefully opened and controlled to match the solids feed rate with the carryover rate so as to maintain a constant inventory in the riser. Beyond a superficial air velocity of about 0.7 m/s, the carryover was so high that it became extremely difficult to match it by feeding solids from the downcomer and the experiment had to be stopped. Using the optical fiber probe described in Chapter 4, the local voidage was measured at ten radial positions at z = 0.38 m for a selected set of superficial air velocities representing bubbling and turbulent conditions. Both the pressure and optical signals were logged into the same data acquisition system described earlier. The apparent solids hold-up was calculated from the measured differential pressures neglecting acceleration and frictional effects (as described in Chapter 3).

6.3 Flow behaviour in different regimes

6.3.1 Differential pressure fluctuations and related quantities

Figure 6.1 plots apparent solids hold-up and standard deviation of differential pressure fluctuations against superficial air velocity. The solids hold-up is a function of superficial gas velocity and falls continuously, reflecting the bed expansion as the superficial air velocity is raised. The transition from the bubbling to turbulent regime is generally considered to occur at U_c, the velocity corresponding to the peak standard deviation. From the plot $U_c \approx 0.46$ m/s, comparing well with $U_c = 0.49$ m/s calculated

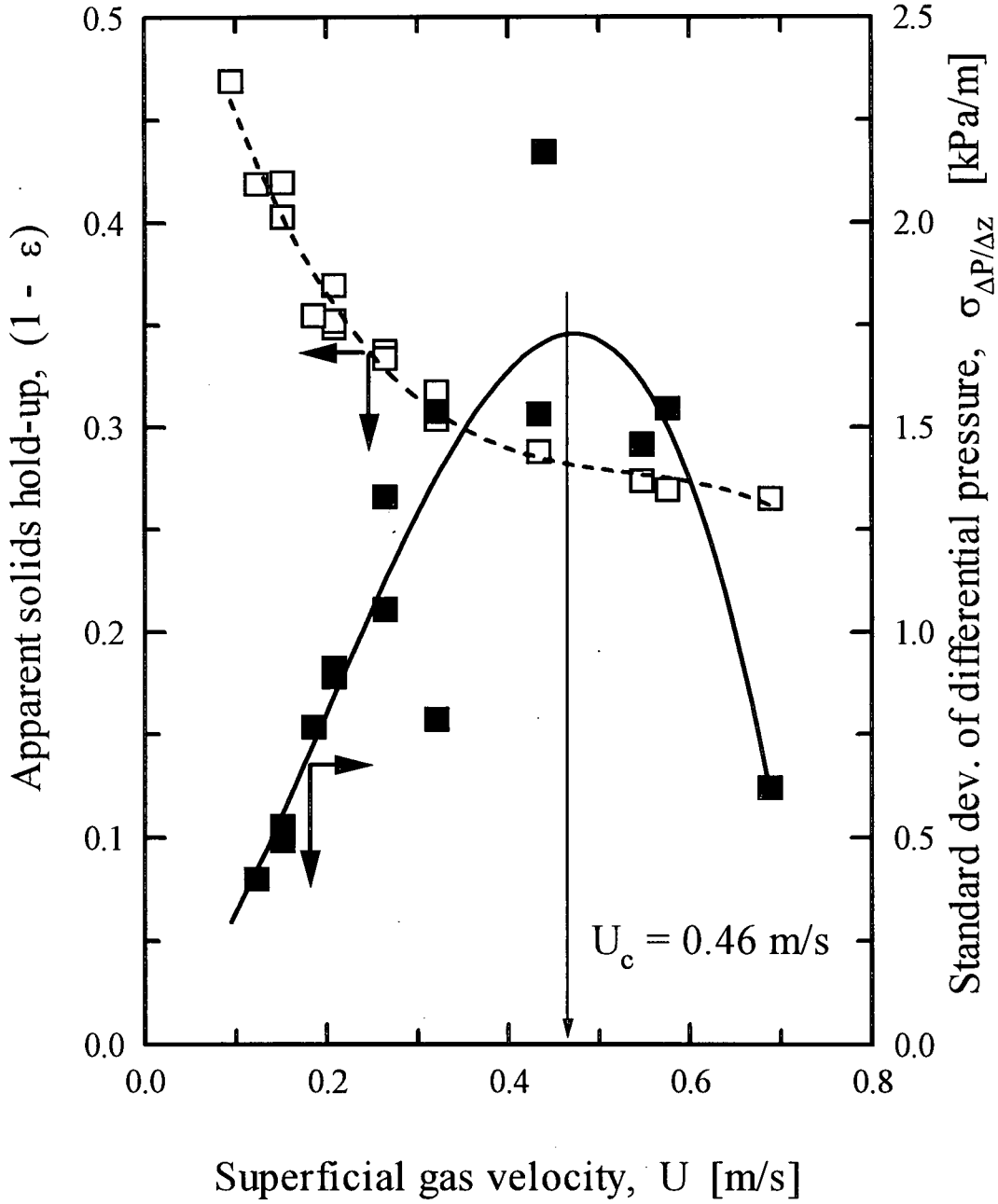

Fig. 6.1: Variation with superficial air velocity of apparent solids hold-up and standard deviation of differential pressure fluctuations measured between z = 0.03 and 0.38 m in a bubbling/turbulent experiment for a static bed height H_O = 0.46 m.

from the correlation of Bi et al. (1995), Eq. (1.4), but it is significantly lower than the value, 0.82 m/s, calculated from Eq. (1.3). The significant entrainment velocity, U_{se}, was estimated from Eq. (1.7) to be 1.46 m/s. The minimum fluidization velocity, U_{mf}, was calculated (Grace, 1982) to be 0.0032 m/s. Therefore, in the present study, the bubbling regime extends from approximately U = 0.0032 to 0.5 m/s, while turbulent conditions prevail from U = 0.5 to 1.5 m/s. Figure 6.2 shows the variation of the cross-sectional mean voidage, calculated from differential pressure data, with superficial air velocity for bubbling and turbulent bed conditions, as well as for the CFB riser at different solids circulation rates. Consistent with other studies, the voidage in the 'captive' fluidized beds, where the bed essentially experiences no net flow, is uniquely defined by the superficial gas velocity. On the other hand, in circulating fluidized beds the suspension density also depends on the solids circulation rate. The dependency on G_s is, however, only strong for dilute CFB conditions, consistent with earlier studies (e.g. Yerushalmi and Cankurt, 1979; see also Chapter 3). Results in Chapter 3 also show the superficial gas velocity to have little effect on the apparent voidage for dense CFB conditions.

Differential pressure fluctuations in bubbling beds are caused primarily (e.g. see Yerushalmi and Avidan, 1985; Chehbouni et al., 1994; Bi et al., 1995) by the passage of bubbles. The increase in the standard deviation of pressure fluctuations as the gas velocity is raised is due to an increase in bubble formation and growth. This increase continues up to the transition velocity U_c at which the fluctuations are highest and the bed has maximum heterogeneity (Chehbouni et al., 1994). Beyond U_c bubbles become unstable and break up into small transient voids and interstitial gas.

Figures 6.3, 6.4 and 6.5 show the influence of solids circulation rate on the standard deviation of differential pressure fluctuations with the apparent solids hold-up also given for reference purposes between z = 0.66 and z = 0.96 m in the CFB riser for

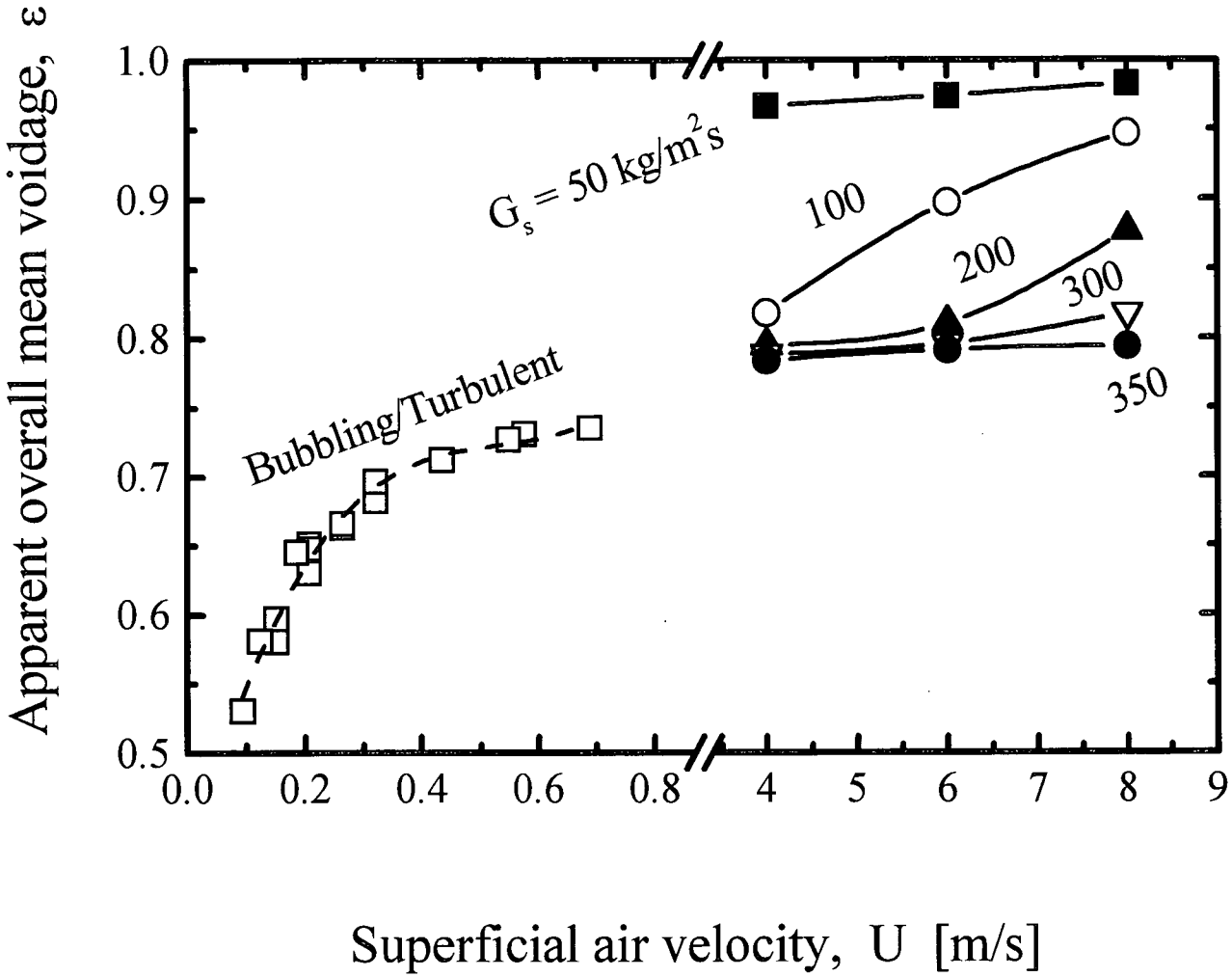

Fig. 6.2: Apparent overall mean voidage as a function of superficial air velocity for bubbling, turbulent and circulating fluidized bed conditions. (CFB data obtained from section between z = 1.88 and 2.18 m).

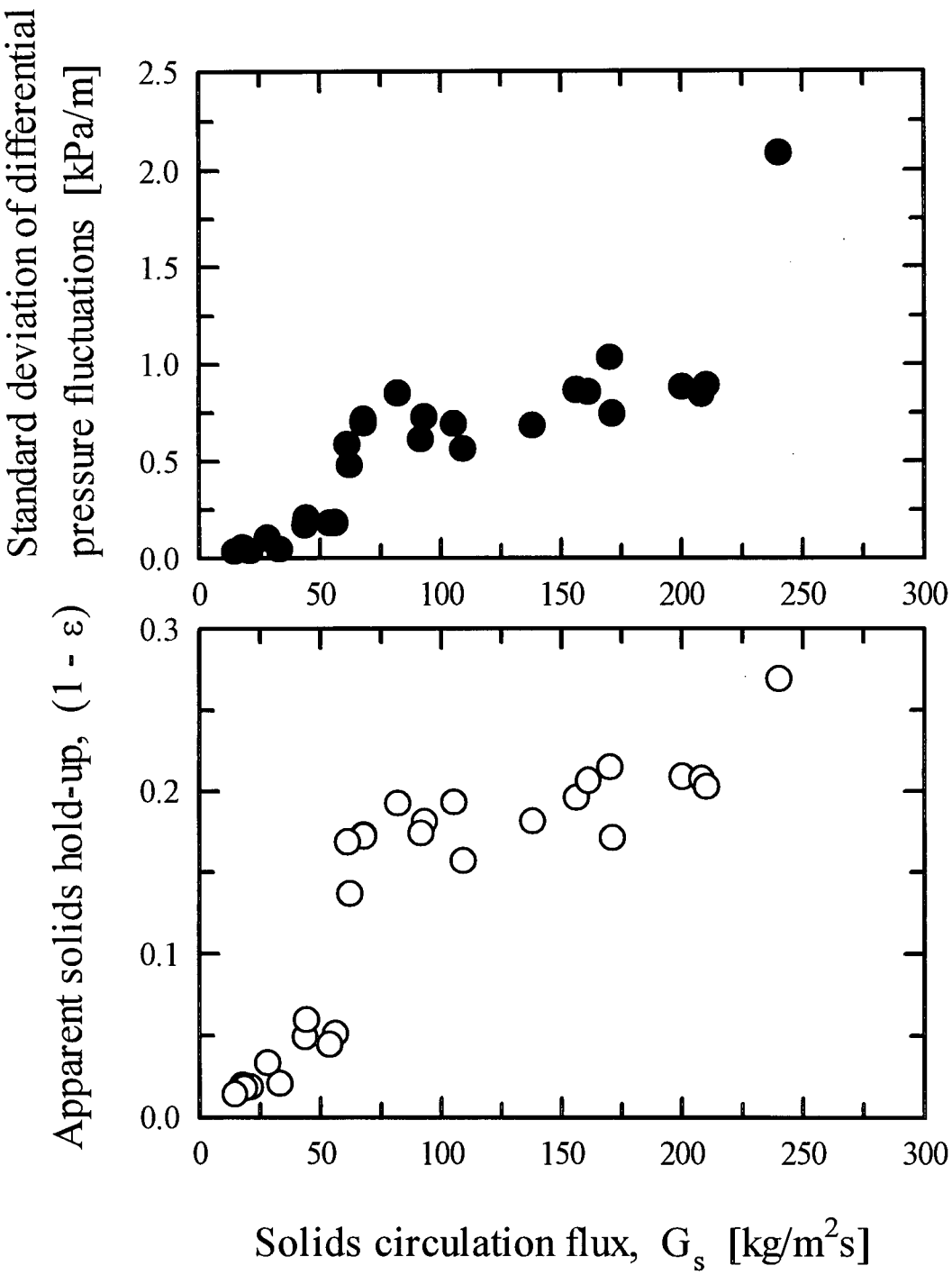

Fig. 6.3: Variation of standard deviation of differential pressure fluctuations and apparent solids hold-up with solids circulation rate for U = 4.0 m/s in the column section between z = 0.66 and z = 0.96 m.

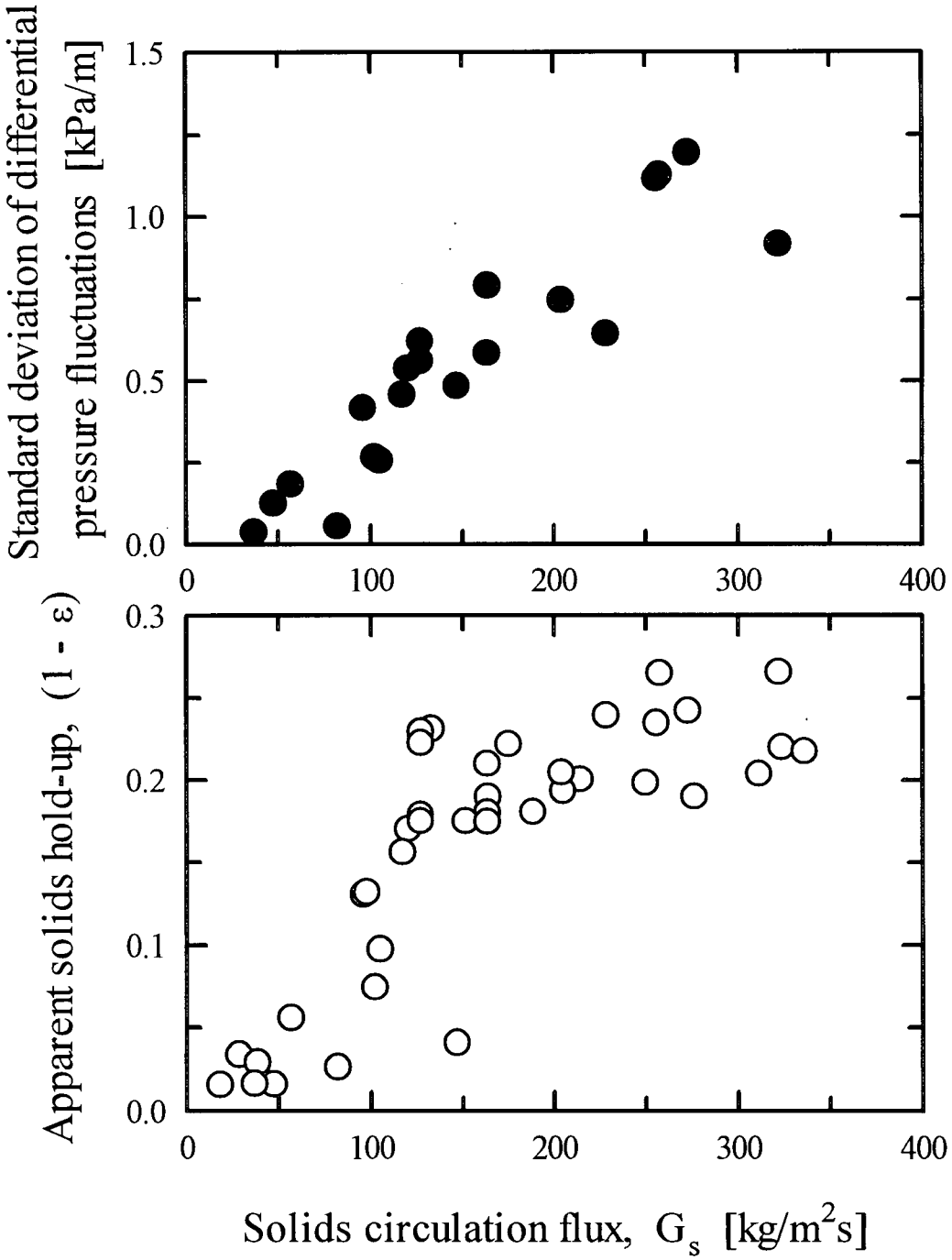

Fig. 6.4: Variation of standard deviation of differential pressure fluctuations and apparent solids hold-up with solids circulation rate for U = 6.0 m/s in the column section between z = 0.66 and z = 0.96 m.

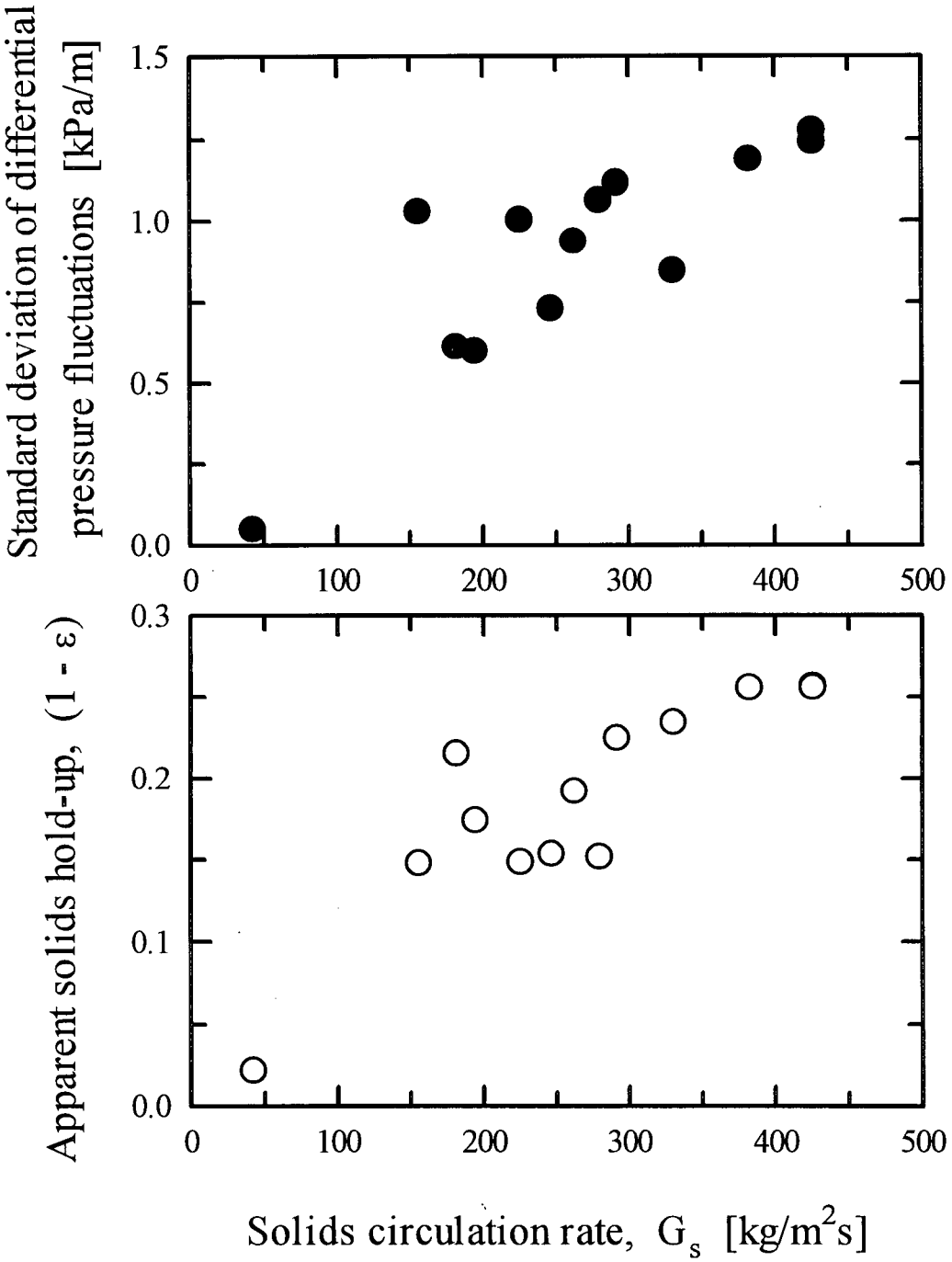

Fig. 6.5: Variation of standard deviation of differential pressure fluctuations and apparent solids hold-up with solids circulation rate for U = 8.0 m/s in the column section between z = 0.66 and z = 0.96 m.

U = 4.0, 6.0 and 8.0 m/s, respectively. In all three cases, the differential pressure fluctuations increase in a manner similar to the solids hold-up with increasing solids circulation rate. For example, on reaching high density conditions (hold-up = 0.2 ± 0.05), the influence of solids circulation rate on both the apparent solids hold-up and on the differential pressure fluctuations is low. The same data are replotted as standard deviation of differential pressure against mean voidage in Fig. 6.6 together with the corresponding data for bubbling and turbulent bed conditions from Fig. 6.1. Also included are other CFB data obtained at U = 5.0 and 7.3 m/s. In the circulating bed, the voidage fluctuations increase as the suspension becomes denser, whereas the fluctuations in the turbulent and bubbling regimes fall continuously as the voidage is lowered further by decreasing the gas velocity.

No bubbles occur under high density CFB conditions. There the flow dynamics are determined by particle-particle interaction and the extent of particle agglomeration, as well as gas-particle interactions. Increasing the suspension density leads to increased cluster formation, hence to higher differential pressure fluctuations. Although small particles, e.g. FCC have been found to damp gas turbulence (e.g. Hetsroni, 1989), solids suspensions in CFB risers are much denser, and the formation of particle clusters enhances rather than damps gas turbulence, further intensifying the fluctuations (Marzocchella et al., 1997). Due to the low suspension density, differential pressure fluctuations are relatively low in dilute CFB risers.

6.3.2 Slip velocities

Slip velocities in both dilute and high-density CFB risers are much higher than in the bubbling and turbulent regimes (calculated as U/ε) as shown in Fig. 6.7. Solid lines on Fig. 6.7 are the predictions of CFB slip velocities by Eq. (3.10).

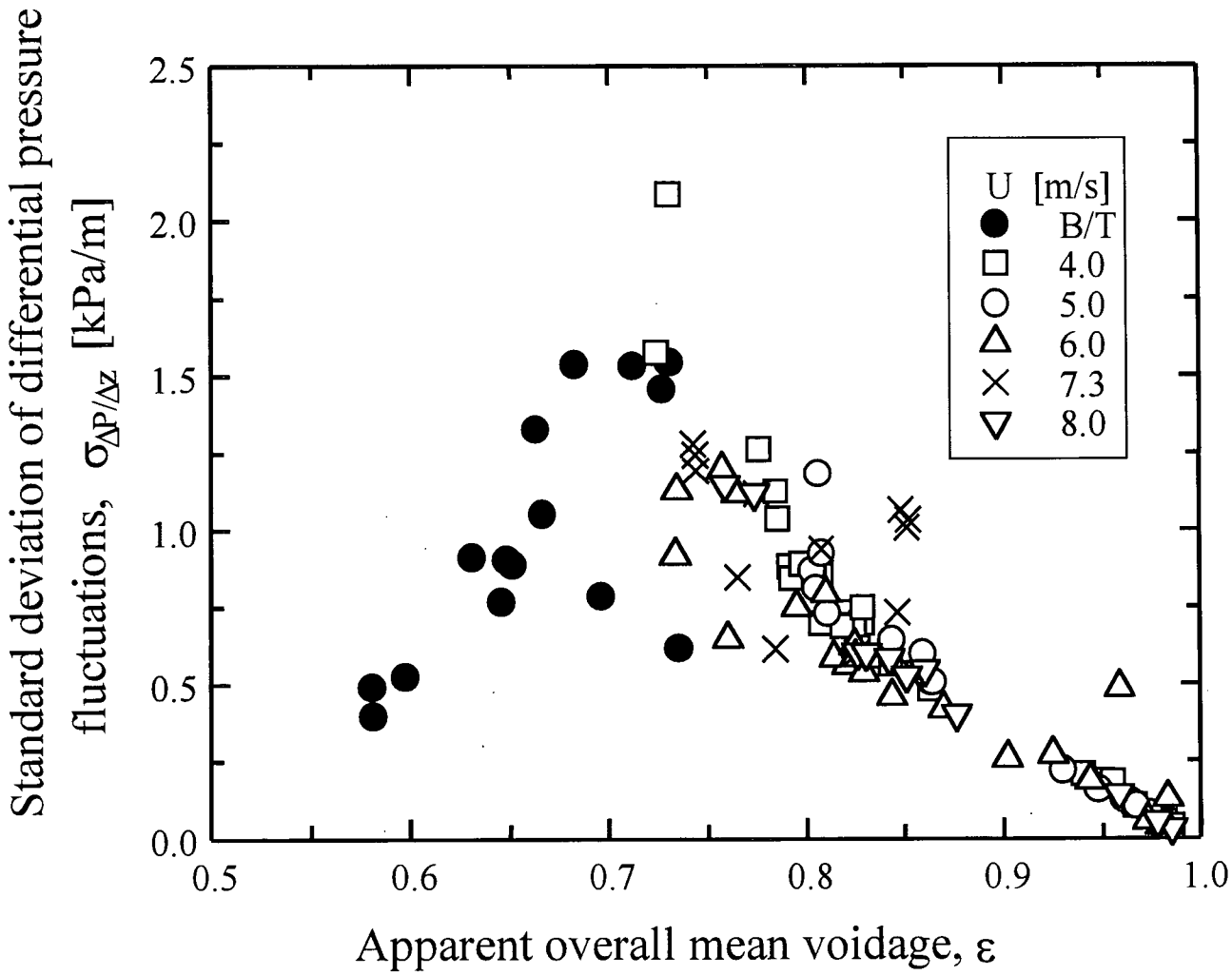

Fig. 6.6: Variation of standard deviation of differential pressure fluctuations with apparent voidage for bubbling and turbulent beds (B/T) and for CFB riser at z = 0.81 m and different superficial gas velocities.

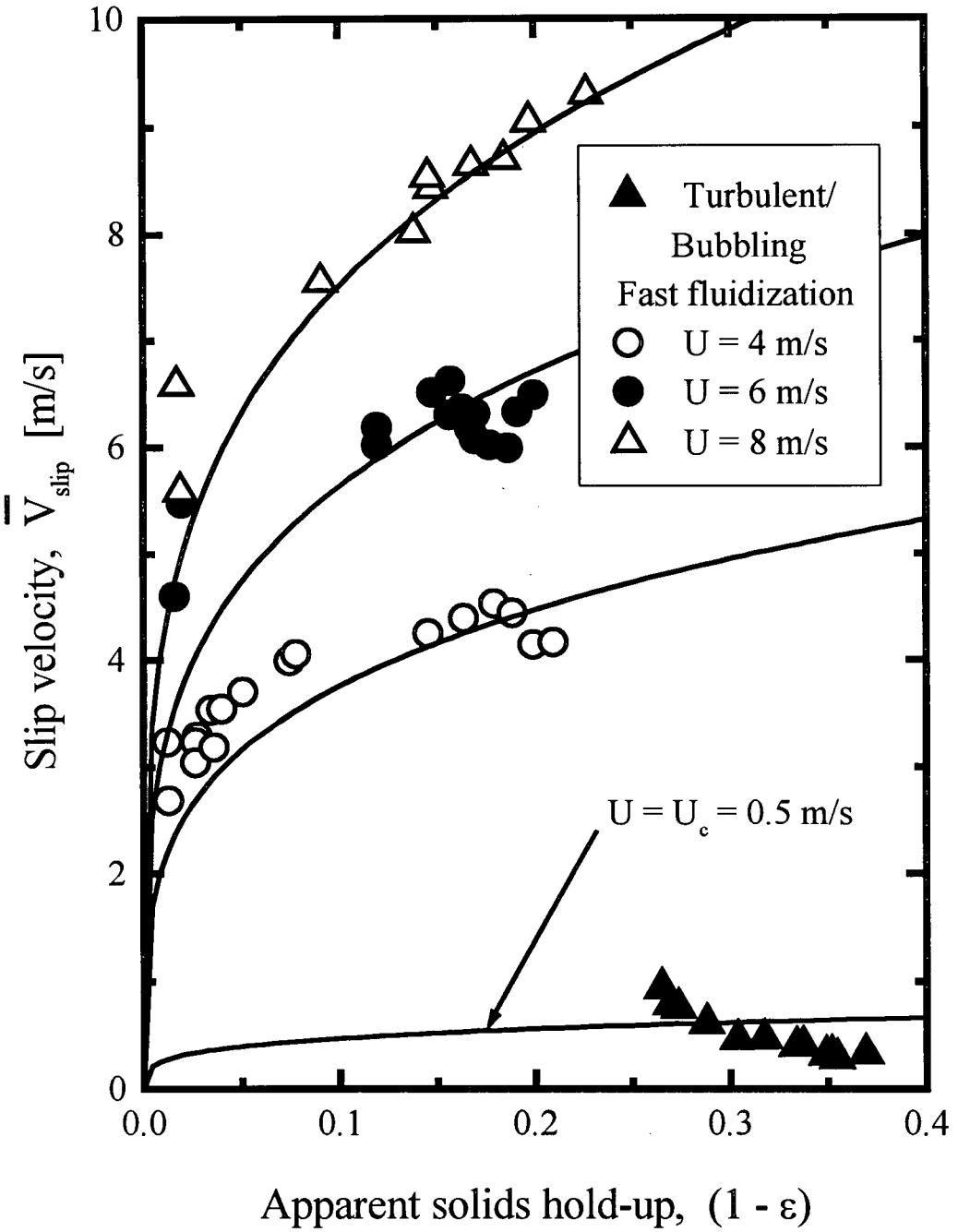

Fig. 6.7: Variation of slip velocity with apparent solids hold-up in CFB riser at z = 2.03 m for U = 4.0, 6.0 and 8.0 m/s, and under bubbling and turbulent bed conditions. Solid lines calculated by Eq. (3.9).

6.3.3. Local voidage fluctuations

Figure 6.8 compares instantaneous local voidage traces at six radial locations (r/R = 0.0, 0.58, 0.75, 0.88, 0.94 and 1.0) for the bubbling (U = 0.15 m/s, ε_m = 0.679) and turbulent (U = 0.67 m/s, ε_m = 0.750) regimes (both z = 0.38 m) and the high density circulating bed (HDCFB) riser for U = 8 m/s, G_s = 425 kg/m^{2}s and z = 1.57 m (ε_m = 0.815). In the bubbling bed the voidage varies between a peak value of nearly 1 and a low value of about 0.5 over the whole cross section, except very close to the wall, showing the coexistence of bubbles and a dense emulsion phase. The corresponding voidage probability distributions in Fig. 6.9 shows that the frequency of bubbles at the measurement level decreases with increasing r. At the wall no bubbles are detected and the suspension consists of an emulsion phase of a mean voidage of approximately 0.5. Such a spatial distribution of bubbles has also been observed in previous studies in freely bubbling beds without internals (e.g. Werther, 1974) and has been explained (Clift and Grace, 1985) to result from the constraint in lateral coalescence of bubbles imposed by the column wall.

The voidage traces for the turbulent regime show a rapidly fluctuating structure with gas phase peaks coexisting with periods where the instantaneous voidage approaches ε_{mf} over a considerable part of the cross-section (to $\Phi \approx 0.75$). The voids are more frequent than in the bubbling regime. Further outward, as observed in Fig. 6.9, the frequency of the high voidage peaks decreases and finally disappear at the wall as the suspension becomes denser. At the same time over the cross-section, peaks of intermediate voidages ($\varepsilon_t > 0.6$) appear scattered in the voidage traces (Fig. 6.8), especially toward the wall. The voidage frequency plots reveal a distribution of voidages over the whole range, in addition to the peaks at the extreme ends. The voidage trace at the axis fluctuates with a higher frequency between $\varepsilon \approx 1$ and ε_{mf} suggesting that the suspension is composed of an emulsion phase coexisting with voids, neither of which can

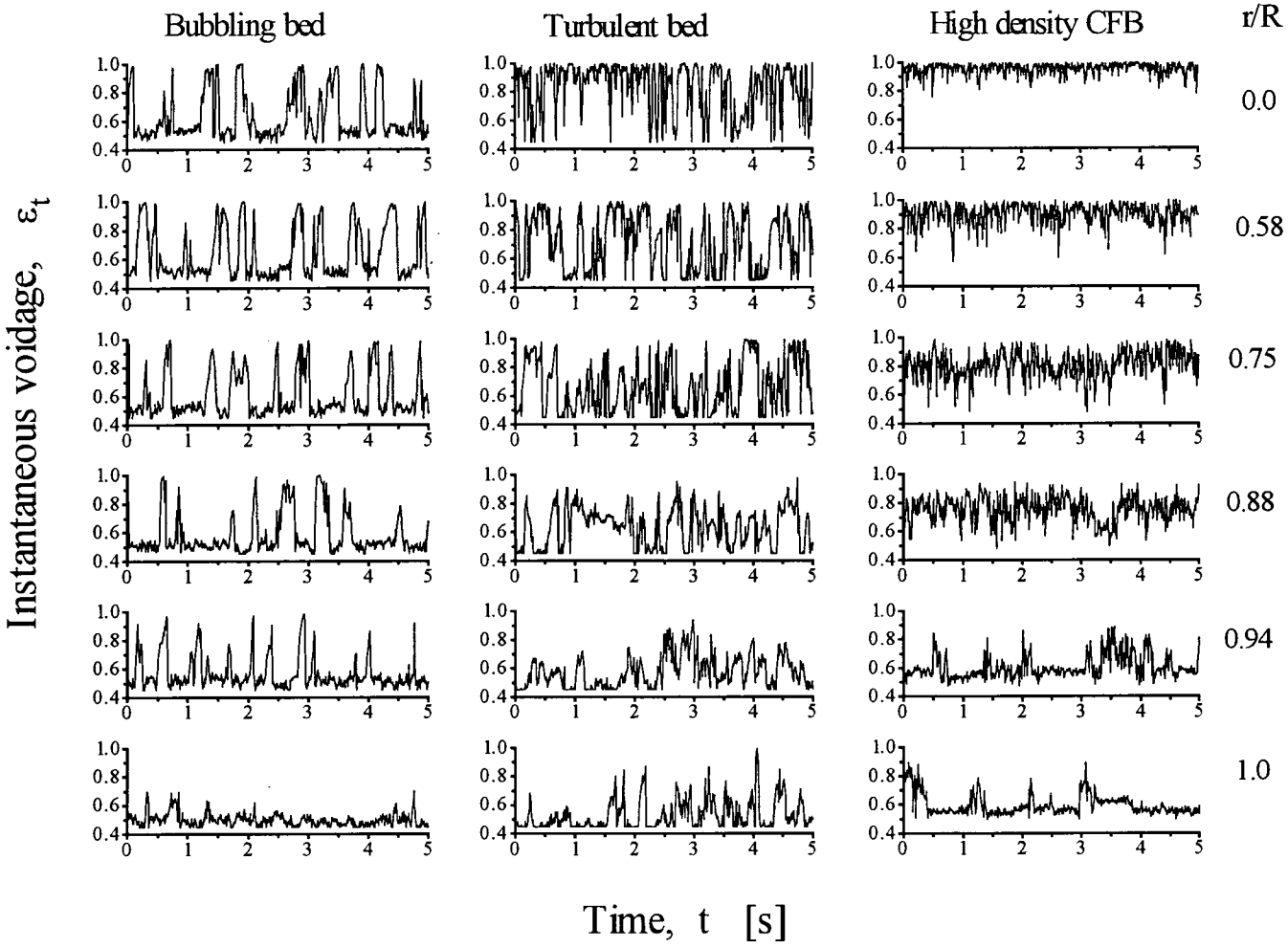

Fig. 6.8: Traces of local instantaneous voidage at six radial locations for bubbling bed (U = 0.15 m/s), turbulent bed (U = 0.69 m/s), both at z = 0.38 m, and high density circulating fluidized bed (U = 8.0 m/s, G_S = 425 kg/m^{2}s, z = 1.57 m).

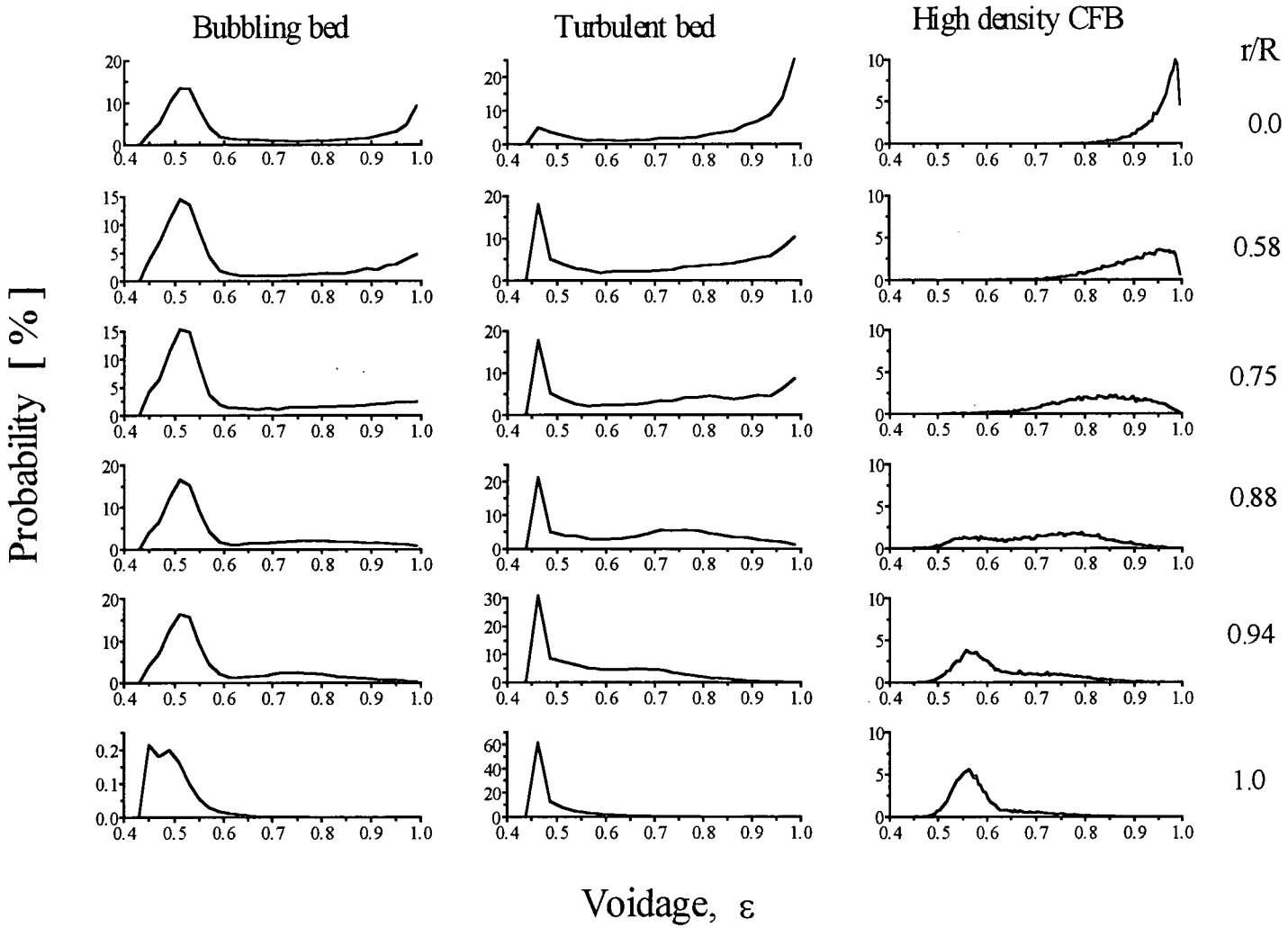

Fig. 6.9: Voidage probability distribution plots at six radial locations for bubbling bed (U = 0.15 m/s), turbulent bed (U = 0.69 m/s), both at z = 0.38 m, and high density circulating fluidized bed (U = 8.0 m/s, G_S = 425 kg/m^{2}s, z = 1.57 m).

be viewed as either continuous or discontinuous. This structure appears to extend outward and is still observable at r/R = 0.58, although the frequency of voids starts to decrease while the proportion of the high density phase grows. Beyond r/R $\approx$ 0.75, fewer and fewer voids are detected (peaks at ε_t = 1) and the voidage trace shows increasingly dense fractions, as well as other periods of voidage of about 0.6 or higher.

The voidage traces and the corresponding probability distribution plots for high density CFB conditions were also discussed in Chapter 4. They appear to differ from those of the bubbling and turbulent regimes. At the axis the suspension is dilute ($\varepsilon_t \approx 0.97$) and no dense periods (with ε_t approaching ε_{mf}) are observed. However, some spikes of voidage $\approx$ 0.8 do appear. The suspension density increases toward the wall where no bubbles or voids (peak voidage = 1) can be inferred from the voidage distribution plots. The suspension can be considered to consist of clusters or other structures dispersed in a relatively dense phase of individual (unagglomerated) particles. Figure 6.10 compares a dilute CFB riser (ε_m = 0.945) with a HDCFB riser (ε_m = 0.806) by plotting instantaneous voidage traces measured at z = 3.4 m and the same six radial locations in the riser. The corresponding probability distribution plots are given in Fig. 6.11. The flow is more dilute over the whole cross-section in the LDCFB, as shown by the persistent high voidage peaks on the voidage probability distribution plots. There are relatively few clusters in the core of the LDCFB but there is a broadening in the voidage frequency distribution towards the wall indicating denser and more frequent clusters.

Typical time-mean voidage profiles for bubbling (B) and turbulent (T) regimes and for LDCFB and HDCFB conditions are compared in Fig. 6.12. A plot for dilute pneumatic transport (P) is also included for completeness. The voidage is relatively uniform over the whole cross-section (about 0.7 in this case) in the bubbling regime, while it decreases from the centre outwards in all other cases. In the pneumatic transport regime the voidage is

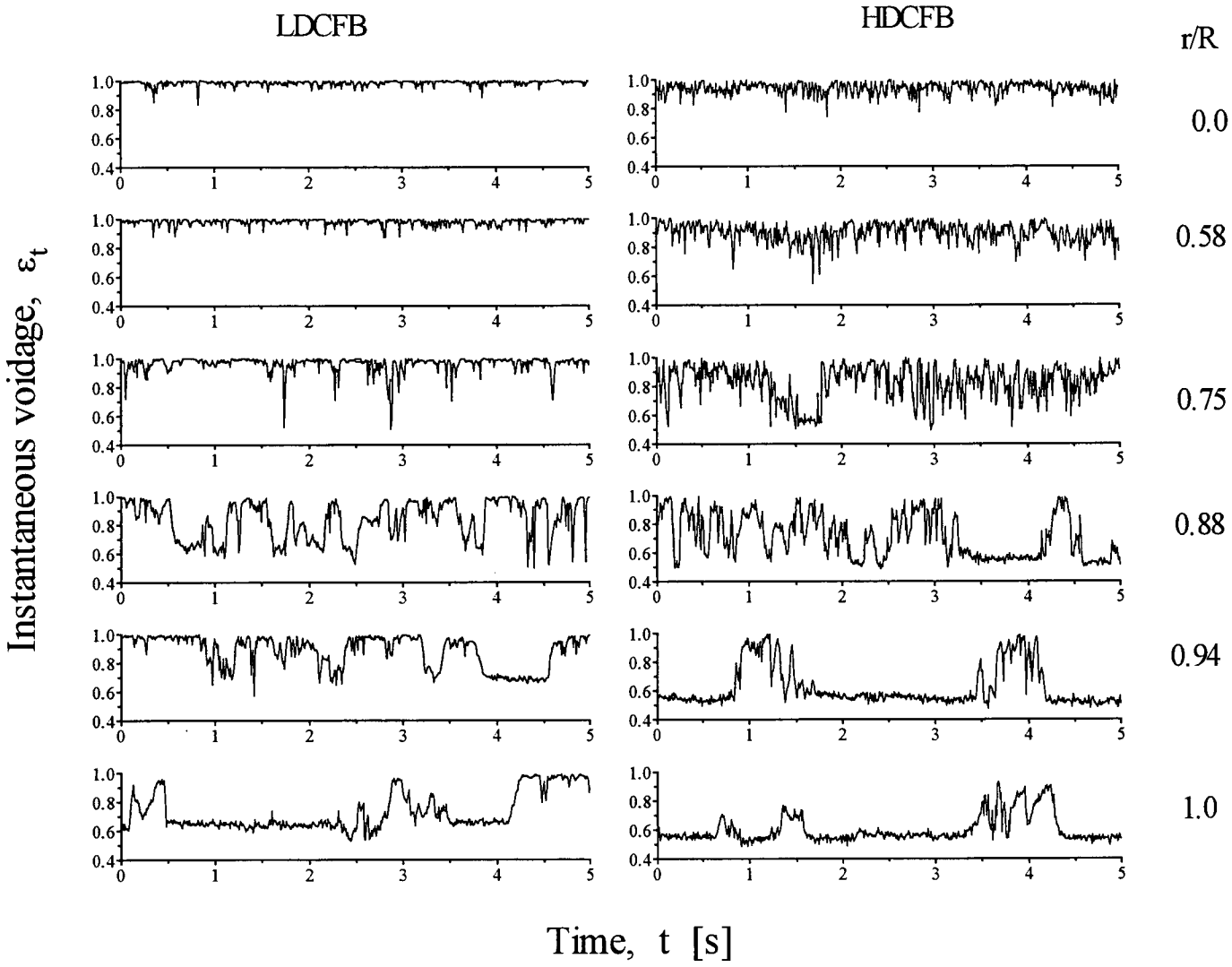

Fig. 6.10: Instantaneous voidage traces at z = 3.4 m in LDCFB (U = 8.0 m/s, G_s = 93 kg/m^{2}s, ε_m = 0.945) and HDCFB (U = 7.7 m/s, G_s = 389 kg/m^{2}s, ε_m = 0.806).

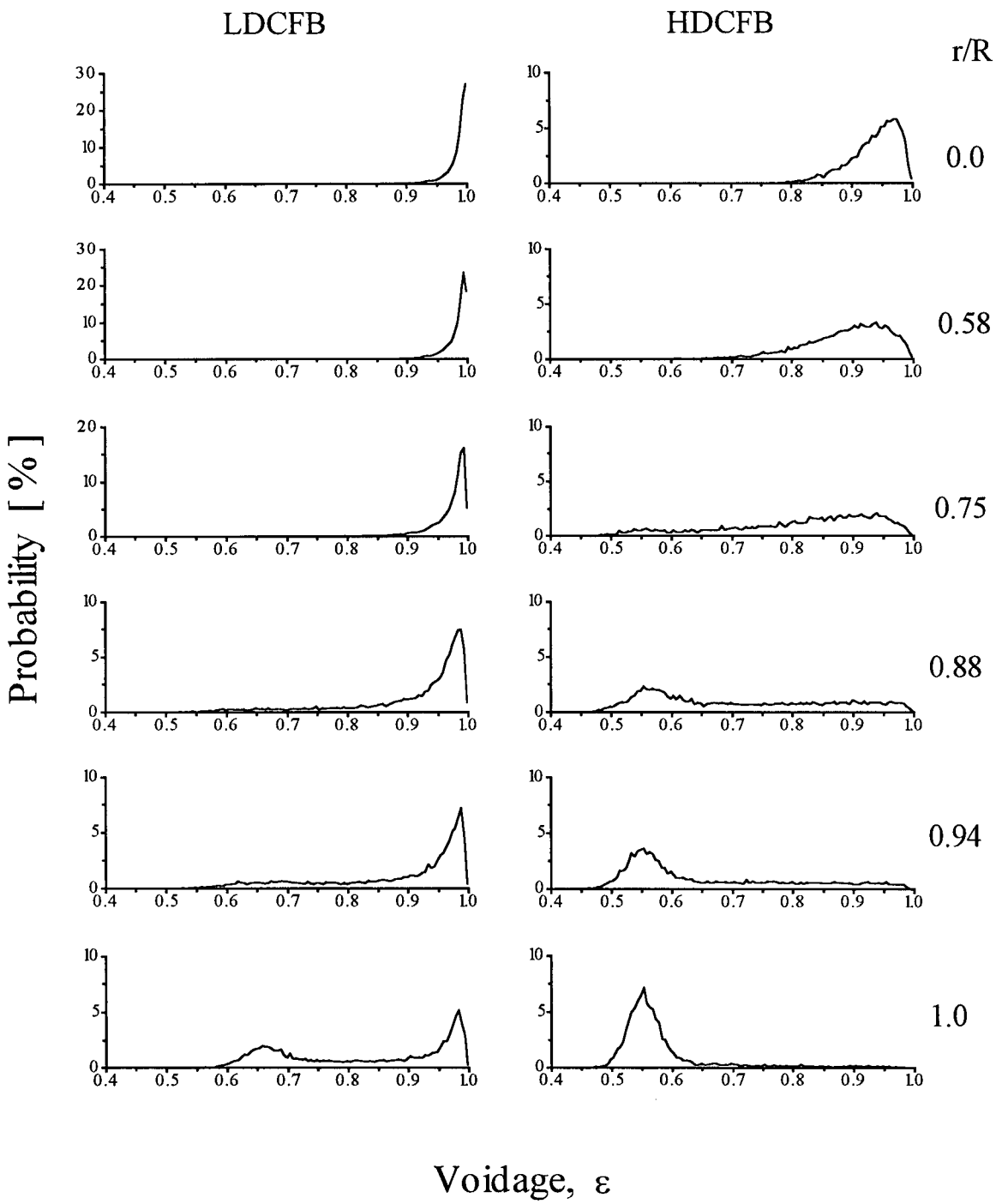

Fig. 6.11: Probability distribution plots of local voidage at z = 3.4 m in LDCFB (U = 8.0 m/s, G_s = 93 kg/m^{2}s, ε_m = 0.945) and HDCFB (U = 7.7 m/s, G_s = 389 kg/m^{2}s, ε_m = 0.806).

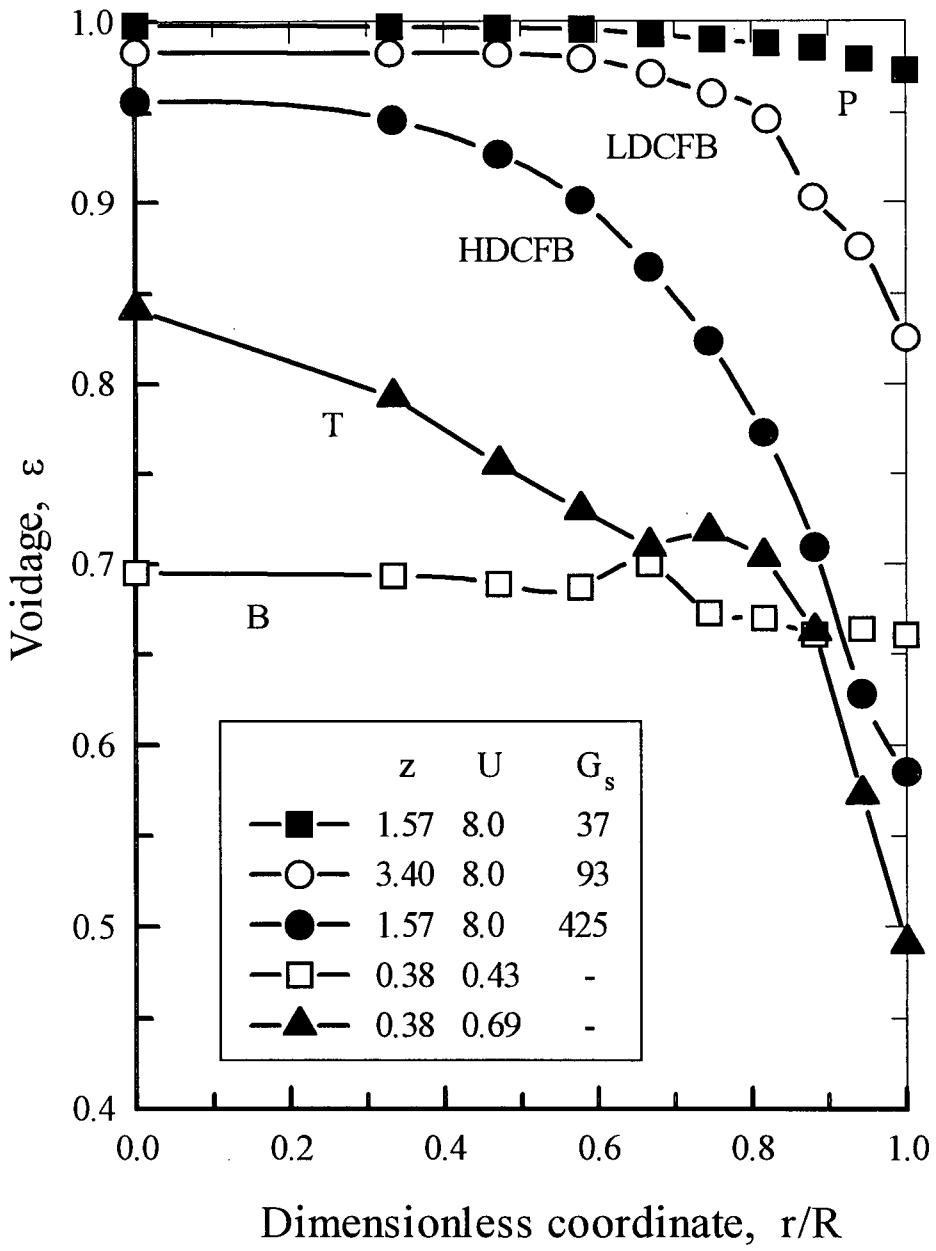

Fig. 6.12: Typical radial profiles of time-mean local voidage for bubbling (B), turbulent (T), dilute pneumatic transport (P) regimes and for low (LDCFB) and high density (HDCFB) circulating fluidized bed conditions.

very high except for the small decrease close to the wall. The voidage in the turbulent regime falls from about 0.70 at the axis to nearly ε_{mf} at the wall. The profiles obtained in the bubbling and turbulent regimes are consistent with those obtained for alumina and glass beads by Zhang et al. (1991). Radial concentration gradients were also found in the turbulent regime by Abed (1984). In the HDCFB the voidage initially decreases less rapidly than in the turbulent regime, changing only from $\varepsilon \approx 0.95$ at the axis to $\varepsilon \approx 0.90$ at $r/R = 0.5$, but it falls rather sharply thereafter to about 0.6 at the wall. A large proportion of the LDCFB is dilute, with the time-mean voidage changing only from about 0.98 at the axis to 0.95 at $r/R = 0.82$. Further outward, the voidage drops sharply to about 0.82 at the wall. Except for the bubbling regime and to some extent the dilute pneumatic transport regime, the suspension exhibits a core - annulus pattern.

The profiles of the standard deviation of local voidage fluctuations for the same conditions as in Fig. 6.12 are plotted in Fig. 6.13, and the corresponding intermittency index profiles appear in Fig. 6.14. In the bubbling regime voidage fluctuations decrease from the centre towards the wall. The intermittency index drops from a relatively high value of about 0.75, indicating a high degree of heterogeneity, to about 0.4 at the wall. The standard deviation in the turbulent regime rises slowly as r increases up to $r/R \approx 0.6$ and then falls off rather rapidly to a much lower value at the wall. The corresponding intermittency index profile follows the same shape, rising only from approximately 0.70 at the axis to 0.73 at $r/R \approx 0.6$ before falling off to approximately 0.45 at the wall. This intermittency index profile and the voidage traces above suggest the turbulent bed, when considered on a time-mean basis, to consist of an inner rather heterogeneous region where voids and dense structures coexist.

The radial profiles of standard deviation of local voidage fluctuations and intermittency index in the LDCFB and HDCFB riser differ significantly from those in the

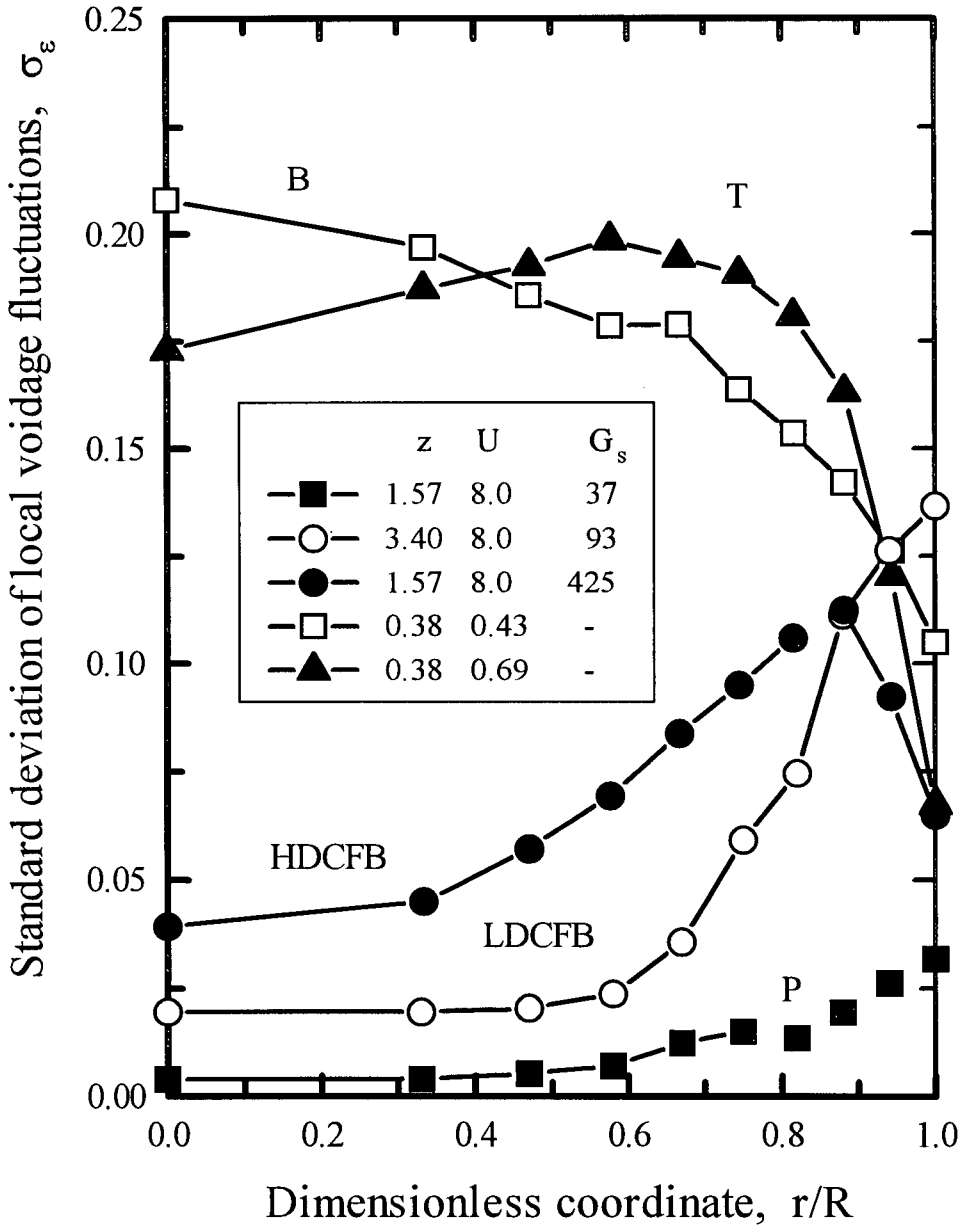

Fig. 6.13: Typical radial profiles of standard deviation of local voidage fluctuations for bubbling (B), turbulent (T), dilute pneumatic transport (P) regimes and for low (LDCFB) and high density (HDCFB) circulating fluidized bed conditions.

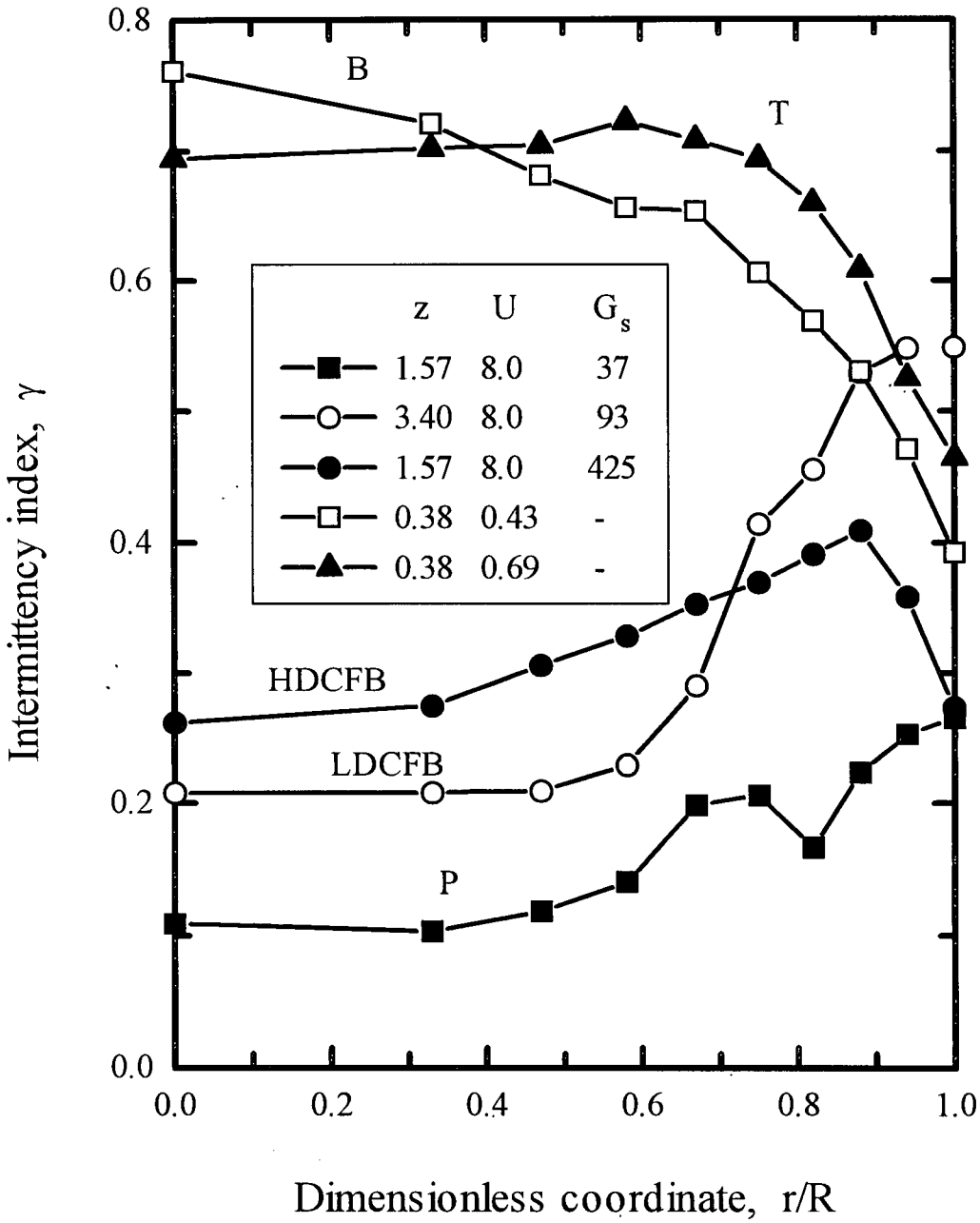

Fig. 6.14: Typical radial profiles of intermittency index for bubbling (B), turbulent (T), dilute pneumatic transport (P) regimes and for low (LDCFB) and high density (HDCFB) circulating fluidized bed conditions.

bubbling and turbulent regimes. In the HDCFB, fluctuations are low at the axis and increase to a peak at r/R $\approx$ 0.9 before falling off towards the wall. Similarly, the intermittency index increases from a low value at the axis to a maximum and then drops towards the wall. As suggested in Chapter 4, away from the axis, up to the position of the peak standard deviation, the suspension becomes more heterogeneous as more clusters or other structures form. Beyond the peak, it is also likely, as for the turbulent regime, that due to the high suspension density, clusters closely resemble the surrounding emulsion so that agglomerates no longer exist individually, but rather "melt away". The result is a more homogeneous suspension. Note that the intermittency index profiles peaks some distance from the wall in both the turbulent bed and the high density CFB riser. Due to its higher voidage, the core region of the LDCFB is more uniform than in the HDCFB. Its annular region is, however, more heterogeneous, with peak voidage fluctuations occurring at the wall. This may be due to the shear between falling clusters and the dilute upflow in the core.

The general observations regarding clusters or particle structures appear to agree closely to the few measurements in CFB risers available in the literature. For example, Lints and Glicksman (1993) measured the solids concentration within clusters near the wall using an impact phonograph needle and found it to increase with the cross-sectional average density. Similarly, Wei et al. (1995) using a set of optical fiber sensors in a CFB riser noted that the size and probability of cluster formation increased with solids concentration and decreased with increasing gas velocity. Horio et al. (1988) observed that in the wall region the cluster size increases while clusters fall downward; clusters in the core region were much smaller than in the annulus region. Soong et al. (1993) determined cluster properties from instantaneous voidage traces based on the criterion that a cluster is present if the local instantaneous solid volume fraction exceeds the time-mean solid fraction by at least 3 times the standard deviation. With this criterion, the frequency

of occurrence and the residence time of clusters was found to increase towards the wall and to decrease with elevation. Although these studies were all based on the dilute region of LDCFB risers, they offer some guidance on the rather complicated subject of particle clustering. More work is certainly needed for high density conditions.

Figure 6.15 plots the standard deviation of local voidage fluctuations against the time-mean local voidage in the bubbling bed, turbulent bed and high density CFB for the same conditions as in Fig. 6.8. For a given time-mean local voidage, the fluctuations are more vigorous in the bubbling and turbulent regimes than in the HDCFB. This is also generally true in Fig. 6.16 (a), where the standard deviation of local voidage fluctuations is plotted for several operating conditions in the bubbling and turbulent regimes as well as in the LDCFB and HDCFB. The corresponding intermittency plot (Fig. 6.16 (b)) clearly shows that the bubbling and turbulent beds are more heterogeneous than the LDCFB and HDCFB.

6.3.4 Spectral density analysis

Another important and widely used measure in the study of the local flow behaviour in fluidized beds is the power spectrum. This establishes the periodicity of the signal fluctuations. The covariance function between two stationary random time history records, x(t) and y(t) for any time delay τ is given (Bendat and Piersol, 1986) by

$$C_{xy}(\tau) = E\left[\{x(t) - \mu_x\}\{y(t+\tau) - \mu_y\}\right]$$
$$= \lim_{T\to\infty} \frac{1}{T}\int_0^T \{x(t) - \mu_x\}\{y(t+\tau) - \mu_y\}dt$$

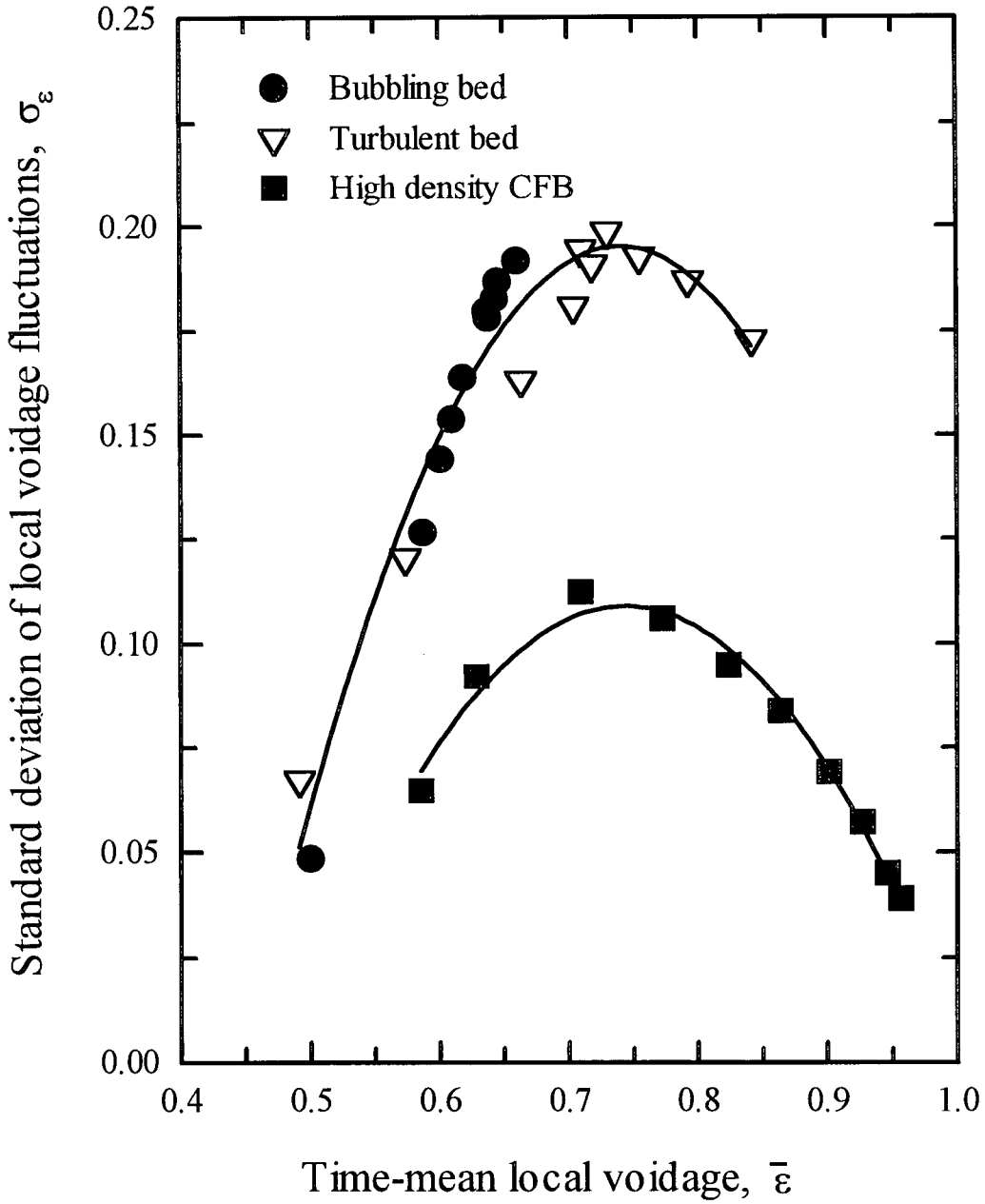

Fig. 6.15: Comparison of influence of time-mean local voidage on standard deviation of local voidage fluctuations for bubbling bed (U = 0.15 m/s), turbulent bed (U = 0.69 m/s) and high density circulating fluidized bed (U = 8.0 m/s, G_S = 425 kg/m^{2}s, z = 1.57 m).

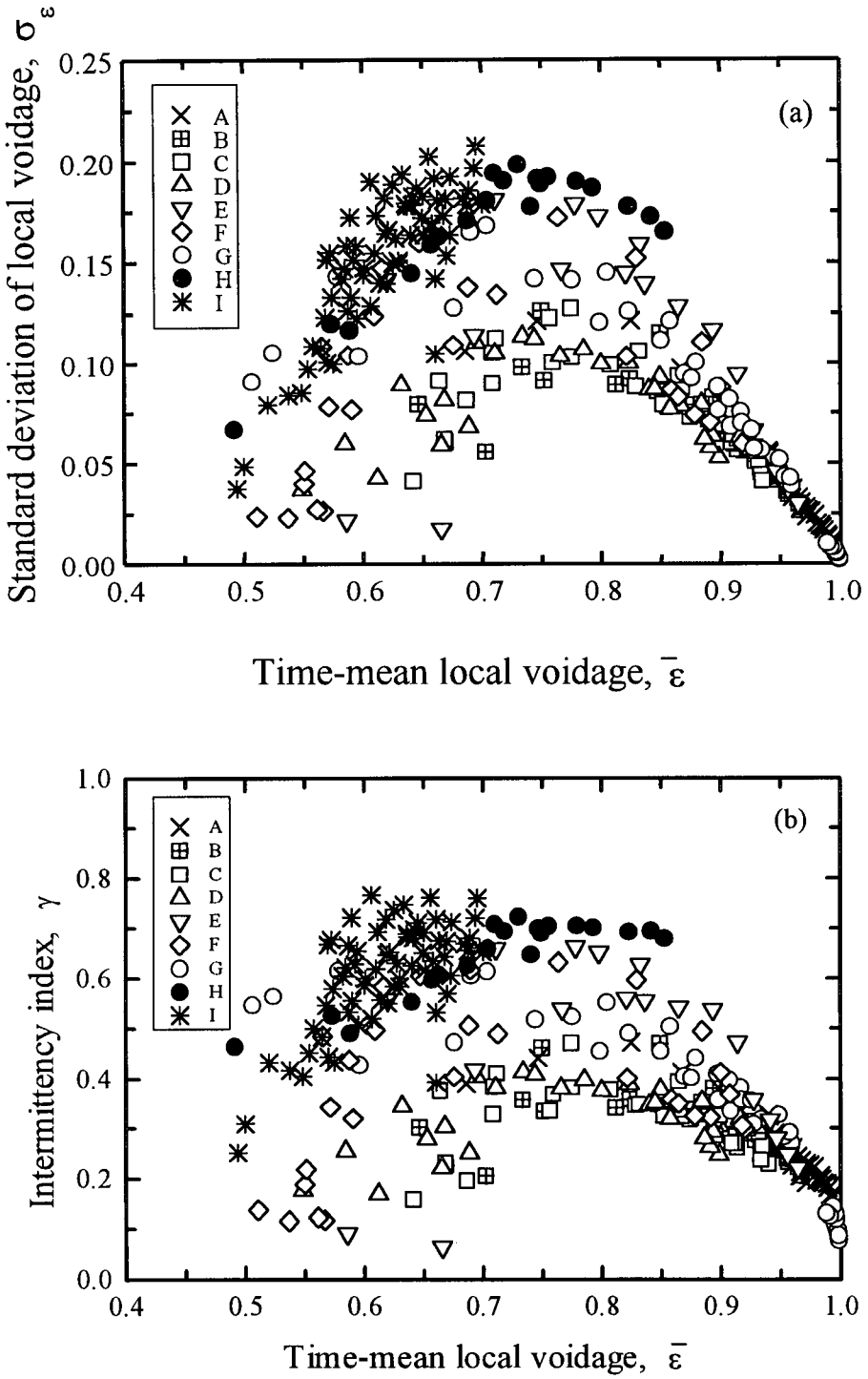

Fig. 6.16: Variation of (a) standard deviation of local voidage fluctuations and (b) intermittency index with local voidage for bubbling bed (I), turbulent bed (H) and different CFB operating conditions. [(A) z = 2.5 m, U = 6 m/s, various G_S; (B) z = 1.57 m, U = 8 m/s, various G_S; (C) U = 6.6 m/s, G_S = 234 kg/m^{2}s, various z; (D) U = 7 m/s, G_S = 249 kg/m^{2}s, various z; (E) z = 0.97 m, U = 4.9 m/s, G_S = 86 kg/m^{2}s; (F) U = 5.3 m/s, G_S = 222 kg/m^{2}s, various z; (G) z = 1.57 m, U = 4 m/s, various G_S)].

$$= \lim_{T\to\infty} \frac{1}{T}\int_0^T x(t)y(t+\tau)dt - \mu_x\mu_y = R_{xy}(\tau) - \mu_x\mu_y \qquad 7.1)$$

$R_{xy}(\tau)$ is called the cross-correlation function between x(t) and y(t). For a special function where x(t) = y(t) the covariance function is called the autocovariance function:

$$C_{xx}(\tau) = \lim_{T\to\infty} \frac{1}{T}\int_0^T x(t)x(t+\tau)dt - \mu_x{}^2 = R_{xx}(\tau) - \mu_x{}^2 \qquad (7.2)$$

and $R_{XX}(\tau)$ is called the autocorrelation function of x(t).

The power spectral density function (also called autospectral density or autospectrum) of x(t) is defined as the Fourier transform of the autocorrelation function of x(t),

$$S_{xx}(f) = \int_{-\infty}^{\infty} R_{xx}(\tau)e^{-j2\pi f\tau}d\tau \qquad (7.3)$$

where $j = \sqrt{-1}$. The power spectral density function is a frequency-domain function, most directly interpreted as a measure of the frequency distribution of the mean square value of the data, i.e. the rate of change of the mean square value with frequency. A mean square value concentrated at a single frequency suggests a cyclical physical phenomenon, whereas if the frequency is distributed over a wide frequency range, the phenomenon is probably broadly stochastic. The Fourier transform at a specific frequency is a complex number, and many spectral density analyses (e.g. Brereton, 1987; Dhodapkar and Klinzing, 1993; Chehbouni et al., 1994; Bi et al., 1995; Svensson, et al., 1996) have only considered its magnitude (also referred to as amplitude, spectral density, absolute value, power etc.). This procedure is adopted in this work.

Power spectral density plots of local voidage at six radial locations for the same bubbling, turbulent and HDCFB conditions as in Fig. 6.8 are presented in Fig. 6.17, while the spectral density profiles for HDCFB are compared to those in LDCFB in Fig. 6.18. The conditions in Fig. 6.18 are similar to those in Fig. 6.9. In the bubbling regime the

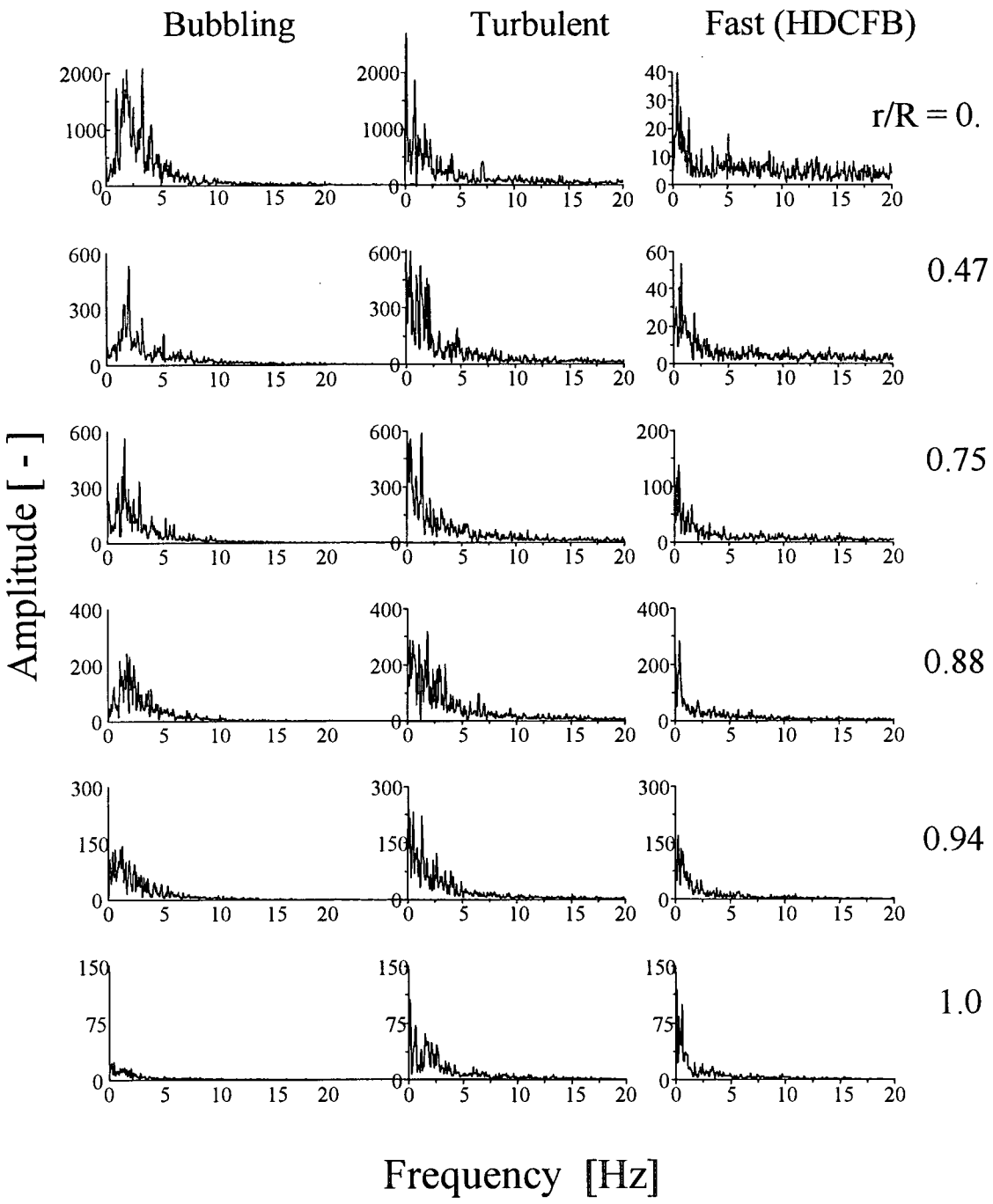

Fig. 6.17: Comparison of power spectral densities of local voidages at six radial locations in bubbling bed (U = 0.15 m/s), turbulent bed (U = 0.69 m/s), both at z = 0.38 m, and high density CFB riser (U = 8.0 m/s, G_S = 425 kg/m^{2}s, z = 1.57 m).

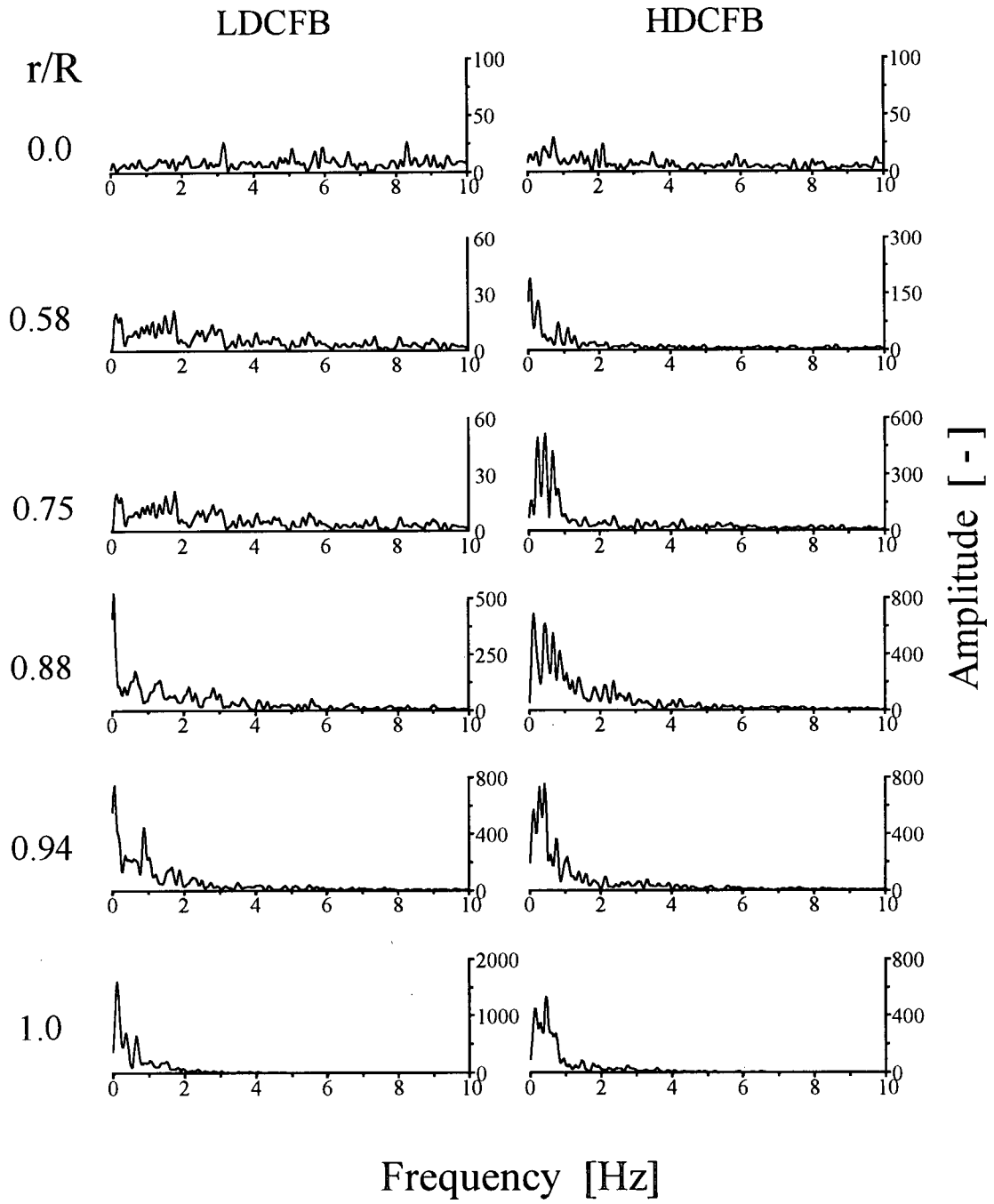

Fig. 6.18: Comparison of power spectral densities of local voidage at six radial locations in low density CFB riser (U = 8.0 m/s, G_S = 93 kg/m^{2}s) and high density CFB riser (U = 8.0 m/s, G_S = 389 kg/m^{2}s); z = 3.4 m in both cases.

amplitudes are distributed over a small range of frequencies with a peak value at approximately 2 Hz. The existence of a dominant frequency is representative of the fluctuations caused by bubbles. Similar findings were found in other studies, e.g. in capacitance probe data (Chehbouni et al., 1994) and differential pressure data (Bi et al., 1995). Radially, the dominant frequency decreases only slightly near the wall, but the peak amplitude decreases significantly, consistent with the decrease in the number of bubbles with increasing r deduced above from voidage probability distribution plots. The amplitudes are distributed over a wide frequency range for the turbulent, LDCFB and HDCFB conditions, and the dominant frequency is less than 1 Hz in all three cases. The broad spectrum of frequencies is indicative of an absence of any significant cyclical phenomenon. Therefore the flow dynamics depend on interactions caused by a multitude of small voids and particle structures, as well as individual particles. The amplitudes for the HDCFB are generally less than for the bubbling and turbulent beds, consistent with the lower heterogeneity in the HDCFB suggested by the intermittency plot (Fig. 7.16 (b)). The amplitudes of LDCFB are even lower than those of HDCFB, with the peak amplitudes increasing from the axis to the wall, while the HDCFB has a maximum value some distance from the wall. These results are also consistent with the voidage standard deviation and intermittency index profiles.

6.4 Summary

The average voidage in bubbling and turbulent beds is lower than in the high density CFB riser. Whereas voidage is a function of superficial gas velocity in the former regimes, the mean voidage is not very significantly affected by either the superficial gas velocity or the solids circulation rate in the HDCFB. These are factors which also influence significantly the voidage in low density CFB conditions.

Differential pressure fluctuations increase with superficial gas velocity in the bubbling bed up to the transition point to the turbulent regime and thereafter continue to fall. In the circulating fluidized bed risers, differential pressure fluctuations are higher in the bottom dense zone and in high density risers than in the dilute upper region of low density risers.

Average slip velocities are lowest in the bubbling and turbulent regimes followed by those in the dilute zone of CFB risers. They are highest in the dense zone of LDCFB units and in HDCFB risers.

The time-mean local voidage is reasonably uniform over the column cross-section in bubbling beds and to a lesser extent in the dilute pneumatic transport regime, while it decreases towards the wall in turbulent beds and in both the dilute upper zone and bottom dense region of dilute CFB risers or throughout high density CFB risers. The suspension is denser in turbulent beds and falls more gradually with radius compared to CFB risers. The voidage decrease with radius in high density risers is more gradual than in dilute risers subject to fast fluidization where there is a core-annulus structure.

While bubbles exist over most of the riser cross-section in bubbling beds, there normally are relatively few bubbles close to the wall, and they are absent in turbulent beds and in high density CFB risers. The core region of the turbulent bed contains small voids and dense structures interacting rapidly with an emulsion phase, but close to the wall the suspension appears to be more uniform with fewer voids and particle streamers. In CFB risers, no voids are found; instead we find a rather dilute suspension in the central region, interspersed with infrequent particle clusters. The number and density of these structures increase with radius. Maximum heterogeneity in the HDCFB occurs at some distance from the wall, while for LDCFB the flow is least uniform at the wall.

Local solids flux measurements presented in Chapter 5 showed that on a time-average basis solids rise rapidly in the core region and much slower close to the wall for high density CFB conditions, whereas in the dilute zone of low density risers solids move downward in the dense annulus and upward in the core. The absence of net downflow close to the wall means that conventional methods of estimating the annular layer thickness in dilute CFB risers are not applicable to high density risers. No measurements of solids velocity were made under bubbling or turbulent conditions in this work, but solids flux patterns in these low velocity beds clearly differ from those in CFB risers. In bubbling beds, particles are transported by bubble wakes and drift induced by bubble motion (Clift and Grace, 1985). Due to bubble coalescence and flow patterns, characteristic solids circulation currents, generally upward near the axis and downwards near the wall, are created in freely bubbling beds. The rapid interaction between voids and solids in turbulent beds also likely cause different solids movement patterns than in CFB risers.

High density flow differs substantially from that in the lower velocity (bubbling and turbulent) regimes. Fast fluidization is widely accepted (e.g. see Grace and Bi, 1997; Horio, 1997) as representing the major flow regime in low density circulating fluidized beds. In fast fluidization the suspension consists of a dense bottom zone with no clear bed surface joined by a transition zone to a relatively dilute top region. There are radial concentration gradients in the top region giving a characteristic core-annulus structure. Solids are carried upwards in the core and travel downwards in the annulus near the wall. This thesis demonstrates that radial and axial concentration gradients are also present in HDCFB; however, solids on average travel upwards at all radial positions. This chapter also demonstrates that there are other significant differences between flow patterns in HDCFB risers and in LDCFB risers subject to fast fluidization. While more work is

needed to investigate other types of solids, riser dimensions and inlet and exit configurations, it appears that the flow regime of fast fluidization needs to be redefined so as to incorporate the high density findings of this work. A possible definition could be as follows. The fast fluidization regime is a void-free regime commonly observed in circulating fluidized bed risers whereby a relatively dense zone forms at the riser bottom giving way to a dilute top region with a gradual transition in between. The height of the dense zone depends on the operating superficial gas velocity and solids circulation rate, as well as the nature of the gas and particles. Radially, the riser consists of a dilute core surrounded by a relatively dense annular region. On a time-average basis, particles travel upward throughout the entire cross-section in the dense zone, while in the dilute region they rise rapidly in the core and move downwards in the annular region.

CHAPTER 7

DETERMINATION OF TYPE A AND TYPE C CHOKING VELOCITIES

7.1 Introduction

The fast fluidization regime is bounded by the type A choking velocity as the upper limit and the type C choking velocity as the lower limit, as reviewed in Chapter 1 (see also Bi et al., 1993). If the superficial gas velocity exceeds the type A choking velocity for a fixed solids circulation rate or if the solids circulation rate is less than that corresponding to type A choking for the given gas velocity, then all particles are conveyed upward in dilute transport mode leaving no accumulation at the riser bottom. On the other hand if the superficial gas velocity falls below that corresponding to type C choking or the solids circulation rate exceeds that at the type C choking, then either slugging occurs, accompanied by severe pressure fluctuations for systems capable of slugging, or the suspension collapses into a turbulent fluidized bed.

Determination of the Type A and C choking velocities, U_{CA} and U_{CC}, has previously required extensive experimental work involving tests at various gas velocities and /or solids fluxes (Knowlton and Bachovchin, 1975). A common method is to increase the solids flux step by step while the superficial gas velocity is held constant, or to reduce the superficial gas velocity gradually while keeping the solids circulation rate constant. Type A choking velocity can then be determined by monitoring the differential pressure over a section at the bottom of the column and finding the solids flux or the superficial velocity at which a sharp jump first occurs in the differential pressure. The type A choking

point indicates the collapse of the suspension as the solids flowrate exceeds the saturation carrying capacity of the gas. If the high solids feed or the reduction in gas velocity is continued beyond this point, then the dense zone at the bottom grows up the riser until the density of the mixture becomes too great for the gas velocity to provide full support and type C choking then occurs. Determination of the velocity at this choking point is, however, difficult and less accurate because, as choking starts to occur, the collapsed solids immediately offer greatly increased resistance to the gas, resulting in a decrease in the gas velocity. This makes it difficult to determine the true choking velocity in most cases (Bai et al., 1997). There is also a possibility, especially in systems using L-valves, that the solids feeder will be unable to continue furnishing the riser with sufficient solids (Knowlton and Bachovchin, 1975). This chapter presents a simple new method of determining both the type A and the type C choking velocities and the corresponding voidages in a single experiment.

7.2 Measurement method

Experiments were carried out in the high density circulating fluidized bed apparatus described in detail in Chapter 2. The dual-loop feature of the system (see Fig. 2.2) facilitates the measurement technique. To ensure reliable results, the starting solids level in the downcomer (5) was kept the same from one run to the next by transferring all solids from the storage tank (3) to the downcomer before each experiment. Pressure taps installed along the first riser (1) were connected to a computer via pressure transducers and an analog-digital board. To record the dynamic change of gas velocity at the bottom of the riser, the pressure drop across the orifice meter and the pressure upstream of the orifice meter were also datalogged. The method requires the facility to be operated in a transient state by controlling the feed of solids to the bottom of the riser from the

downcomer and accumulating solids carried over from the top of the riser in the storage tank as outlined below.

Prior to time t = 0, the solids valve (7a) between riser 1 and the downcomer is closed and gas flows through empty riser 1 at a preset velocity. At t = 0 one starts to open valve (7a), while simultaneously recording the pressures. Typical results appear in Figs. 7.1 and 7.2. Over the initial period, gradual opening of the valve leads to an increase in the solids flux, and consequently to an increase in pressure drop (very nearly proportional to solids hold-up) in the riser. Since valve (7b) between the storage tank and riser 2 (4) and valve (7c) between the storage tank and riser 1 were kept closed, i.e. no particles were being returned to the top of the downcomer during the process, the solids inventory in the downcomer decreases. This can be seen from the fall of the pressure drop, ΔP_d, across the downcomer with time in Fig. 7.2. Further opening of valve (7a), thereby increasing the solids flux, eventually results in a sharp increase in the pressure drop at the riser bottom (see Fig. 7.1, z = 0.81 m, time t_1). This means that a relatively dense region has started to form at the bottom of the riser due to accumulation of solids. As a result, both the solids hold-up, (1 - ε), and the pressure at the riser bottom, P_r, begin to increase sharply with time (Fig. 7.2). This corresponds to type A choking, marking the transition from dilute pneumatic transport to fast fluidization. Beyond this point, any further opening of the valve makes the solids level in the downcomer fall linearly with time since the solids flux has reached the saturation carrying capacity. Since valves (7b) and (7c) were closed, this feature allows the net solids flux to be calculated from the slope of ΔP_d vs. time between t_1 and t_2 since

$$\Delta P_d = \rho_p (1 - \varepsilon_{mf}) g L_d \qquad (7.1)$$

and

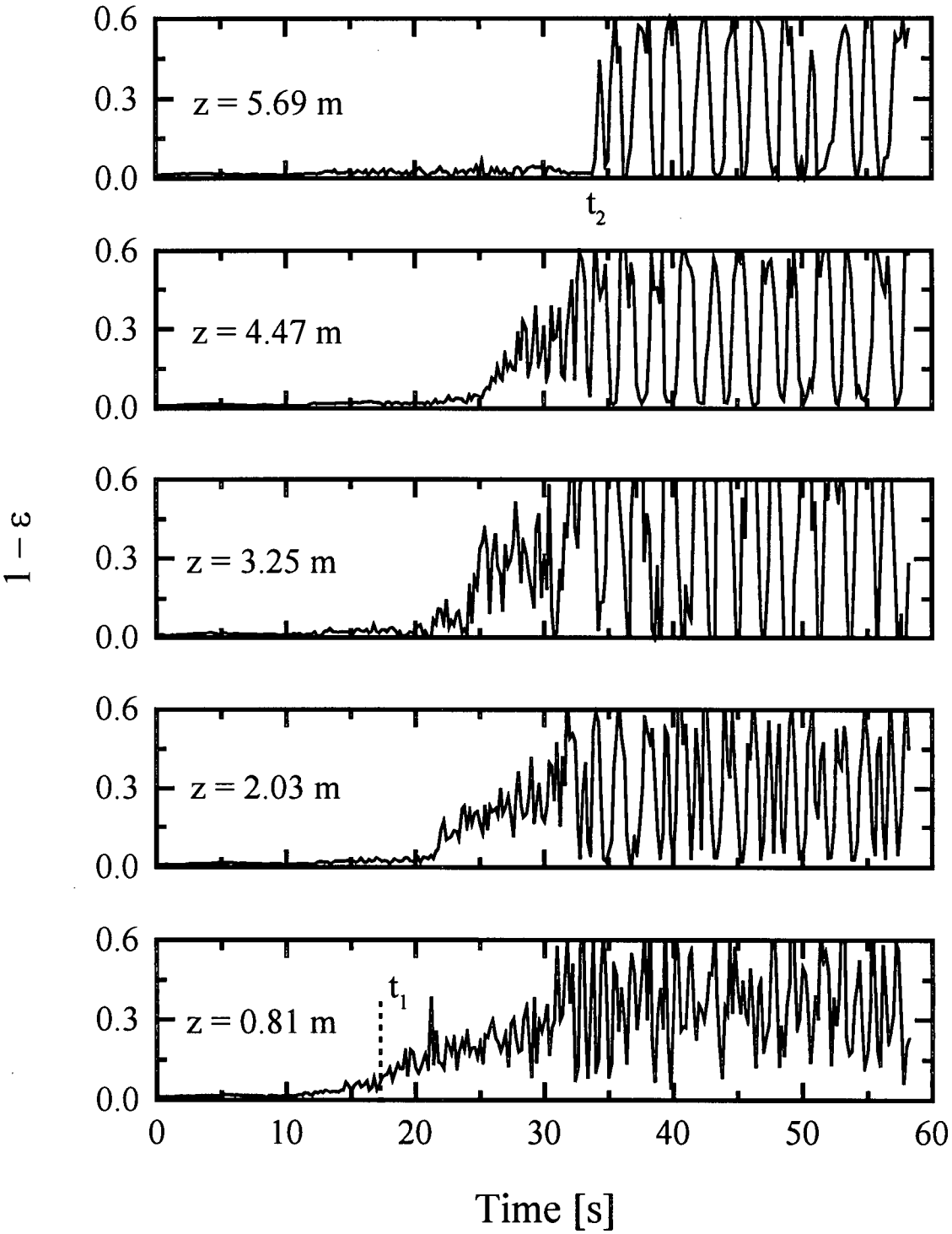

Fig. 7.1: Differential pressure fluctuations at various heights in riser 1 for a preset gas velocity of 7.2 m/s after commencing solids flow to the bottom of the riser. Values of z are to midpoints of 0.3 m tall measuring intervals.

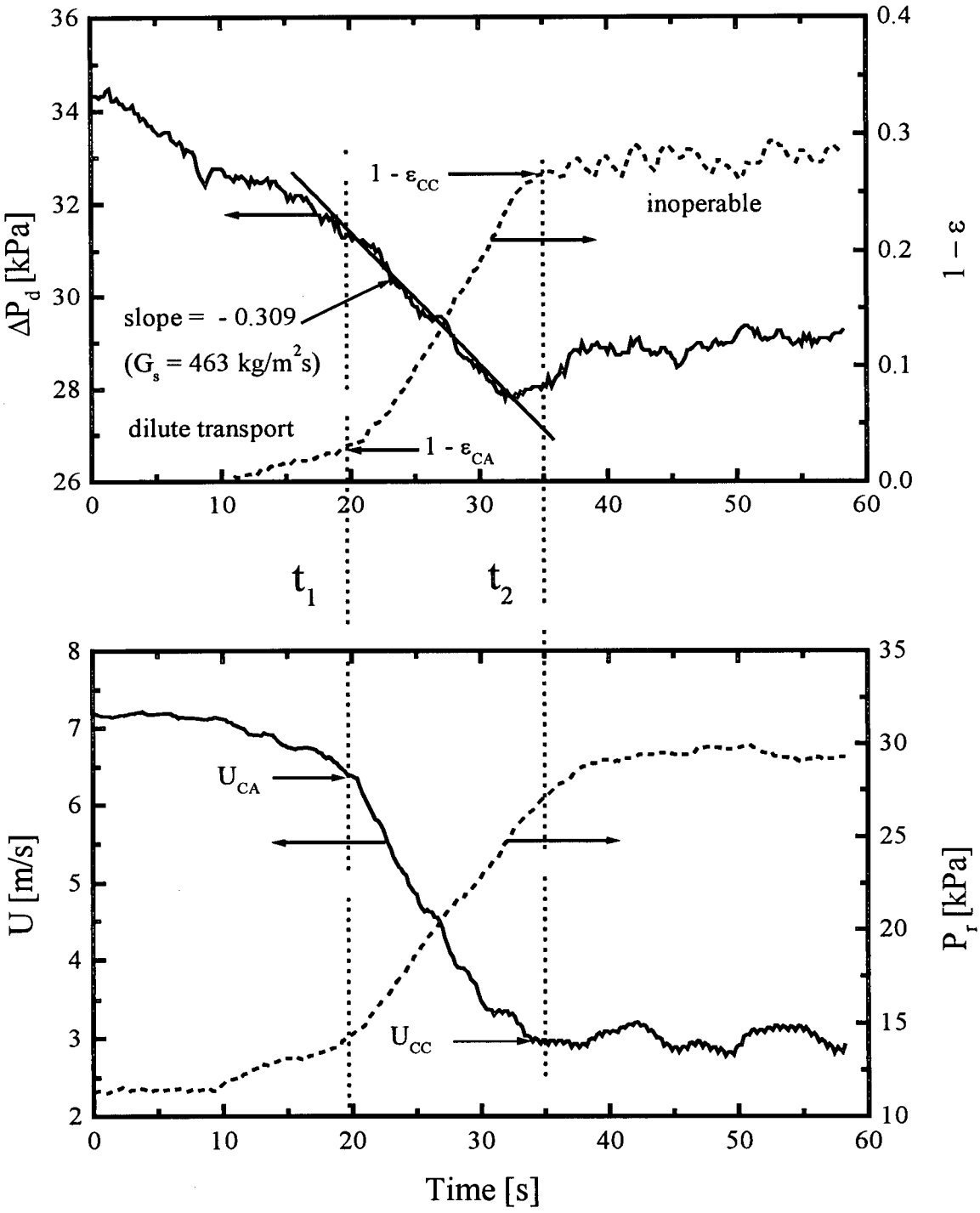

Fig. 7.2: Determination of choking velocities, U_{CA} and U_{CC}, and corresponding voidages in riser 1 for an initial gas velocity of 7.2 m/s.

$$G_s = -\rho_p(1-\varepsilon_{mf})\left(\frac{D_d}{D}\right)^2 \frac{dL_d}{dt} \tag{7.2}$$

Combining equations (7.1) and (7.2) gives

$$G_s = -\frac{1}{g}\left(\frac{D_d}{D}\right)^2 \frac{d\Delta P_d}{dt} \tag{7.3}$$

Experience has shown that once the net solids flux in riser 1 has reached its maximum, any further opening of gate valve (7a) no longer affects solids flow. While solids accumulate in the riser, the pressure drop (and therefore solids hold-up) increases progressively as solids build up in the lower part of riser 1. Finally a point is reached where slugs form at the bottom and rise through the dense zone. Due to the augmented resistance to gas flow, the gas velocity in the riser drops significantly. Once slugs have developed in the whole riser (marked as point $t = t_2$), the local pressure drop fluctuates with a considerable amplitude This can be taken as the type C choking point.

Note that the valve opening rate may influence the results. Opening the valve quickly may trigger bed collapse since the system has insufficient time to follow the changes in the flow pattern. It is therefore important to open the valve slowly to allow reliable results to be obtained (typically over a span of 2 minutes in the apparatus used here). The experiments were repeated for various initial gas velocities, giving a series of choking velocities (U_{CA}, U_{CC}) and corresponding voidages (ε_{CA}, ε_{CC}), for a series of different solids fluxes. All experiments were for the same FCC particles as in the rest of this study.

7.3 Results

The solids velocities U_{CA} and U_{CC}, determined in the manner described above, are plotted against the solids flux in Fig. 7.3. U_{CA} and U_{CC} both appear to increase with

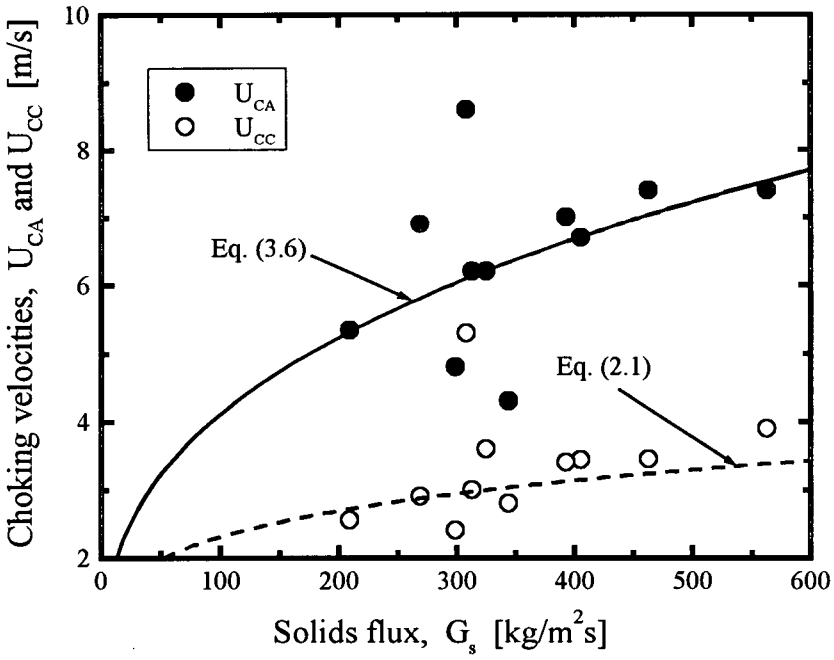

Fig. 7.3: Choking velocities as functions of the solids circulation flux compared with correlations recommended by Bi et al. (1993).

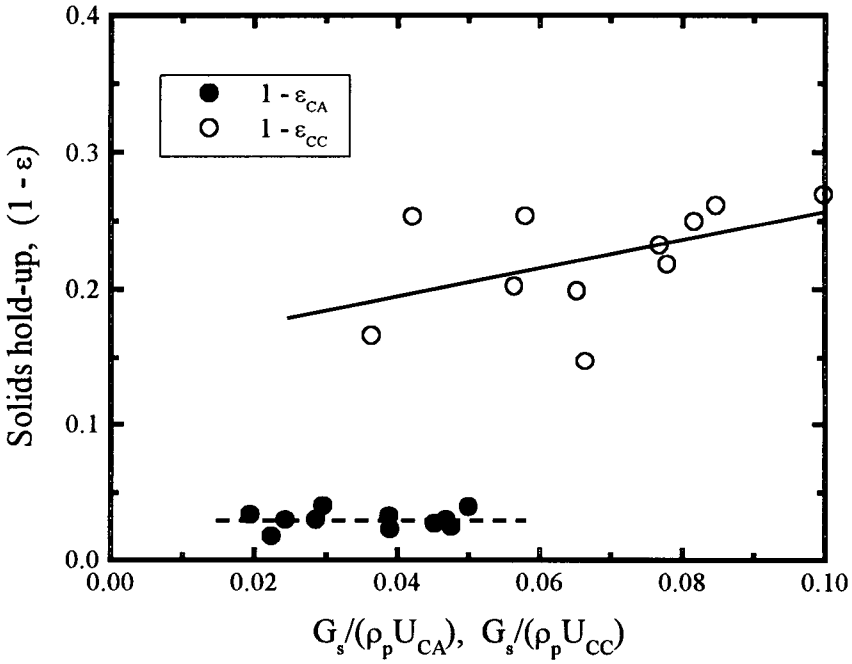

Fig. 7.4: Voidages at choking conditions as functions of $G_S/(\rho_p U_{CA})$ and $G_S/(\rho_p U_{CC})$ corresponding to results in Fig. 7.3.

increasing solids flux. For the same solids flux, U_{CA} is greater than U_{CC} as expected, and the difference between the two choking velocities increases as the solids flux is increased. These trends are consistent with results in the literature. The correlations recommended by Bi et al. (1993) are also plotted on Fig. 7.3. There appears to be favorable agreement between the measured U_{CA} values and the predictions of Eq. (3.5) by Bi and Fan (1991), and also between the experimental U_{CC} points and the Yousfi and Gau (1975) correlation (Eq. 2.1), supporting the recommendation of Bi et al. (1993) that the lower and upper bounds of fast fluidization can be predicted by the above two correlations.

The average solids hold-ups at the choking conditions, $(1 - \varepsilon_{CA})$ and $(1 - \varepsilon_{CC})$, are plotted as functions of corresponding solids-to-gas flow ratios, $G_s/(\rho_p U_{CA})$ and $G_s/(\rho_p U_{CC})$ in Fig. 7.4. No significant dependence of $(1 - \varepsilon_{CA})$ on $G_s/(\rho_p U_{CA})$ or of $(1 - \varepsilon_{CC})$ on $G_s/(\rho_p U_{CC})$ is observed. On average, $(1 - \varepsilon_{CA})$ and $(1 - \varepsilon_{CC})$ are around 0.03 and 0.22, respectively, consistent with earlier findings (Yang, 1975; Smith, 1978; Bi, 1994)

7.4 Summary

A new simple method has been proposed to determine the type A and type C choking velocities and their corresponding voidages in a single experiment. The method offers ease of operation and considerable experimental economy, thereby outweighing the drawback of having an extra solids recycle loop. Results obtained for FCC particles compare well with previously recommended correlations for the two types of choking that set the bounds of the fast fluidization regime.

CHAPTER 8

OVERALL CONCLUSIONS AND RECOMMENDATIONS

8.1 Conclusions

A dual-loop circulating fluidized bed unit has been designed, constructed and operated to study the flow dynamics of risers operating at high suspension densities and high solids flux. The main riser has an inside diameter of 76.2 mm and a height of 6.1 m. The unit is capable of achieving solids hold-ups as high as 15 to 25% by volume over the entire riser and FCC circulation fluxes of 400 kg/m^2s and beyond for superficial air velocities up to 8 m/s. These solids hold-ups and circulation rates are well above those of most previous studies. A new criterion has been proposed to indicate a transition between low density (LDCFB) and high density CFB (HDCFB) conditions. The total pressure drop across the riser has been found to be directly proportional to the solids-to-air mass flow ratio over a wide range, but levels off at higher solids flowrates when the riser is wholly under high density conditions. Previous studies had only suggested the initial linear relationship.

Voidages for bubbling, turbulent, low-density CFB and dilute pneumatic conditions have been compared to those for high density CFB conditions. The cross-sectional average solids hold-up in bubbling and turbulent beds is a function of superficial gas velocity and is higher than in HDCFB risers. Gas velocity and solids circulation rate also significantly influence the voidage in low density CFB conditions, but not for HDCFB operation.

Average slip velocities are lowest in the bubbling and turbulent regimes followed by those in the dilute zone of CFB risers. HDCFB risers have the highest slip velocities, with values as high as 40 times the single particle terminal velocity. Except for some scatter at high voidages, the average slip velocity in CFB risers at a given superficial air velocity appears to be a function only of voidage. Slip factors as high as 15 have been obtained for HDCFB operation, compared to about 2 to 5 reported in the literature for the developed region of low-density CFB risers. The higher values are however, within the range of values for the dense region of risers reported in previous studies.

Better correlations for predicting longitudinal profiles of mean solids hold-up have been established and used in a pressure and overall material inventory balance analysis to determine minimum solids inventories needed to maintain steady operation of the dual-loop HDCFB unit for fixed G_S and U. The analysis supports observations from this work and the literature which suggests that, at a fixed solids circulation rate and air velocity, raising solids inventories in the downcomer has no significant effect on solids hold-ups in risers.

Radial profiles of time-mean local voidage were studied using a reflective-type optical fiber probe. For the FCC particles used in this work, the intensity of the reflected light is not a linear function of the solids concentration as assumed in many previous studies. A new method of calibrating the probe was developed.

As for low solids flux and dilute conditions, voidages for high density conditions are lower near the wall than in the core, with time-mean voidages nearly as low as ε_{mf} at the wall and as high as 0.9 at the axis. The superficial air velocity and solids circulation rate have more influence on the voidage at the wall than in the core. The voidage decrease with radius in high density risers is more gradual than in dilute risers. The local voidage

data have been correlated as a function of the cross-sectional mean voidage. The resulting correlation gives better predictions than previous correlations based on limited ranges of suspension density.

The local flow dynamics of a high density CFB riser are characterized by local voidage traces, voidage frequency distribution plots, voidage power spectra and intermittency index profiles. The riser core is a relatively uniform predominantly dilute flow interspersed by particle clusters. The frequency and density of the clusters increase with radius. While the standard deviation of local voidage fluctuation is always highest at the wall in dilute CFB risers, the radial profile of standard deviation of local voidage fluctuations in HDCFB risers shows a characteristic peak at some distance from the wall. The location corresponding to the peak shows maximum heterogeneity. Further towards the wall the suspension becomes more homogeneous, probably because individual clusters no longer exist. Instead they join the dense 'emulsion phase', leading eventually to dense and relatively uniform conditions near the wall. The presence of bubbles or voids makes flow patterns in bubbling and turbulent beds differ significantly from HDCFB riser.

Solids sampling tubes have been used to measure local solids fluxes. While strong radial gradients exist in dense risers, as for dilute risers, there is a substantial difference in that there is no region of net downflow near the wall for high-density risers. The core-annulus concept commonly used in characterizing and modelling low-density CFB risers, appears, therefore, to have little or no applicability under high-density conditions. While the location of the peak standard deviation of voidage fluctuations can be used to delineate a boundary between a more dilute core region and a denser region at the wall, the wall layer thickness defined in this manner is quite different from that obtained from local solids flux measurements.

HDCFB flow behaviour differs significantly from that of the standard fluidization regimes. However, rather than proposing a new flow regime, the fast fluidization regime is redefined to incorporate the findings of this study.

A novel method has been developed to determine the type A and type C choking velocities and their corresponding voidages in a single experiment, offering ease of operation and considerable experimental economy. Results obtained for FCC particles compare well with predictions from recommended correlations.

8.2 Recommendations for Future Work

1. This study provides new data for testing CFB hydrodynamic models at higher suspension densities. Future modelling approaches need to incorporate the various differences between LDCFB and HDCFB pointed out in this study.

2. Formation of clusters, streamers, etc. appears to intensify with increasing suspension density. Measuring techniques need to be established which provide a better picture of the flow structure under high density conditions, thereby leading to more realistic and predictive hydrodynamic models.

3. Solids exchange between the core and the wall region is of importance in accounting for the radial solids distribution pattern found in this work. Studies are needed to confirm and quantify the exchange rate.

4. Highly exothermic or endothermic reactions may require internals for heat removal or addition to maintain temperature uniformity. Research is needed on the influence of internals on flow dynamics and catalyst attrition, as well as tube erosion and heat transfer. Heat transfer between the solids and the membrane walls in CFB combustors has been well documented. Similar studies need to be conducted for high density risers.

5. Studies of HDCFB at elevated pressures and temperatures as well as the study of the influence of riser diameter and height, riser inlet and exit geometries and particle properties need to be conducted to aid scale-up.

6. From a gas-solid reaction point of view, an increase in the solids hold-up and solids circulation rate should lead to a high capacity of the CFB reactor. However, the contact efficiency between gas and solids probably decreases with increasing solids hold-up. Research in this area is needed. It also needs to be established whether the best operating condition occurs when the riser is wholly occupied by dense phase or when there is a mixture of the dilute and dense phases.

7. Modifications need to be made to the air supply and the HDCFB unit so that the present work can be extended to even higher solids circulation rates.

NOMENCLATURE

A	Cross-sectional area	m^2
Ar	Archimedes number, $[\rho(\rho_p - \rho)gd_p^3]/\mu^2$	-
C_d	Discharge coefficient	-
D	Diameter of riser	m
D_d	Diameter of downcomer	m
d_p	Mean particle diameter	m
d_p^*	Dimensionless particle diameter, $d_p[\rho(\rho_p - \rho)g/\mu^2]^{1/3}$	-
F	Force	N
f_g	Fanning friction coefficient	-
Fr	Froude number, $U/\sqrt{gd_p}$	-
g	Acceleration due to gravity	m/s^2
G_s	Net solids circulation flux	kg/m^2s
G_s^*	Net solids circulation flux at high-density transition point	kg/m^2s
H	Riser height	m
K	Constant in Eqs. (3.25) and (5.2)	
k	Constant in Eqs. (3.26) and (5.3)	
L	Solids inventory expressed as height of packed bed in downcomer	m
m	Constant in Eq. (3.25)	-
m	Solids-to-gas mass flow ratio, $G_s/\rho U$	-
N	Number of data points	-
P	Instantaneous absolute pressure	Pa
P_d	Pressure at bottom of downcomer	Pa
r	Radial coordinate	m
R	Riser inner radius	m

Re	Gas Reynolds number, $\rho UD/\mu$	-
Re_c	Reynolds number based on U_c , $\rho U_c d_p/\mu$	-
Re_{mf}	Reynolds number based on U_{mf}, $\rho U_{mf} d_p/\mu$	-
Re_t	Reynolds number based on v_T, $\rho v_T d_p/\mu$	-
T	Sampling duration	s
t	Time	s
U	Superficial gas velocity	m/s
U^*	Dimensionless gas velocity, $U(\rho^2/(\rho_p - \rho)g\mu)^{1/3}$	-
U_B	Bubble rise velocity	m/s
U_c	Superficial air velocity corresponding to maximum standard deviation of differential pressure	m/s
U_{CA}	Accumulative (Type A) choking velocity	m/s
U_{CC}	Classical (Type C) choking velocity	m/s
U_{ch}	Classical choking velocity given by Eq. (2.1)	m/s
U_{mb}	Minimum bubbling velocity	m/s
U_{se}	Velocity for onset of significant solids entrainment	m/s
V	Voltage	V
V_g	Interstitial gas velocity, U/ε	m/s
V_p	Average particle velocity, $G_s/\rho_p(1-\varepsilon)$	m/s
v_T	Single particle terminal velocity	m/s
$\overline{V}_{slip}$	Average slip velocity, $V_g - V_p$	m/s
Ws	Solids mass flow rate	kg/s
Y	Ratio of actual bubble flow rate to value predicted by simple two-phase theory	-
z	Height above distributor	m
z_i	Height of inflection point in longitudinal solids hold-up profiles	m
z_o	Constant in Eq. (3.12)	m

Greek letters

α	Constant in Eqs. (5.1) and (5.3)	
γ	Intermittency index	-
ΔP	Pressure difference	Pa
ΔP_d	Pressure drop in downcomer	Pa
ΔP_{mo}	Momentum probe pressure drop	Pa
ΔP_r	Total pressure drop across riser	Pa
ΔP_v	Pressure drop across solids flow control valve	Pa
Δz	Distance between differential pressure ports	m
$\Delta\rho$	Difference between solids and gas density, $\rho_p - \rho$,	kg/m^3
φ	Dimensionless radial coordinate, r/R	-
δ_σ	Distance from wall of maximum standard deviation of local voidage fluctuations	m
δ_{Gs}	Annulus layer thickness from local time-mean net solids flux profile	m
$\delta_{\Delta P,mo}$	Annulus layer thickness from local time-mean net momentum probe pressure drop profile	m
ε	Apparent cross-sectional average voidage	-
$\bar{\varepsilon}$	Time-mean local voidage	-
ε	Limiting average dilute region voidage	-
ε_a	Limiting average dense zone voidage	-
ε_D	Average voidage at riser bottom	-
ε_e	Average voidage at riser exit	-
ε_m	Cross-sectional average voidage	-
ε_{mf}	Voidage at minimum fluidization	-
ε_t	Instantaneous local voidage	-
μ	Gas viscosity	kg/ms

μ_x	Mean value of any time series data x(t)	
μ_y	Mean value of any time series data y(t)	
ν_d	Effective kinematic viscosity of the emulsion phase	m^2/s
ρ	Gas density	kg/m^3
ρ_b	Bulk density, $\rho_p(1-\varepsilon)$	kg/m^3
ρ_p	Particle density	kg/m^3
σ_ε	Standard deviation of local voidage	-
$\sigma_{\Delta P/\Delta z}$	Standard deviation of differential pressure fluctuations per unit length	Pa/m
$\sigma_{\Delta P}$	Standard deviation of differential pressure fluctuations	Pa
ϕ	Valve opening ratio, A_o/A_{dis}	-
Φ	Slip factor, i.e. ratio of the interstitial gas velocity to the average particle velocity, V_g/V_p	-
τ	Time delay	s

Subscripts

0	Empty, without solids
1	Riser 1, Storage tank
2	Riser 2, Downcomer
ac	Acceleration
CA	Accumulative choking
calc.	Calculated, predicted
CC	Classical choking
cy	Cyclone
d	Downcomer
D	Drag

dis	Solids discharge pipe
expt.	Experimental, measured
fg	Friction from gas flow
fs	Friction from solids
G	Gravitational
max	Maximum
mf	Minimum fluidization
o	Orifice
p	Primary
r	Riser
ref	Reference
s	Secondary
w	Wall
ε	Voidage

REFERENCES

Abed, R., (1984), The characterization of turbulent fluid-bed hydrodynamics, in ***Fluidization IV***, D. Kunii and R. Toei, eds., Engineering Foundation, New York, 137 - 144.

Abrahamsen, A. R. and D. Geldart, (1980), Behavior of gas-fluidized beds of fine powders, Part 1: Homogeneous expansion, ***Powder Technol.***, **26**, 35 - 46.

Adanáz, J., L. F. de Diego and P. Gayán, (1994), Axial voidage profiles in fast fluidized beds, ***Powder Technol.***, **81**, 259 - 268.

Agbim, J. A., A. W. Nienow and P. N. Rowe, (1971), Inter-particle forces that suppress bubbling in gas fluidized beds, ***Chem. Eng. Sci.***, **26**, 1293 - 1294.

Aguillon, J., K. Shakourzadeh, and P. Guigon, (1996), A new method for local solid concentration mesurement in circulating fluidized bed, ***Powder Technol.***, **86**, 251 - 255.

Arena, U., A. Cammarota, L. Pistone, and P. V. Tecchio, (1986), High velocity fluidization behaviour of solids in a laboratory scale circulating bed, in ***Circulating Fluidized Bed Technology***, P. Basu, ed.., Pergamon Press, Toronto, 119-125.

Arena, U., A. Cammarota, L. Massimilla, and D. Pirozzi, (1988), The hydrodynamic behavior of two circulating fluidized bed units of different sizes, in ***Circulating Fluidized Bed Technology II***, P. Basu and J. F. Large, eds., Pergamon Press, Oxford, 223-230.

Arena, U., L. Massimilla, and D. Pirozzi, (1987), Analysis of a circulating fluidized bed system, ***Proc. 9th. Intern. Conf. Fluid. Bed Comb.***, ASME, New York.

Arena, U., A. Malandrino, A. Marzocchella, and L. Massimilla, (1991), Flow structures in the risers of laboratory and pilot CFB units, in ***Circulating Fluidized Bed Technology III***, P. Basu, M. Horio, and M. Hasatani, eds., Pergamon Press, Oxford.

Arena, U., A. Marzocchella, L. Massimilla, and A. Malandrino, (1992), Hydrodynamics of circulating fluidized beds with risers of different shape and size, ***Powder Technol.***, **70**, 237.

Arena, U., Cammarota, A., Pistone, L.,Tecchio, P. V., The high velocity fluidization behavior of solids in a laboratory scale circulating bed, in ***Circulating Fluidized Bed Technology***, P. Basu, ed., Pergamon Press, New York, 1986, 119-125.

Avidan, A. A., (1997), Fluid catalytic cracking, Chapter 13 in Circulating Fluidized Beds, J. R. Grace, A. A. Avidan and T. M. Knowlton, eds., Blackie Academic & Professional, 466 - 488.

Avidan A., M. Edwards, and H. Owen, (1989), Fluid Catalytic Cracking - Past and future challenges, in ***Fluidization***, J. R. Grace, L. W. Shemilt, and M. A. Bergougnou, eds., Engineering Foundation, New York

Avidan A. J. and J. Yerushalmi, (1982), Bed expansion in high velocity fluidization, ***Powder Technol.***, **32**, 223-232.

Azzi, M., P. Tulier, J. F. Large and J. R. Bernard, (1991), Use of a momentum probe and gammadensitometry to study local properties of fast fluidized beds, in ***Circulating Fluidized Bed Technology III***, P. Basu, M. Horio and M. Hasatani, eds., Pergamon, Oxford, 189 - 194.

Bader, R., J. Findlay and T. M. Knowlton, (1988) Gas/Solid flow patterns in a 30.5-cm-diameter circulating fluidized bed, in ***Circulating Fluidized Bed Technology II***, P. Basu and J. F. Large, eds., Pergamon Press, Oxford.

Bai, D., A. Issangya, J. -X. Zhu and J. R. Grace, (1997), Analysis of overall pressure balance around a high-density circulating fluidized bed, ***Ind. Eng. Chem. Res.***, **36**, 3898 - 3903

Bai, D. and K. Kato, (1995), Saturation carrying capacity of gas and flow regimes in CFB, ***J. Chem. Eng. Japan***, **28**, 179 - 185.

Bai, D. and K. Kato, (1994), Generalized correlations of solids holdups at dense and dilute regions of circulating fluidized beds, ***Proceedings of 7th. Symposium on Circulating Fluidized Beds, Tokyo, 137 – 144.***

Bai, D-R., Y. Jin, Z.-Q. Yu, J.-X. Zhu, (1992), The axial distribution of the cross-sectionally averaged voidage in fast fluidized beds, ***Powder Technol.***, **71**, 51-58.

Bai, D., E. Shibuya, Y. Masuda, N. Nakagawa and K. Kato, (1996), Flow structure in a fast fluidized bed, ***Chem. Eng. Sci.***, **51**, 957 - 966.

Bai, D, E. Shibuya, Y. Masuda, K. Nishio, N. Nakagawa and K. Kato, (1995b), Distinction between upward and downward flows in circulating fluidized beds, ***Powder Technol.***, **84**, 75 - 81.

Bai, D., E. Shibuya, N. Nakagawa and K. Kato, (1996), Characterization of gas fluidization regimes using pressure fluctuations, ***Powder Technol.***, **87**, 105 - 111.

Bai, D-R., J. -X. Zhu, Y. Jin and Z. -Q. Yu, (1995), Internal recirculation flow structure in vertical upflow gas-solids suspensions. Part I. A core - annulus model, ***Powder Technol.***, **85**, 171 - 177.

Bartholomew, R. N. and R. M. Casagrande, (1957), Measuring solids concentration in fluidized systems by gamma-ray absorption, ***Ind. Eng. Chem.***, **49**, 428 - 431.

Bendat and Piersol, (1986), Random Data - Analysis and Measurement Procedures, John Wiley and Sons

Berruti, F., J. Chaouki, L. Godfroy, T. S. Pugsley and G. S. Patience, (1995), Hydrodynamics of circulating fluidized bed risers: A review, ***Can. J. Chem. Eng.***, **73**, 579-602.

Berruti, F. and N. Kalogerakis, (1989), Modelling of internal flow structure of circulating fluidized beds, ***Can. J. Chem. Eng.***, **67**, 1010 - 1014.

Bi, H. T., (1994), Flow patterns of gas-solid fluidization and transport, Ph.D. dissertation, University of British Columbia, Vancouver, Canada.

Bi, H. T. and L.-S. Fan, (1991), Regime transition in gas-solid circulating fluidized beds, Paper #101e presented at the AIChE Annual Meeting, Los Angeles, Nov. 17-22.

Bi, H. T., J. R. Grace and K. S. Lim, (1995), Transition from bubbling to turbulent fluidization, ***Ind. Eng. Chem. Res.***, **34**, 4003 - 4008.

Bi, H. T., J. R. Grace and J. X. Zhu, (1995), Regime transitions affecting gas-solids suspensions and fluidized beds, ***Chem. Eng. Res. Des.***, **73**, 154 - 161.

Bi, H. T., J. R. Grace and J. X. Zhu, (1993), Types of choking in vertical pneumatic systems, ***Int. J. Multiphase Flow***, **19**, 1077 - 1092.

Bi H. T. and J. R. Grace, (1995), Effect of measurement method on velocities used to demarcate the onset of turbulent fluidization, ***Chem. Eng. J.***, **57**, 261 - 271.

Bi H. T. and J. R. Grace, (1996), Effects of pressure and temperature on flow regimes in gas-solid fluidization systems, ***Can. J. Chem. Eng.***, **74**, 1025 - 1027.

Bi H. T., J. Zhou and J. R. Grace, (1996), Annular wall layer thickness in circulating fluidized bed risers, ***Can. J. Chem. Eng.***, **74**, 811 - 814.

Bi, H. and J. Zhu, (1993), Static instability analysis of circulating fluidized beds and concept of high-density risers, ***AIChE J.***, **39**, (8), 1272-1280.

Bierl, T. W., L. J. Gadjos, A. L. McIver and J. J. McGovern, (1980), Studies in support of recirculating bed reactors for the processing of coal, US Department of Energy, Contract No. EX-C-76-01-2449.

Bird, R. B, W. E. Stewart and E. N. Lightfoot, (1960), Transport Phenomena, John Wiley & Sons, New York.

Bolton, L. W. and J. F. Davidson (1988), Recirculation of particles in fast fluidized beds, in ***Circulating Fluidized Bed Technology II***, P. Basu and J. F. Large, eds., Pergamon Press, Oxford, 139-152.

Breault, R. W. and V. K. Mathur, (1989a), High velocity fluidized bed hydrodynamic modeling. 1. Fundamental studies of pressure drop, ***Ind. Eng. Chem. Res.***, **28**, 684-688.

Breault, R. W. and V. K. Mathur, (1989b), High velocity fluidized bed hydrodynamic modeling. 2. Circulating bed pressure drop modeling, ***Ind. Eng. Chem. Res.***, **28**, 688.

Brereton, C. M. H. and J. R. Grace, (1993), Microstructural aspects of the behavior of circulating fluidized beds, ***Chem. Eng. Sci.***, **48,** 2565-2572.

Brereton, C. M. H., (1987), Fluid mechanics of high velocity fluidized beds, Ph.D. dissertation, University of British Columbia, Vancouver.

Brereton, C. M. H. and J. R. Grace, (1992), The transition to turbulent fluidization, ***Trans. Inst. Chem. Eng.***, **70A**, 246 - 251.

Brereton, C. M. H. and J. R. Grace, (1994), End effects in circulating fluidized bed hydrodynamics, in ***Circulating Fluidized Bed Technology IV***, A. A. Avidan, ed., 137 - 144.

Burkell, J. J., J. R. Grace, J. Zhao, and C. J. Lim, (1988), Measurement of solids circulation rates in circulating fluidized beds, in ***Circulating Fluidized Bed Technology II***, P. Basu and J. F. Large, eds., Pergamon Press, Oxford.

Chang, H. and M. Louge, (1992), Fluid dynamic similarity of circulating fluidized beds, ***Powder Technol.***, **70**, 259-270.

Chang, H. and M. Louge, (1991), Hydrodynamic scale-up of circulating fluidized beds, ***Proc. 11th. Intern. Conf. Fluid Bed Comb.***, ASME, New York, 1215 - 1218.

Chehbouni, A., J. Chaouki, C. Guy and D. Klvana, (1994), Characterization of the flow transition between bubbling and turbulent fluidization, ***Ind. Eng. Chem. Res.***, **33**, 1889 - 1896.

Cheremisinoff, N. P., (1986), Review of experimental methods for studying the hydrodynamics of gas-solid fluidized beds, ***Ind. Eng. Chem. Process Des. Dev.***, **25**, 329 - 351.

Choi, J. H. C. K. Yi, and J. E. Son, (1991), Axial voidage profile in a cold model circulating fluidized bed, in ***Circulating Fluidized Bed Technology III***, P. Basu, M. Horio, and M. Hasatani, eds., Pergamon Press, Oxford.

Clark, N. N. and C. M. Atkinson, (19988), Amplitude reduction and phase lag in fluidized bed pressure measurements, ***Chem. Eng. Sci.***, **43**, 1547 - 1557.

Clift, R. and J. R. Grace, (1985), Continuous bubbling and slugging, Chapter 3 in Fluidization, 2nd. ed., Academic Press, London, 73 - 131.

Comas, M., J. Comas, C. Chetrit and J. Casal, (1991), Cyclone pressure drop and efficiency with and without an inlet vane, ***Powder Technol.***, **66**, 143 - 148.

Contractor, R. M., (1988), Butane oxidation to maleic anhydride in a recirculating solids riser reactor, in ***Circulating Fluidized Bed Technology II***, P. Basu and J. F. Large, eds., Pergamon Press, Oxford, 467 - 474.

Contractor R. and J. Chaouki, (1991), Circulating fluidized bed as a catalytic reactor, in ***Circulating Fluidized Bed Technology III***, P. Basu, M. Horio, and M. Hasatani, eds., Pergamon Press, Oxford.

Corella, J. and Frances, (1991), Analysis of the riser reactor of a fluid catalytic cracking unit - Model based kinetics of cracking and deactivation from laboratory tests, in ***Fluid Catalytic Cracking II - Concept in Catalyst Design***, M. L. Occelli, ed., American Chemical Society, Washington, DC, 165 - 182.

Darton, R. C., R. D. LaNauze, J. F. Davidson and D. Harrison, (1977), Bubble growth due to coalescence in fluidized beds, ***Trans. Instn. Chem. Engrs.***, **55**, 274 - 280.

Dasgupta, S., R. Jackson and S. Sundresan, (1994), Turbulent gas-solid flow in vertical risers, ***AIChE J.***, **40**, 215 - 228.

de Diego, L. F., P. Gayan, and J. Adanez, (1995), Modelling of the flow structure in circulating fluidized beds, ***Powder Technol.***, **85**, 19 - 27.

Dhodapkar, S. V. and G. E. Klinzing, (1993), Pressure fluctuation analysis for a fluidized bed, ***AIChE Symp. Ser.***, **89** (296), 170 - 183.

Doig, I. D. and G. H. Roper, (1963) The minimum gas rate for dilute-phase solids transportation in a gas stream, ***Australian Chem. Eng.***, **1**, 9.

Drahos, J. J. Cermak, R. Guardani, and K. Schugerl, (1988), Characterization of flow regime transition in a circulating fluidized bed, ***Powder Technol.***, **56**, 41.

Dry, R. J. and C. J. Beeby, (1997), Applications of CFB technology to gas-solid reactions, Chapter 12 in Circulating Fluidized Beds, J. R. Grace, A. A. Avidan and T. M. Knowlton, eds., Blackie Academic & Professional, 441 - 465.

Engstrom, F. and Y. Y. Lee, (1991), Future challenges of circulating fluidized bed combustion technology, in ***Circulating Fluidized Bed Technology III***, P. Basu, M. Horio and M. Hasatani, eds., Pergamon, New York, 15 - 37.

Foscolo, P. U. and L. G. Gibilaro, (1987), Fluid dynamic stability of fluidized suspensions: the particle bed model, ***Chem. Eng. Sci.***, **42**, 1489 - 1500.

Gadjos L. J. and T. W. Bierl, (1978), Studies in support of circulating bed reactors for processing of coal, Topical Report for the US Department of Energy, Contract No. EX-C-76-01-2449, US Department of Energy, Washington, D.C . (Quoted from Yerushalmi and Avidan, 1985).

Galtier, P. A., R J. Pontier and T. E. Patureaux, (1989), Near full-scale cold flow model for the R2R catalytic cracking process, in ***Fluidization VI***, J. R. Grace, L. W. Shemilt and M. A. Bergougnou, eds., Engineering Foundation, New York, 17 - 24.

Geldart, D., (1986), Single particles, fixed and quiscent beds, Chapter 2 in Gas Fluidization Technology, D. Geldart, ed., John Wiley & Sons, New York, 11 - 32.

Geldart, D., (1986), Particle entrainment and carryover, Chapter 6 in Gas Fluidization Technology, D. Geldart, ed., John Wiley & Sons, New York, 123 - 153.

Geldart, D. and S. J. Ling, (1990), Dense phase conveying of fine coal at high total pressure, ***Powder Technol.***, **62**, 243 - 252.

Gianetto A., S. Pagliolico, G. Rovero and B. Ruggeri, (1990), Theoretical and practical aspects of circulating fluidized bed reactors (CFBRs) for complex chemical systems, ***Chem. Eng. Sci.***, **45**, 2219-2225.

Gibilaro, L. G., R. DiFelice, and P. U. Foscolo, (1988), On the minimum bubbling voidages and the Geldart classification for gas-fluidized beds, ***Powder Technol.***, **56**, 21 - 29.

Gidaspow, D. Y. P. Tsuo and K. M. Luo, (1989), Computed and experimental cluster formation and velocity profiles in circulating fluidized beds, in ***Fluidization VI***, J. R. Grace, L. W. Shemilt and M. A. Bergougnou, eds., Engineering Foundation, 81 - 88.

Glicksman, L. R. (1994), quoted from Louge (1997).

Glicksman, L. R. and P. D. Noymer, (1997), Measurement of the velocity and acceleration of clusters at the wall of a circulating fluidized bed, ***Preprints of AIChE Annual Meeting***, Chicago, 45 - 52.

Goedicke F. and L. Reh, (1993), Particle induced heat transfer between walls and gas-solid fluidized beds, ***AIChE Symp. Ser.***, **89**, (296), 123 - 136.

Grace, J. R., (1982), Fluidized bed hydrodynamics, Chapter 8.1 in Handbook of Multiphase Systems, G. Hetsroni, ed., Hemisphere Publishing, Washington.

Grace, J. R., (1986a), Contacting modes and behavior classification of gas-solid and other two-phase suspensions, ***Can. J. Chem. Eng.***, **64**, 353 - 363.

Grace J. R., (1986b) Heat transfer in circulating fluidized beds, in ***Circulating Fluidized Bed Technology***, P. Basu and, ed. Pergamon Press, Toronto, 63 - 81.

Grace, J. R., (1990), High-velocity fluidized bed reactors, ***Chem. Eng. Sci.***, **45**, 1953-1966.

Grace, J. R., (1996), Riser geometry influence on CFB particle and fluid dynamics, in ***Circulating Fluidized Bed Technology V***, J. Li and M. Kwauk, eds., Science Press, Beijing.

Grace, J. R. and J. Baeyens, (1986), Instrumentation and experimental techniques, Chapter 13 in Gas Fluidization Technology, D. Geldart, ed., Wiley, New York, 415 - 462.

Grace, J. R. and J. Tuot, (1979), A theory for cluster formation in vertically conveyed suspensions of intermediate density, ***Trans. Inst. Chem. Eng.***, **57**, 49 - 54.

Grewal, N. S., R. D. Maurer, W. Fox, and M. D Mann, (1991), Axial particle loading in a circulating fluidized bed, ***Proc. 11th. Intern. Conf. Fluid Bed Comb.***, ASME, New York.

Harris, B. J. and J. F. Davidson, (1994), A core/annulus deposition model, in ***Circulating Fluidized Bed Technology IV***, A. A. Avidan, ed., AIChE, New York, 32 - 39.

Harris, B. J., J. F. Davidson and Y. Xue, (1994), Axial and radial variations of flow in circulating fluidized bed risers, in ***Circulating Fluidized Bed Technology IV***, A. A. Avidan, ed., AIChE, New York, 103 -110.

Hartge, E.-U., Y. Li and J. Werther, (1986), Analysis of the local structure of the two phase flow in a fast fluidized bed, in ***Circulating Fluidized Bed Technology***, P. Basu (ed.), Pergamon Press, Oxford, 153-160.

Hartge, E. U., D. Rensner, J. Werther, (1988), Solids concentration and velocity patterns in circulating fluidized beds, in ***Circulating Fluidized Bed Technology II***, P. Basu and J. F. Large, eds., Pergamon Press, Oxford, 165-180.

Hartge, E. U., D. Rensner, J. Werther, (1989), Chem. Ing. Tech., **9**, 744

He, Y. L., (1995), Ph.D. dissertation, University of British Columbia, Vancouver, Canada.

Herb, B., K. Tuzla, and J. C. Chen, (1989), Distribution of solid concentrations in circulating fluidized bed, in ***Fluidization VI***, J. R. Grace, L. W. Shemilt, and M. A. Bergougnou, eds., Engineering Foundation, New York.

Herb, B., S. Dou, K. Tuzla, and J. C. Chen, (1992), Solid mass fluxes in circulating fluidized beds, ***Powder Technol.***, **70**, 197 - 205.

Herbert, P. M., T. A. Gauthier, C. L. Briens and M. A. Bergougnou, (1994), Application of fiber optic reflection probes to the measurement of local particle velocity and concentration in gas-solid flow, ***Powder Technol.***, **80**, 243 - 252.

Hirama, T., Takeuchi, H., Chiba, T., (1992), Regime classification of macroscopic gas-solid flow in a circulating fluidized-bed riser, ***Powder Technol.***, **70**, 215- 222.

Hoffmann, A. C., A. van Santen, R. W. K. Allen and R. Clift, (1992), Effects of geometry and solid loading on the performance of gas cyclones, ***Powder Technol.***, **70**, 83 - 91.

Horio, M., (1991), Hydrodynamics of circulating fluidization - Present status and research needs, in ***Circulating Fluidized Bed Technology III***, P. Basu, M. Horio, and M. Hasatani, eds., Pergamon Press, Oxford, 3 - 14.

Horio, M., K. Morishita, O. Tachibana, and N. Murata, (1988), Solid distribution and movement in circulating fluidized beds, in ***Circulating Fluidized Bed Technology II***, P. Basu and J. F. Large, eds., Pergamon Press, Oxford, 147 - 154.

Horio, M. and H. Kuroki, (1994), Three-dimensional flow visualization of dilutely dispersed solids in bubbling and circulating fluidized beds, ***Chem. Eng. Sci.***, **49**, 2413 - 2421.

Ishida, M. and T. Shirai, (1980), Measurement of the velocity and direction of flow of solid particles in a fluidized bed, ***Powder Technol.***, **27**, 1 - 6.

Ishida, M., A. Nishiwaki and T. Shirai, (1980), Movement of solid particles around bubbles in a three-dimensional fluidized bed at high temperatures, in Fluidization, J. R. Grace and J. M. Matsen, eds., Plenum, 357 - 364.

Ishii, H., T. Nakajima and M. Horio, (1989), ***J. Chem. Eng. Japan***, **22**, 484.

Issangya, A. S., D. Bai, H. T. Bi, K. S. Lim, J. Zhu and J. R. Grace, (1997), Axial solids hold-up profiles in a high-density circulating fluidized bed riser, in ***Circulating Fluidized Bed Technology V***, M. Kwauk and J. Li, eds., Science Press, Beijing, 60 - 65.

Issangya, A. S., D. Bai, J. R. Grace, and K. S. Lim, (1997), Flow behavior in the riser of a high-density circulating fluidized bed, ***AIChE Symp. Ser.***, **93** (317), 25 - 30.

Issangya, A. S., D. Bai, H. T. Bi, K. S. Lim, J. Zhu and J. R. Grace, (1996), Radial voidage profiles in a high-density circulating fluidized bed riser, ***46th Can. Chem. Eng. Conference***.

Jahnig, C. E., Campbell, D. L., and Martin, H. A., (1980), History of fluidized solids development at EXXON, in Fluidization, J. R. Grace and J. M. Matsen, eds., Plenum Press, New York, 3 - 24.

Jazayeri, B., (1991), Optimize FCC riser design, ***Hydrocarbon Process.***, May, 93 - 95.

Jiang, P. J., H.-T. Bi, R.-H. Jean and L.-S. Fan, (1991), Baffle effects on performance of catalytic circulating fluidized bed reactor, ***AIChE J.***, **37**, 1392-1400.

Jin, Y., Z. Yu, C. Qi, and D. Bai, (1988), The influence of exit structures on the axial distribution of voidage in fast fluidized bed, in ***Fluidization'88 - Science and Technology***, M. Kwauk and D. Kunii, eds. Science Press, Beijing, China.

Johnsson, F., A. Svensson and B. Leckner, (1992), Fluidization regimes in circulating fluidized bed boilers, in ***Fluidization VII***, O. E. Potter and D. J. Nicklin, eds., Engineering Foundation, New York, 471 - 478.

Jones, D. R. M. and J. F. Davidson, (1965), The flow of particles from a fluidized bed through an orifice, ***Rheologica Acta***, **4**, 180 - 192.

Karri and Knowlton, (1990), A practical definition of the fast fluidization regime, in ***Circulating Fluidized Bed Technology III***, P. Basu, M. Horio, and M. Hasatani, eds., Pergamon Press, Oxford.

Kato, K., T. Takarada, T. Tamura, and K. Nishino, (1991), Particle holdup distribution in a circulating fluidized bed, in ***Circulating Fluidized Bed Technology III***, P. Basu, M. Horio, and M. Hasatani, eds., Pergamon Press, Oxford.

Kehoe, P. W. K. and J. F. Davidson, (1971), ***Inst. Chem. Eng. (London) Symp. Ser.***, **33**, 97 - 116.

King, D. F., (1989), Estimation of dense phase bed voidage in fast and slow fluidized beds of FCC catalyst, in ***Fluidization VI***, J. R. Grace, L. W. Shemilt, and M. A. Bergougnou, eds., Engineering Foundation, New York.

King, D. F., (1992), Fluidized catalytic crackers: An engineering review, in ***Fluidization VII***, O. E. Potter and D. J. Nicklin, Engineering Foundation, New York.

Knowlton, T. M., (1992), Pressure and temperature effects in fluid-particle systems, in ***Fluidization VII***, O. E. Porter and D. J. Nicklin, eds., Engineering Foundation, New York, 27 - 46.

Knowlton, T. M. and D. M. Bachovchin, (1975), The determination of gas-solids pressure drop and choking velocity as a function of gas velocity in a vertical pneumatic conveying line, in ***Fluidization Technology I***, D. L. Keairns, ed., Hemisphere, Washington, D.C., 253 - 282.

Kunii, D and O. Levenspiel, (1991), Fluidization Engineering, 2nd edn., Butterworth, Boston.

Kunii, D. and O. Levenspiel, (1996), The vertical distribution of solids in circulating fluidized beds, in ***Fluidization VIII***, J. F. Large and C. Laguerie, eds., 229 - 236.

Kunii, D. and O. Levenspiel, (1991), Flow modelling of fast fluidized beds, in ***Circulating Fluidized Bed Technology III***, P. Basu, M. Horio, and M. Hasatani, eds., Pergamon Press, Oxford, 91 - 98.

Kunii, D. and O. Levenspiel, (1988), Entrainment of solids from fluidized beds - I. Holdup of solids in the freeboard, II. Operations of fast fluidized beds, ***Powder Technol.***, **61**, 193.

Kwauk, M., N. Wang, Y. Li, B. Chen, and Z. Shen, (1986), Fast fluidization at ICM, in ***Circulating Fluidized Bed Technology***, P. Basu, ed., Pergamon Press, Toronto, 33 - 62.

Leva, M., (1959), Fluidization, McGraw-Hill, New York.

Leuenberger, B. J. and L. J. Wilbert, (1987), Octane catalysts raise heat at cracking, reduce coke make, ***Oil & Gas J.***, 85, 38-44, May 25.

Leung, L. S., (1980), The ups and downs of gas-solid flow - A review, in ***Fluidization***, J. R. Grace and J. M. Matsen, eds., Plenum, New York, 25 - 68.

Leung, L. S. and R. J. Wiles, (1976), A quantitative design procedure for vertical pneumatic conveying systems, ***Ind. Eng. Chem. Process Des. Dev.***, **15**, 552.

Li, Y. and M. Kwauk, (1980), The dynamics of fast fluidization, in ***Fluidization***, J. R. Grace and J. M. Matsen (eds.), Plenum Press, New York, 537-544.

Li, J., Y. Tung, and M. Kwauk, (1988), Axial voidage profiles of fast fluidized beds in different operating regions, in ***Circulating Fluidized Bed Technology II***, P. Basu and J. F. Large, eds., Pergamon Press, Oxford.

Lim, K. S., J. X. Zhu and J. R. Grace, (1995), Hydrodynamics of gas-solid fluidization, ***Int. J. Multiphase Flow***, **21**, 141 - 193.

Lints, M. C. and L. R. Glicksman, (1993), The structure of particle clusters near the wall of a circulating fluidized bed, ***AIChE Symp. Ser.***, **89**, (296), 35 - 52.

Lischer, D. J. and M. Y. Louge, (1992), Optical fiber measurement of particle concentration in dense suspensions: calibration and simulation, ***Applied Optics***, **31**, 5106-5113.

Louge, M., (1997), Experimental techniques, Chapter 9 in ***Circulating Fluidized Beds***, J. R. Grace, A. A. Avidan and T. M. Knowlton, eds., Blackie Academic & Professional, 312 - 368.

Louge, M., D. J. Lischer, and H. Chang, (1990), Measurement of voidage near the wall of a circulating fluidized bed riser, ***Powder Technol.***, **62**, 267 - 274.

Louge M. and H. Chang, (1990), Pressure and voidage gradients in vertical gas-solid risers, Powder Technol., **60**, 197-201.

Martin, M. P., P. Tulier and J. R. Bernard, (1992), Gas and solid behavior in cracking circulating fluidized beds, ***Powder Technol.***, **70**, 249-258.

Marzocchella, A., R. C. Zijerveld, J. C. Schouten and C. M. van den Bleek, (1997), Chaotic behaviour of gas-solids flow in the riser of a laboratory-scale circulating fluidized bed, ***AIChE J.***, **43** (6), 1458 - 1468.

Matsen, J. M., (1976), Some characteristics of large solids circulation systems, in ***Fluidization Technology***, Keairns, D. L., ed., Hemisphere Publishing, New York, 135 - 149.

Matsen, J. M., (1982), Mechanisms of choking and entrainment, ***Powder Technol.***, **32**, 21 - 33.

Matsen, J. M., (1997), Design and scale-up of CFB catalytic reactors, Chapter 14 in Circulating Fluidized Beds, J. R. Grace, A. A. Avidan and T. M. Knowlton, eds., Blackie Academic & Professional, 489 - 503.

Matsuno, Y., H. Yamaguchi, T. Oka, H. Kage and K. Higashitani, (1983), The use of optic fiber probes for the measurement of dilute particle concentrations: calibration and application to gas-fluidized bed carryover, ***Powder Technol.***, **36**, 215 - 221.

Miller A. L. and D. Gidaspow, (1992), Dense vertical gas-solid flow in a pipe, ***AIChE J.***, **38**, 1801 - 1815.

Monceaux, L., M. Azzi, Y. Molodtsof and J. F. Large, (1986), Overall and local characterization of flow regimes in a circulating fluidized bed, in ***Circulating Fluidized Bed Technology***, P. Basu, ed., Pergamon, Toronto, 185 - 191.

Monceaux, L., M. Azzi, Y. Molodtsof, and J. F. Large, (1986), Particle mass flux profiles and flow regimes characterization in a pilot scale fast fluidized bed unit, in *Fluidization V*, K. Ostergaard and A. Sorensen, eds., Engineering Foundation, New York, 337 - 344.

Mori, S., K. Kato, E. Kobayashi, D. Liu, M. Hasatani, H. Matsuda, M. Hatori, T. Hirama, and H. Takeuchi, (1991), Effect of apparatus design on hydrodynamics of circulating fluidized bed, ***AIChE Symp. Ser.***, **289**, (88), 17 - 25.

Mori, S., Y. Yan, K. Kato, K. Matsubara, and D. Liu, (1991), Hydrodynamics of a circulating fluidized bed, in ***Circulating Fluidized Bed Technology III***, P. Basu, M. Horio, and M. Hasatani, eds., Pergamon Press, Oxford, 113 - 118.

Myler, C. A., A. Zaltash and G. E. Klinzing, (1986), Gas-solid transport in a 0.0508 m pipe at various inclinations with and without electrostatics I: Particle velocity and pressure drop, ***J. of Powder & Bulk Sol. Technol.,*** **10**, 5 - 12.

Nieuwland, J. J., R. Meijer, J. A. M. Kuipers and W. P. M. van Swaaij, (1996), Measurements of solids concentration and axial solids velocity in gas-solid two-phase flows, ***Powder Technol.***, **87**, 127 - 139.

Nowak, W., H. Mineo, R. Yamazaki, and K. Yoshida, (1991), Behavior of particles in a circulating fluidized bed of a mixture of two different sized particles, in ***Circulating Fluidized Bed Technology III***, P. Basu, M. Horio, and M. Hasatani, eds., Pergamon, Oxford.

Okhi, K., T. and T. Shirai, (1976), Particle velocity in fluidized beds, in ***Fluidization Technology***, D. L. Keairns, ed., Hemisphere, New York, 95 - 119.

Ouyang, S. and O. E. Potter, (1993), Consistency of circulating fluidized bed experimental data, ***Ind. Eng. Chem. Res.***, **32**, 1041-1045.

Park, D. W. and G. Gau, (1986), Simulation of ethylene epoxidation in a multitubular transport reactor, ***Chem. Eng. Sci.***, **41**, 143-150.

Patience, G. S. and J. Chaouki, (1991), Solids circulation rate determined by pressure drop measurements, in ***Circulating Fluidized Bed Technology III***, P. Basu, M. Horio, and M. Hasatani, eds., Pergamon Press, Oxford, 627 - 632.

Patience, G. S. and J. Chaouki, (1995), Solids hydrodynamics in the fully developed region of CFB risers, in ***Fluidization VIII***, J. F. Large and C. Laguerie, eds..

Patience, G. S., J. Chaouki, F. Berruti and R. Wong, (1992), Scaling considerations for circulating fluidized bed risers, ***Powder Technol.***, **72**, 31-37.

Patience, G. S., (1990), Ph.D. Dissertation, Ecole Polytechnique de Montréal, Canada.

Perales, J. F., T. Coll, M. F. Llop, L. Puigjaner, J. Arnaldos and J. Casal, (1991), On the transition from bubbling to fast fluidization regimes, in ***Circulating Fluidized Bed Technology III***, P. Basu, M. Horio, and M. Hasatani, eds., Pergamon Press, Oxford, 73 - 78.

Perry, R. H. and D. W. Green, (1984), Perry's Chemical Engineers' Handbook, McGraw-Hill, New York, p. 20 - 84.

Pita, J. A. and S. Sunderesan, (1993), Developing flow of a gas-particle mixture in a vertical riser, ***AIChE J.***, **39**, 541 - 552.

Pugsley, T. S., G. S. Patience, F. Berruti, and J. Chaouki, (1992), Modelling the catalytic oxidation of n-butane to maleic anhydride in a circulating fluidized bed reactor, ***Ind. Eng. Chem. Res.***, **31**, 2652-2660.

Pugsley, T. S., F. Berruti, L. Godfroy, J. Chaouki and G. S. Patience, (1994), A predictive model for the gas-solid flow structure in circulating fluidized bed riser, in ***Circulating Fluidized Bed Technology IV***, A. A. Avidan, ed.

Qin, S. and G. Liu, (1982), Application of optical fibers to measurement and display of fluidized bed systems, in ***Fluidization, Science and Technology***, M. Kwauk and D. Kunii, eds., Science Press, Beijing, 258-267.

Ravisankar, S. and T. N. Smith, (1986), Slip velocities in pneumatic transport, ***Powder Technol.***, **47**, 167 - 194.

Reh, L., (1971), Fluidized bed processing, ***Chem. Eng. Prog.***, **67**, 58 - 63.

Reh, L., (1985), The circulating fluidized bed reactor - A key to efficient gas/solid processing, in ***Circulating Fluidized Bed Technology***, P. Basu, ed., Pergamon Press, Toronto, 105 - 118.

Reh, L. and J. Li, (1991), Measurement of voidage in fluidized beds by optical probes, in ***Circulating Fluidized Bed Technology III***, P. Basu, M. Horio and M. Hasatani, (eds.), Pergamon Press, Oxford, 163-169.

Reichle, A. D., (1992), Fluid catalytic cracking hits 50 year mark on the run, ***Oil & Gas J.***, **90** (20), 41 - 48.

Rhodes, M. J. and P. Laussmann, (1992), A study of the pressure balance around the loop of a circulating fluidized bed, ***Can. J. Chem. Eng.***, **70**, 625-630.

Rhodes, M. J., Z. Shihui and H. Benkreira, (1992), Flow of dilute gas-particle suspensions, ***AIChE J.***, **38**, (12), 1913 - 1915.

Rhodes, M. J. and D. Geldart, (1986), Transition to turbulence, in ***Fluidization V***, K. Ostergaard and A. Sorensen, (ed.), Engineering Foundation, New York, 281 - 288.

Rhodes, M. J., H. Mineo, T. Hirama, (1991), Particle motion at the wall of a 305 mm diameter riser of a cold model circulating fluidized bed, in ***Circulating Fluidized Bed Technology III***, P. Basu, M. Horio, and M. Hasatani, eds., Pergamon Press, Oxford.

Rhodes, M. J., T. Hirama, G. Gerutti, and D. Geladart, (1989), Non-uniformities of solids flow in the risers of circulating fluidized beds, in ***Fluidization VI***, J. R. Grace, L. W. Shemilt and M. A. Berougnou, eds., Engineering Foundation, New York.

Rhodes, M. J. and D. Geldart, (1986), The hydrodynamics of recirculating fluidized beds, in ***Circulating Fluidized Bed Technology***, P. Basu, ed., Pergamon Press, Toronto, 193 - 206.

Rhodes, M. J. and D. Geldart, (1987), A model for the circulating fluidized bed, ***Powder Technol.***, **53**, 155-162.

Rhodes, M. J., (1990), Modeling the flow structure of upward-flowing gas-solid suspensions, ***Powder Technol.***, **60**, 27-38.

Rhodes, M. J., P. Laussmann, F. Villain, and D. Geladart, (1988), Measurement of radial and axial solids flux variations in the riser of a circulating fluidized bed, in ***Circulating Fluidized Bed Technology II***, P. Basu and J. F. Large, eds., Pergamon Press, Oxford.

Rhodes, M. J. and P. Laussmann, (1992), Characterizing non-uniformities in gas-particle flow in the riser of a circulating fluidized bed, ***Powder Technol.*** **72**, 277 - 284.

Rhodes, M. J., Laussmann, P., (1992), A study of the pressure balance around the loop of a circulating fluidized bed, ***Can. J. Chem. Eng.***, **70**, 625-630.

Rudolph, V., Y. O. Chong and D. J. Nicklin, (1991), Standpipe modelling for circulating fluidized beds, in ***Circulating Fluidized Bed Technology III***, P. Basu, M. Horio and M. Hasatani, eds., Pergamon Press, Oxford, 49 - 64.

Saxton, A. L. and A. C. Worley, (1970), Modern catalytic cracking design, ***Oil & Gas J.***, **68**(20), 82-99.

Schnitzlein, M. G. and H. Weinstein, (1988), Flow characterization in high-velocity fluidized beds using pressure fluctuations, ***Chem. Eng. Sci.***, **43**, 2605-2614.

Schuurmans, H. J. A., (1980), Measurements in a commercial catalytic cracking unit, ***Ind. Eng. Chem. Process Des. Dev.***, **19**, 267 - 271.

Senior, R. C. and C. M. H. Brereton, (1992), Modelling of circulating fluidized bed solid flow and distribution, ***Chem. Eng. Sci.***, **47**, 281-296.

Shaheen, E. I., (1983), Catalytic processing in petroleum refining, Penwell Books, Tulsa.

Shohji, Y, N. Fujita, Y. Kamugai, H. Kubo and T. Murayama, (1983), Production of olefins from heavy oils in a fluidized coke bed, ***Fluidization IV***, D. Kunii and R. Toei, (eds.), Engineering Foundation, New York.

Simons, S. J. R., J. P. K. Seville, R. Clift, W. B. Gilboy and M. E. Hosseini-Ashrafi, (1993), Application of gamma-ray tomography to gas fluidised and spouted beds, in Tomographic Techniques for Process Design and Operation, M. S. Beck, E. Campogrande, M. Morris, M. Williams and R. C. Waterfall, eds., Computational Mechanics Publications, Southampton, U. K., 227 - 238.

Sinclair, J. L. and R. Jackson, (1989), Gas-particle flow in a vertical pipe with particle-particle interactions, ***AIChE J.***, **35**, 1473 - 1486.

Sinclair, J. L., (1997), Hydrodynamic modelling, in Circulating Fluidized Beds, J. R. Grace, A. A. Avidan and T. M. Knowlton, eds., Blackie Academic & Professional, 149 - 177.

Sitnai, O and A. B. Whitehead, (1985), in Fluidization, J. F. Davidson, R. Clift and D. Harrison, eds., Academic, London, 473 - 493.

Sobocinski, D. A., B. J. young, H. I. de Lasa, (1995), New fiber-optic method for measuring velocities of strands and solids hold-up in gas-solids downflow reactors, ***Powder Technol.***, **83**, 1 - 11.

Soong, C. H., K. Tuzla and J. C. Chen, (1994), Identification of particle clusters in circulating fluidized bed, in ***Circulating Fluidized Bed Technology IV***, A. A. Avidan, ed., AIChE, New York, 615 - 620.

Squires, A. M., (1986) The story of fluid catalytic cracking: The first circulating fluid bed, in ***Circulating Fluidized Bed Technology***, P. Basu, ed., Plenum Press, Toronto, 1 - 19.

Stemerding, S. (1962), The pneumatic transport of cracking catalyst in vertical risers, ***Chem. Eng. Sci.***, **17**, 599-608.

Stripinis, V. J., (1991), Long-residue processing in a riser pilot plant, in ***Fluid Catalytic Cracking II - Concept in Catalyst Design***, L. M. Occelli, ed., American Chemical Society, Washington, DC, 308 - 317.

Sun, G. and G. Chen, (1989), Transition to turbulent fluidization and its prediction, in ***Fluidization VI***, J. R. Grace, L. W. Shemilt and M. A. Bergougnou, eds., Engineering Foundation, New York, 33 - 40.

Sun, G. and J. R. Grace, (1992), The effect of particle size distribution in different fluidization regimes, ***AIChE J.***, **38**, 716 - 722.

Svarovsky, L., (1986), Solid-gas separation, Chapter 8 in Gas Fluidization Technology, D. Geldart, ed., John Wiley & Sons, New York, 197 - 210.

Svensson, A., F. Johnsson and B. Leckner, (1996), Fluidization regimes in non-slugging fluidized beds: the influence of pressure drop across the air distributor, ***Powder Technol.***, **86**, 299 - 312.

Takeuchi, H., T. Hirama, T. Chiba, J. Biswas, and L. S. Leung, (1986), A quantitative regime diagram for fast fluidization, ***Powder Technol.***, **47**, 195.

Teo, C. S. and L. S. Leung, (1984), Vertical flow of particulate solids in standpipes and risers. Chapter 11 in Hydrodynamics of Gas-Solids Fluidization, N. P. Cheremisnoff and P. N. Cheremisnoff, eds., Gulf Publishing Company, Houston.

Toomey, R. D. and H. F. Johnstone, (1952), Gaseous fluidization of solid particles, ***Chem. Eng. Prog.***, **48**, 220 - 226.

Trefz, M. and E. Muschelknautz, (1993), Extended cyclone theory for gas flows with high solids concentrations, ***Chem. Eng. Technol.***, **16**, 153 - 160.

Tsuo, Y. P., and D. Gidaspow, (1990), Computation of flow patterns in circulating fluidized beds, ***AIChE J.***, **36**, 885 - 896.

Tung, Y., J. Li and M. Kwauk, (1988), Radial voidage profiles in a fast fluidized bed, in ***Fluidization 88: Science and Technology***, M. Kwauk and D. Kunii, eds., Science Press, Beijing, 139 - 145.

Tuzla, K and J. C. Chen, (1992), Performance of a cyclone under high solid loadings, ***AIChE Symp. Ser.***, **88**, (289), 130 - 136.

van Breugel, J. W., J. M. Stein and R. J. de Vries, (1970), Isokinetic sampling in a dense gas-solids stream, ***Proc. Inst. Mech. Eng.***, **184**, 18 - 23.

van der Ham, A. G. J. Prins and W. P. M. van Swaaij, (1993), Hydrodynamics of a pilot plant scale regularly packed CFB, ***AIChE Symp. Ser.***, **89** (296), 53 - 72.

van Swaaij, W. P. M., (1978), The design of gas-solids fluid bed and related reactors, ***ACS Symp. Ser.***, **72**, 193 - 222.

van Swaaij, W. P. M, C. Buurman and J. W. van Breugel, (1970), Shear stresses on the wall of a dense phase riser, ***Chem. Eng. Sci.***, **25**, 1818 - 1820.

Vergel, C. H., (1990), quoted from Pugsley et al. (1994).

Viitanen, P. I., (1993), ***Ind. Eng. Chem. Res.***, **32**, 577-583.

Wainwright, M. S. and T. W. Hoffman, (1974), Chem. Reaction Eng. II, Advances in Chem. Sciences, 113, H. M. Hulburt, ed., ACS, Washington D.C.

Wang, X. S., and B. M. Gibbs, (1991), Hydrodynamics of a circulating fluidized bed with secondary air injection, in ***Circulating Fluidized Bed Technology III***, P. Basu, M. Horio, and M. Hasatani, eds., Pergamon Press, Oxford, 225 - 230.

Wang, Z., F. Wei, Y. Jin and Z. Yu, (1996), Effect of flow direction on hydrodynamics and mixing of circulating fluidized beds, Paper DB4, ***Preprint of 5th. International Conference on Circulating Fluidized Bed Technology***, Beijing.

Wei, F., G. -Q., Yang, Y. Jin and Z. -Q., Yu, (1995), The characteristics of cluster in a high density circulating fluidized bed, ***Can. J. Chem. Eng.***, **73**, 650 - 655.

Wei, F., L. Fangbin, J. Yong and Y. Zhiqing, (1997), Mass flux profiles in a high density circulating fluidized bed, ***Powder Technol.***, **91**, 189 - 195.

Weimer, A. W., D. C. Gyure and D. E. Clough, (1985), Application of a gamma-radiation density gauge for determining hydrodynamic properties of fluidized beds, ***Powder Technol.***, **44**, 179 - 194.

Weinstein, H., Graff, R. A., Meller, M., and Shao, M. J., (1983), The influence of the imposed pressure drop across a fast fluidized bed, in ***Fluidization IV***, D. Kunii and R. Toei, eds., Engineering Foundation, New York, 299 - 306.

Weinstein, H, M. Shao and L. Wasserzug, (1984), Radial solid density variations in a fast fluidized bed, ***AIChE Symp. Ser.***, **80** (241), 117 - 121.

Weinstein, H., M. J. Shao, M. Schnitzlein, and R. A. Graff, (1986), Radial variation in void fraction in a fast fluidized bed, in ***Fluidization V***, K. Ostergaard and A. Sorensen, eds., Engineering Foundation, New York, 329 - 336.

Weinstein, H., M. J. Shao, and M. Schnitzlein, (1986), Radial variation in solid density in high velocity fluidization, in ***Circulating Fluidized Bed Technology***, P. Basu, ed., Pergamon Press, Toronto, 201-206.

Weinstein, H. and J. Li, (1989), An evaluation of the actual density in the acceleration section of vertical risers, ***Powder Technol.***, **57**, 77-79.

Weinstein, H., H. J. Feindt, L. Chen and R. A. Graff, (1992), The measurement of turbulence quantities in a high velocity fluidized bed, in ***Fluidization***, O. E. Potter and D. J. Nicklin, eds., Engineering Foundation, New York, 305 - 312.

Werther, J., (1974), ***AIChE Symp. Ser.***, **141**, (70), 53 - 62.

Werther, J., (1994), Fluid mechanics of large-scale CFB units, in ***Circulating Fluidized Bed Technology IV***, A. A. Avidan, ed., 1-14.

Werther, J., E. -U. Hartge and D. Rensner, (1993), Measurement techniques for gas-solid fluidized bed reactors, ***Int. Chem. Eng.***, **33**, 18-26.

Williams, R. A., C. G. Xie, F. J. Dickins, S. J. R. Simons and M. S. Beck, (1991), Multi-phase flow measurements in powder processing, ***Powder Technol.***, **66**, 203 - 224.

Wirth, K. E., M. Seiter and O. Molerus, (1991), Concentration and velocities of solids in areas close to the walls in circulating fluidized bed systems, ***VGB Kraftwerkstechnik***, 10.

Wong, R., T. Pugsley and F. Berruti (1992), Modeling the axial voidage profile and flow structure in risers of circulating fluidized beds, ***Chem. Eng. Sci.***, **47**, 9-11, 2301-2306.

Wu, R. L., J. R. Grace and C. J. Lim, (1990), A model for heat transfer in circulating fluidized beds, ***Chem. Eng. Sci.***, **45**, 3389 - 3398.

Yamazaki, H., K. Tojo and K. Miyanami, (1992), Measurement of local solids concentration in a suspension by an optical method, ***Powder Technol.***, **70**, 93 - 96.

Yang, W. C., (1975), A mathematical definition of choking phenomenon and a mathematical model for predicting choking velocity and choking voidage, ***AIChE J.***, **29**, 1013 - 1015.

Yang, W. C., (1993), The hydrodynamics of circulating fluidized beds, Chapter 9 in Encyclopedia of Fluid Mechanics, Supplement 2: Advances in Multiphase Flows, ed., Gulf Publishing, Houston.

Yang, W. C., (1988), A model for the dynamics of a circulating fluidized loop, ***in Circulating Fluidized Bed Technology II***, P. Basu and J. F. Large, eds., Pergamon Press, Oxford, 181 - 191.

Yang, W. C. and T. M. Knowlton, (1993), L-valve equations, ***Powder Technol.***, 77, 49 - 54.

Yang, J. S., A. Y. Liu and A. M. Squires, (1987), A simple light-probe method for quantitative measurement of particle volume fractions in fluidized beds, ***Powder Technol.***, **49**, 177 - 187.

Yang, Y.-L., Y. Jin, Z. -Q. Yu, J. -X Zhu and H. -T. Bi, (1993), Local slip behaviors in the circulating fluidized bed, ***AIChE Symp. Ser.***, 89, (296), 81 - 90.

Yates, J. G. and J. R. Simons, (1994), Experimental methods in fluidization research, ***Int. J. Multiphase Flow***, Vol. **20** Suppl., 297 - 330.

Yerushalmi, J. and N. T. Cankurt, (1979), Further studies of the regimes of fluidization, ***Powder Technol.***, **24**, 187 - 205.

Yerushalmi, J. and A. M. Squires, (1977), The phenomenon of fast fluidization, ***AIChE Symp. Ser.***, **73** (161), 44 - 50.

Yerushalmi, J., D. H. Turner and A. M. Squires, (1976), The fast fluidized bed, ***Ind. Eng. Chem. Process Des. Dev.***, **15**, 47-53

Yerushalmi, J., Cankurt, N. T., Geldart, D., and Liss, B. (1978), Flow regimes in vertical gas-solid contact systems, ***AIChE Symp. Series***, **74** (176), 1.

Yerushalmi, J. and A. A. Avidan, (1985), High velocity fluidization, Chapter 7 in Fluidization, J. F. Davidson, R. Clift and D. Harrison, eds. 2nd. Ed., Academic Press, London, 225 - 291.

Yoshida, K. and H. Mineo, (1989), High-velocity fluidization, in Transport in Fluidized Particle Systems, L. K. Doraiswamy and A. S. Mujumdar, eds., Elsevier Science, Amsterdam, 241 - 285.

Yousfi, Y. and G. Gau, (1974), Aérodynamique de l'écoulement vertical de suspensions concentrées gaz-solides - I. Régimes d'écoulement et stabilité aérodynamique, ***Chem. Eng. Sci.***, **29**, 1939-1946.

Yousfi, Y. and G. Gau, (1974), Aérodynamique de l'écoulement vertical de suspensions concentrées gaz-solides - II. Chute de pression et vitesse relative gas-solide, ***Chem. Eng. Sci.***, **29**, 1947-1953.

Zenz, F. A., and Othmer, D. F., (1960), Fluidization and fluid-particle systems, Rheinhold Publishing Corp., New York.

Zenz, F. A. (1949), Two-phase fluidized-solid flow, ***Ind. Eng. Chem.***, **41**, 2801

Zhang, W., Y. Tung and F. Johnsson, (1991), Radial voidage profiles in fast fluidized beds of different diameters, ***Chem. Eng. Sci.***, **46**, 3045 - 3052.

Zhang, W., F. Johnsson and B. Leckner, (1994), Characteristics of the lateral particle distribution in circulating fluidized bed boilers, in ***Circulating Fluidized Bed Technology IV***, A. Avidan, ed., 266 - 273.

Zhang, W., F. Johnsson and B. Leckner, (1995), Fluid-dynamic boundary layers in CFB boilers, ***Chem. Eng. Sci.***, **50**, 201 - 210.

Zhou, J., J. R. Grace, S. Qin, C. M. H. Brereton, C. J. Lim, and J. Zhu, (1994), Voidage profiles in a circulating fluidized bed of square cross-section, ***Chem. Eng. Sci.***, **49**, 3217-3226.

Zhou, J., (1995), Circulating fluidized bed hydrodynamics in a riser of square cross-section, PhD dissertation, University of British Columbia, Canada.

Zhu, J.-X. and H.-T Bi, (1995), Distinctions between low density and high density circulating fluidized beds, ***Can. J. Chem. Eng.***, **73**, 644-649.

Zhu, J., J. R. Grace, and C. J. Lim, (1989), Erosion-causing particle impacts on tubes in fluidized beds, in ***Fluidization VI***, J. R. Grace, L. W. Schemilt, and M. A. Bergougnou, eds., Engineering Foundation, New York, 613 - 620.

Zoonen, D. van, (1962), Measurements of diffusional phenomena and velocity profiles in a vertical riser, ***Proc. Symp. on the Interaction between Fluids and Particles***, London, 64 - 71.

APPENDICES

Appendix A-1: Details of Riser 1

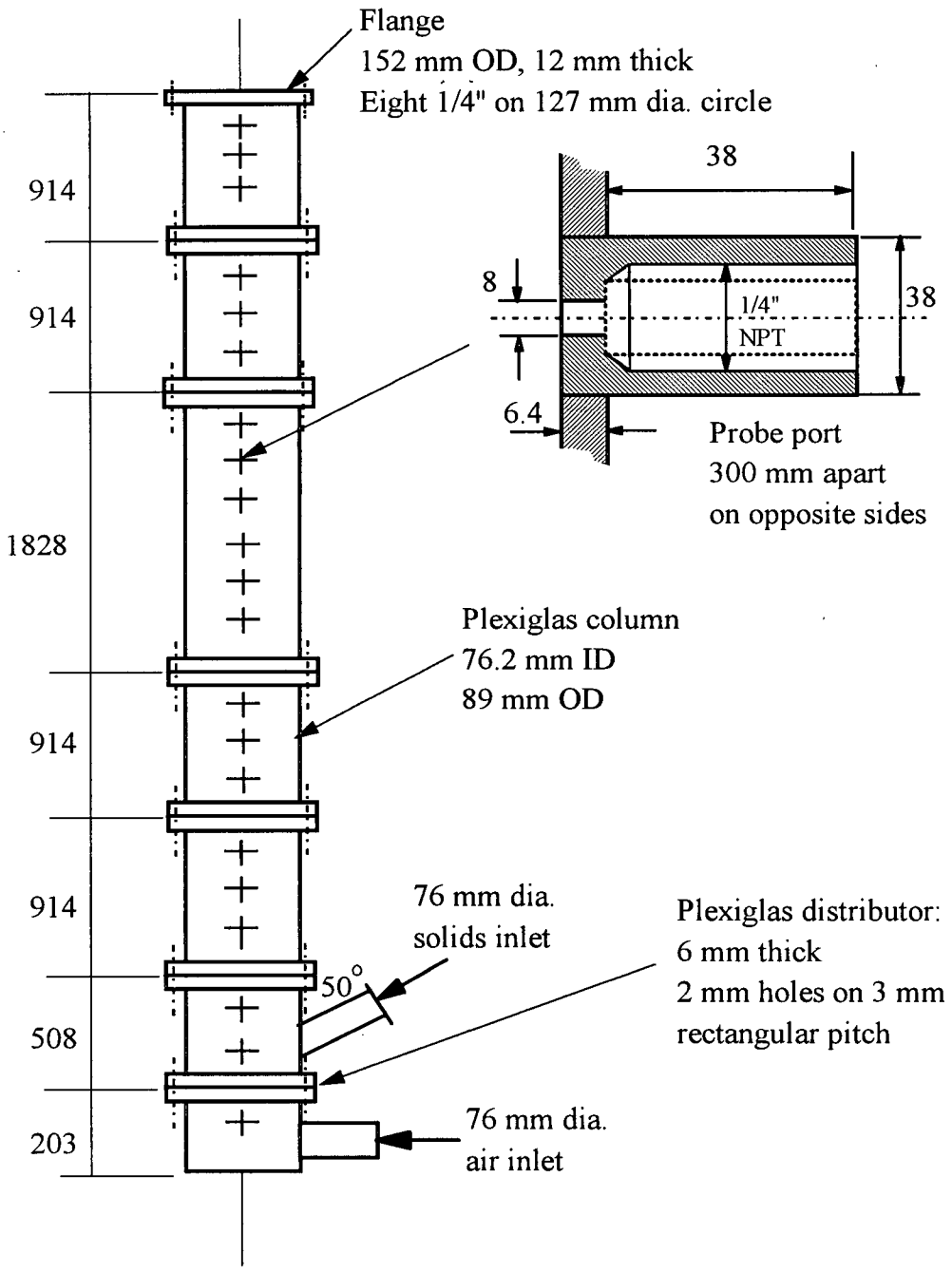

Dimensions in mm

Appendix A-2: Details of Riser 2

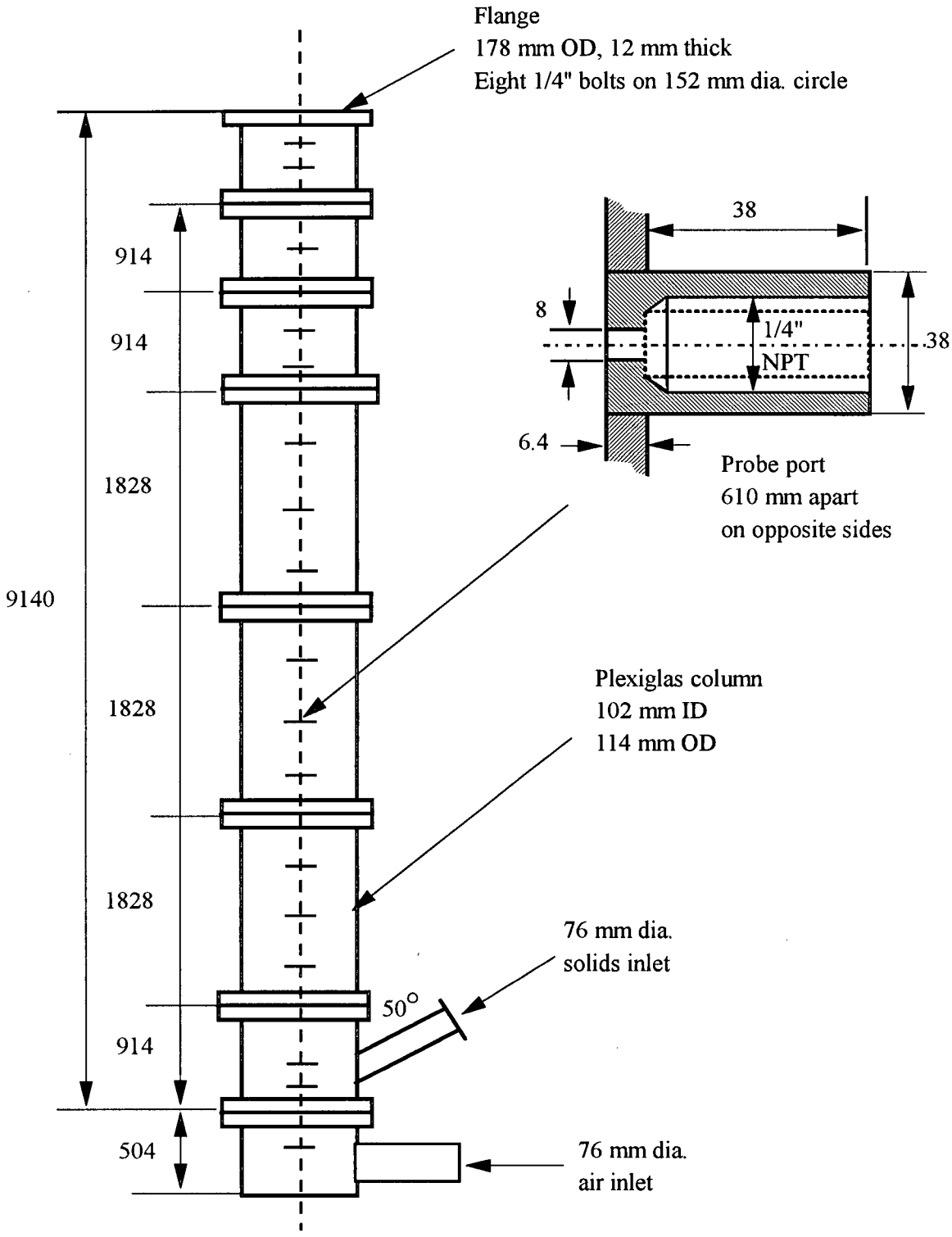

Dimensions in mm

Appendix A-3: Details of Downcomer

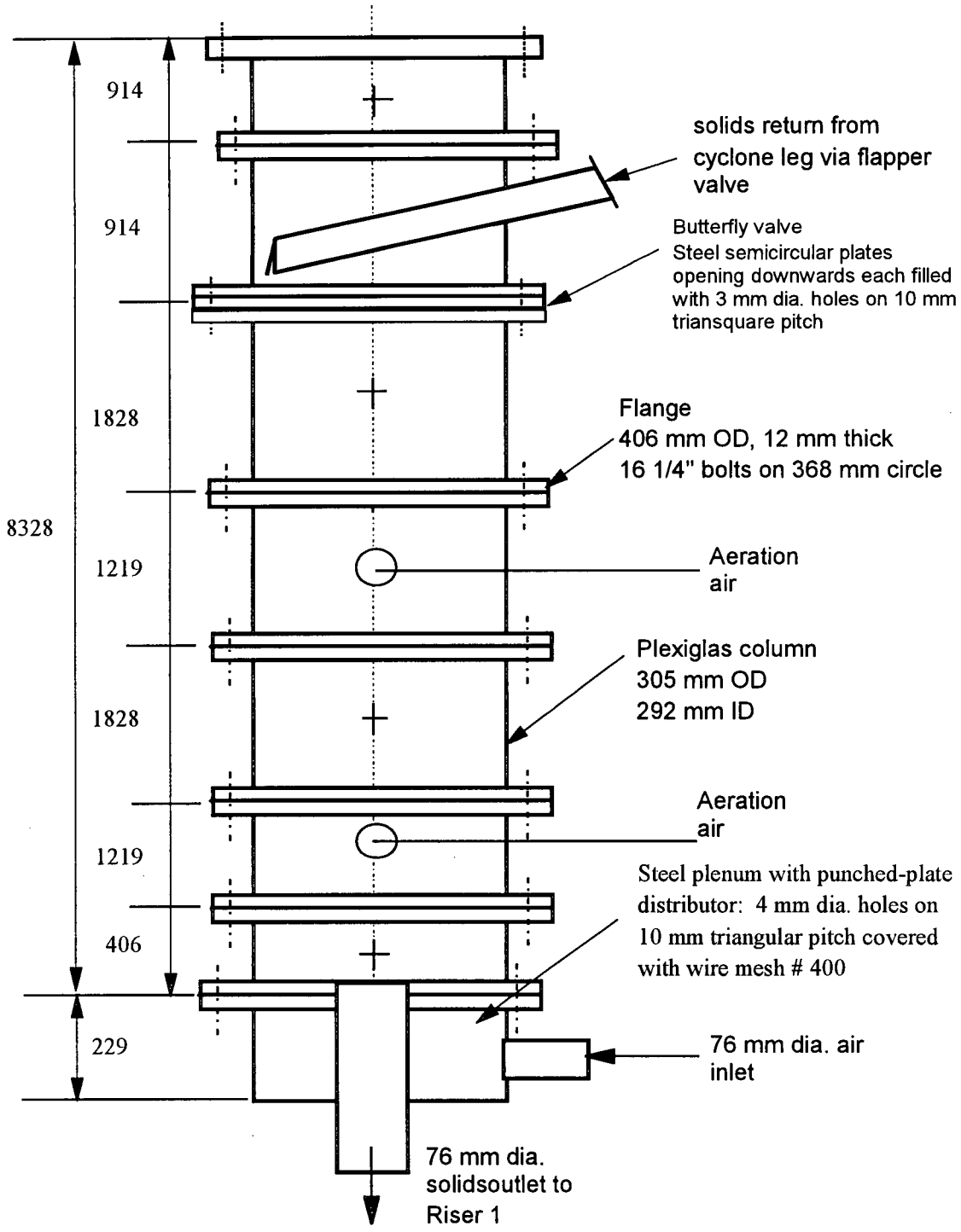

Dimensions in mm

Appendix A-4: Details of Storage Tank

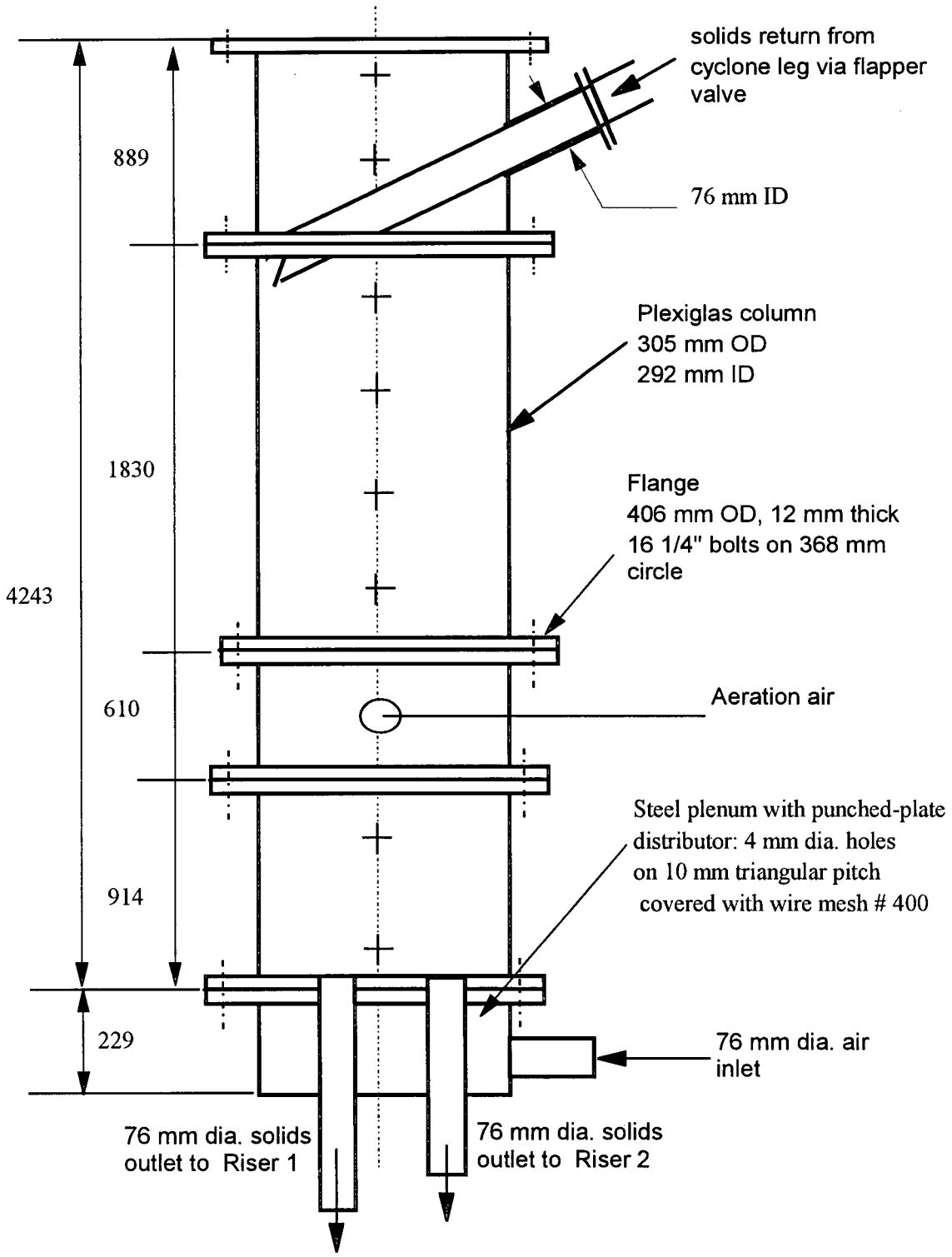

Dimensions in mm

Appendix A-5: Details of Impingement Separator

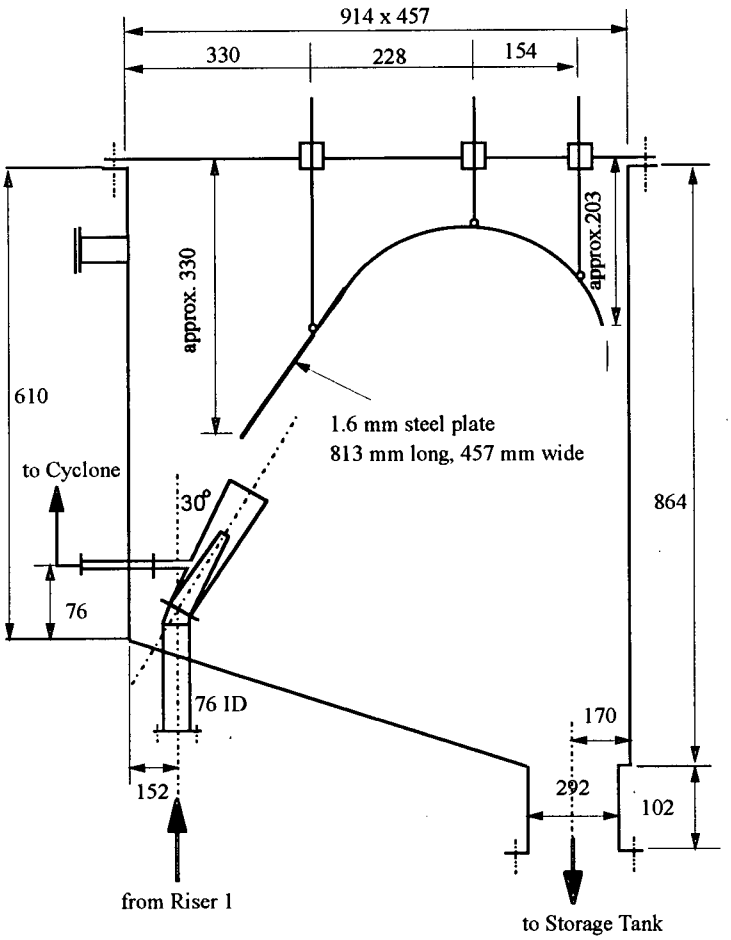

Separator nozzle

Dimensions: mm

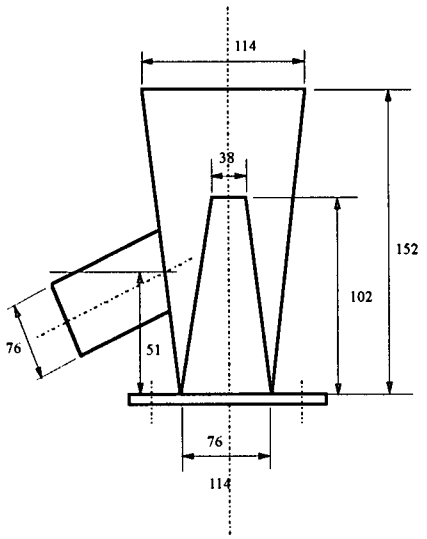

Appendix A-6: Details of Cyclones

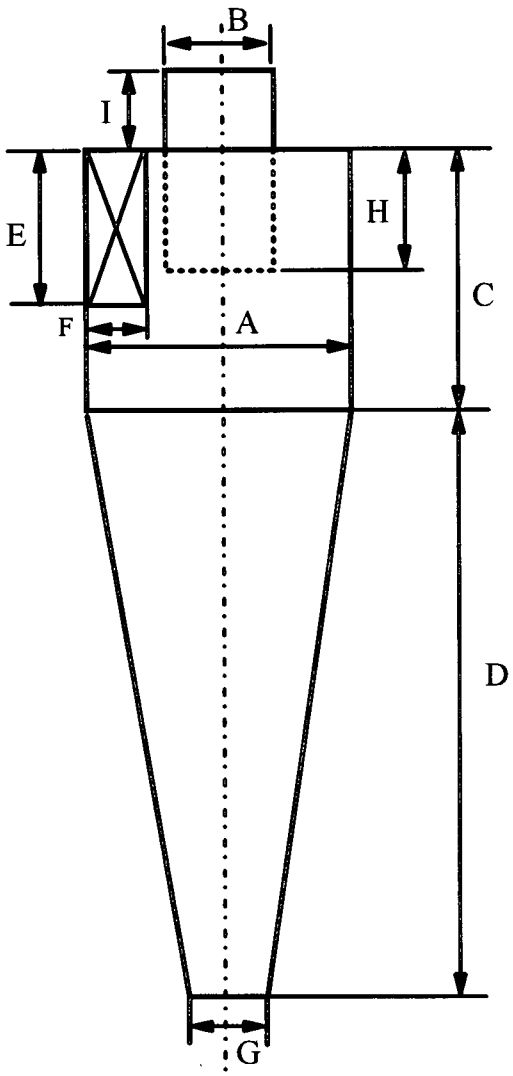

Dimension	Cyclone 1	Cyclone 2	Cyclone 3
A	102	203	152
B	51	102	76
C	152	508	229
D	254	-	381
E	51	102	76
F	21	41	30
G	38	-	57
H	51	102	76
I	102	102	102

Fig. A6: Dimensions of cyclones in mm (1. Secondary - Riser 1, 2. Primary - Riser 2, 3. Secondary - Riser2; Material - Mild steel).

Appendix A-7: Details of Baghouse

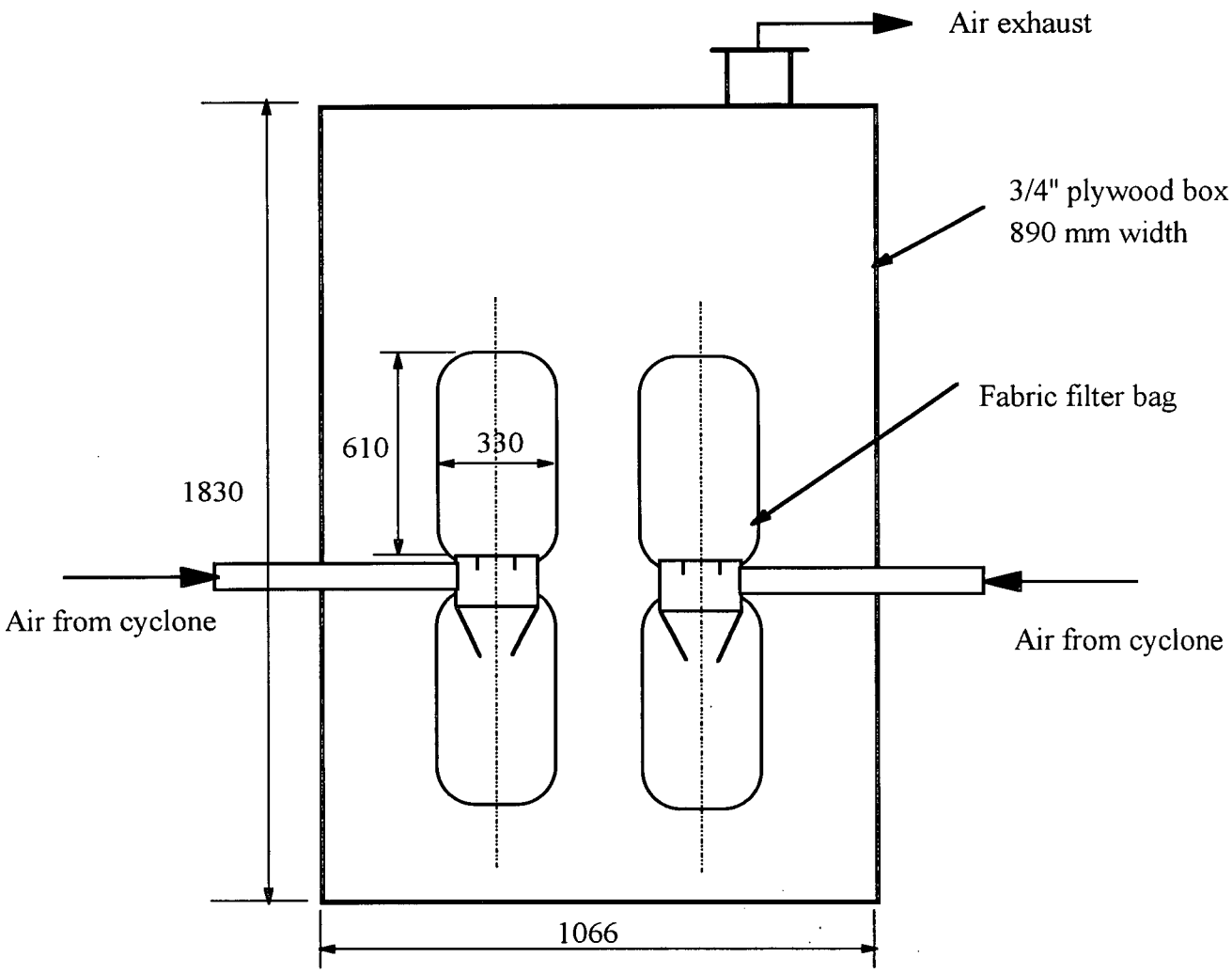

Dimensions in mm

Appendix A-8: Details of Solids Sampling Section

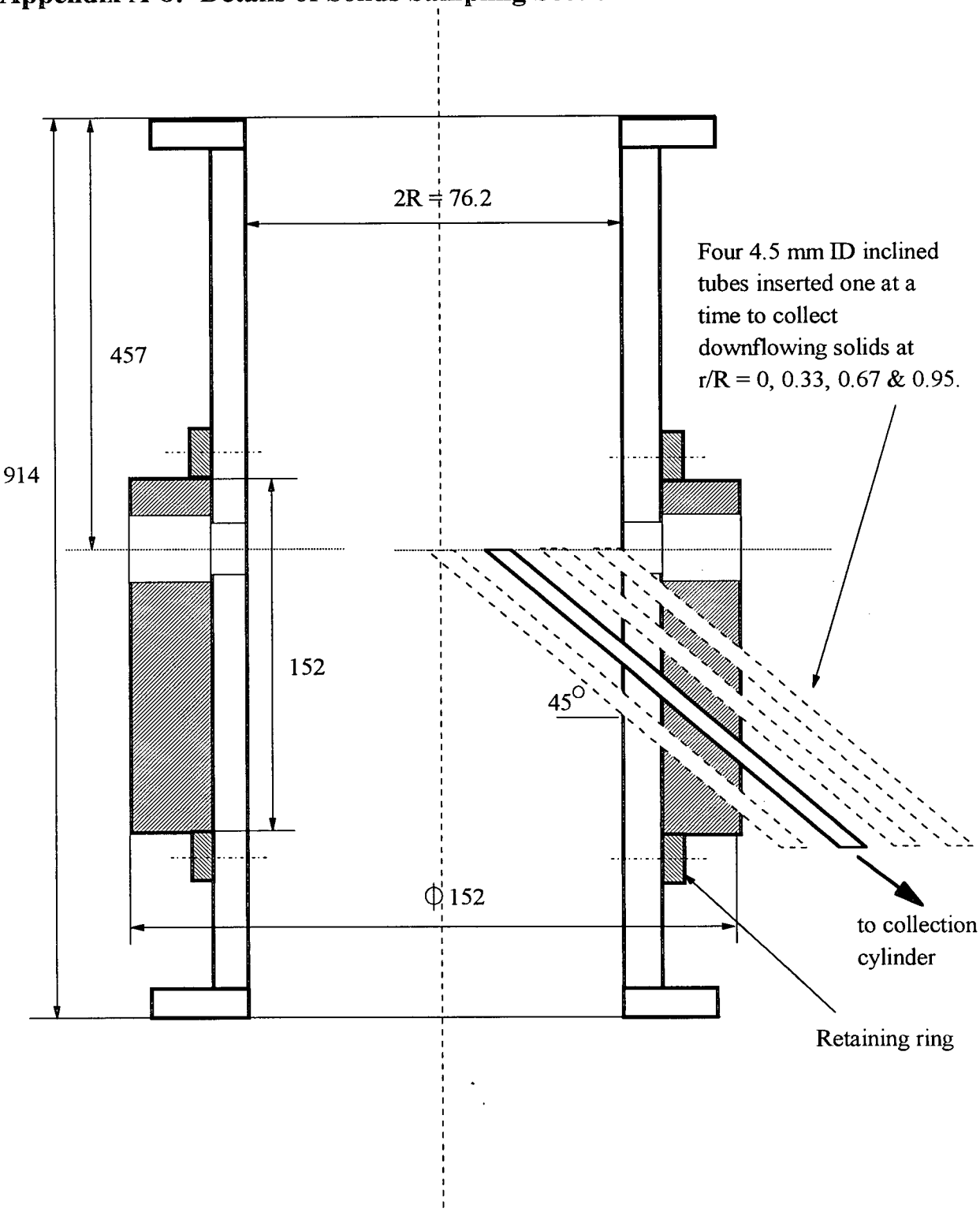

Dimensions in mm

APPENDIX B-1

Evaluation of Mean Solids Hold-up from Pressure Drop Data

In circulating fluidized bed studies measurements of time-averaged axial differential pressure profiles are commonly used to establish average solids hold-ups in a section of the riser by equating the pressure drop per unit length over a section, $\Delta P/\Delta z$, to the bulk weight per unit area, i.e. by writing

$$\frac{\Delta P}{\Delta z} \approx [\rho_p (1-\varepsilon) + \rho\varepsilon]g \qquad \text{(B-1)}$$

where ρ_p and ρ are the densities of the solid and the gas and ε is the voidage averaged over the cross-section and over Δz. This equation assumes that the pressure drop due to the combined effects of gas-wall friction, solids-wall friction and solids acceleration are negligible compared to the weight of the solids. This assumption has, however, been questioned (e.g. Arena et al., 1986; Stemerding, 1962; Hartge et al., 1986; Kato et al., 1988). Weinstein and Li (1989) assumed the flow pattern to be one-dimensional and showed that the actual voidage could be evaluated from differential pressures in the bottom region of a CFB riser, provided that the length of the acceleration section is known. Louge and Chang (1990) also assumed the flow to be one-dimensional and calculated the actual voidage by solving continuity and momentum balance equations. However, they neglected solid and gas-to-wall friction terms. We present below a similar approach with these terms included.

Assuming that radial variations of voidage and velocity observed in CFB risers (e.g. Saxton and Worley, 1970; Brereton and Grace, 1993; Chapter 4) do not contribute significantly to the transfer of momentum in the vertical direction, steady-state one-

dimensional continuity and momentum balance equations can be written for the solids and gas phases as follows:

Continuity equations:

Gas phase: $$\frac{d}{dz}(\rho\varepsilon V_g) = 0 \qquad \text{(B-2)}$$

Solids phase: $$\frac{d}{dz}(\rho_p(1-\varepsilon)V_p) = 0 \qquad \text{(B-3)}$$

Momentum equations:

Gas phase: $$\frac{d}{dz}(\varepsilon\rho V_g{}^2) = -\frac{dP}{dz} - \varepsilon\rho_g g - F_D - F_{Rg} \qquad \text{(B-4)}$$

Solids phase: $$\frac{d}{dz}(1-\varepsilon)\rho_p V_p^2 = -(1-\varepsilon)\rho_p g + F_D - F_{Rp} \qquad \text{(B-5)}$$

F_{Rg} and F_{Rp} are gas/wall and solids/wall frictional forces, respectively, while F_D is the drag force exerted on the solids by the gas.

Adding equations (B-4) and (B-5) leads to

$$\frac{d}{dz}(\varepsilon\rho V_g^2) + \frac{d}{dz} - [(1-\varepsilon)\rho_p V_p^2] = -\frac{dP}{dz}[\rho_p(1-\varepsilon) + \rho_g\varepsilon]g - F_{Rg} - F_{Rp} \qquad \text{(B-6)}$$

Integrating (B-2) and (B-3), we obtain

$$\varepsilon\rho V_g = \text{const.} = G_g \text{ and } (1-\varepsilon)\rho_p V_p = \text{const.} = G_s \qquad \text{(B-7)}$$

Both ρ and ρ_p can be taken to be invariant with height. Therefore equation (B-6) can be rewritten as

$$\frac{d}{dz}\left(G_g V_g\right) + \frac{d}{dz}\left(G_s V_p\right) = -\frac{dP}{dz} - [\rho_p(1-\varepsilon) + \rho_g\varepsilon]g - F_{Rg} - F_{Rp} \qquad \text{(B-8)}$$

In view of equation (B-7), the left side can be simplified leading to

$$G_g\frac{dV_g}{dz} + G_s\frac{dV_p}{dz} = -\frac{dP}{dz} - [\rho_p(1-\varepsilon) + \rho_g\varepsilon]g - F_{Rg} - F_{Rp} \qquad \text{(B-9)}$$

From equation (B-7) we can also show that

$$\frac{dV_g}{dz} = -\frac{G_g}{\rho}\varepsilon^{-2}\frac{d\varepsilon}{dz} \text{ and } \frac{dV_p}{dz} = \frac{G_s}{\rho_p}(1-\varepsilon)^{-2}\frac{d\varepsilon}{dz} \tag{B-10}$$

Substituting (B-10) in (B-9) and rearranging, we obtain

$$[\frac{G_g^2}{\rho_g\varepsilon^2} + \frac{G_s^2}{\rho_p(1-\varepsilon)^2}]\frac{d\varepsilon}{dz} = -\frac{dP}{dz} - [\rho_p(1-\varepsilon) + \rho_g\varepsilon]g - F_{Rg} - F_{Rp} \tag{B-11}$$

Solution of this first order ordinary differential equation requires knowledge of the vertical pressure gradient profile and an initial voidage condition at any location in the riser. The flow is considered to be fully developed when the pressure gradient becomes constant (Arena et al., 1986; Bai et al., 1990). For low density conditions, the flow near the top of the riser often approaches being fully developed. As a result, acceleration and frictional effects are negligible there, and the voidage can then be estimated at the top from the static head using equation (B-1). For high density risers, the boundary condition can be taken at the exit point if the dense phase occupies the whole riser, or at a point in the dense region where the profile is flat if the dense region occupies only part of the riser. In the latter case, the integration is then carried out partly upwards and partly downwards.

F_{Rg} can be estimated from the Fanning equation for gas flow through a circular duct:

$$F_{Rg} = \frac{2f_g\rho U^2}{D} \tag{B-12}$$

with the Fanning friction coefficient, f_g, estimated by Eq. (3.23). There are very few equations for predicting solids friction in dense suspension flows. Figure B-1 shows predicted ratios of the solids frictional-to-static pressure drop according to three different correlations for FCC particles for our high density CFB riser. In all cases this ratio is less than 10%. Equation (3.24) by Geldart and Ling (1990) is adopted in our above calculation since it was obtained for a wider range of solids and gas flows and for voidages as low as 0.55.

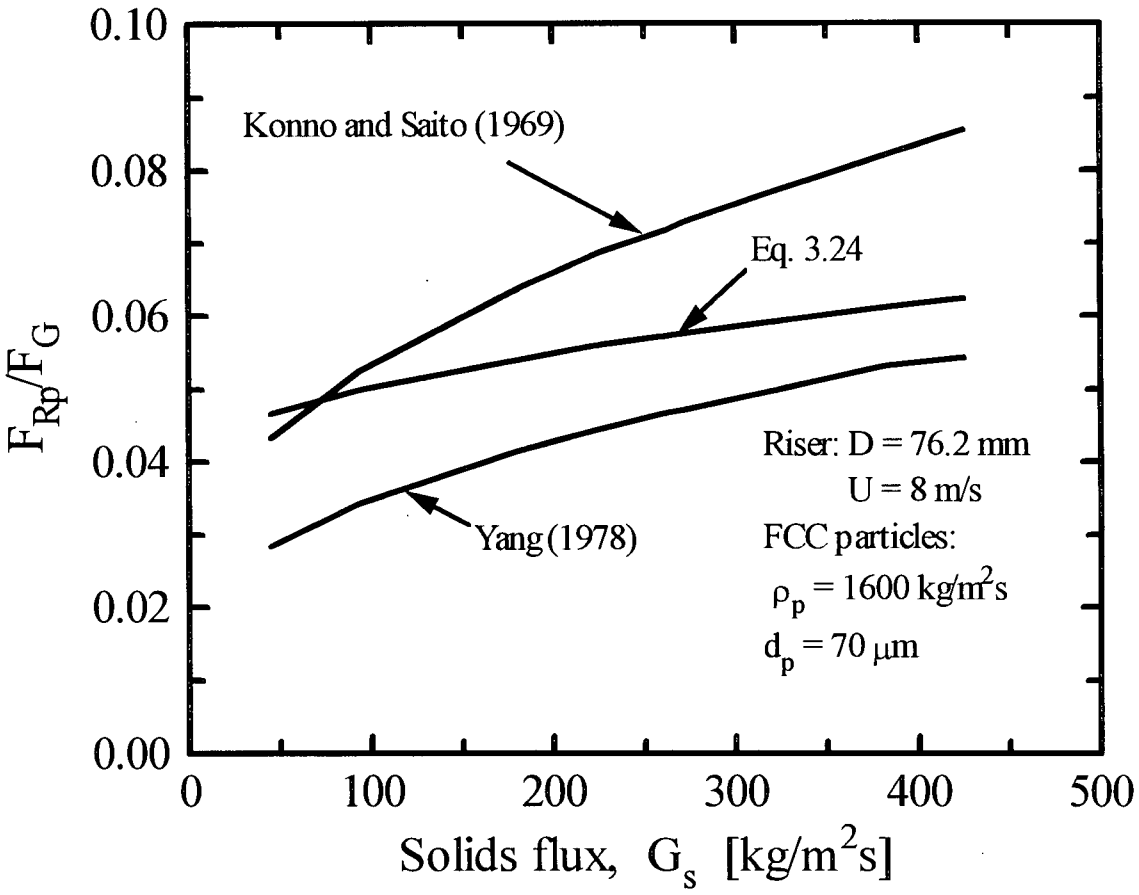

Fig. B-1: Ratio of solids friction to static pressure drop in a high density riser.

Figure B-2 compares measured and calculated solid hold-ups for G_s = 181 and 425 kg/m^{2}s at U = 8 m/s. The calculation is limited to heights above about 1 m from the distributor to minimize entry effects which tend to make the flow pattern three-dimensional.

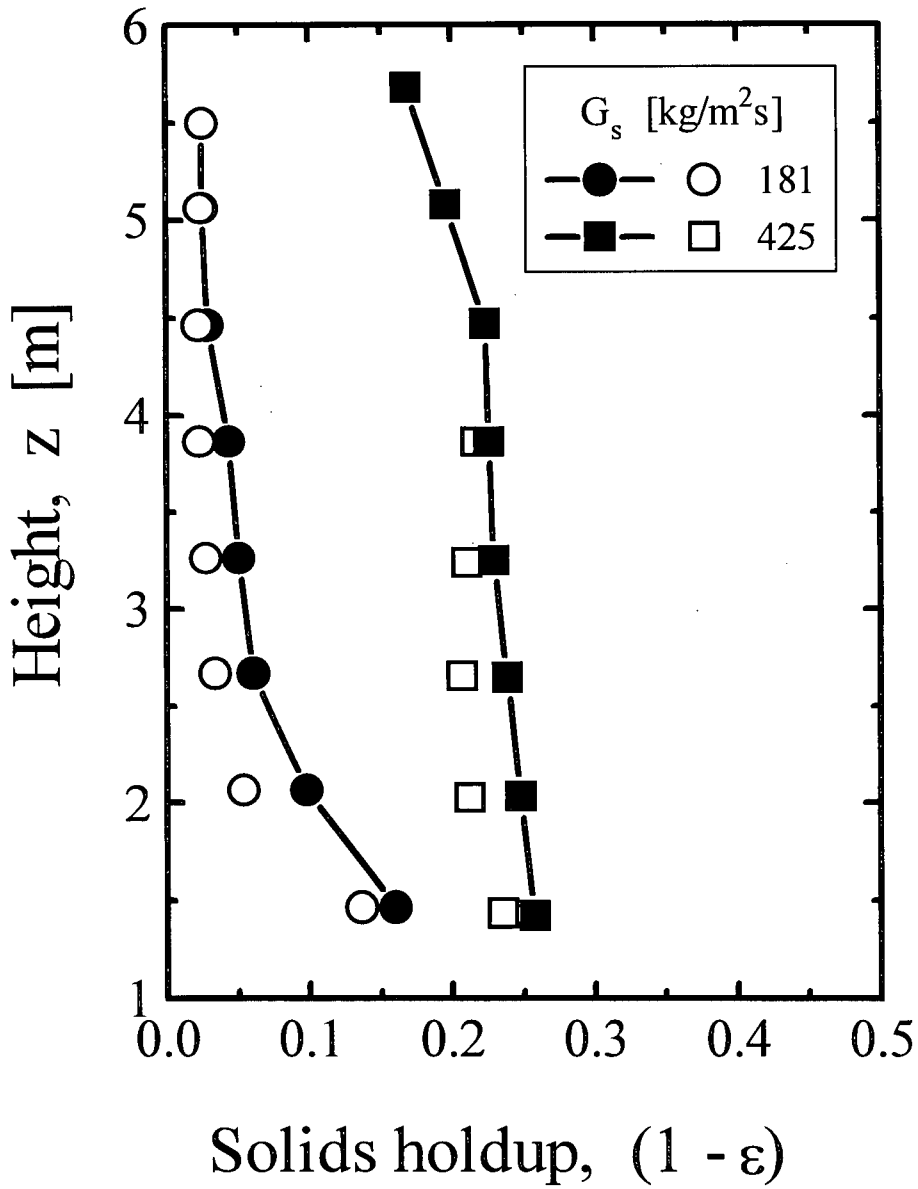

Fig. B2: Apparent (solid symbols) and actual (open symbols) solids hold-up profiles at U = 8 m/s for G_S = 181 and 425 kg/m^{2}s.

APPENDIX B-2

Data used to correlate bottom and exit cross-sectional mean voidages.

Ref.	d_p [μm]	ρ_p [kg/m^3]	D [m]	U [m/s]	G_s [kg/m^{2}s]	ε_D [-]	ε_e [-]
A	65	1380	0.254	2.27	54.1	0.771	0.962
A	65	1380	0.254	3.95	117.9	0.847	0.952
A	65	1380	0.254	5.71	157.1	0.781	0.962
A	65	1380	0.254	5.68	183.3	0.746	0.954
A	65	1380	0.254	7.66	103.1	0.860	0.978
A	65	1380	0.254	7.47	206.3	0.741	0.951
B	81	3090	0.09	2.2	73	0.877	0.974
B	81	3090	0.09	4	73	0.911	0.984
B	81	3090	0.09	5.6	73	0.927	0.988
C	56	3050	0.09	1.5	129	0.877	0.962
D	105	4510	0.09	4	135	0.879	0.976
D	105	4510	0.09	5.5	135	0.899	0.982
E	54	930	0.09	1.5	14.3	0.819	0.974
E	54	930	0.09	1.5	15.4	0.819	0.974
E	54	930	0.09	1.5	26.6	0.826	--
E	54	930	0.09	1.5	48.2	0.810	0.940
E	54	930	0.09	2.1	24.1	0.850	0.978
E	54	930	0.09	2.1	32	0.850	0.963
E	54	930	0.09	2.1	64.2	0.843	0.888
E	54	930	0.09	2.1	96.3	0.812	0.850
F	60	881	0.076	2.44	50	0.852	0.926
F	60	881	0.076	4.51	120	0.858	0.909
F	60	881	0.076	4.51	212	0.790	0.844
G	49	1450	0.152	1.9	113	0.768	0.940
G	49	1450	0.152	2.5	137	0.800	0.947
G	49	1450	0.152	3.3	153	0.807	0.947
G	49	1450	0.152	4.1	173	0.827	0.960
H	64	1800	0.152	2.5	41	0.760	0.970
H	64	1800	0.152	3.5	67	0.830	0.970
H	64	1800	0.152	3.5	80	0.781	0.965
H	64	1800	0.152	4.5	107	0.801	0.966
I	270	2600	0.152	6	70	0.839	0.975
I	270	2600	0.152	6	90	0.740	0.965
I	270	2600	0.152	8	100	0.954	0.990

Appendix B2

Ref.	d_p [μm]	ρ_p [kg/m^3]	D [m]	U [m/s]	G_s [kg/m^{2}s]	ε_D [-]	ε_e [-]
I	270	2600	0.152	8	160	0.894	0.986
J	56	2600	0.05	3.4	72	0.850	0.987
J	56	2600	0.05	3.8	75	0.900	0.988
J	56	2600	0.05	4	90	0.807	0.978
K	56	2600	0.4	4.2	64	0.800	0.985
K	56	2600	0.4	5	65	0.920	0.984
K	56	2600	0.4	4.9	118	0.850	0.980
L	72	1300	0.203	2	40	0.720	0.957
L	72	1300	0.203	3.7	84	0.820	--
M	76	1714	0.305	4.3	147	0.818	0.961
N	280	706	0.186	3.7	84.4	0.820	0.910
N	280	706	0.186	6	93.9	0.900	0.950
N	280	706	0.186	6	133.8	0.801	0.930
O	220	794	0.115	5.3	132	0.800	0.950
O	220	794	0.115	5.3	160	0.750	0.943
P	90	2543	0.12	5	92	0.800	0.977
P	90	2543	0.12	5	115	0.788	0.976
P2	90	2543	0.4	5	251	0.764	0.973
Q	49	1450	0.152	2.9	75	0.846	0.973
Q	49	1450	0.152	2.9	108	0.794	0.960
Q	49	1450	0.152	2.9	118	0.793	0.953
Q	49	1450	0.152	2.9	74	0.833	0.967
Q	49	1450	0.152	2.9	106	0.820	0.947
Q	49	1450	0.152	2.9	118	0.800	--
Q	49	1450	0.152	3.4	71	0.833	0.962
Q	49	1450	0.152	3.4	106	0.800	0.961
Q	49	1450	0.152	3.4	140	0.770	0.942
Q	49	1450	0.152	3.4	79	0.852	0.962
Q	49	1450	0.152	3.4	112	0.814	0.945
Q	49	1450	0.152	3.4	129	0.785	--
R	49	1450	0.152	3	68	0.750	--
R	49	1450	0.152	3	70	0.717	--
R	49	1450	0.152	3	73	0.711	--
R	49	1450	0.152	3	78	0.710	--
R	49	1450	0.152	3	101	0.710	--
R	49	1450	0.152	3	103	0.718	--

Appendix B2

Ref.	d_p [μm]	ρ_p [kg/m^3]	D [m]	U [m/s]	G_s [kg/m^{2}s]	ε_D [-]	ε_e [-]
R	49	1450	0.152	3	106	0.713	--
R	49	1450	0.152	3	106.4	0.700	--
R	49	1450	0.152	3	109	0.713	--
R	49	1450	0.152	3	116	0.713	--
R	49	1450	0.152	3	128	0.711	--
R	49	1450	0.152	3	139	0.706	--
R	49	1450	0.152	4	78	0.756	--
R	49	1450	0.152	4	99.6	0.733	--
R	49	1450	0.152	4	105	0.779	--
R	49	1450	0.152	4	131	0.729	--
R	49	1450	0.152	4	145	0.713	--
R	49	1450	0.152	3	118	0.720	--
S	60	1000	0.05	1.17	11.7	0.844	0.975
S	60	1000	0.05	1.2	13.6	0.850	0.975
S	60	1000	0.05	1.29	11.3	0.875	0.975
T	69	1690	0.097	1.5	11	0.760	--
T	69	1690	0.097	1.5	21	0.740	--
T	69	1690	0.097	1.5	22	0.717	--
T	69	1690	0.097	1.5	10	0.745	--
T	69	1690	0.097	1.5	11	0.733	--
T	69	1690	0.097	1.5	15	0.750	--
T	69	1690	0.097	1.5	17	0.745	--
T	69	1690	0.097	1.5	16	0.755	--
T	69	1690	0.097	2	30	0.795	--
T	69	1690	0.097	2	37	0.775	--
T	69	1690	0.097	2	20	0.903	--
T	69	1690	0.097	2	24	0.780	--
T	69	1690	0.097	2	32	0.780	--
T	69	1690	0.097	2	35	0.750	--
T	69	1690	0.097	3	49	0.850	--
T	69	1690	0.097	3	63	0.800	--
T	69	1690	0.097	3	75	0.775	--
T	69	1690	0.097	3	84	0.765	--
T	69	1690	0.097	3	41	0.910	--
T	69	1690	0.097	3	50	0.818	--
T	69	1690	0.097	3	53	0.845	--
T	69	1690	0.097	3	93	0.838	--
T	69	1690	0.097	3	62	0.883	--
T	69	1690	0.097	3	118	0.800	--
T	69	1690	0.097	4	65	0.840	--
T	69	1690	0.097	4	84	0.790	--
T	69	1690	0.097	4	107	0.775	--
T	69	1690	0.097	4	93	0.855	--

Appendix B2

Ref.	d_p [μm]	ρ_p [kg/m^3]	D [m]	U [m/s]	G_s [kg/m^{2}s]	ε_D [-]	ε_e [-]
T	69	1690	0.097	4	52	0.785	--
T	69	1690	0.097	4	86	0.843	--
T	69	1690	0.097	4	87	0.790	--
T	69	1690	0.097	4	200	0.775	--
U	62	1020	0.09	1.18	12.2	0.800	--
U	62	1020	0.09	1.39	18	0.819	--
V	205	760	0.09	4.25	82	0.790	--
V	205	760	0.09	3.37	60	0.788	--
V	205	760	0.09	2.7	37.3	0.775	--
W	82	1780	0.09	2.5	35	0.800	--
X	59.1	1623	0.15	1.5	18.3	0.738	0.983
X	59.1	1623	0.15	1.5	22.3	0.707	0.984
X	59.1	1623	0.15	2	27.5	0.820	0.972
X	59.1	1623	0.15	2	32.8	0.795	0.982
X	59.1	1623	0.15	2	34.9	0.732	0.976
X	59.1	1623	0.15	2	49.6	0.642	0.925
X	59.1	1623	0.15	2.5	36.8	0.712	0.965
X	59.1	1623	0.15	2.5	49.4	0.771	0.964
X	59.1	1623	0.15	2.5	64.7	0.765	0.972
X	59.1	1623	0.15	2.5	87.6	0.751	0.961
Y	59.1	1623	0.097	1.5	9.79	0.694	0.974
Y	59.1	1623	0.097	1.5	15.6	0.746	0.982
Y	59.1	1623	0.097	1.5	20.3	0.761	0.990
Y	59.1	1623	0.097	2	20.3	0.788	0.986
Y	59.1	1623	0.097	2	26.1	0.795	0.977
Y	59.1	1623	0.097	2.5	18.1	0.782	0.994
Y	59.1	1623	0.097	2.5	29.3	0.815	0.981
Y	59.1	1623	0.097	2.5	47.1	0.795	0.996
Y	59.1	1623	0.097	3	36.1	0.817	0.975
Y	59.1	1623	0.097	3	63.6	0.820	0.976
Z	59.1	1623	0.066	1.5	7.85	0.752	0.997
Z	59.1	1623	0.066	1.5	25.2	0.821	0.976
Z	59.1	1623	0.066	2	41.2	0.847	0.992
Z	59.1	1623	0.066	2.5	32	0.846	0.979
Z	59.1	1623	0.066	2.5	37.8	0.742	0.988
Z	59.1	1623	0.066	2.5	35.8	0.776	0.979
Z	59.1	1623	0.066	2.5	37.8	0.796	0.988
Z	59.1	1623	0.066	3	25.7	0.702	0.989
A1	70	1400	0.3	11.1	147	0.9308	0.973

Appendix B2

Ref.	d_p [μm]	ρ_p [kg/m^3]	D [m]	U [m/s]	G_s [kg/m^{2}s]	ε_D [-]	ε_e [-]
A2	150	2500	0.05	6.5	270	0.837	0.952
A2	150	2500	0.05	6.5	385	0.650	0.929
A3	275	2630	0.0828	6	102	0.931	0.988
A3	275	2630	0.0828	6	198	0.876	0.982
A4	70	1570	0.15	5.7	294	0.916	0.931
A4	70	1570	0.15	5.7	389	0.879	0.905
A4	70	1570	0.15	5.7	538	0.818	0.871
A4	70	1570	0.15	5.7	685	0.813	0.843
AA	70	1600	0.0762	8	93	0.927	0.986
AA	70	1600	0.0762	8	225	0.825	--
AA	70	1600	0.0762	8	262	0.797	--
AA	70	1600	0.0762	8	272	0.754	0.919
AA	70	1600	0.0762	8	382	0.722	0.842
AA	70	1600	0.0762	8	425	0.717	0.832
AA	70	1600	0.0762	8	77	0.950	0.983
AA	70	1600	0.0762	8	262	0.794	--
AA	70	1600	0.0762	8	225	0.826	--
AA	70	1600	0.0762	8	279	0.838	--
AA	70	1600	0.0762	8	291	0.790	--
AA	70	1600	0.0762	8	382	0.733	0.842
AA	70	1600	0.0762	8	181	0.739	--
AA	70	1600	0.0762	8	194	0.816	--
AA	70	1600	0.0762	8	330	0.787	0.941
AA	70	1600	0.0762	8	163	0.841	0.985
AA	70	1600	0.0762	8	225	0.830	0.975
AA	70	1600	0.0762	8	323	0.781	0.943
AA	70	1600	0.0762	7.3	235	0.849	--
AA	70	1600	0.0762	7.3	286	0.834	--
AA	70	1600	0.0762	7.3	246	0.823	--
AA	70	1600	0.0762	6	98	0.884	0.983
AA	70	1600	0.0762	6	151	0.819	--
AA	70	1600	0.0762	6	205	0.787	--
AA	70	1600	0.0762	6	276	0.783	0.957
AA	70	1600	0.0762	6	311	0.775	0.908
AA	70	1600	0.0762	6	336	0.768	0.852
AA	70	1600	0.0762	4	68	0.811	0.984
AA	70	1600	0.0762	4	138	0.798	--
AA	70	1600	0.0762	4	200	0.778	0.921
AA	70	1600	0.0762	4	240	0.742	0.813
AA	70	1600	0.0762	4	109	0.828	0.984

References:

A	Ouyang and Porter (1993)	P2	Arena et al. (1991)
B	Li and Kwauk (1980)	Q	Weinstein et al. (1984)
C	Li and Kwauk (1980)	R	Schnitzlein (1987)
D	Li and Kwauk (1980)	S	Horio et al. (1988)
E	Li et al. (1988)	T	Nishino (1990)
F	Yerushalmi et al. (1979)	U	Gao (1990)
G	Yerushalmi and Avidan (1985)	V	Gao (1990)
H	Rhodes and Geldart (1986)	W	Gao (1990)
I	Rhodes and Geldart (1986)	X	Bai and Kato (1995)
J	Hartge et al. (1986)	Y	Bai and Kato (1995)
K	Hartge et al. (1986)	Z	Bai and Kato (1995)
L	Louge and Chang (1990)	A1	Vergel (1990)
M	Bader et al. (1988)	A2	Pugsley (1990)
N	Bi et al. (1989)	A3	Patience (1990)
O	Yang et al. (1984)	A4	Contractor et al. (1993)
P	Arena et al. (1991)	AA	This work

APPENDIX B-3

Comparison between solids inventories predicted from mass and pressure balance analysis in HDCFB unit and measured values.

G_s [kg/m^{2}s]	U_1 [m/s]	U_2 [m/s]	$L_{1,expt.}$ [m]	$L_{1,calc.}$ [m]	$L_{2,expt.}$ [m]	$L_{2,calc.}$ [m]	$M_{inv,expt}$ [kg]	$M_{inv,calc.}$ [kg]
278	6.5	7.2	3.258	1.721	2.964	2.368	367	257
185	5.8	6.7	2.988	1.377	3.614	1.860	389	204
126	7.8	6.0	2.648	1.154	4.354	1.293	413	154
200	9.5	5.5	3.148	1.561	3.554	1.674	395	203
184	8.0	6.6	2.708	1.377	4.644	1.595	433	186
275	8.0	5.4	2.928	1.944	4.054	2.042	412	252
294	8.0	6.3	3.028	1.834	3.954	2.135	412	250
163	8.0	6.0	3.028	1.332	4.104	1.491	421	177
203	8.0	6.0	3.048	1.507	4.004	1.691	416	201
288	8.0	6.0	2.678	1.858	4.174	2.103	404	250
319	8.0	6.0	2.638	1.998	4.054	2.248	395	268
354	8.0	7.0	2.938	1.948	3.954	2.406	406	274
95	5.7	7.5	3.108	0.994	3.714	1.181	402	136
98	5.7	7.2	3.353	0.998	3.334	1.201	394	138
205	5.6	6.6	3.008	1.460	3.554	2.071	387	223
255	6.1	5.8	3.038	1.758	2.914	2.301	351	257
232	6.0	5.8	3.018	1.659	2.884	2.158	348	242
222	6.1	5.4	--	1.683	--	2.055	--	237
425	8.0	7.5	--	2.115	--	3.077	--	326
184	8.0	7.0	--	1.358	--	1.595	--	185
275	8.0	7.0	--	1.687	--	2.042	--	234
78	6.0	7.8	2.533	0.930	4.522	1.023	416	121
57	6.0	7.8	2.993	0.831	4.132	0.853	420	104
62	6.0	7.7	3.103	0.851	4.022	0.897	420	108
133	5.6	7.5	3.163	1.153	3.742	1.498	407	166
288	5.2	7.7	3.103	1.692	3.852	3.316	410	315
268	8.3	9.0	2.403	1.628	4.162	1.988	387	225
282	6.1	8.0	2.918	1.665	3.814	2.540	397	264
333	6.1	8.0	2.998	1.814	3.764	3.179	399	314
47	6.0	8.0	2.878	0.796	4.092	0.771	411	97
228	5.5	7.1	3.264	1.519	3.923	2.321	424	242
322	5.5	7.4	3.194	1.811	3.938	3.361	421	326
77	7.7	7.1	3.224	0.899	3.962	1.008	424	118
127	5.5	9.7	2.098	1.240	3.884	1.467	353	168
134	5.5	9.7	1.788	1.263	3.934	1.524	337	173
164	5.5	9.7	2.368	1.357	2.634	1.769	295	195
28	4.1	16.3	3.038	1.984	2.964	0.639	354	157
39	4.1	16.3	2.858	2.017	3.139	0.790	354	169
95	5.7	7.5	3.108	0.994	3.714	1.181	402	136
98	5.7	7.2	3.353	1.000	3.334	1.205	394	138

G_s [kg/m^{2}s]	U_l [m/s]	U_2 [m/s]	$L_{1,expt.}$ [m]	$L_{1,calc.}$ [m]	$L_{2,expt.}$ [m]	$L_{2,calc.}$ [m]	$M_{inv,expt}$ [kg]	$M_{inv,calc.}$ [kg]
205	5.6	6.6	3.008	1.460	3.554	2.071	387	223
151	5.5	7.7	2.468	1.226	4.034	1.663	383	181
214	5.5	7.7	2.508	1.452	4.074	2.190	388	229
249	5.5	7.2	2.508	1.588	3.834	2.548	374	261
276	5.7	7.0	2.628	1.689	3.794	2.738	379	279
311	5.7	6.9	2.628	1.818	3.744	3.220	376	318
323	5.6	6.7	3.353	1.881	--	3.323	--	329
336	5.5	6.5	2.543	1.960	3.814	3.433	375	341
280	6.5	7.2	1.858	1.692	3.014	2.346	287	254
183	6.2	8.0	2.833	1.345	2.209	1.761	297	194
365	7.3	8.0	3.353	1.901	--	2.655	--	286
218	6.2	8.0	1.853	1.464	2.859	2.002	278	217
18	6.0	8.0	3.913	0.631	2.339	0.504	369	69
45	6.0	8.0	3.353	0.786	1.929	0.754	311	95
118	6.0	8.0	3.063	1.106	3.169	1.328	367	152
217	6.0	8.0	3.753	1.462	2.309	2.049	357	220
28	6.1.	8.0	4.023	0.694	2.279	0.605	372	80
133	6.1	8.0	3.233	1.162	2.819	1.424	357	161
257	6.1	8.0	3.053	1.589	2.709	2.318	340	245
127	6.1	8.0	2.463	1.141	3.189	1.383	333	157
175	6.1	8.0	3.513	1.316	2.019	1.721	326	190
163	6.1	8.0	3.363	1.275	1.989	1.640	316	182
188	6.1	8.0	2.963	1.362	2.159	1.815	302	199
149	6.0	8.0	3.353	1.223	--	1.555	--	174
156	6.0	8.0	3.353	1.249	--	1.605	--	179
227	6.0	8.0	3.353	1.493	--	2.120	--	227
77	6.0	8.0	3.353	0.936	--	1.016	--	121
234	6.0	8.0	3.353	1.516	--	2.019	--	222
223	7.6	8.0	3.353	1.480	--	1.819	--	206
194	7.8	7.6	3.128	1.423	4.364	1.695	442	195
330	7.8	7.6	2.928	1.823	4.304	2.327	426	260
359	7.2	7.6	2.558	1.906	4.164	2.661	396	287
291	8.2	7.6	2.708	1.705	3.754	2.100	381	239
382	7.8	7.6	3.098	1.971	3.124	2.550	367	284
181	8.1	7.6	3.158	1.337	3.514	1.578	393	182
190	7.9	7.6	3.078	1.367	2.564	1.628	333	187
120	7.8	7.6	3.078	1.102	4.094	1.259	423	147
53	7.8	7.6	2.488	0.798	4.554	0.860	415	102
126	7.8	6.0	2.648	1.154	4.354	1.293	413	154
200	9.5	5.5	3.148	1.561	3.554	1.674	395	203
37	8.1	6.7	2.178	0.664	4.944	0.778	420	89
62	8.0	6.6	2.678	0.810	4.604	0.930	429	108
365	7.3	7.6	1.938	1.923	2.684	2.655	273	288
359	5.8	6.7	2.988	2.149	3.614	3.553	389	359
165	5.4	4.2	3.353	1.663	--	1.800	--	221
329	4.1	7.0	2.728	1.865	3.404	4.300	362	389